

Final Report

European Stratospheric Research Aircraft

Design Synthesis Exercise Group 14

Delft University of Technology



Final Report

European Stratospheric Research Aircraft

by

Design Synthesis Exercise Group 14

Student Name	Student Number
Maximilian Reinhard	5298903
Jurgen de Groot	5303133
Gleb Martjanovs	5295882
Cheng Shun Chak (Jack)	4835549
Álvaro Baillet Bolívar	5243750
Carlo Filippo Capano	5268281
Jonas Candries	4842979
Tom Weering	5009057
Marco Rubaga	5031680
Antonio Minafra	5027993

Instructor: Dr. S.J. Hulshoff
Coach: Marco Desiderio
Coach: P. Pai Raikar
Project Duration: April, 2023 - June, 2023
Faculty: Faculty of Aerospace Engineering, Delft

Contents

Executive Overview	<i>Jack</i>	1
I Project context		6
1 Market Analysis	<i>Marco & Antonio & Jack</i>	6
1.1 Roadmap to ESRA		6
1.2 Competing aircraft		7
1.3 Budgeting for an Airborne Science Mission		8
1.4 Scientific missions		9
1.5 Aircraft Lifetime		9
2 Functional Analysis	<i>Carlo</i>	11
2.1 Functional Flow Diagram (FFD) - Diagram 2.1		11
2.2 Function Breakdown Structure (FBS) - Diagram 2.2		11
3 Requirements	<i>Jurgen, Tom, Carlo, Marco</i>	14
3.1 Stakeholder requirements		14
II Technical design		16
4 Sub-system Interface	<i>Jonas</i>	16
4.1 N2		16
5 Configuration selection	<i>Antonio, Maximilian, Carlo, Gleb, Jonas, Marco</i>	17
5.1 General Design Challenges		17
5.2 Past work		17
5.3 Engine configuration		17
5.4 Wing configuration		19
5.5 Tail configuration		21
6 Payload design	<i>Jack</i>	23
7 Methodology and Budgets	<i>Alvaro, Gleb</i>	26
7.1 Design Methodology		26
7.2 Fuel, Structural Mass and Drag Budgets		27
8 Propulsion	<i>Jonas, Carlo</i>	33
8.1 Model Analysis		33
8.2 Engine Design Considerations		33
8.3 Engine selection		37
8.4 Engine characteristics and off design		38
8.5 Verification and Validation		40
8.6 Recommendations		40
9 Aerodynamics	<i>Jack, Maximilian</i>	41
9.1 Airfoil design		41
9.2 Planform Design		42
9.3 Wing characterization		44
9.4 Wing optimization		45
9.5 Verification and Validation		45
9.6 Recommendations		45

10 Structures	<i>Jurgen, Tom</i>	47
10.1 Wing box design methodology		47
10.2 Wing box design parameters		47
10.3 Material selection		50
10.4 Wing box modelling		52
10.5 Normal Loading		54
10.6 Loading diagrams		55
10.7 Failure analysis		58
10.8 Wing box design		62
10.9 Recommendations		64
11 Aeroelasticity		66
11.1 Verification & Validation		68
11.2 Recommendations		68
12 Stability and control	<i>Alvaro, Gleb</i>	69
12.1 Longitudinal stability and controllability		69
12.2 Lateral stability		70
12.3 Tail Planform Sizing		71
12.4 Dynamic stability		73
12.5 Control surfaces		75
12.6 Gear design and placement		77
13 Performance Analysis	<i>Alvaro, Gleb</i>	79
13.1 Detailed Profile Characterization and Optimization		79
13.2 Take-off and Landing		83
13.3 Flight Envelope, Climb and Descent Performance		84
13.4 Turning Analysis		87
14 Internal layout and aircraft systems	<i>Maximilian</i>	89
14.1 System communication		89
14.2 Electrical subsystem		89
14.3 Fuel subsystem		91
14.4 Hydraulic subsystem		92
14.5 Recommendations		93
15 Final Design	<i>Gleb</i>	94
15.1 Aircraft system characteristics		94
15.2 Technical Drawings		95
III Operations		97
16 Operations and Logistics	<i>Antonio & Marco</i>	98
16.1 Home bases for operation		98
16.2 Flight Operations		98
16.3 Ground Operations		100
16.4 Operational Limitations		101
17 Sustainable Development Approach	<i>Jonas, Carlo</i>	102
17.1 Climate impact and emissions		102
17.2 Social sustainability		105
17.3 End of life		106
18 Production Plan, Assembly and Integration plan	<i>Jack</i>	107
18.1 Manufacturing		107
18.2 Assembly plan		107

19 Technical Risk Assessment	<i>Maximilian</i> 109
20 Reliability, Availability, Maintainability, and Safety (RAMS) Analysis	<i>Maximilian, Jonas, Marco, Antonio</i> 113
20.1 Reliability	113
20.2 Availability	118
20.3 Maintainability	118
20.4 Safety	119
20.5 Recommendations	121
21 Cost	<i>Marco, Antonio</i> 122
21.1 Cost Breakdown Structure	122
21.2 User Fee and campaign costs	126
21.3 V&V of the cost tool	127
21.4 Sensitivity Analysis	128
21.5 Recommendations	129
22 Requirement compliance	<i>All</i> 131
22.1 System Requirements	131
22.2 Aerodynamics sub-system	132
22.3 Structure sub-system	133
22.4 Propulsion sub-system	133
22.5 Communication sub-system	134
22.6 Power sub-system	134
22.7 Payload sub-system	134
22.8 Life Support	135
22.9 Avionics	135
22.10Landing Gear	135
23 Future planning	<i>Tom, Maximilian</i> 136
23.1 Project design and development logic	136
23.2 Project Gantt chart	137
References	<i>Maximilian</i> 139
IV Appendix	144
A Appendix A	144

Nomenclature

			wrt	With Respect To	
a.c	Aerodynamic Centre		α	Angle of attack	
AM	Additive Manufacturing		σ	Axial stress	Pa
AoA	Angle of Attack		τ	Shear stress	Pa
APU	Auxiliary Power Unit		A	Area	m^2
ATC	Air Traffic Control		C_D	Wing drag coefficient	-
c.p	Centre of Pressure		c_d	Airfoil drag coefficient	-
CG	Center of Gravity		C_L	Wing lift coefficient	-
DOC	Direct operating cost	FY 23 USD\$	c_l	Airfoil lift coefficient	-
EC	European Commission		$C_{L\alpha}$	Wing lift slope	-
EoL	End of life		C_m	Airfoil pitching moment coefficient	-
ESRA	European Stratospheric Research Aircraft		C_r	Root chord length	m
EUFAR	European Facility for Airborne Research in Environmental and Geoscience		C_t	Tip chord length	m
FCS	Flight Control System		E	Young's modulus	Pa
FLS	Flight Logging System		G	Shear modulus	Pa
GH	Global Hawk		I	Second moment of area	m^4
GPU	Ground Power Unit		K_θ	Wing section torsional stiffness	Nm/rad
LE	Leading Edge		K_h	Wing section bending stiffness	N/m
MAC	Mean Aerodynamic Chord		K_{IC}	Fracture toughness	MPa · m ^{1/2}
MOF	Margin Of Failure		M	Moment	Nm
MTBF	Mean Time Between Failures		q_b	Base shear flow	N/m
MTBM	Mean Time Between Maintenance		q_{div}	Torsional divergence dynamic pressure	Pa
MTBPM	Mean Time Between Preventive Maintenance		q_{rev}	Control reversal dynamic pressure	Pa
MTOM	Maximum take off mass	kg	q_{s0}	Constant shear flow	N/m
MTOW	Maximum take off weight	N	t	Thickness	m
NavCom	Navigation and Communication System		V_∞	Freestream velocity	m/s
OEW	Operational empty weight	N	V_y	Shear force in y-direction	N
RAT	Ram Air Turbine		x_{cg}	Centroid x location	m^4
RTU	Rectifier Transformer Unit		y_{cg}	Centroid y location	m^4
SFC	Specific fuel consumption	$\frac{g}{kNs}$	c	Chord length	m
TE	Trailing Edge		D	Drag	N
VHF	Very High Frequency		L	Lift	N
			S	Wing area	m^2

Executive Overview

Climate change continues to pose the greatest threat to Earth and human society inhabiting the planet. It leads to a myriad of extreme weather events, one of which is the general warming of the planet. Other than the drastic cut in greenhouse gas emission, scientists have proposed Solar Aerosol Injection (SAI) as a last resort, to inject particles into the stratosphere, these particles reflect incoming solar radiation back into space to provide cooling effects for the planet. As the method has never been attempted before and may lead to serious consequences without sufficient research supporting the solution. Following this line of thought, the need for a stratospheric aircraft tailored for scientific research purposes (not limited to SAI) has been discovered. Along with the main stakeholders that explained the current climate in stratospheric research the following mission need statement had been formulated.

To provide a platform for scientific experiments in the stratosphere, beginning operations from 2030.

The 2030 scheduled timeline is due to the opportunity to fill a market gap since the current fleet of stratospheric aircraft is due to retire by 2030. Stakeholders have also conveyed to the project team that a low direct operating cost is vital in enabling scientific research. Hence, the project objective statement is formulated as follows.

Within 10 weeks, elaborate on the conceptual design of an aircraft capable of carrying a scientific payload to the stratosphere, minimizing its direct operating costs.

Market analysis

The project is named European Stratospheric Research Aircraft (ESRA), it started off with project tutor Dr. Ir. Steven Hulshoff and external expert Mr. Wake Smith specify a set of top-level requirements that characterize the project. From this, a market analysis is conducted to increase understanding of where ESRA should stand to increase its competitiveness as well as to assist in steering the design towards some direction.

The main takeaways from the market analysis are cost and performance data on existing stratospheric aircraft such as the NASA-operated ER-2, Global Hawk and WB-57. This information provides the ESRA team with a compass as to roughly how ESRA should perform in terms of cost and aircraft performance. User fees of the existing fleet expressed per flight hour are shown in Table 1. This is a main input in formulating ESRA's own cost requirement in a later stage. Next, to cost, the team had a closer look into the scientific missions that these aircraft undertake, the objective of these missions, payload carried, flight profiles, and logistics data are all valuable inputs to the design.

Functional analysis

Functional analysis of the aircraft relies on market analysis to determine the exact functions that the aircraft should be able to perform. They are mapped out in the form of a functional flow diagram (FFD) and function breakdown structure (FBS) with the former focusing on the functions to be performed in a sequenced manner and the latter providing higher resolution into functions and sub-functions. Requirements generation follows from functional analysis, where systems requirements are formulated, and subsystems requirements are also formulated but to a lesser extent and are updated as the design

Aircraft	User Fee [2023US\$/hour]	Additional Costs [US\$/week]
ER-2	13,520.42	80,000
WB-57	12,844.40	80,000
M-55	11,577.89	Unknown

Table 1: User fee of ER-2 and WB-57

process progresses. Stakeholder requirements were reformulated into system requirements to be more precise, the most crucial of them all are listed below:

- ESRA-STAKE-1-SYS-1 : The aircraft shall be able to fly at an altitude of 20.5 km or higher.
- ESRA-STAKE-5-SYS-12 : The direct operating cost of the aircraft shall be no more than \$11557 FY23 USD per hour.
- ESRA-STAKE-2-SYS-13 : The aircraft shall enter operation by 2030.

Configuration selection

Technical design of the aircraft starts with performing a series of configuration tradeoffs including engine integration, wing, and tail configuration. Amongst engine configurations, the wing podded scored the highest due to the possibility of using a higher bypass ratio engine compared to other options. The fuselage podded option scored quite close and was considered due to the commercial availability of the AE3007 engine used on the Global Hawk. Upon further analysis, it was determined that this engine option was no longer suitable due to the lack of thrust at high altitudes, and a twin-engine option was chosen. The engine configuration was thus changed to twin-wing podded engines.

Wing configuration was largely determined by the weight a particular configuration would incur. Hence low wing and strutted high wing options scored best. Initial studies show that strut-braced wings can bring more weight savings than low-wing designs while also providing larger ground clearance, which is why a strutted high-wing configuration was chosen. Initially, a V-tail configuration was opted to prevent placing the tail in the exhaust of the engine which was mounted on the fuselage. With the change of engine configuration, a T-tail was chosen due to its' simplicity and to avoid interactions between the horizontal surface and the engine exhaust.

Payload design

As the main objective of ESRA is to facilitate stratospheric research, extensive effort has been put into designing payload compartments to accommodate a wide range of different payloads and to ensure ease of payload integration. According to the market analysis, payload integration is a major challenge, which is why ESRA aims to optimize the payload compartments to minimize integration time. The design features of the payload areas of ESRA includes environmentally controlled (pressurized and temperature controlled) pallets that can be slotted into the fuselage via a rail from the back of the aircraft. Space is also available in the nose cone of the aircraft mainly for imaging purposes. This will have a full field of view of the entire frontal hemisphere of the aircraft. A range of existing research missions uses in-situ sampling equipment that is best far from interference of the fuselage which is why wing pods are included specifically for this type of equipment. Due to the nose area being reserved for imaging equipment, a weather radar will be integrated into one of the wing pods. Figure 1 to Figure 3 illustrates the payload bays of ESRA.



Figure 1: ESRA wingpods



Figure 2: Pressurized payload pallet



Figure 3: Nose cone imaging equipment bay

Engine selection

Working towards a cost and schedule requirement, the project team determined it would be necessary to purchase a commercially available and proven engine. A list of engines was gathered and considered

mainly on their thrust lapse performance as it was the most important performance parameter for ESRA's purpose. Eventually, the Pratt & Whitney Canada PW535A engine was chosen. Table 2 tabulates some engine performance parameters at various altitudes.

Table 2: PW535A Engine performance at various operational conditions

Flight point of interest	Altitude [m]	M [-]	Thrust [kN]	TSFC [g/kN*s]	m_f [kg/s]
Take off	0	0.2	11.64	17.57	0.2044
Cruise Climb start	11000	0.65	4.57	17.43	0.0796
On station	20500	0.65	0.94	18.94	0.0178

Cost

The costs of the aircraft were estimated utilizing the "Airplane Cost Estimation: Design, Development, Manufacturing and Operating" book written by Dr. Jan Roskam [69]. This costing method has been widely used in past projects and in industry, however, this method is quite old, being developed in 1989 and furthermore, it is based on empirical relations from commercial aircraft collected up until 1989. Therefore limitations of this method were known but given a lack of widely available, reliable open-source methods to estimate the costs of a whole aircraft program it was chosen to go forward with the Roskam costing tool.

The costs were divided into acquisition costs and direct operating costs. The acquisition costs include R&D, Certification, and Manufacturing all costs that would just need to be paid once for the life of the aircraft. Total acquisition costs divided by the number of aircraft produced result in a cost to acquire a single aircraft of 26.54 million USD. The direct operating costs were divided into insurance, flying costs (fuel and crew costs), and maintenance. According to the Roskam costing tool, the direct operating costs are measured in USD per nautical mile, this has been calculated as being 5.05 USD/nautical mile. The largest component of the operating cost is the maintenance burden for running the aircraft with the fuel costs being the second largest.

The acquisition and direct operating costs were collected into a single user fee per hour. This user fee would cover the direct operating costs and a over the 30-year lifespan of the aircraft would repay the user for the acquisition costs. This total user fee was calculated as being 4217 USD per hour, significantly lower than our competitors ER-2, M-55, and WB-57.

A standard campaign model was produced describing a campaign made up of 45 science hours plus 14 testing hours over 50 days. This model was produced based on schedule delays and timelines of past missions done by the WB-57 and ER-2. Applying the costing model to the standard campaign model a cost for a campaign conducted from a home-based of 304703 USD was calculated. This campaign cost is lower than competitor aircraft's campaign costs.

Final design

A multitude of tools have been developed to size all major components of the aircraft, which leads to the final design of ESRA. A number of these tools take mission flight profiles as input. The mission profile was made with reference to existing mission profiles observed in the market analysis. The final design of ESRA is shown in Figure 4.

Operations and logistics

To enable global operations for ESRA, the fleet of aircraft will be distributed across multiple regions, with 10 selected airports serving as home bases. This approach eliminates the need for ferry flights and allows for significant time and cost savings. The critical flight profile during a campaign was produced and can be seen in Figure 16.2. ESRA's routine flight duration is 6 hours, extendable to 9 hours if needed. Pilots and crew have a 12-hour duty day with 12 hours of off-duty time between flights. Pre-flight operations include checks, inspections, fueling, and oxygen replenishment. In flight, pilots must adhere to performance limitations, considering factors like altitude and weather conditions. The ground crew maintains communication with the pilot and instrument teams at all times. After

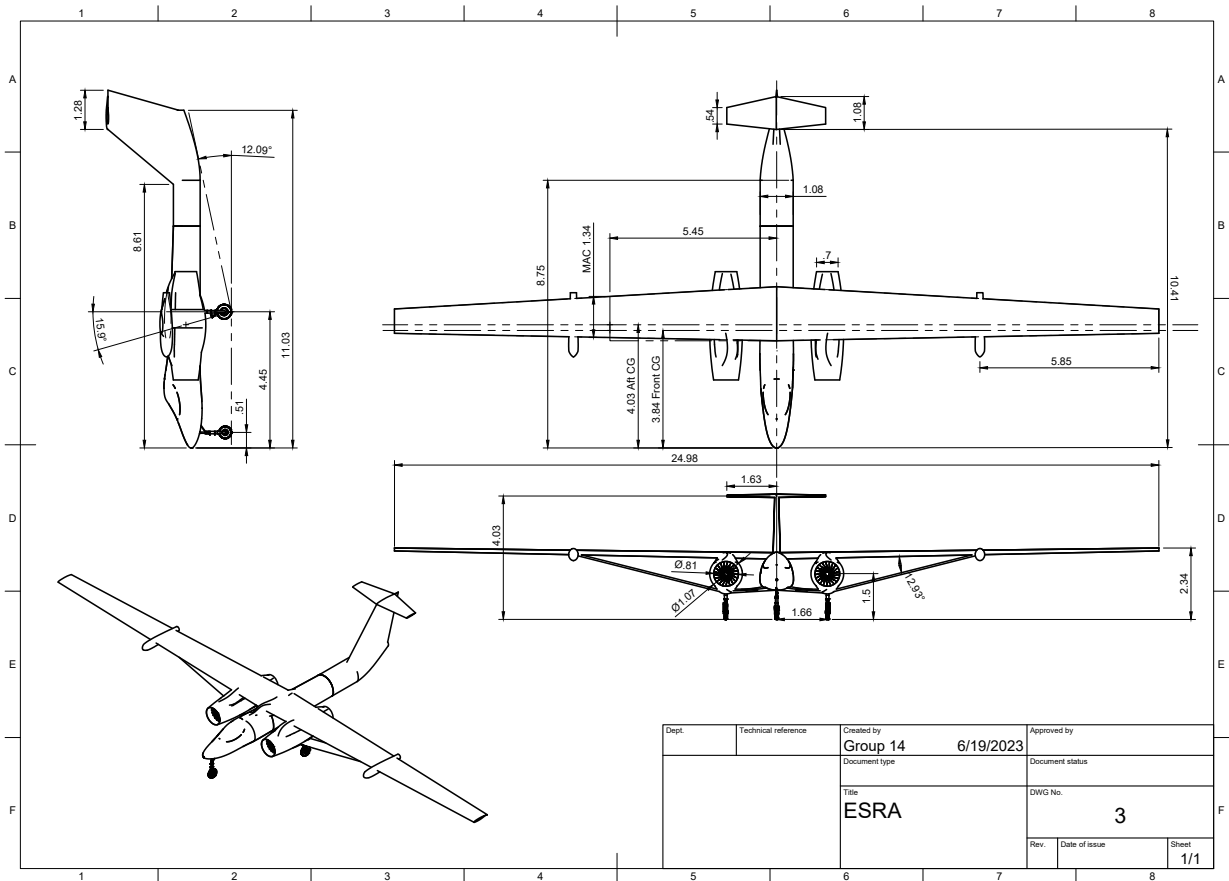


Figure 4: Three view of ESRA

landing, instruments are turned off, and the aircraft undergoes inspection, servicing, and towing. The payload is integrated through a rear hatch in the fuselage, with dollies and wing pods for mounting and electrical connection. Electrical power is provided in flight by generators and on the ground by local infrastructure. Data recording is done on a hard drive in the payload compartment, which scientists are responsible for downloading and securely storing.

Future planning

The future plannign outlines the phases of the ESRA project beyond the design synthesis exercise, including preliminary design, detailed design, manufacturing, certification and testing, operational phase, and end-of-life considerations. The operational lifetime is estimated at 30 years, and sustainability principles guide the end-of-life phase. A project Gantt chart visualizes the timeline and milestones (Figure 23.2). Overall, the chapter provides a comprehensive overview of the ESRA project, its development phases, and the involvement of the ESRA design bureau in various aspects of the aircraft’s lifecycle.

Introduction

It is without debate that climate change has been and will continue to disrupt numerous aspects of human society. Annual CO_2 emission has increased by more than seven folds since the end of the Second World War, the vast amount of greenhouse gases in Earth's atmosphere continues to warm its' climate and subsequently causes extreme weather conditions. Since the problem of climate change was first raised, there have been increasing calls for drastic actions to cut greenhouse gas emissions. Despite this, emissions have been shown to continue increasing. This is why some scientists have been researching ways to cool the planet with geoengineering. A notable method is Stratospheric Aerosol Injection (SAI) whereby particles are injected into the upper atmosphere to reflect solar radiation back to space thereby cooling the atmosphere. Extensive research is however required to investigate potential side effects of SAI on the long term effects such interventions might have.

The need for stratospheric research aircraft has emerged due to the extensive research required to understand the effects of SAI and the significance of conducting scientific studies in the stratosphere. However, the current fleet of stratospheric aircraft, predominantly converted from military platforms and operated by NASA, presents two challenges. Firstly, their high cost of operation, considering their military origins, poses financial constraints, especially with limited budgets for scientific projects compared to other industries. Secondly, the dominance of NASA in operating these aircraft restricts opportunities for scientists from other regions to conduct research. This monopolistic situation limits the progress of scientific investigations. Addressing urgent climate change concerns necessitates facilitating research, be it for gaining a deeper understanding of Earth's atmosphere or exploring potential solutions. Furthermore, the impending retirement of NASA's stratospheric aircraft fleet by 2030 creates a market gap for a new aircraft specifically designed for scientific research.

To act on this need for a new platform to perform stratospheric research, the ESRA design bureau has come forward with a design solution. Namely, the European Stratospheric Research Aircraft (ESRA). This aircraft's design is motivated with the main aim of enabling stratospheric research through an aircraft that is affordable to operate and is driven by the scientists' needs. This will be reflected in the detailed cost analysis in the report as well as the design decisions which are designed around the scientific payload that ESRA will be carrying to the stratosphere.

A market analysis is presented in Chapter 1 which provides an overview of the project as well as ESRA's stand in the market. This is followed by a functional analysis in Chapter 2. Requirements for ESRA follow from the functional analysis, they are listed in Chapter 3. Technical design begins with mapping all the subsystem interfaces and ESRA's design methodology in Chapter 4. After that, a rough aircraft configuration selection is outlined in Chapter 5. The design of the payload area in the aircraft is then presented in Chapter 6, this is a major part of ESRA's design, and a lot of effort has been put into designing the aircraft around the payload areas. General aircraft sizing, propulsion system, and aerodynamic analysis are presented in Chapter 7, Chapter 8, and Chapter 9 respectively. Following these are the structural design which mainly analyses ESRA's wings and strut in Chapter 10. An aerolastic analysis of the design is perform in Chapter 11. Landing gear sizing is included in Chapter 12 due to its interaction with ground control capabilities. Chapter 13 address a few separate performance parameters such as take-off rotation and flight envelope etc. Following this is Chapter 14 which contains the preliminary layout of communication, electric, hydraulic systems etc. Chapter 21 presents the cost of the project based on the design of the aircraft, this is a particularly crucial part for ESRA as it aims to lower cost for scientific purposes. With cost input taken into account, the design is finalized in Chapter 15. The last part of the report mainly deals with operational matters. An operations and logistics plan, sustainability approach of the project, and a crude production plan are discussed in Chapter 16, Chapter 17 and Chapter 18. Risk analysis is presented in Chapter 19 followed by RAMS analysis in Chapter 20. The aircraft's compliance with the requirement is listed Chapter 22. Chapter 23.2 concludes the report.

Market Analysis

This chapter will cover the market analysis performed that shaped the ESRA project. The market analysis starts with explaining a roadmap of the project in Section 1.1. After this in Section 1.2 an analysis is performed on the current competing aircraft. With this budgeting for airborne science mission is done in Section 1.3. In Section 1.4 different types of stratospheric scientific missions are discussed. At last, Section 1.5 discusses how the aircraft lifetime was approximated using the market analysis.

1.1. Roadmap to ESRA

Before delving into the role of ESRA in the market, the context in which the ESRA design bureau operates and the source of funding for aircraft design need to be understood. The European Commission (EC) collaborates with scientists to identify areas where research capability is lacking. In response, funding for a call that aims to develop a technology to address these scientific gaps is provided. In 2023 the EC has allocated 905 million euros to *LIFE Climate Change Mitigation and Adaptation*,¹ a program aimed at developing and implementing ways to respond to climate challenges. Within these programs, the EC issues call for scientific research solutions. Previously, calls for research in ESRA's field of expertise have been issued, such as the 2022 grant for *Improved knowledge in cloud-aerosol interaction*,² directed at integrating the latest advancements in science and observation methods, including airborne remote sensing, to better understand complex cloud-aerosol interactions. Based on this information, it is likely that the development, funding, and market expansion of the ESRA program will follow the roadmap outlined in Figure 1.1.

A program sponsored by the EC was the European Facility for Airborne Research in Environmental and Geoscience (EUFAR).³ In 2011 EUFAR produced a Whitebook [76] titled *Stratospheric aircraft in Europe* where scientists discussed the future scientific needs for stratospheric aircraft in Europe, presenting options such as the M-55 Geophysica, ER-2, and WB-57 for the short and midterm time frames. Scientists also expressed their interest in developing a new European carrier, which should enter service 5 to 10 years after a funding decision, and is required to

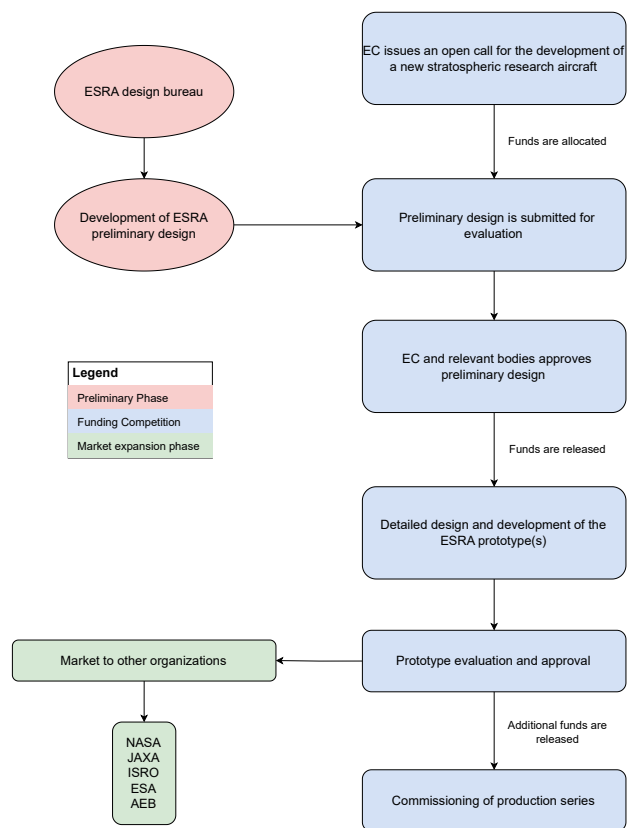


Figure 1.1: Diagram for the ESRA program.

¹URL: <https://climate.ec.europa.eu/eu-action/funding-climate-action/life-climate-change-mitigation-and-adaptation> cited on 08/06/2023

²URL: <https://rb.gy/c39gx> cited on 08/06/2023

³URL: <https://cordis.europa.eu/project/id/227159/reporting>

satisfy the scientists' requirements to increase observational options for remote sensing instrumentation. This interest could potentially translate into a call from the EC for new proposals, which the ESRA design bureau would respond to. The above argument provides evidence that the DSE exercise being conducted is realistic.

The ESRA design bureau will be selling the aircraft to space agencies and research facilities that will be renting it out to individual scientists for a research campaign. This needs to be taken into account when designing the aircraft. In the end, to convince a space agency to buy the research aircraft, two documents need to be prepared: one with the technical characteristics and performance of the aircraft, the second a costing plan detailing how much a space agency needs to charge a user per hour and per campaign.

1.2. Competing aircraft

The current active fleet of aircraft that can operate in the stratosphere consists of four aircraft: the ER-2, M-55 Geophysics, WB-57, and the RQ-4 (Global Hawk). For each of these aircraft, mass and mission profiles will be quantified by a market analysis.

1.2.1. Mass

Mass budgets and breakdowns on the three manned aircraft can be found in Table 1.1 and Table 1.2. A non-civil version of the U-2 was also considered for comparison.

Table 1.1: Mass budgets of existing aircraft stratospheric aircraft fleet data originates from [36]

Breakdown/Aircraft	WB-57	M-55	ER-2	U-2S
OEW [kg]	18143.7	14000	7257.5	7257.5
MTOW [kg]	32658.7	21553	18145	18143
Payload [kg]	4400 available 680 used for missions	2553 (2000)	1156	2268
Fuel [kg]	10115	5000	8617.5	8617.5
Engine Mass [kg]	2 x 1978	2 x 2640	1500	1500

Table 1.2: Mass fraction of different components with respect to the max takeoff weight of the aircraft (Table 1.1)

A/C Breakdown	WB-57	M-55	ER-2	U-2S
OEW (%)	55	65	40	40
Payload (%)	13 available 2 used for missions	11.8	6.4	12.5
Fuel (%)	30.9	23	47.5	47.5
Engine Mass (%)	12	24.5	8.3	8.3

1.2.2. Aircraft characteristics

ER-2

One of the most frequently used aircraft for stratospheric research is the ER-2, a civilianized version of the U-2. The different costs regarding production and operation can be assumed to be similar. As for its operation, the recurring cost per flying hour was reported to be \$ 35706 on average [58]. This includes maintenance and logistics but excludes acquisition and certification costs. As the development and production cost of this kind of military aircraft is classified, only educated guesses can be made with regard to these costs.

One more thing of note when considering the U-2 and its derivatives is its destruction rate per million flight hours, which was reported to be 22.81. At first sight, this might not seem like a lot, but it is on par with some of the military drones for which extra cost is calculated for this matter. Normally, for piloted aircraft, one would expect this number to be close to zero. In practical terms, this equates to a 0.01% chance of an aircraft being crashed beyond repair on every sortie. The magnitude of this number could be explained by the challenging operation of this aircraft, especially during landing as the aircraft has only two landing gears and performs a bicycle landing which requires a spotter car to follow the aircraft on the runway.

RQ-4

NASA operates two RQ-4A block 10 "Global Hawks". Examples of its operational deployment are the ATTREX mission⁴ and the SHOUT program.⁵ A cost study of the SHOUT program reports an operational cost of \$5,491.68 per flight hour. However, this cost is derived through an assumption

⁴URL <https://espo.nasa.gov/attrex>[cited 08/05/2023]

⁵URL <https://airbornescience.nasa.gov/category/Mission/SHOUT>][cited 08/05/2023]

Table 1.3: Percentage of different research campaigns that are employed for science days. Data is based on NASA's flight calendar for WB-57 and ER-2.

Aircraft	Mission Name	Duration	Science days	Percentage science days
ER-2	ALOFT	57	30	52.6
ER-2	DCOTSS	64	35	54.7
ER-2	IMPACTS	84	52	61.9
WB-57	ACCLIP	89	43	48.3
WB-57	SABRE-I&II	80	36	45
RQ-4A	ATTREX	390 flight hours over 3 years	N/A	N/A

that NASA Airborne Science Program base funding and in-kind contribution from the Space Act Agreement between NASA and Northrup Grumman Corporation are present [45]. The air force reported a recurring cost of \$18,677.71 per flight hour [58]. Moreover, NASA loaned these early production vehicles from Northrop Grumman,⁶ thus, development, certification, and production cost are not included. These can however be modeled when looking at the acquisition cost of the craft, which was reported to be \$239.44 million apiece [79]. Nonetheless, the competitive edge achieved by funding and relations of NASA cannot be neglected as the same scientific audience is targeted in the ESRA project.

Currently, the RQ-4s are not available for booking and one has been retired.⁷ No official statement has been given, but the RQ-4s currently appear to be inoperable for research purposes. Thus, for future (private) operations this operating cost might be higher. Reports from inside the Airforce state that an operating cost of \$18,708.26 [2023USD] per flight hour of the RQ-4 was reported by the United State Air Force in 2014 [23]. This operating cost might be more representative of potential competition.

WB-57

The WB-57 is a civilian derivative of the B-57 bomber. It has the unique benefit that it can carry a pilot and a passenger, which makes it especially popular for scientific missions. In addition to this, it is significantly more efficient in operation, with more flight hours per campaign than the ER-2. The cost per flight hour is slightly higher than for the ER-2. A disadvantage is that the WB-57 has a service ceiling of 60 000 ft compared to 80 000 ft of the ER-2.

1.2.3. Mission Distribution

The number of science days for each mission was based on the NASA flight calendars, this data is reported Table 1.3. Unfortunately, no detailed data for the ATTREX mission was freely available.

1.3. Budgeting for an Airborne Science Mission

The cost of an airborne science mission can be split up into two parts. The 'user fee', which includes all usage-based costs: personnel, fuel, and aircraft operational costs. The rest of the total cost is typically attributed to general deployment costs, overtime, personnel augmentation costs, and aircraft support costs that are classified as 'additional costs'. These costs are given in Table 1.4 for both the ER-2 and the WB-57.

Table 1.4: User fee and additional cost for the ER-2 and WB-57 in 2023US\$ **Table 1.5:** Cost breakdown for DSCOTTS, WDTS and ACCLIP missions in 2023US\$

Aircraft	User Fee [\$/hour]	Additional Costs [\$/week]	Mission	Aircraft	Duration	Hours Flown	Cost [\$]
ER-2	13,520.42	80,000	DCOTTS ⁸	ER-2	2 years	102.5	700,000 for flight hours 960,000 for integration and testing 1,660,000 total
WB-57	12,844.40	80,000	WDTS ⁹	ER-2	59 days	72.6	255,000 total breakdown unknown
M-55	11,577.89	Unknown	ACCLIP ¹⁰	WB-57	59 days	18.9	170,000 for flight hours integration and testing unknown

⁶URL <https://spaceref.com/press-release/nasa-dryden-receives-two-early-global-hawk-aircraft/>[cited 08/05/2023]

⁷URL https://airbornescience.nasa.gov/aircraft/Global_Hawk_-_AFRC[cited 08/05/2023]

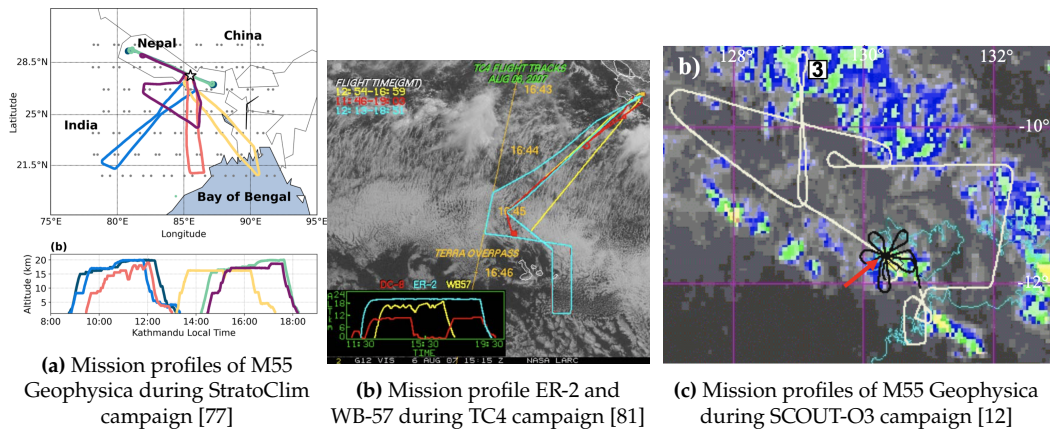


Figure 1.2: Example of mission profiles

Some examples of cost estimations of actual missions can be found in Table 1.5

1.4. Scientific missions

In order to understand the capability that a high-altitude research aircraft should have, the scientific missions that the current operating fleet has conducted were analyzed. A comprehensive study of how the missions influence the aircraft characteristics that are of value to research were cataloged. This is done to best design the chosen mission profile.

Below is a list of missions and certain characteristics that were beneficial to the particular research missions.

SCOUT-O3: This mission uses the M-55 to investigate the diurnal weather system 'Hector'. Deployment speed is of importance due to the short-lived weather system. Some weather systems decay within 40 minutes. Specific flight profiles are also required. [12].

GRIP experiment: This mission uses the Global Hawk (GH) and WB-57 to investigate hurricanes. The long endurance and range of the GH bring significant advantages to scientific research. [10].

2017 solar astronomy: This mission uses two WB-57s to observe the solar eclipse in 2017. High mobility of aircraft allows more observation time of eclipse as well as flying in a formation beneficial for the research. Imaging equipment is in the nose cone, which enhances tracking capabilities and is controlled by separate operators in flight. [14]

1980 Mount St. Helens eruption plume: The NASA U-2 was used to fly through the volcanic eruption plume to obtain aerosol and gas measurements. The plume travels at a zonal speed of approximately 25m/s. The U-2 plane also intercepted the plume 4 days after the initial eruption [20].

Figure 1.2a and Figure 1.2b are examples of altitude flight profiles flown during the TC4 and StratoClim campaign. A specific flight profile as seen from a top view is also shown in Figure 1.2c. Different missions will have different flight profiles tailored to the specific scientific objective. These would serve as a reference to generate a mission profile as input to the design of the aircraft.

1.5. Aircraft Lifetime

In order to estimate the cost of the aircraft, its operational life should be taken into account. Market research has been conducted to find typical campaign profiles which are used to estimate the aircraft's lifetime activities. During a campaign, the main activities are ferry flights, payload integration, maintenance, flight tests, and research flights. The time required for these activities makes up the campaign duration, the time values used are based on existing missions and scaled down due to the comparably smaller size of ESRA. Table 1.6 summarizes the duration of the individual activities which makes up a standardized campaign and is used to estimate ESRA's operational lifetime. In addition to the standard activities, it has been noted that a significant contributor to low flight hours of

stratospheric aircraft is payload malfunction and subsequent troubleshooting. This is not something that can be actively prevented by the ESRA design team but has been considered in operational profiles. Since this additional payload integration time is highly unpredictable, the number of days between 0 and 10 is randomly generated and added to each mission.

In an estimation tool, the standard campaign duration described in Table 1.6 is repeated until an assumed service lifetime of 30 years is reached. The tool also incorporates the different types of maintenance which is performed once a certain amount of flight hours is accumulated. These maintenance checks and their estimated time required are presented in Table 1.7. Taking this maintenance into account results in approximately 500 flight hours per year over the entire lifespan of ESRA, which is significantly higher than current stratospheric aircraft and will contribute to lowering ESRA's operating cost.

Table 1.6: Standard campaign

Activity	Duration
Ferry flight	2 days
Payload integration	4 days
Maintenance	1.5 days
Flight tests	14 hours
Research flight	45 hours
Additional payload integration	0-10 days
Total days	46-56 days

Table 1.7: Types of maintenance over aircraft lifespan

Type	Accumulated flight hours	Required time [man hours]
A	80-90	10-20
B	500-600	300-500
C	6000	10000-30000
D	18000	50000

A standard campaign for the ESRA aircraft is composed of 2 days of payload integration, followed by two or three test flights totaling 14 hours of troubleshooting for the scientific instruments. The plane then either commences its mission or has to be ferried over to its destination. During the ferrying flight, the plane cannot be airborne for more than 8 hours at a time due to regulations. Once the plane has arrived at its destination there are a set number of flight hours that the scientists seek to collect data. On average the plane flies for 6 hours a day for 8 days, these are referred to as flying days. According to historical data or schedules from previous missions, there needs to be approximately four times the amount of scheduled flying days that actual flying days need to be scheduled to account for weather delays, instrument failures, and other common delays associated with experimental research programs. Finally, once the science objectives have been reached, the airplane is flown back to a destination where payload de-integration takes place.

⁸URL <https://dcotss.org/index.html>[cited on 24/05/23]

⁹URL https://science.gsfc.nasa.gov/sci/content/uploadFiles/highlight_files/ASP2021_AnnualReport_0.pdf[cited on 24/05/23]

¹⁰URL https://science.gsfc.nasa.gov/sci/content/uploadFiles/highlight_files/ASP2021_AnnualReport_0.pdf[cited on 24/05/23]

Functional Analysis

The functional analysis is a detailed view of the overall mission which answers the question: what does the product need to do to accomplish the mission? The functional flow diagram (Diagram 2.1) sequentially orders the functions the product must perform. The functional breakdown sequence (Diagram 2.2) takes each function of the functional flow diagram and orders them in the form of a hierarchical tree while going into more depth. These give a visual overview that highlights the functions and their sequential interdependencies. In the previous baseline report, the functional analysis was done prior to the selection of the final design configuration and hence was not design-specific. This functional analysis keeps the same overall structure while tweaking the functions to be more specific to a fixed-wing jet aircraft, especially for the end-of-life section. Additionally, the layout of the functional flow diagram (FFD) has been altered for a more clear view of the analysis.

2.1. Functional Flow Diagram (FFD) - Diagram 2.1

The FFD is divided into seven main mission sections: Plan mission, initialize mission, go to the research area, science, return to base, finalize mission, and end of life. Each main part is numbered from 1 to 7 which corresponds to the first index for each function inside each part.

These main functions are placed in purple blocks as explained in the legend (figure 2.1). From there, the more specific lower-level functions follow to complete the sequence. The lower-level functions fall into the category of their respective higher-level block. This is shown by color (figure 2.1) and by the number index. The deeper levels have a longer index number which shows traceability and connects them to the higher-level functions. A function with three digits X.X.X is a level 3 function and a two-digit X.X is a level 2.

For example, at the beginning of the flow diagram on the top left, the "produce mission plan" block is a level two function with index 1.1. The block then expands into the three blue blocks: "Check research objective satisfaction" - "Check weather" - "Make flight plan" which are all numbered 1.2.X to show they are a sub-function of block 1.2. For a more clear view of the hierarchy, the FBS should be used.

To incorporate the nonlinearity of the flow, diamond blocks are used for decision junctions where the sequence splits up based on circumstance. Special functions (orange bubbles) relate to necessary functions for the missions that do not affect the design but are more of an organizational nature. They are placed for completeness' sake and hence do not fit in the hierarchy of the FBS.

2.2. Function Breakdown Structure (FBS) - Diagram 2.2

The FBS incorporates every single block from the FFD to highlight the different functional levels. The coloring of the blocks is also the same as the FFD apart from the fourth level. The analysis is then built upon by adding a fourth level which corresponds to the bullet point text in the FBS and the green blocks in the FFD. Using the more in-depth FBS allows for a more precise and detailed approach for the next phases of the preliminary design.

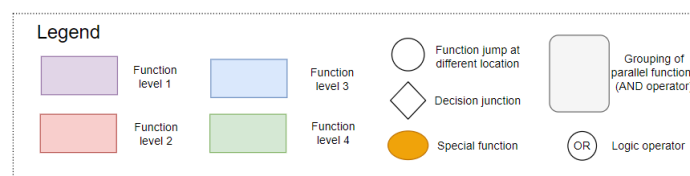
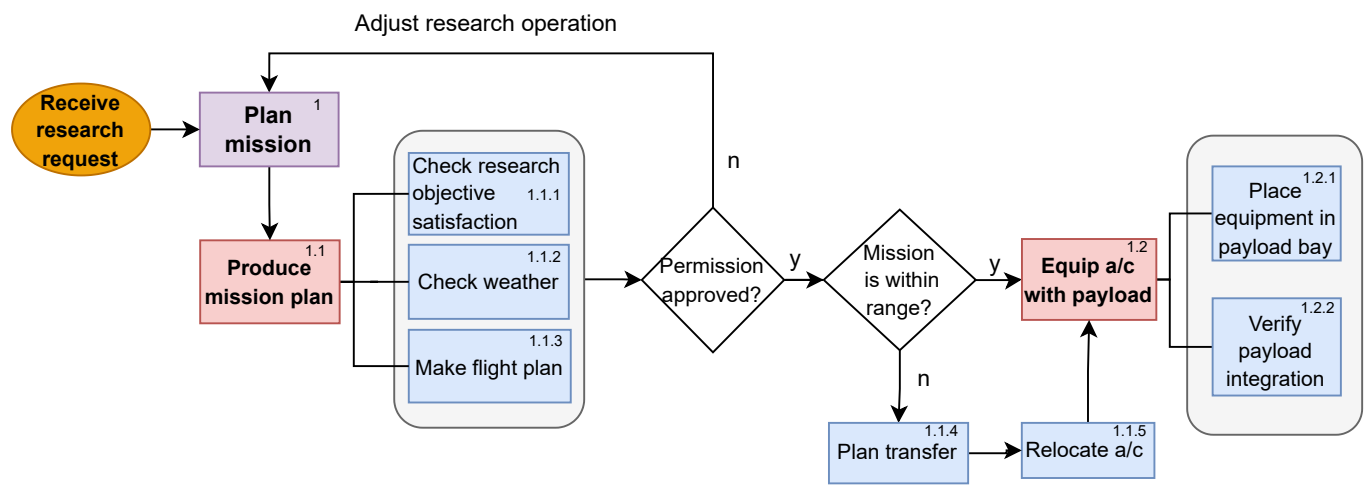


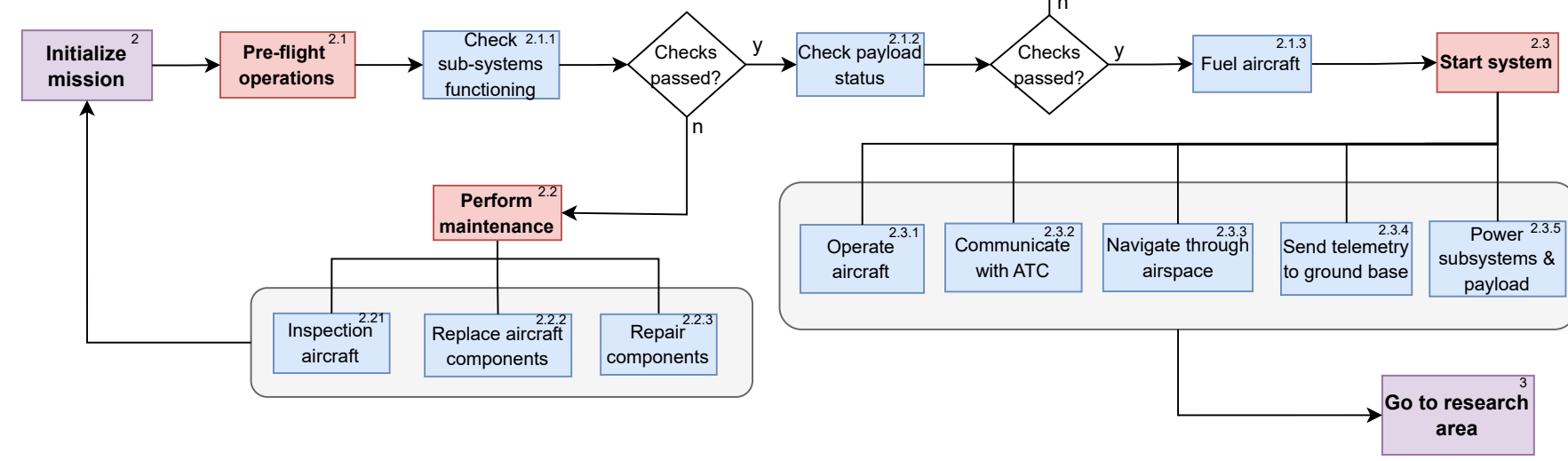
Figure 2.1: Legend of the functional flow diagram

Diagram 2.1: Functional flow diagram of the stratospheric research aircraft

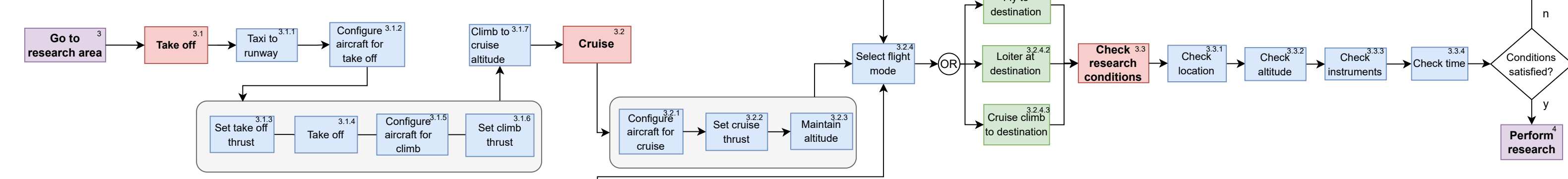
1: PLAN MISSION



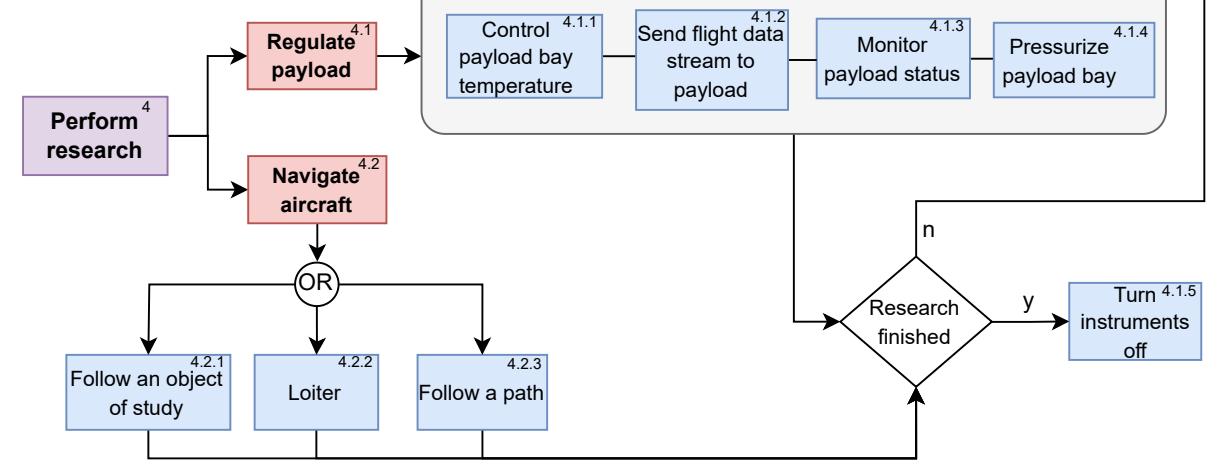
2: INITIALIZE MISSION



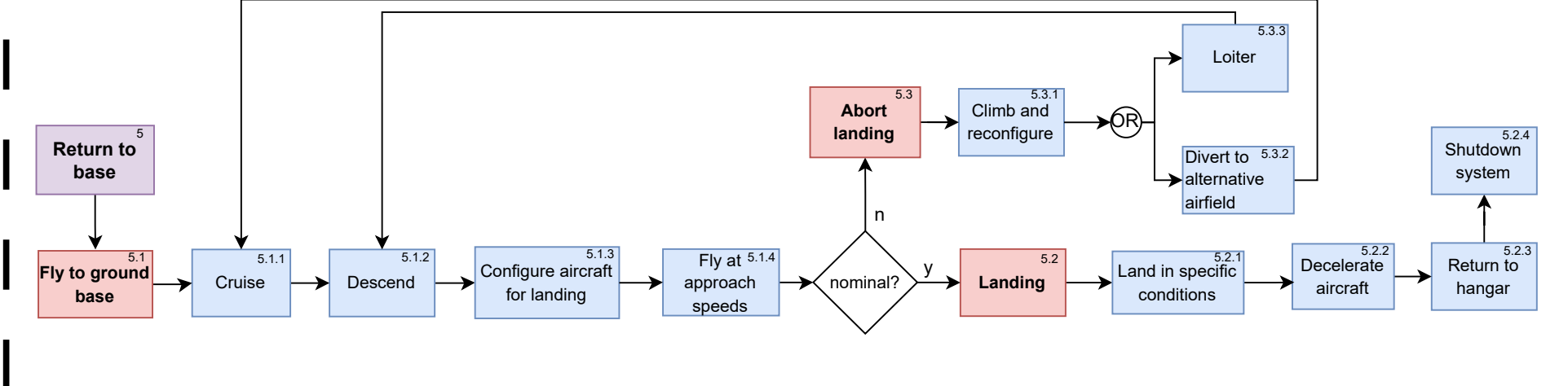
3: GO TO RESEARCH AREA



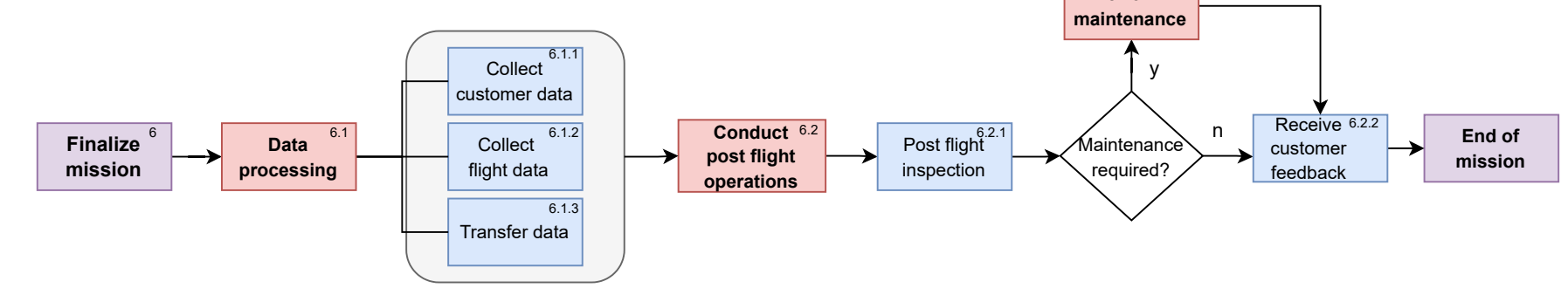
4: SCIENCE



5: RETURN TO BASE



6: FINALIZE MISSION



7: END OF LIFE

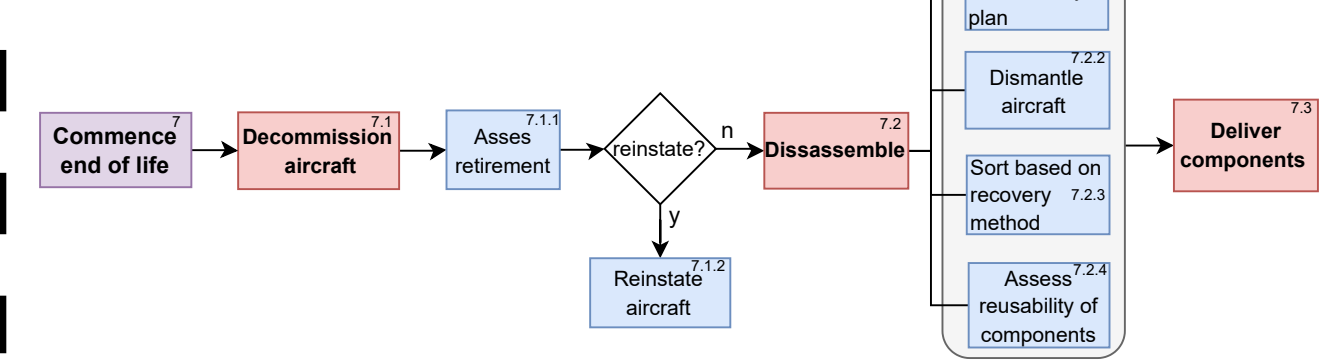
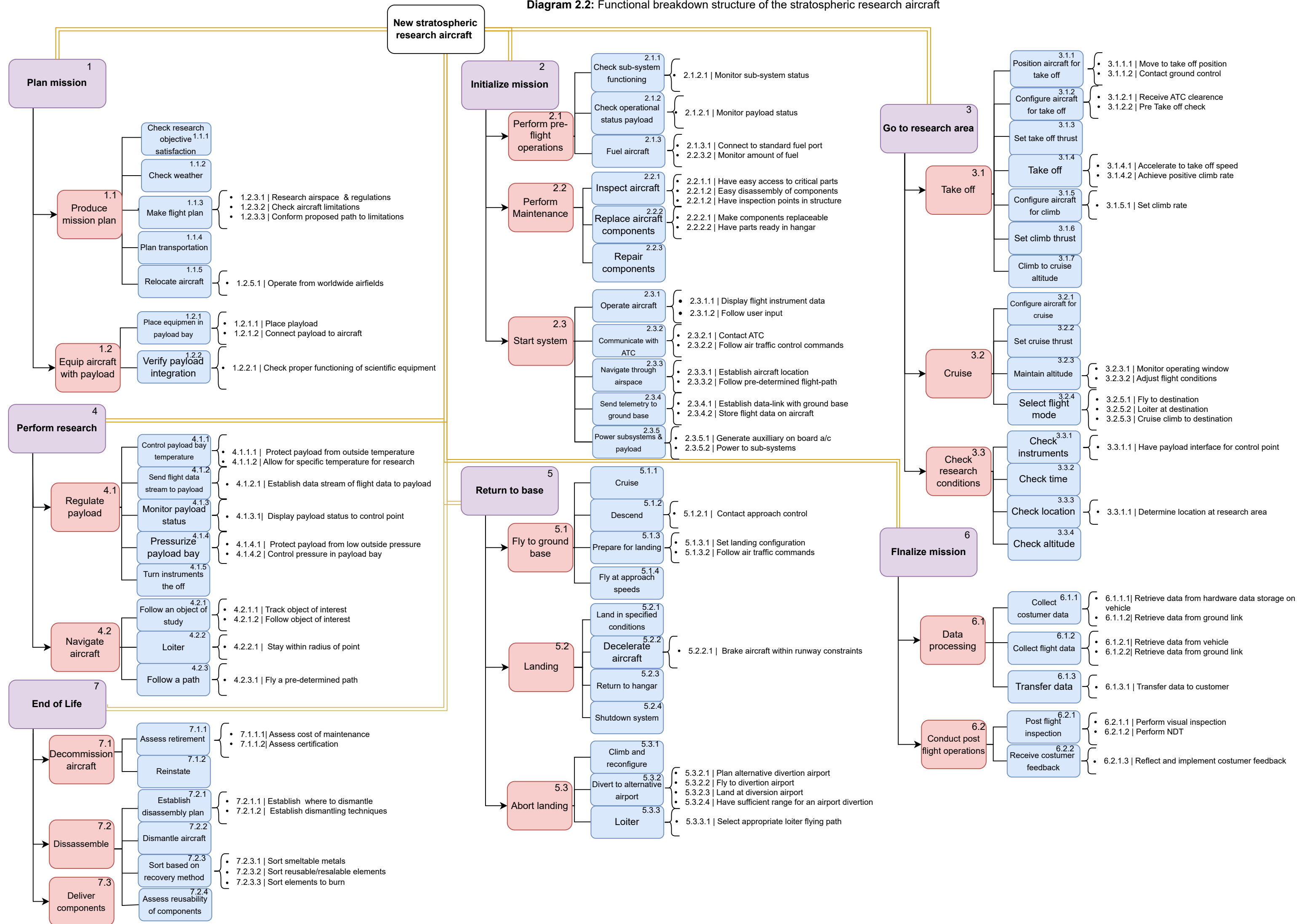


Diagram 2.2: Functional breakdown structure of the stratospheric research aircraft



Requirements

This chapter covers the initial requirement analysis performed for the ESRA project. The requirement analysis is a crucial part of system engineering as it ensures that the stakeholder needs are clearly translated into technical requirements used to constrain the design space. This chapter will cover the generation of the stakeholder requirements for the ESRA project.

3.1. Stakeholder requirements

Aircraft design projects are always guided by requirements, which are in turn set by stakeholders, as these are the entities affected by the product. Some stakeholders have already been discussed in Chapter 1 and are given again below, along with some new stakeholders.

Key Stakeholders

- **The scientists**, commissioning and performing stratospheric research. The scientists will influence payload integration methods, cost requirements due to their limited research budget, and most importantly, the mission profile which drives the aircraft design.
- **The aircraft operators**, who will be flying and maintaining the aircraft. They will determine many technical requirements.

Other Stakeholders

- **Launch providers**, as they need to observe rockets and the rocket plumes during and after launch.
- **Manufacturing parties**, that will have to set constraints on parts production.
- **Airports**, from which the aircraft will operate and be maintained/serviced.
- **Regulators**, who will provide guidelines from which requirements are generated in order to ensure safe operations.
- **The general public**, as the findings of the scientific research, could contribute to the reduction of excursions in global temperature. Furthermore, aircraft operations must have a limited amount and severity of disturbance for the public.

It is important to distinguish between key stakeholders and non-key stakeholders due to time and resource constraints. The key stakeholder's needs and requirements are given priority since those are the ones that are going to impact the project the most. From the stakeholder needs, the stakeholder requirements can be then formulated. Firstly, a short description of the needs of the key stakeholders is given.

The first key stakeholders are the scientists. Currently, stratospheric research is performed by either balloons or old military airplanes such as the WB-57¹ and the ER-2.² Where missions that require significant range and specific positioning are mostly performed by the aforementioned airplanes. The current fleet of aircraft is expected to retire by 2030, with the airframes already having exceeded their expected lifetimes. Stratospheric research, however, is only expected to increase in this time frame, thereby raising the need for a new stratospheric research platform. These aircraft usually perform research missions in the stratosphere, with altitudes ranging from 15 to 20 km. External expert Wake Smith, who has performed design exercises concerning stratospheric aerosol injection aircraft with

¹URL https://airbornescience.nasa.gov/aircraft/WB-57_-_JSC[cited 11/05/2023]

²URL https://airbornescience.nasa.gov/aircraft/ER-2_-_AFRC[cited 11/05/2023]

similar characteristics as required for ESRA [8], suggests that expanding the altitude capabilities would enhance the value of such research platforms. Therefore, a minimum height of 20.5 km was identified as a stakeholder requirement. As discussed in Chapter 1, scientific research budgets are limited, and often a large portion is spent on performing a stratospheric research campaign, therefore there is a need for the researchers to have a lower or equal price tag compared to the current platforms. Furthermore, the current platforms have payload capabilities ranging between 600-1000 kg. According to external expert Wake Smith, this current payload capability is not a key necessity for scientific missions and 100 kg would also suffice according to his surveys. Sometimes scientific experiments are at remote locations, where no nearby airports are present. Therefore, another need of the platform is to be able to travel to a destination of interest for experiments located 3000km from the base of the scientific mission. When doing experiments on a station, the scientists need to loiter at the research area for a varying amount of time, according to Wake Smith a minimal on-station time would be approximately 1 hour.

The second key stakeholders are the aircraft operators. This group of people will directly be involved in operating and maintaining the aircraft. These operators want an aircraft that is certified for civil operations globally, which falls in line with the need of the regulations stakeholders. The operators of the aircraft also need a reliable and maintainable aircraft to ensure smooth operations. As operations are expected to be global, there is also a need to have the aircraft travel between destinations and be operable from remote airports. Furthermore, sustainability is becoming an important aspect of any operation, especially aviation, the operator also is in need of a platform that is sustainable and future-proof in terms of upcoming regulation.

From the described key stakeholder needs, stakeholder requirements have been generated and are listed below.

- ESRA-STAKE-1: The aircraft shall be able to reach the lower layers of the stratosphere (20.5 km)
- ESRA-STAKE-2: The aircraft shall enter service by 2030.
- ESRA-STAKE-3: The aircraft shall be sustainable.
- ESRA-STAKE-4: The aircraft shall be certified for civil operations globally.
- ESRA-STAKE-5: The operating price of the aircraft shall be lower or equal to the current operating fleet.
- ESRA-STAKE-6: The aircraft shall be able to perform a 1-hour research operation at 20.5 km within a 3000 km radius.
- ESRA-STAKE-7: The aircraft shall be able to have scientific payload capabilities of 100 kg.
- ESRA-STAKE-8: The aircraft shall be operable from varying airports around the world
- ESRA-STAKE-9: The aircraft shall be able to fulfill scientific research mission requirements.

From the stakeholder requirements, the system-level requirements are given. Subsequently, a set of preliminary sub-system requirements is also generated. The extensive list of requirements is found at the end of the report in section 22 where the compliance to the requirements are discussed.

Sub-system Interface

4.1. N2

To effectively design a complete system that adheres to all the requirements, the interdependencies between sub-systems should first be properly understood and mapped out. For this purpose, an N2 chart was made as a visual representation of which subsystem impacts other subsystems and in what way. This chart can be seen in Figure 4.1. This overview embodies the way systems engineering is done and served as a basis to coordinate the systems engineering.

Using the N2 chart, a roadmap can be created from which the design sequence can be established. Iterations also become more evident and efficient as the inputs that will change are known in advance and preparations can be made. This enables others to keep working on subsystems where no significant impact will be felt by certain changes. By keeping track of all changes and managing the time allocation well, more design iterations can be made, and as a result the end design can be better optimized.

Aerodynamics	Wing planform, C_L, C_D, drag bucket	C_D, V_cruise	Aerodynamic loads, dynamic pressure, natural frequencies	Payload location, fairing		Wing and tail location, control derivatives	
V_cruise, V_stall, Climb rate, Turn rate, required C_L, W_F	Flight performance	Thrust required, cruise altitude	Maneuver loads, Gust load, W_F	Maximum payload weight		Control surface size, dynamic stability coefficients	Performance parameters
Engine size, thrust	Thrust, SFC, number of engines, engine mass	Propulsion	Engine mass, integration options, vibrational loads		Power available	Engine status	Engine status
CG location, wing stiffness, W_OE, engine location	W_OE, CG location	Mass budget	Structures	Structural interface		CG location	
Payload dimension, payload location, W_P	Mission profile		W_P	Payload	Power required	weight and location of payload	Payload status
		Startup power	Battery mass, battery location	Electrical power, power interface	Power	Electric supply	Electric supply, power status
	Pitch, roll, yaw rate, controller gain		Control surface loading			Control	
				Flight Data		Flight Data	Avionics

Figure 4.1: N2 chart of sub-systems

Configuration selection

5.1. General Design Challenges

The stratosphere is a very challenging environment, primarily due to the very low density, which at 20.5 km is only 6.6% of the sea level density.

A crucial aerodynamic challenge lies in finding the optimal combination of wing surface area (S), lift coefficient (C_L), and velocity (V) to enable efficient cruising at altitude. This requires a careful trade-off, as large wings increase weight and drag, a large C_L increases the induced drag, and flying at high V may induce transonic effects. Increasing the aspect ratio A is a good way to improve performance. However, high aspect ratio wings are more prone to aeroelastic effects like flutter, have reduced handling qualities, and are heavier.

A second, perhaps more important, aerodynamic challenge is the so-called “coffin corner”. This is a region of the flight envelope, where the margin between stall speed and critical Mach number is very small. In this situation, any increase in speed or decrease in altitude can cause the aircraft to exceed its critical Mach number and enter an unrecoverable stall, resulting in a loss of control and potentially catastrophic consequences. A way to counter this is to ensure the stall speed is lower, either by decreasing the wing loading or increasing $C_{L_{max}}$. However, the achievable $C_{L_{max}}$ of the airfoil decreases with altitude due to compressibility effects.

The challenges posed by the low density of high altitudes also extend to propulsion. As altitude increases, the engine’s air intake capacity diminishes, resulting in a significant decline in thrust. In consideration of time and cost constraints, the decision was made to utilize an off-the-shelf engine instead of investing in the development of a new one. This choice presents an additional hurdle in the design of the ESRA, requiring careful analysis of the performance of the selected engine and of its integration into the overall system.

5.2. Past work

During the baseline and midterm reports done by group 14 a number of different preliminary options were evaluated to complete the ESRA mission. In order to conduct scientific research at 20.5 km four distinct options were considered, namely: a fixed-wing manned airplane, a fixed-wing unmanned airplane, a propeller fixed-wing airplane, and a lighter-than-air airship. A preliminary design was conducted on each of these options to see which one best met the requirements and the gaps in the market identified. A trade-off was done on these preliminary designs, which resulted in the fixed-wing manned option being chosen. The reasons for it being chosen were its low cost, readiness, and good performance, complying with two of the most important requirements: ESRA-STAKE-2-SYS-12 and ESRA-STAKE-2-SYS-13. In the following sections, focus will be put on the configuration selection for the manned fixed wing aircraft.

5.3. Engine configuration

There are various configurations available for a jet aircraft, offering different advantages and disadvantages depending on the number and placement of engines. Due to the results obtained in our preliminary design, a maximum of two engines were considered to meet the required thrust. However, after a more thorough analysis, a configuration making use of more than two smaller engines might be beneficial. No conclusions could be made on the number of engines without a more in-depth analysis of the propulsion subsystem. This is because more engines do not necessarily come with a weight penalty. Therefore, this preliminary trade-off only dictates the location and integration of the engines, while the number of engines is kept as a design variable to consider in the detailed design in section 8.

An important driving design parameter is the bypass ratio of the engine, as it classifies different types of engines. High bypass relates to a highly efficient engine at the cost of a larger and heavier engine [21]. Various configurations pose limits to engine bypass ratio due to the integration methods. Fuselage-podded engines are bypass limited, as too large of an engine results in a large lateral moment arm. Fuselage-integrated engines can only be small, low bypasses to not ruin the aerodynamics of the fuselage. Wing integrated cannot be too large with high bypass due to structural limitations. Finally, wing-podded engines are limited only due to clearance, which allows for high bypass engines.

Therefore, the options taken into account are the following:

- Fuselage podded engine(s) - Low to medium bypass
- Fuselage integrated engine(s) - Low bypass
- Wing integrated engine(s) - Low to medium bypass
- Wing podded engine(s) - High bypass

Initially, mixed configurations such as wing-podded engines in combination with fuselage-podded engine configurations were considered. After analyzing the impact of the added weight and higher absolute fuel consumption in combination with more complicated maintenance, these configurations were deemed to be not viable.

In order to identify the best possible engine layout, a trade-off has been performed on the propulsion system. Five different criteria are identified and given a weight between one and five:

- **Efficiency** will be the main factor that influences the direct operating cost of the mission. A highly efficient engine consumes less fuel, resulting in lower costs per flight hour. Therefore, this criterion was assigned the highest weight in the trade-off analysis.
- **Accessibility** will largely dictate the level of maintainability of the engine for the ESRA aircraft. An integrated engine poses challenges in terms of access and extraction for inspections and maintenance. Since the ESRA aircraft is expected to undergo extended maintenance periods, ensuring engine accessibility is a crucial aspect of the design, and was assigned a weight of four.
- **Weight** is an important parameter in the cost estimations and thus needs to be minimized. Due to the impact of weight on cost, it was decided to award this criterion a weight of three.
- **Cost** for procuring and integrating the engine must be considered, but since the group's goal is to minimize direct operational costs, this criterion has been assigned a weight of two.
- **Aerodynamics** of an engine can be advantageous, however, performance is not the primary focus of this project. As a result, it has been assigned the lowest score in the trade-off analysis.

The tradeoff is illustrated in Table 5.1, revealing that the fuselage-podded single engine achieved the highest score. Accordingly, our configuration will feature a single jet engine podded on top of the fuselage. This choice of engine configuration will subsequently impact the tradeoff considerations for wing and tail configuration.

Table 5.1: Trade-Off Matrix for engine layout selection

Criteria Option	Efficiency	Accessibility	Weight	Cost	Drag	Total Score
Weights	5	3	4	2	3	-
Fuselage podded engine(s)	4: Higher fuel consumption for the same thrust. Limited bypass. [Y]	3: Mounting height of the engines limits accessibility, removal possible. [Y]	4: Fuselage reinforcement increases the weight, low bypass engines are lighter. [B]	4: Common mounting method on fuselage [B]	2: Mounting on fuselage causes interference, increasing drag [R]	6.94
Fuselage integrated engine(s)	2: Higher fuel consumption for the same thrust, low bypass. [R]	1: Integrated engines are hard to get to, making maintenance hard, no removal [R]	4: Structural reinforcement needed on the fuselage, no compensation for moment arm [B]	2: Complex airframe more extensive development [R]	5: Little to no disturbance to the airflow. [G]	5.65
Wing integrated engine(s)	3: Larger bypass possible, but limited by the wing. [Y]	2: Integrated engines limit accessibility, complicating maintenance, though better than fuselage integrated. [R]	3: No need for a podded engine's support structure, wings need to be reinforced. [Y]	3: Integration results in additional design & development cost of planform [Y]	4: Integration reduces drag Smaller intake [B]	6.00
Wing podded engine(s)	5: Low fuel consumption for the same thrust, large bypass possible. [B]	5: Easily accessible for on ground maintenance & easy removal [G]	3: Need additional support structure & high bypass heavier. [Y]	4: A most common method for mounting but hinders possible strut [B]	2: High bypass podded engine creates drag but less interference drag. [R]	7.18

The trade-off in Table 5.1, shows that two configurations are feasible for the design: fuselage podded engine(s) and wing podded engine(s). Both configurations are still under consideration due to their relatively small difference in scores. The wing-podded engine configuration achieved a higher score primarily because it offers the ability to mount high bypass engines. As an off-the-shelf engine has to be used that is compatible with the current design while also providing sufficient performance at altitude, the effect bypass of the engine has not yet been determined, and thus the advantage of the wing podded could dissipate when a low bypass engine is used.

The bypass of the turbofan has a few direct implications for the design and the weight of the aircraft. Higher bypass engines tend to be more fuel efficient than their respective low bypass equivalents, though this also means that a higher mass flow is needed to produce the same amount of thrust. At high altitudes, the air becomes increasingly thin, reducing air mass flow through the engine. This, in turn, increases the thrust lapse, and for a set thrust requirement at altitude, comparatively larger engines will have to be used, inducing an increase in weight. This will again require more fuel and add to the weight of the aircraft, increasing the thrust required at altitude. This iterative process will increase the total weight and size of the aircraft, eventually mitigating the added effect of better fuel efficiency, as the total fuel use will eventually become the same.

5.4. Wing configuration

With the two feasible engine configurations in mind, wing configuration options are generated and a trade-off formulated, keeping in mind both engine configurations.

A trade-off for the wing position can be made with the following criteria:

- **Weight** is a crucial factor for all systems as it significantly influences costs and must be minimized

accordingly. The wing’s structure contributes significantly to the overall structural weight, making any savings in this area highly meaningful. As a result, a weight of five was assigned to this criterion.

- **Operations** are also a large driver for cost as a configuration making payload integration or maintenance more difficult will cost time and thus money. This criterion was thus awarded a weight of four
- **Landing Gear integration** is heavily influenced by the wing position as a low wing for example enables easy integration of the main gear assembly into the wing providing a sufficiently wide track with short, relatively light, struts. A high wing however will force heavy fuselage integrated gear with a low track width or heavy and long wing integrated gear. Due to the potential impact on weight, though it is less important than wing the weight of the wing itself, this criterion was awarded a weight of three.
- **Ground clearance** will be achieved regardless of the choice of wing position as it is mandated for certification. That being said, a high wing will make the ground clearance requirements easier to fulfill as the wing is inherently higher off the ground thus making some wing droop allowable. For these reasons, a weight of two was chosen.
- **Roll stability** is considered as well because of the influence that the wing position, and specifically the interactions between the wing and fuselage, can have on roll stability. This criterion is treated similarly to the ground clearance as stability will be achieved regardless of configuration although some configurations will be easier to stabilize than others. This criterion was thus assigned a weight of one.

Table 5.2: Trade-Off Matrix for different wing layout

Criteria Option	Weight	Operations	Landing gear integration	Ground clear- ance	Roll stability	Total Score
Weights	5	4	3	2	1	-
Strutted high wing	5: Strut saves lots of weight[G]	3: Strut can get in the way[Y]	2: High wing makes LG integration difficult[R]	5: High wing[G]	5: High wing has better effective dihedral[G]	3.86
High wing	2: High wings require heavier structures[R]	5: Lots of space bellow the wing[G]	2: High wing makes LG integration difficult[R]	5: High wing[G]	5: High wing has better effective dihedral[G]	3.40
Mid wing	4: Wing structure combined with fuselage structure[B]	1: Payload integration difficult due to large wing structure[R]	4: LG can be integrated easily enough[B]	3: Ground clearance between the other options[Y]	4: Good effective dihedral[B]	3.06
Low wing	4: Wing structure combined with LG structure[B]	3: Worse for ground handling but has space for payload[Y]	5: Very easy and light LG integration[G]	1: Low wing[R]	3: Requires more dihedral[Y]	3.46

The trade-off shown in Table 5.2 shows that the most optimal wing configuration is the strutted high wing option. This choice will enable the use of high aspect ratio wings while minimizing their weight. Furthermore, this option will enable the easy use of wing-mounted payload bays as well as a fuselage-integrated bay. It must be said that this configuration will make landing gear integration difficult due to the height of the wing.



Figure 5.1: Three tail types potentially compatible with centrally mounted engines

5.5. Tail configuration

Aircraft empennage configurations vary depending on engine placement, wing positioning and many other factors. It has already been decided that ESRA would be equipped with a high strutted wing and engines podded on either the fuselage or the wings. As the number of engines is yet to be fixed, multiple design options must be considered and described. Indeed, a single fuselage podded engine would constrain the design in that no vertical surface could be placed behind the engine exhaust.

In case of an uneven number of engines, one will be constrained to the top of the fuselage as it cannot be integrated and must be on the longitudinal axis of the aircraft to avoid unbalanced lateral moments. An example of this configuration is given in Figure 5.1a where it can be seen that it is combined with a V-tail configuration.

The V-tail configuration is advantageous for a single fuselage podded configuration as it enables the engine to be mounted dorsally while minimizing the exhaust interference with the tail. Furthermore, the V-tail option enables a reduction in drag as it has only two surfaces. On the other hand, a V-tail does bring somewhat more complexity for control as the yaw and pitch controls are coupled and need to be mixed by a flight computer. Furthermore, the V-tail causes an increase in adverse roll characteristics and a decrease in dutch roll stability. It can also be said that the V-tail would function for purely wing mounted engines as well as two engines podded on the side of the fuselage although other more conventional tail options then become possible.

Other tail configurations compatible with a dorsally mounted engine would be an H-tail such as is shown in Figure 5.1b or even a boom mounted tail such as on the M-55 Geophysica in Figure 5.1c could be considered. These two options would however cause an increase in structural weight and a large increase in drag for the boom mounted tail due to the additional wetted area. These two options do simplify the control of the aircraft relative to the V-tail as the control axes are decoupled. Considering the extreme operating conditions of ESRA however, it can be said that weight savings would be more important than a simplification of the control system and thus the V-tail configuration would be selected in the case of centrally podded engine.

In the case of wing podded engines there are fewer constraints from the jet blast although it has been found that low horizontal surfaces such as the one on a conventional tail, shown in Figure 5.2b, would not be possible as they would be placed in the engine wake. Configurations considered for an aircraft with wing podded engines were the T-tail Figure 5.2a, the V-tail shown in Figure 5.1a and the cruciform tail shown in Figure 5.2c. The T-tail is advantageous in that it doesn't suffer from coupled control as the V-tail does. Furthermore, the horizontal surface acts as an endplate for the vertical surface thus increasing its effectiveness [82]. A T-tail does bring some structural complexity though as the vertical surface must be made strong enough to hold all loads generated by the horizontal surface and delay the onset of aeroelastic effects. A cruciform tail would also enable the horizontal surface

¹URL: <https://news.northropgrumman.com/news/releases/photo-release-northrop-grumman-built-nasa-global-hawk-soars> [cited 02/06/2023]

²URL: <https://www.kitplanes.com/h-tails-and-triple-tails/> [cited 02/06/2023]

³URL: <https://www.airliners.net/photo/Geophysica/Myasishchev-M-55-Geophysica/2149757> [cited 02/06/2023]



Figure 5.2: Three tail configurations compatible with wing-podded engines

to be outside of the jet blast. However, a cruciform tail would share disadvantages with the T-tail without reaping its benefits. Indeed, it must also be structurally stronger than a conventional tail but does not have performance gain due to the endplate effect. For these reasons, the cruciform tail was not considered further. The disadvantages of the V-tail explained above mean that, if there aren't any centrally podded engines, the T-tail would be selected.

In summary, ESRA will be fitted with a V-tail or a T-tail depending on the chosen engine configuration. If an engine is podded on top of the fuselage, a V-tail must be chosen but if the final decision does not outright disqualify the T-tail, this configuration will be chosen.

⁴URL: https://www.nasa.gov/centers/dryden/Features/F-104G_final_flight.html [cited 24/06/2023]

⁵URL: <https://www.nasa.gov/centers/armstrong/news/FactSheets/FS-046-DFRC.html> [cited 24/06/2023]

⁶URL: <https://mybusinessjet.com/buyers-guide/cessna-citation-latitude/> [cited 24/06/2023]

Payload design

Since ESRA will serve a general scientific research purpose, it will be undertaking a wide range of missions and hence will have drastically different payloads. As mentioned in Section 1.5, a significant amount of time during a scientific campaign is spent on integrating payload onto the aircraft. Whilst ESRA cannot ensure the functionality of the payload themselves, payload integration has been a main design objective, aiming to accommodate as much different equipment as possible, provide the payload with a suitable environment and minimize integration time. These objectives are understood to facilitate scientific research and contribute to the increased utilization and cost efficiency of aircraft.

The main payload area of ESRA is located along the bottom of the fuselage. The motivation for the location is due to the majority of nadir-looking equipment during missions that overfly atmospheric features. This area is made up of three standardized modular pallets that can be slotted into the aircraft on a rail from the aft of the fuselage. The bottom part of one of the pallets is flat and made with transparent material for imaging purposes. The volume of these pallets adds up to $2.53 m^3$ and is calculated by averaging the payload capabilities of existing aircraft and scientific equipment used in previous missions. Regarding payload environmental control, the WB-57 incorporates a pressurization system operating at 34.5kPag [56], while the ER-2's nose cone is equipped with temperature control set to -20°C at its maximum altitude [25]. It has been determined that utilizing the same values for the payload pallets is the most appropriate course of action. Figure 6.2 illustrates the standard pallets. ESRA's payload environment located in the fuselage and nose cone will have the option to be moderated according to these conditions. A volume of $0.027 m^3$ in the nose cone is available for cameras to allow a full frontal hemisphere view, this is shown in Figure 6.4.

A very common piece of equipment used in atmospheric research is a dropsonde that is used to map the vertical profile of atmospheric features. ERSA can be equipped with such a system, a simplified dropsonde launcher system has been modeled with reference to the launcher on the Global Hawk[85]. ESRA's dropsonde launcher integrated into one of the standard pallets is shown in Figure 6.1.

In addition to the payload areas within the fuselage, it is feasible to mount two wing pods underneath the wings, positioned near the strut. These pods are expected to be connected through a nacelle or a lofted geometry arrangement. It is important to note that the weather radar will not serve as a load-carrying member and is placed outboard for aerodynamic reasons and to provide bending moment relief. Each wing pod offers a weight and volume capacity of $0.03 m^3$. According to ESRA's market research, equipment mounted on the wings is usually sampling equipment and generally without environmental control, therefore, the wing pods will not be heated or pressurized. Dimensions

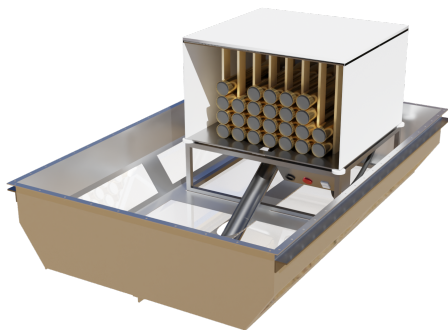


Figure 6.1: Dropsonde launcher system

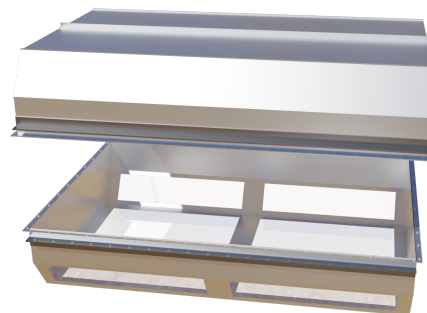


Figure 6.2: Standard pressurized payload pallet



Figure 6.3: Weather radar in ESRA wingpod

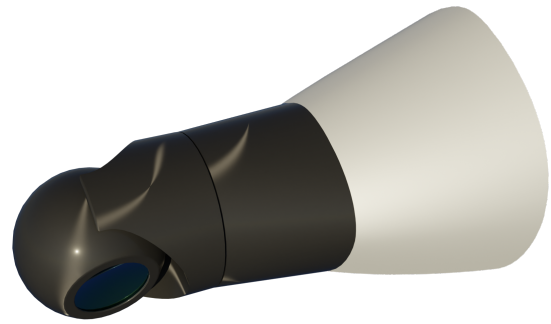


Figure 6.4: ESRA nose cone payload compartment



Figure 6.5: Payload bay

of the wing pods are sized according to existing scientific payload such as the 2D-S Stereo Probe¹ and Closed-path Laser Hygrometer². Since the nose cone is reserved for imaging equipment, a weather radar is placed in one of the wing pods as opposed to the conventional nose position. The wing pods are visualized in Figure 6.3.

To further support payload onboard, standard electrical power connections are available at each payload area, the options are 230 Vac at 50A, 115 Vac at 50A, 115 Vac at 100A, and 28Vdc, combined electrical power available for payload usage is 3 kW. Note that current and voltage values are obtained from ER-2 [25] and WB-57 [56], they can be modified in later design phases should scientists show a need for a different power supply. The entire payload bay is depicted in the Figure 6.5.

6.0.1. Fuselage design

The fuselage design was based on two inputs, namely the payload and pilot. The payload design mainly depicted the design of the aft and middle of the fuselage. Whereas the nose of the aircraft was designed around the cockpit.

Market analysis revealed that for scientific purposes it is very beneficial for the fuselage to have a flat base since it would ease scientific experiments providing ample space for cameras and sensors [25]. In line with the idea of payload modularity, first, the payload bay was designed. The bay consists of 3 trolleys designed to accommodate the scientific payload Figure 6.5.

Considering that a mission could extend to a maximum of 11 hours it was crucial to prioritize the

¹URL: <https://airbornescience.nasa.gov/instrument/2DS> [cited 16/06/2023]

²URL: <https://airbornescience.nasa.gov/instrument/CLH> [cited 16/06/2023]

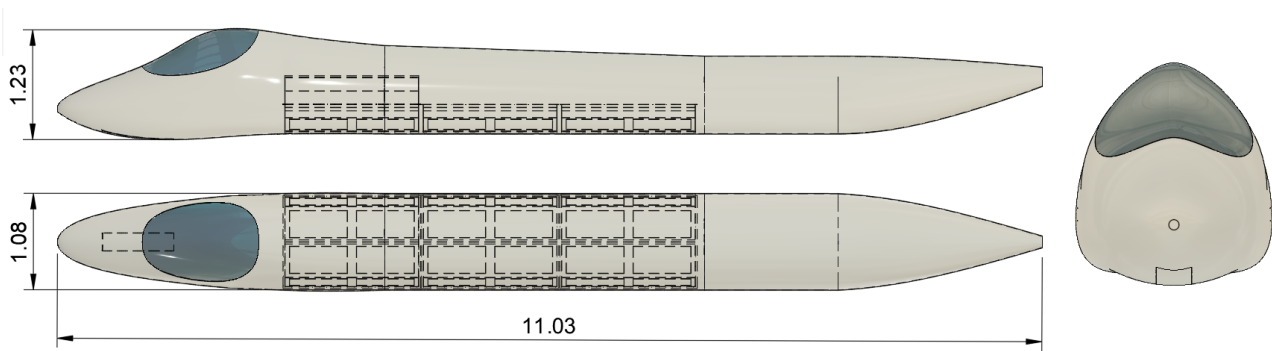


Figure 6.6: ESRA's fuselage 3-views



Figure 6.7: ESRA's offloading ramp for the payload pallets

pilot's comfort on board. For this, standard one-seater cockpit dimensions were utilized in the design process such as described by Torenbeek [82].

Taking into account the constraints that the payload and the cockpit introduce, the design of the fuselage can start. Sensitivity analysis has shown that a wetted area of the fuselage and an upsweep angle are crucial parameters for parasite drag. That is why the design was done trying to minimize these values.

After several iterations design converged to the one depicted in Figure 6.6. With wetted area equal to $32.5 [m^2]$ and upsweep angle approaching zero fuselage minimizes its contribution to the parasite drag while meeting established requirements. Note that the payload compartment is depicted with dashed lines in the middle of the fuselage on Figure 6.6. Moreover, the aft ramp, as depicted in Figure 6.7, facilitates the loading of pallets into the aircraft.

Methodology and Budgets

7.1. Design Methodology

This section presents the iterative procedure of the design. In Chapter 5 the basic configuration was selected based on several trade-offs. In Chapter 6 a detailed analysis of the payload was carried out. An initial flight profile was assumed, based on some considerations about maximizing the specific range. The airplane was determined to fly at $M = 0.65$ cruising at $h = 19.2\text{km}$ and to loiter at 20.5km at the same velocity. A diversion capability of 500 km was established at an altitude of 11 km to optimize the specific fuel consumption. The critical mission profile was determined to be: cruise for 3000km , loiter for one hour, cruise back for 3000km and divert for 500 km . Knowing the mission profile it is possible to establish a fuel budget for ESRA in Section 7.2, using statistical fuel fractions and Breguet formulas.

Based on this OEW the T/W - W/S diagram has been created based on the following constraints: stall speed at landing, stall speed in clean configuration, sizing for take-off, sizing for landing, sizing for cruise, sizing for climb rate, and sizing for climb gradient. The driving constraints turned out to be a stall at altitude and a cruise at altitude.

The key findings of the T/W - W/S diagram are the surface area of the wing, $S = 32[m]$, and the thrust required at altitude, $T_{alt} = 1725.8[N]$. Usually, the T/W-W/S yields a thrust requirement for take-off, T_{TO} , however, for ESRA this was not very useful information, since thrust lapse at service altitude is so high that this is no longer limiting. Hence why thrust loading at altitude was of much more interest since it enabled the selection of an engine that can perform up to par in all situations. This constrains the number of available engines drastically. More detailed analysis and justification are described in [64].

Once the rough OEW is known and the configuration is selected, the Class II weight estimation method proposed by Torenbeek was implemented to define a structural budget for ESRA Subsection 7.2.2. This weight estimation yields a different value for the OEW which usually differs significantly from the one obtained from a Class I estimation. This is why an iteration is needed using the OEW obtained from the Class II estimation instead of a statistical-based regression. This process continues until the estimations from both Class I and Class II converge to the same value.

The Class II weight estimation allows to perform initial sizing. This way, the drag budget can consequently be defined as described in Subsection 7.2.3. At this point, the design has to be reiterated again since the C_{d_0} obtained here differs from the one assumed in the Class I estimation and thus a different amount of fuel will be needed to fulfil the mission profile. In turn, this will lead to different structural requirements. Again, iterations are done until drag C_{d_0} converges to the same value.

Once an initial sizing was performed, the stability and controllability analysis was carried out, which yielded new dimensions for the horizontal and vertical tail. This means that the entire design has to be reiterated, to comply with new tail dimensions since it influences both structural and drag budgets. In practice, this iteration process included doing another Class II weight and drag estimation. The gear placement concludes the initial design. Here, controllability and stability considerations have to be made as well.

Following the previous process, the analysis of the take-off rotation constraint was performed, to verify that no further adjustments are needed for the horizontal tail. Finally, the overall analysis of the take-off, landing, turn, and climb performance was conducted. Flight profile optimization was carried out and full calculations of the fuel used were carried out to assess the margins to the fuel budget.

7.2. Fuel, Structural Mass and Drag Budgets

This section presents the fuel, mass, and drag budgets of the aircraft. These were determined from the sizing of the aircraft with respect to an initial flight profile with a set of assumptions that are shown in Table 7.2. Of these, the most relevant is that c_j is constant with altitude and that C_L is constant throughout the mission. Once the aircraft was sized to meet the requirements of this profile, detailed structural design was carried out and these assumptions about the flight profile were loosened. Then, an evaluation was carried out to determine the margins that should be included in the different budgets. Due to the tight margins inherent to flying in the stratosphere, a result of the low air density at these altitudes, it is essential that throughout the future design and production of the aircraft, these budgets are adhered to as this will ensure the proper operation of ESRA.

Table 7.2: Assumptions for Initial Profile

Parameter	value
Mach	0.65
A	19.5
e	0.7
C_{d_0}	0.022
$c_{j_{cruise}}$	1.85e-05
c_{alt}	1.95e-05
$C_{L_{cruise}}$	0.77

Table 7.1: Altitude effects on a specific range.

h [m]	C_L	C_{D_0}	c_j [g/kNs]	$\frac{1}{c_j} \frac{L}{D}$ [$sg \times 10^6$]
11000	0.205	0.017	17.4	6.57
15000	0.383	0.019	17.7	9.71
19500	0.720	0.022	18.5	11.59

7.2.1. Initial Profile Determination and Fuel Budget

ESRA-STAKE-6-SYS-36, ESRA-STAKE-1-SYS-1, ESRA-STAKE-6-SYS-2, and ESRA-STAKE-4-SYS-27 are the main requirements that determine the mission profile for ESRA. There are three fuel-intensive phases: the 6000 km cruise, the one-hour loiter, and the 500 km diversion. To calculate the fuel burnt at each of these stages, the Breguet range and endurance equations (7.1) (7.2) were used.

$$R = \frac{V}{g} \frac{L}{c_j} \ln \frac{W_s}{W_e} \quad (7.1)$$

$$E = \frac{1}{g} \frac{L}{c_j} \ln \frac{W_s}{W_e} \quad (7.2)$$

It was necessary to determine the altitude at which each of the fuel-intensive segments takes place. ESRA-STAKE-6-SYS-2 specifies that loitering for one hour must take place at 20.5 km. Concerning cruise, the approach taken was to find the altitude that maximized the specific range in equation (7.1), which amounts to an optimization for $\frac{V}{g} \frac{L}{c_j}$. In [64] it was found that loitering at $M = 0.65$ offered the best altitude margin to the service ceiling so it was decided, as a first assumption, that ESRA would also cruise at this velocity. This is comparable to the cruise speed of the ER-2 which holds a constant Mach number of 0.7 throughout its operation. Since the speed of sound is constant in the tropopause, where cruise would take place, the parameter to be optimized became $\frac{1}{c_j} \frac{L}{D}$.

As can be seen in Chapter 8 and Chapter 9, at lower altitudes both c_j and C_{D_0} are lower, however, the required C_L to maintain cruise is also significantly lower. Table 7.1 shows the characteristics of three altitudes that were considered for the initial sizing. It is clear that the negative effect of decreasing C_L is more severe than the positive effects of decreasing both C_{D_0} and c_j . Therefore, it was decided that the long-range cruise would take place at 19.5 km.

Table 7.3 shows the computed fuel mass for both the fuel-intensive and non-intensive phases of flight (take off, landing, climb, descent, and taxi). For the latter, these values were obtained from statistics [62]. The validity of these statistics is questionable, as they are compiled from airliners with significantly different operational domains. The design of aircraft is a highly iterative procedure and these values correspond to an iteration where the structural weight of the aircraft was already estimated and several subsystems had been sized. This means they are a good indication of the budget that should be respected to ensure the completion of the profile. Adding the fuel mass to the payload, crew, and structural mass results in an MTOW of 4446 kg.

Sensitivity Analysis

Table 7.4 shows the results of a sensitivity analysis considering the fuel weight and the Mach number, specific fuel consumption and parasite drag. The method used was standard regression coefficients (SRC), described in [64] and [73]. Values of β close in magnitude to 1 indicate that the fuel weight is most sensitive to that variable and the sign of β indicates whether an increase in the independent variable leads to an increase in the output.

Table 7.3: Fuel budget.

Phase	Fuel Required [kg]
Cruise	1040
Loiter at 20.5 km	142
Diversion	218
Non-intensive phases	143
Total	1543

Table 7.4: Sensitivity of fuel weight to selected parameters.
 $R^2 = 0.88$

Parameter	β
M	-0.228
C_{D0}	0.331
c_j	0.638
A	-0.501
e	-0.182

It is clear that the fuel weight is most sensitive to the specific fuel consumption and that focus should be put into minimizing this to ensure healthy margins for the fuel budget. The sensitivity to the Mach number is also notable as flying faster leads to reductions in fuel consumption. This will be considered when optimizing the flight profile in Chapter 13. Note that this sensitivity analysis does not take into account a number of dependencies, such as the way increasing the aspect ratio increase structural weight.

Verification and Validation

Verification was carried out by comparing hand calculations of the range and endurance equations to the predicted values. The method is quite simple and no discrepancies were found in machine precision so the tool can be considered verified to a high degree of confidence. Validation is more challenging as experimental data on fuel burnt is not readily available and very sensitive to atmospheric conditions. A degree of validation may be carried out by comparing the predicted fuel fraction of the ESRA to other similar aircraft. Table 7.5 shows the fuel fraction of some aircraft with similar ranges. Of these the most valuable data point is the M-55, as it has similar performance characteristics, being a medium-range stratospheric aircraft. The ER-2 and RQ-4 have significantly higher fuel fractions, both in the order of 0.45, however, they also have a range of 11,500 and 22,800 km respectively.

Analysis of the data from Table 7.5 indicates that the fuel fraction is reasonable as the discrepancies between the aircraft are quite slight.

7.2.2. Structural Mass Budget

Accurate prediction of the structural mass is a significant challenge in the conceptual phase as detailed design has not taken place. Nevertheless, prediction is important as it can set constraints on the performance of the aircraft and on the maximum weight that the structure can achieve.

¹https://customer.janes.com/display/JAU_A235-JAU

²<https://customer.janes.com/display/JAWA1244-JAWA>

³<https://customer.janes.com/display/JAWAA584-JAWA>

⁴https://customer.janes.com/display/JAU_A216-JAU

Table 7.5: First order validation of fuel budget.

Aircraft	Fuel fraction	Range [km]	Type
ESRA	0.35	6000	Stratospheric research aircraft
M55 ¹	0.33	5000	Stratospheric research aircraft
Cessna Citation Sovereign ²	0.37	5900	Business Jet
Legacy 500 ³	0.31	5400	Business Jet
Challenger 300 ⁴	0.36	5700	Buisness Jet

The Torenbeek weight estimation method was implemented and resulted in the following weight breakdown, which should also be read as a budget.

Component	Mass [kg]	Percentage
Propulsion group	729.1	34.3%
Wing	651.88	30.7%
Fuselage	305.68	13.4%
Nacelles	155.72	7.3%
Main landing gear	135.98	6.4%
Empennage	132.85	6.3%
Nose landing gear	34.56	1.6%

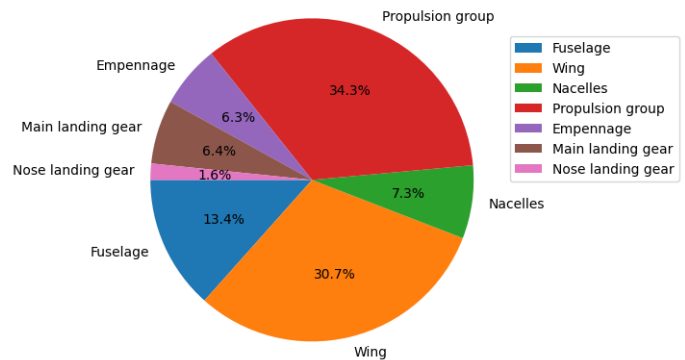


Figure 7.1: ESRA mass breakdown

It can be seen from Figure 7.1 that the propulsion group accounts for the largest proportion of the overall weight. This is primarily due to the intentionally overpowered design of ESRA, which ensures its capability to reach the required service altitude. The subsequent component is the wing, which possesses significant weight due to its exceptionally large aspect ratio. The high aspect ratio can also cause undesired aeroelastic effects. To mitigate both significant weight and aeroelastic response the struts were added. According to Torenbeek, the implementation of struts can reduce wing weight by up to 30%. However, to maintain a conservative approach Raymer’s suggested 18% was utilized in the calculations [63].

Validation and Verification

The accuracy of this method along with Roskam and Raymer methods has been studied by NASA Langley Research Center [13]. For smaller subsystems errors can become significantly high and reach up to 80%, however for bigger subsystems such as the wing and propulsion group, the errors usually do not exceed 2.5%. The paper shows that eventually, the combination of all methods converges to the same value. However, each individual method can either overestimate or underestimate the weight of an aircraft. That is why both verification and validation of Torenbeek’s method were conducted.

Verification Roskam provides a detailed mass breakdown for a variety of aircraft [69]. For verification purposes, the Fokker F28-1000 was utilized since it is one of the aircraft used to build the empirical relationship for the Class II method. The geometrical parameters of the aircraft were used for Class II method setup.⁵ The by-hand calculations were performed and compared with data listed in Roskam database. The maximum deviation did not exceed 2%.

Validation For validation, the data of U2 which was the main reference aircraft for ESRA design, again provided by Roskam, was used [69]. The results are summarized in Table 7.6. It shows very little discrepancy in wing weight and OEW percentage. The one percent difference in the empennage weight comes from the conservative approach that has been followed during tail sizing, and the high end of tail weight approximation was utilized. The landing gear weight also differs significantly and is more than two times higher for ESRA, this can be explained rather easily since U-2 does not utilize a tricycle landing gear and utilizes pogos instead, drastically decreasing the weight. The fuselage weight is much smaller for ESRA due to the fact that it is carrying a much lighter payload compared to the U-2.

Overall, the results obtained during validation were considered satisfying, since there were no discrepancies that could not be justified.

⁵https://www.the-blueprints.com/blueprints/modernplanes/fokker/46934/view/fokker_f-28/

7.2.3. Drag Budget

This section presents the method to estimate the drag of the aircraft throughout the mission. Given the limited operational margins of the plane when flying in the stratosphere, it is necessary to create a drag budget that must be adhered to during later design and production phases to ensure fulfillment of the critical mission profile.

Drag is assumed to consist of parasite and induced drag components. The former accounts for skin friction, pressure, wave, and miscellaneous drag, whereas the latter takes into account the drag due to downwash at the wingtips, which is a function of lift. Equation (7.3) shows the representation of C_D , the drag coefficient.

$$C_D = C_{D_0} + \frac{C_L^2}{\pi A e} \quad (7.3)$$

For the drag budget, it is necessary to estimate C_{D_0} . The estimation of e is described in Section 9.2. A is a design variable, justified in Section 9.2, and C_L is within the control of the pilot as a function of the weight, altitude, and velocity.

Estimation of C_{D_0}

To estimate C_{D_0} the component drag build-up method was used, as described in [62], which is reflected in equation (7.4).

$$C_{D_0} = \frac{1}{S} \sum (C_{f_c} FF_c Q_c S_{wet_c}) + C_{D_{misc}} + C_{D_{l\&p}} \quad (7.4)$$

The method captures the effect of skin friction in the coefficient C_{f_c} , pressure drag due to separation in the form factor FF_c and interference in the coefficient Q . The term S_{wet} describes the amount of area immersed in the flow. The additional terms refer to miscellaneous and leakage drag. Leakage drag is estimated to be 2% of the total C_{D_0} [62]. $C_{D_{misc}}$ accounts for wave drag, and separation due to upsweep.

The skin friction of the components was computed using a flat-plate approximation. This method computes a weighted average of the skin friction due to turbulent- and laminar flow. Accurate prediction of the transition point is required because the skin friction drag due to turbulent is in the order of five times greater than the drag due to laminar flow. This is considered outside the scope of this project, as it requires high-fidelity CFD or experimental measurement. Some high-fidelity results for a transonic strut-braced wing operating at Mach 0.7 with a $C_{L_{cruise}} = 0.81$ are presented in [80]. For this aircraft, laminar flow occurs until 50% of the mean aerodynamic chord. As a conservative approximation, transition was assumed to occur at 35% of the MAC for the wing and at 10% of the length for all other components. Figure 7.2 shows the results of the effect of the transition point on the computation of $C_{D_{0wing}}$.

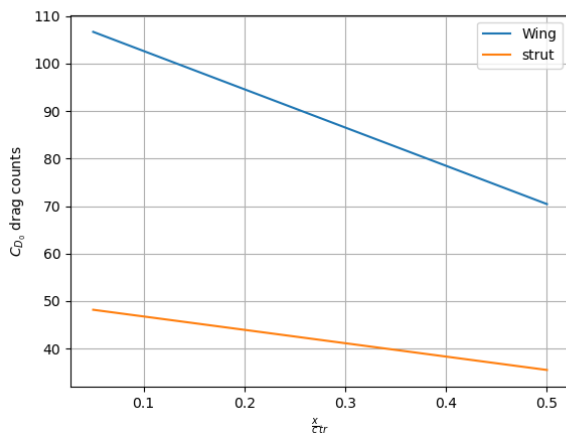


Figure 7.2: Sensitivity of drag of the wing and strut to the transition point

Table 7.6: Class II weight estimation method verification and validation results

Group [%]	U-2 [%] [67]	ESRA [%]	delta [%]
OEW	60.3	59.8	-0.471
Wing	12	12.72	0.72
Fuselage	8.3	6.03	-2.26
Empennage	1.9	2.9	1.09
Landing gear	1.5	3.83	2.34

Table 7.7: Parasite drag breakdown in counts for different flight conditions

Mach	0.2	0.65	0.65	0.65	Average Percentage Contribution
Altitude (m)	0	11000	19500	20500	-
Fuselage	26.0	22.4	27.2	28.3	13.60
Wing	60.1	60.6	78.3	82.5	36.07
Vertical Tail	9.9	10.3	12.7	13.3	5.96
Horizontal Tail	7.2	7.3	9.2	19.6	5.19
Engine group	27.8	23.5	29.0	30.2	14.43
Strut	34.8	34.5	44.5	46.8	20.64
Wing payload pods	5.1	4.3	5.3	5.6	2.65
Wave drag	0.7	4.0	4.0	4.0	1.43
Leakage drag	1.7	1.7	2.1	2.2	0.99
Total $C_{D_0} \times 10,000$	173	169	212	222	100

C_{D_0} was evaluated in different flight conditions throughout the mission. Table 7.7 shows the results. The breakdown per component of the parasite drag at high cruise is shown in Figure 7.3.

This table should be read as a budget for each flight condition that should not be exceeded to ensure the optimum performance of the aircraft in its critical mission profile. A proposal to ensure this will now be discussed.

The largest contributions to the drag come from the wing and the strut. Currently, it is assumed that the strut has 10% laminar flow over its surface. A significant drag reduction may be achieved if this is increased. In order to optimize the drag behavior of large surface areas, like the wing, the transition between laminar and turbulent flow has to be controlled and delayed as much as possible. Major factors in this transition are flow instabilities and attachment-line contamination[75]. Improving the aerodynamic behavior is done through laminar flow control: by making the boundary layer more full, the growth of disturbances is generally lowered, resulting in the more laminar flow over the wing[75]. Boundary layer behavior can be influenced by the roughness of the surface [74]. By applying rough patches on the leading edge of the wing, the flow can be kept laminar for longer, thus decreasing the overall drag over the wing.

The spanwise position of the strut also plays a significant role in the drag of the component. Figure 7.4 shows how the angle between the strut and the horizontal (θ), shown in Figure 10.6, correlates to drag. This angle is directly related to the length of half of the strut by (7.5).

$$l_{strut/2} = \frac{y_{strut}}{\sin \theta} \tag{7.5}$$

As expected, the more shallow angles of the strut lead to an increase in length, surface area and consequently parasite drag. It appears that past 30° the reduction of drag due to a steeper angle begins to diminish, suggesting this is a good value to size the strut for. Detailed sizing of the strut and its placement may be found in Subsection 10.2.4.

A breakdown of the induced drag is shown in Section 13.1, as the lift coefficient is known to a higher fidelity.

7.2.4. Verification and validation

Verification of the zero-lift drag estimation was carried out by unit testing each function compared to hand calculation until all results had a discrepancy of, at most, 10^{-12} . A second layer of verification and validation was conducted by comparing the results of the drag estimation to those of the digital DATCOM method, of which examples with data may be found in the footnote.⁶ In this case, the data was for a Cessna Citation II. The inputs are the flight Mach number and altitude, and the geometry

⁶https://github.com/arktools/pydatcom/blob/master/test/data/Citation_simple.out

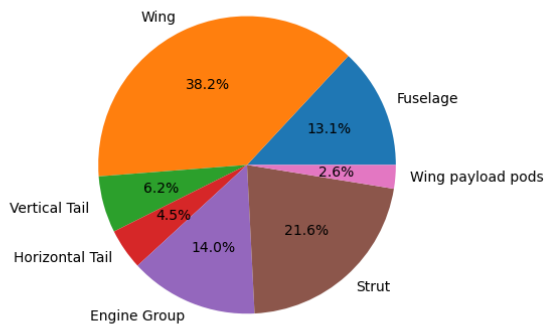


Figure 7.3: Parasite drag breakdown per component

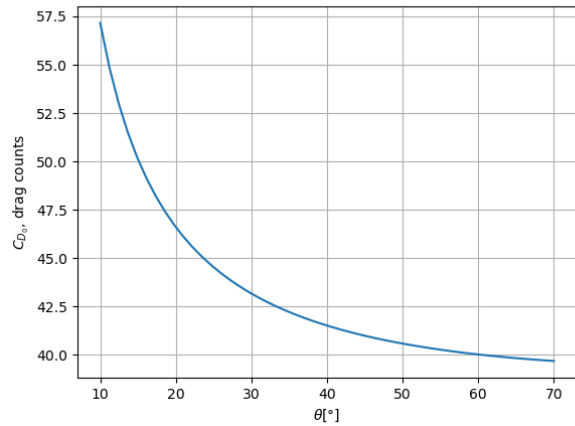


Figure 7.4: Sensitivity of the drag of the strut to θ

Table 7.8: Verification table for the zero-lift drag estimation

Component	Datcom value (drag counts)	Predicted value (drag counts)	Difference %
Fuselage	42.85	42.7	-0.35
Wing	61.7	65.3	5.83
Vertical Tail	11	11.4	3.63
Horizontal Tail	15.4	16.2	5.19

of the aircraft, particularly the surface area of the wing, empennage, and fuselage, as well as the characteristic lengths of each of these components. A value for transition was assumed to be 10% for the wing and empennage, and 5% for the fuselage. The results are shown in Table 7.8.

There are no significant outliers between the prediction and the DATCOM value. The estimation from [62] appears to be more conservative, which is favourable for the conceptual design phase as the budget will be easier to adhere to.

Propulsion

From the midterm report, it has been concluded that a jet engine is required for our design. Rather than developing a new engine, an off-the-shelf engine is considered due to certification costs and limited development time since ESRA aims to be operational by 2030. This section focuses on selecting an appropriate engine, modeling it to sufficient standards, and correctly implementing it into the design such that it works with the other sub-systems. It has been found that the propulsion system is largely coupled with the performance of the aircraft because of the imposing thrust requirements, leading the engine to be a large contributor to the aircraft's weight and drag. The engine acts as a large concentrated mass that has to be integrated effectively into the aircraft. The required thrust of the aircraft has been found to be sensitive to the mass of the engine and its efficiency as this directly influences the fuel mass. This coupling has led to a largely concurrent engineering design process with the performance sub-system.

8.1. Model Analysis

Two modeling techniques are utilized to analyze the behavior of a turbofan engine, a first principle model based on the method highlighted in [53] and [28] and using industry-level software *GasTurb14*. Such models require a lot of inputs that are hard to quantify in real life such as various isentropic efficiencies and pressure ratios, the turbine inlet temperature, and the nozzle geometry. After doing research on engines, all this information is hard to find as engine manufacturers do not disclose this kind of data.

The first method, in [28], is based on principles of thermodynamics and aerodynamics. Modeling existing engines with this method is difficult because of the lack of data available. Simplifications and assumptions had to be made where inputs are missing. This method splits the engine into six main stations: inlet, fan, compressor, combustion chamber, turbine, and exhaust nozzle. It was assumed that a single turbine powers both the compressor and fan connected via a single spool. This allows complicated configurations such as multi-spool layouts to be neglected and simply consider a lumped thermodynamic power balance between the compressing elements and turbine. In the end, however, it was noted that to be able to model engine performance at altitude, more input are required to obtain accurate results and prevent oversimplifying the problem.

Industry level software *GasTurb14* is built on similar principles but in considerably more detail and with more possibilities for analysis and optimization. However, the software requires text files containing a platitude of inputs that are needed to run the simulation. This is because Gas Turb is built for designing new engines rather than modelling existing ones. Therefore, both the first principle model and Gas Turb model require parametrization. As doing so would add a layer of uncertainty to the already simplified first principles model, it has been concluded that the most accurate representation of an existing engine would be achieved using Gas Turb. This is because it offers higher resolution at each engine section calculation and is a recognized industry-level software. Therefore, Gas Turb is used to model existing engines where the inputs required are found by parametrizing and iterating. On the other hand, the first principles model is used to provide insight into the thermodynamic functioning of turbofan engines.

8.2. Engine Design Considerations

Since the available information on existing engines does not include their performance at our target altitude of 20.5 km, it is vital that the engines are modelled to provide indicative estimates for ESRA's design. Understanding how some main engine parameters affect its' performance will narrow down a list of possible options that meet our mission profile.

When choosing a commercially available engine, considerations should be made about the convergence of a design. For each engine option, varying amounts of fuel is required to adhere to the mission profile, depending on the fuel consumption of the engine, and the added weight of the engine itself. This increased fuel mass in turn requires the engines to provide more thrust than was originally required, resulting in an additional design iteration. Additionally, the drag generated by the engine nacelle area also influences the thrust requirements of the aircraft, especially for multiple engine configurations. Since the engines are a main weight contributing member, the shifting of the cg due to fuselage-mounted engines is considered for stability. There is a risk that the cg is moved too far aft and would cause instability hence this additional analysis is conducted. In case the engine cannot provide the thrust required either at sea level or at altitude, the engine is not suitable for the design and should be discarded as an option.

8.2.1. Propulsion performance metrics

A few performance metrics can be used to describe the overall compatibility of an engine. First, the thrust-specific fuel consumption (TSFC) describes the fuel efficiency of the engine and is expressed as a function of the fuel used per unit of time per unit of thrust.

Another metric used to describe the engine performance is the thrust-to-weight ratio. This metric expresses the ability of an engine to provide a certain amount of thrust while not being unnecessarily heavy. An engine with a higher thrust-to-weight ratio will enable an aircraft to achieve a better overall performance.

The last metric that will be considered is the thrust lapse. As the design is required to fly at a considerable altitude, deterioration of engine performance at altitude should be analyzed. Due to the lower pressures at altitude, for a given flight speed, air mass flow through the engine decreases compared to sea level, reducing the effective thrust of any air-breathing engine. This effect is further accelerated by increasing bypass, as for those engines, a higher mass flow is required to provide sufficient thrust. The effect of these three performance metrics are analyzed in the next section via sensitivity analysis.

8.2.2. Engine performance and sensitivity analysis

In order to be able to select a suitable engine, the effect of the performance metrics above should be analyzed through a sensitivity analysis. With this information, a general qualitative analysis was conducted to rule out some engine options that does not meet our mission profile. A default two-spool turbofan engine in Gas Turb is used to illustrate the relationship between the performance metrics. The engine has a bypass ratio of 6, and is designed to operate at an altitude of 11000km at a Mach number of 0.8. An important emphasis is placed on the bypass ratio due to its effect on TSFC and its sensitivity to altitude but also it is readily available information for any existing engine. Therefore, the bypass ratio will affect our choice of engine.

Specific fuel consumption

The TSFC can be influenced by changing some design parameters, most notably the bypass ratio. Flight conditions can also be altered to optimize for minimum fuel consumption. If the critical mission profile allows, determining the optimum cruise altitude and Mach number could greatly impact the weight, mission fuel consumption and cost of ESRA. In order to visualize the effect of these parameters, some graphs are presented below in Figure 8.2 and Figure 8.1. In these graphs, a reference two-spool unmixed flow turbofan was used. As can be seen in Figure 8.1, TSFC is minimal for a bypass ratio of 6, this is logical as the design bypass ratio of this specific engine is equal to 6. In addition to that, the engine is clearly optimized for its' respective cruise altitude of about 11km. From these graphs, some conclusions can be drawn. In general, for increasing bypass, the TSFC goes down, up to a certain point after which it rapidly increases again. As this is one of the main design parameters of any engine, we can conclude that generally, an increase in bypass ratio will result in a decrease in TSFC, up to a certain point. With increasing altitude, the TSFC increases gradually. As for the Mach number, the specific fuel consumption goes up with increasing Mach.

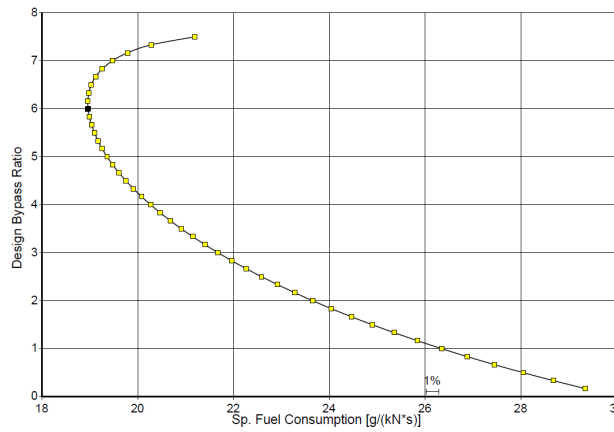
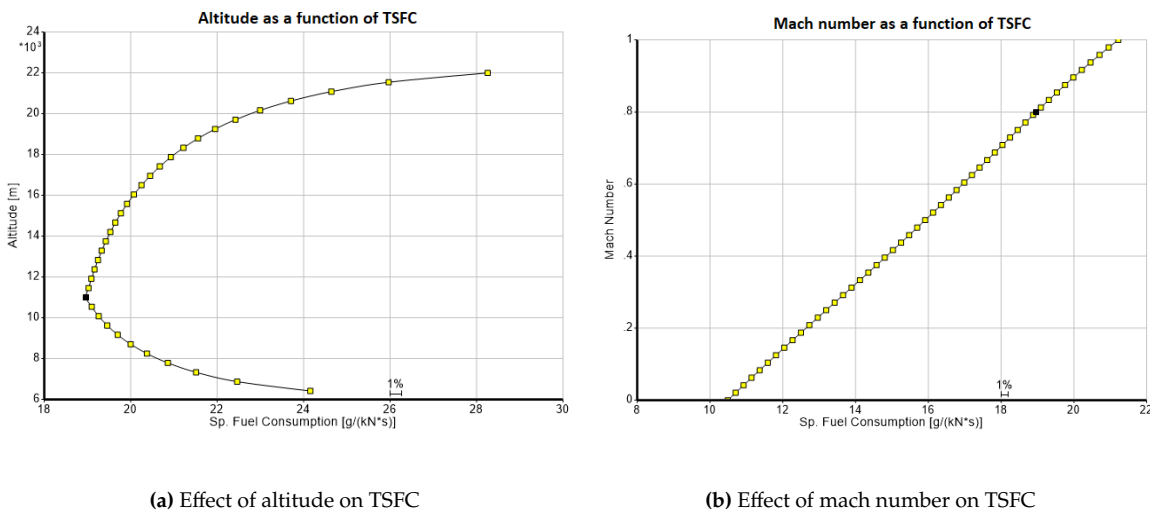


Figure 8.1: Effect of bypass on TSFC



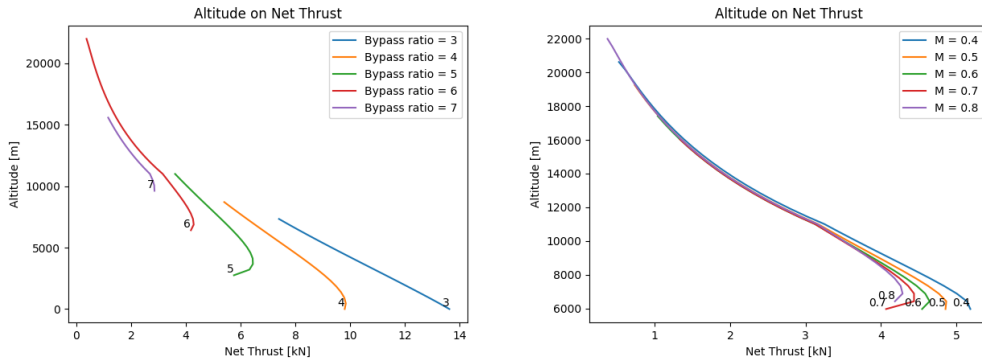
(a) Effect of altitude on TSFC

(b) Effect of mach number on TSFC

Figure 8.2: Variables impacting TSFC

Performance at altitude

To ensure that existing engines, which are designed for general cruise altitude, can indeed be used at our target altitude (20.5 km) it is important to understand how altitude, bypass, and Mach number affect net thrust and specific fuel consumption of turbofan engines. To analyze this, the same reference two-spool turbofan engine is used. It is important to note that this particular engine is optimally designed for a bypass ratio of 6, a cruise altitude of 11km, and a Mach number of 0.8. Altering these parameters, especially the design bypass ratio will cripple efficiency as explained above. In figure 8.3(a), models which differ from the design bypass ratio of 6 are shown to be incomplete. This is because the simulation does not converge for the given parameters. This is only the case as the engine is tailored to function at specific conditions and no in-depth conclusions of how different bypass engines are affected by thrust should be taken from the said graph. However, the modeling still highlights the thrust behavior. Models in figure 8.3(a) are kept at the design Mach number of 0.8 and in figure 8.3(b) are kept at the design bypass ratio of 6.



(a) Effect of altitude on thrust with varying bypass (b) Effect of altitude on thrust with varying mach

Figure 8.3: Altitude effect on thrust

What is evident is that thrust deteriorates as altitude increases due to the lack of airflow in the engines. When all parameters are kept constant (including intake mass flow), a lower bypass ratio results in a greater net thrust. This is because the engine core (compressor, combustion chamber, turbine) can generate more thrust with the same amount of airflow compared to the fan. This is important to consider at high altitudes due to the limited airflow. Figure 8.3 (b) shows the effect of flying at different mach numbers. At low altitudes, increasing the Mach number reduces the net thrust. This is due to compressibility effects decreasing the static density of the air hence decreasing the mass flow.

Another important consideration is that the fuel mass flow decreases as altitude increases. This is because the engine operates at a specific air-to-fuel ratio which changes only slightly with altitude, therefore, since air mass flow decreases at altitude due to density, so does the fuel flow to maintain the air-to-fuel ratio.

Thrust to weight

In order to evaluate engines' thrust-to-weight ratio, both the thrust and the weight have to be known. For this purpose, relevant data on some engines were collected and displayed in Table 8.1. One of the first things to note is that older engines (age is not included here), tend to have less bypass and a worse thrust-to-weight ratio. A good comparison can be made when looking at the F101 and F119 engines. Both of these are made to power military jets but differ significantly in age. Even though the F101's bypass is considerably larger than the F119's, one can conclude that there is a significant increase in the power to weight ratio. This general increase in bypass can also be observed when comparing the CF700-2C and the HTF7500E, where the thrust-to-weight ratio does not change for a larger bypass.

Table 8.1: comparison of some engines with varying weight and bypass, containing thrust to weight and TSFC

Name	Bypass ratio [-]	Thrust [kN]	Weight [kg]	Fuel consumption [g/kN*s]	Thrust to weight [-]
PW305A ¹	4.3:1	23.24	450	10.99	5.27
PW535A ²	2.6:1	15.12	317	12.46	4.86
CF700-2C ³	1.6:1	18.68	329	18.46	5.79
HTF7500E ⁴	4.4:1	34.0	618.7	11.87	5.60
CF34-10E ⁵	5.3:1	83.68	1724	10.75	4.95
Progress D-436 ⁶	4.91:1	73.55	1360	18.17	5.51
LEAP-1A [54] ⁷	11:1	146.35	3153	15.579	4.73
Passport 20-18 ⁸	5.6:1	82	2066	/	4.05
F119 [18] ⁹	0.3	113 (W/O reheating)	1769	22.66	6.51
F101 [18] ¹⁰	2	75.6 (W/O reheating)	2023	16.43	3.81

As a result, looking at newer engines will generally result in a higher bypass engine which generally consumes less fuel but is more impacted by the thrust lapse. As the effects of the combination of parameters described above cannot be accurately predicted due to the implications of the change in (fuel) weight, all engines have to be evaluated case by case when selecting an engine.

8.3. Engine selection

For the engine selection, a shortlist of engines to consider was made. For this purpose, the three performance metrics in Section 8.2 were used to compare the different options. Engines that scored poorly in any of these metrics were discarded as they would not be able to fulfill the performance requirements at altitude or would result in a very heavy or no solution at all. When selecting an engine, the first thing taken into consideration is the number of engines of each type that would be needed to power the aircraft. For this, the most critical requirement was the thrust available at altitude. As low bypass engines generally experience a smaller reduction in thrust compared to the sea level situation, these were considered first.

There are few modern very low-bypass (0 - 1 BPR) engines due to their relatively high fuel consumption and emissions. This in turn implies that most modern low bypass engines are developed for military applications. These engines also tend to be of considerable length and weight. The increase in overall weight and fuel consumption resulted in heavy, unfeasible designs where the engine would make up a significant portion of the total aircraft weight. As either a fuselage-podded or wing-podded engine configuration was selected, the engine would be mounted on top of the fuselage, towards the tail of the plane, complicating the stability and controllability of the craft. For these reasons, engines with a bypass ratio of 0 - 1 were discarded as an option.

When looking to minimize fuel usage to keep the additional weight as low as possible, some engines with a higher bypass ratio were considered next. Characterized by poor performance at altitude, and overall poorer thrust to weight than their low bypass counterparts, these engines proved to be unfeasible as well. This was not caused by the fuel weight but by the engine weight. As the thrust required at high altitudes remains the same for the same weight of the engine, this type of engine had to be significantly larger to deliver the same performance. With this, the engine weight went up and so did the thrust requirement at altitude as the overall design became heavier.

The conclusion was rather simple: a relatively low bypass engine (1-3 BPR) with good fuel consumption and a proper thrust-to-weight ratio would be ideal for the purpose. With these criteria in mind, large engine databases are narrowed down to yield a shortlist of possible viable engines. Each engine was then tested with the performance model to see if the thrust requirements are met and to quantify the integration of the engine with the design. The most suitable engine is the Pratt and Whitney PW535A, a low bypass option of the PW500 series. As this is one of the most recent small low bypass engines, the thrust-specific fuel consumption was found minimal in combination with a low weight per engine. Due to the low bypass, the thrust lapse was also kept to a minimum. In addition, two of these engines can provide enough thrust at altitude, meaning that they can be wing mounted. This is mainly done for stability reasons as mounting two such engines on the fuselage would move the center of gravity too far aft. Furthermore, wing-podded engines allow for easier accessibility hence lower maintenance costs and time.

¹URL: https://customer.janes.com/display/JAE_0486-JAE_ [cited on 21/06/2023]

²URL: https://customer.janes.com/display/JAE_0487-JAE_ [cited on 21/06/2023]

³URL: https://customer.janes.com/display/JAE_0286-JAE_ [cited on 21/06/2023]

⁴URL: https://customer.janes.com/display/JAE_0721-JAE_ [cited on 21/06/2023]

⁵URL: https://customer.janes.com/display/JAE_0737-JAE_ [cited on 21/06/2023]

⁶URL: https://customer.janes.com/display/JAE_0699-JAE_ [cited on 21/06/2023]

⁷URL: https://customer.janes.com/display/JAE_A047-JAE_ [cited on 21/06/2023]

⁸URL: https://customer.janes.com/display/JAE_A054-JAE_ [cited on 21/06/2023]

⁹URL: https://customer.janes.com/display/JAE_0573-JAE_ [cited on 21/06/2023]

¹⁰URL: https://customer.janes.com/display/JAE_0733-JAE_ [cited on 21/06/2023]

8.4. Engine characteristics and off design

After having selected the PW535A engine, it is imperative that the engine is extensively analyzed, especially in off-design conditions to evaluate its flight envelope. This allows the understanding of the performance of the engine at the target altitude of 20.5km but also the climb performance of the aircraft. As such, the engine characteristics as found in [59] and [83], are used to parameterize the input values in Gas Turb. Information available from the EASA certification [83] includes the geometry and weight of the engine which is used for sizing as well as the technical characteristics presented in table 8.2.

Using the data in table 8.2, Gas Turb inputs are iterated to match the PW535A rated take-off thrust and take-off SFC. The main inputs that are parameterized this way are the various pressure ratios and efficiencies at each station of the engine leading to the final model for the PW535A. For the modeling itself, a template for a two-spool low bypass turbofan was modified. The intake pressure ratio and LPC and HPC compression ratios were iterated until the thrust and fan spool speeds were consistent with test data provided by EASA [83]. The interturbine temperature was set to be consistent with the measured one by modifying the temperature in the combustion chamber. When all of these inputs were set, and the design converged, the design was saved and used for the modeling of the performance at altitude. Doing this resulted in the engine behavior that can be observed in Figure 8.4 and Figure 8.5.

Table 8.2: Engine characteristics used to parameterize Gas Turb inputs

Bypass ratio (BPR)	2.6
inlet diameter	0.953 [m]
Interturbine Temperature (IIT)	973 [K]
Low pressure rotor rpm	15850
High pressure rotor rpm	33970
Rated take off thrust	15.12 [kN]

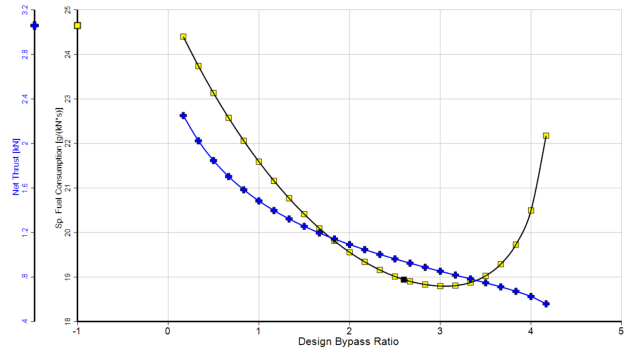
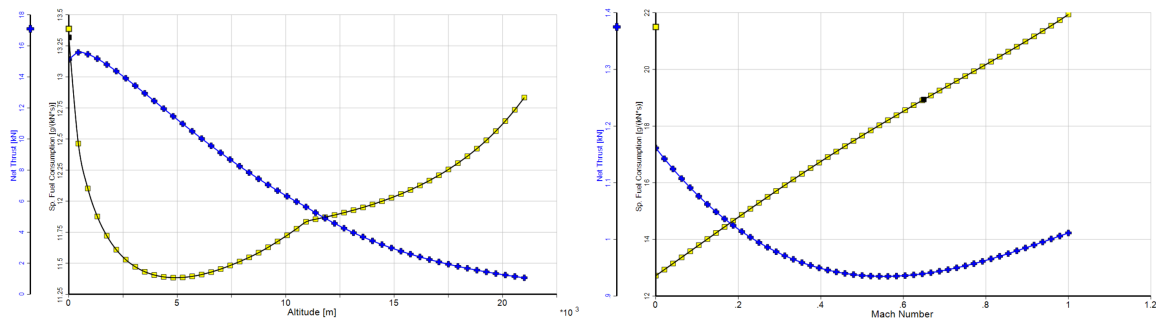


Figure 8.4: Effect of design bypass ratio on TSFC and net thrust for the PW535A, at 20.5 km



(a) Effect of altitude on TSFC and net thrust for the PW535A, assuming static conditions **(b)** Effect of mach number on TSFC and net thrust for the PW535A, at 20.5 km

Figure 8.5: Variables impacting TSFC and net thrust

The flight envelope generated by the model is shown in Figure 8.6. The contour lines highlight the net thrust the engine produces at combinations of altitude and Mach number. The same graph is produced for the SFC shown in Figure 8.6. These envelopes are crucial in the selection of optimum flight profiles and are to be analyzed together with the performance flight envelopes in Chapter 7. Namely, the engine performance will be constraining for the specific range optimal performance point.

Table 8.3: PW535A Engine performance at various operational conditions

Flight point of interest	Altitude [m]	M [-]	Thrust [kN]	SFC [g/kN*s]	m_f [kg/s]
Take off	0	0.2	11.64	17.57	0.2044
Diversion Cruise	11000	0.65	4.57	17.43	0.0796
Cruise	19500	0.65	1.22	18.48	0.0226
On station	20500	0.65	0.94	18.94	0.0178

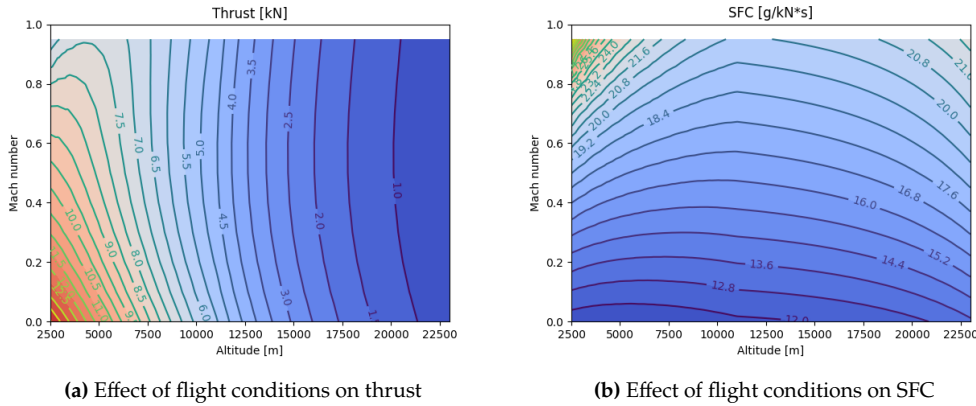


Figure 8.6: Flight envelope on engine performance

The behavior highlighted in the graphs is consistent with that of the preliminary engine analysis done previously in Subsection 8.2.2. The thrust (Figure 8.6a) decreases steeply at low altitudes while at a lower rate at higher altitudes varying only slightly with Mach number. It should be noted in the top right corner, low altitude, and high Mach numbers show the same behavior as Figure 8.3(b)) where the high mach number curves of $M=0.7$ and $M=0.8$ wherein the thrust slightly increases with altitude before decreasing again. Similarly, the SFC graph (Figure 8.6b) shows the parabolic relation with altitude where the peak of a contour curve (constant SFC curves) highlight the minimum value of an SFC vs altitude curve at a given Mach number. The behavior is the same as figure 8.2(b).

The data will also be used to verify compliance with the requirements imposed by the performance of the aircraft. Additionally, it will highlight in what conditions our engine utilizes the most fuel and is most efficient.

Based on our flight profiles expanded upon in section 16, flight conditions of interest are selected to give a numerical overview of the engines' performance. The first point of interest is the take-off point and the last one is the on-station loiter point. The off-design performance of the engine is highlighted in table 8.3. GasTurb modeling data can be found in Appendix A.

The most driving engine requirement was that of our thrust at altitude. The entire system is required to provide a thrust of 1.98 kN at the altitude of 20500m based on class II drag estimations in section 7. This value includes a margin of 0.075 kN due to the high risk associated with high-altitude operations. Since a two-engine configuration is used and one engine produces 0.94 kN of thrust at 20500m, this requirement is met.

Additionally, Pratt & Whitney Canada is still producing this engine and the engine itself is still in service on similar size aircraft such as the Cessna Citation V encore [59]. This further proves the claim that the PW535A engine is ideal for the ESRA mission.

8.5. Verification and Validation

8.5.1. Verification

The industry-level Gas Turb software is already in itself a verified tool as it is used by many engine manufacturers.¹¹ Additionally, modeling of the engines as done in section 8.2 exhibits similar behavior according to physical principle found in literature. Additionally, the thrust decrease due to altitude graphs matches those derived by the model based on [28] which is based on first principles. It highlights that the thermodynamics and physics of the flow are affected in the same way in both methods.

8.5.2. Validation

Validating Gas Turb is more important, especially due to the fact that engines operating at high altitudes are niche and the software developers probably put more emphasis on modeling engines and commercial aircraft altitudes. It is also important to validate the parameterization of the inputs for GasTurb.

However, it has been shown to be arduous to perform validation as the Gas Turb simulation needs to be parameterized using existing engine characteristics to be able to model said engine accurately. What is therefore done, is to use existing data on the performance of the engine at different operating conditions.

The parametrization has been done only by matching the takeoff thrust and take-off SFC, not by utilizing off-design data. This data is also not readily available and only the cruise rating of the PW535A has been found. Comparing this data would validate the PW535A model used.

The PW535A has a performance rating of 3.67 kN at an altitude of 12200m and a Mach number of 0.8 [59]. The GasTurb model at the same conditions outputs a thrust of 3.85 kN. The values are displayed in table 8.4.

Table 8.4: Comparison of PW535A cruise performance with Gas Turb model

Data (h = 12200m, M = 0.8)	GasTurb model (h = 12200m, M = 0.8)	Percentage difference
Thrust = 3.67 kN	Thrust = 3.85 kN	4.9%

A percentage difference of 4.9% is sufficiently accurate for the level of this conceptual design phase. This difference is also accounted for by the thrust margin imposed at altitude of 75N.

8.6. Recommendations

The weakest part of the model used in the analysis of the PW535A engine is the fact that only one data point is used to parametrize the GasTurb model. Ideally, data on thrust and SFC at various operating conditions is used for a more complete and correct parametrization of the model. However, with the available data and considering the early stage of the design, the modelling method is apt. At further stages, Pratt & Whitney Canada will be contacted to purchase the engines. Real life tests will be conducted on the engines to obtain more extensive data to improve the accuracy of our model. Extensive sensors will be used to extract as much input parameters for the model such as mass flows, pressure and temperature values at various stations of the engine. This would decrease the parametrization needed and lead to a more precise model. If the engine performance were to differ notably from the present model, then the rest of the design would need to be tweaked in further iterations to comply with the engines performance.

¹¹URL <https://www.gasturb.com/> [cited on 21/06/2023]

Aerodynamics

9.1. Airfoil design

Given the extreme operating conditions of ESRA, special care has to be given to high lift capabilities while ensuring the ability to fly at high speeds without encountering drag divergence. Due to the high cruise altitude of ESRA, the design team was anticipating transonic effects, therefore, supercritical airfoils were considered for ESRA. A trade-off can be set up in order to select the best airfoil with the following criteria and weights:

- **The drag divergence mach number** is relevant as the aircraft will need to fly close to the coffin corner where the drag divergence mach number is assumed to be the upper speed limit. In order to maximise the speed margins, it is critical to push this number as high as possible. Consequently, the drag divergence mach number criterion was given a weight of five. Furthermore, the drag divergence mach number is given by :

$$M_{DD} = M^* - \frac{t}{c} - 0.1C_l^{1.5} \quad (9.1)$$

Where $M^* = 0.935$ is a technology factor for supercritical airfoils [84].

- **The maximum lift coefficient** controls the lower speed limit of the flight envelope as it dictates when the aircraft will stall. In addition, the maximum lift coefficient for the wing will be significantly lower than that of the airfoil thus making it critical to maximise this quantity. Given the importance of this quantity, it was decided to award this criterion a weight of four.
- **The lift to drag ratio** at cruise quantifies the airfoil efficiency in cruise conditions. This quantity is important as the engine efficiency will significantly decrease with altitude and efficiency will be critical to achieving performance goals. This criterion is important but as it does not directly affect the mission, it was awarded a lower weight of three.
- **The zero lift moment coefficient** will give an indication of the required tail size as a larger moment will require a larger tail to trim the aircraft. This will also translate into more drag and weight which will snowball into even more weight. As the computed moment coefficients vary with the lift coefficients, it was decided that C_{m_0} should not be given a significant weight. Thus, this criterion was awarded a weight of two.
- **The zero lift drag coefficient** is a critical as it directly influences the total wing drag. That being said, the number obtained from XFLR5 are unreliable as the software does not properly simulate viscous effects. Thus this criterion was assigned a low weight of one.

From Table 9.1, it is shown that the SC(2)-0612 scores the best amongst the selection of supercritical airfoils and was chosen for ESRA's wing design.

Table 9.1: Trade-Off Matrix for airfoil

Criteria Option	M_{DD}	$C_{l_{MAX}}$	$(\frac{L}{D})_{cruise}$	C_{m_0}	C_{d_0}	Total Score
Weights	5	4	3	2	1	-
SC(2)-0612	0.746 [G]	1.67 [B]	68.7 [B]	-0.11 [B]	0.0063[B]	3.33
SC(2)-0614	0.725 [Y]	1.67 [B]	67.85 [Y]	-0.114 [G]	0.0062 [G]	2.67
SC(2)-0712	0.746 [B]	1.629 [Y]	69.98 [G]	-0.122 [Y]	0.0073 [Y]	2.73
SC(2)-0714	0.726 [R]	1.7 [G]	66.75[R]	-0.132 [R]	0.0078 [R]	1.8

9.2. Planform Design

The trapezoidal wing configuration was chosen to simplify the design process. An elliptical wing would be expensive to manufacture due to its complex shape whereas the rectangular wing would become too heavy because of the high aspect ratio.

The main design parameters are thus sweep, aspect ratio, dihedral angle, and taper ratio. All other dimensions such as span, root chord, and tip chord follow from simple relations

$$b = \sqrt{SA} \quad c_r = \frac{2S}{(1 + \lambda)b} \quad c_t = \lambda c_r$$

The sweep angle helps to increase the critical Mach number however reduces lifting force. Since ESRA's Mach cruise is below 0.7, a sweep angle is unnecessary since compressibility effects can be avoided with supercritical airfoil technology [84, 64]. Thus, $\Lambda_{c/4} = 0$. M.Nita and D.Scholz from the Hamburg University of Applied Science claim that for unswept wings the optimal taper ratio is $\lambda_{opt} = 0.45$ [48].

A dihedral angle of $\Gamma = 1^\circ$ has been chosen from a statistical relationship in [61]. In Chapter 12 it is shown that all stability and controllability requirements are met without the need to modify the dihedral.

The aspect ratio is the crucial design parameter. Sensitivity analysis showed that it strongly affects the weight of the aircraft which in its turn affects the cost. Going beyond 17 the aspect ratio actually increases the weight of the aircraft however it is needed to decrease the required thrust that the engine has to provide at altitude. The engines can provide up to 880 N of thrust at service altitude, represented by the orange line in Figure 9.1. This leads to the optimum aspect ratio of 18.75. Conservatively, the aspect ratio of 19.5 has been chosen to provide more thrust range at altitude.

9.2.1. Oswald factor

The Oswald efficiency factor, e , is a measure of the aerodynamic efficiency of the aircraft. It is an important parameter as it plays a significant role in the induced drag, and thus the required thrust and fuel burn. This section presents an estimation for this parameter based on the method proposed in [57].

The method is based on computing a theoretical value for e based on the aspect and taper ratios, using (9.2), and then adding corrections for the fuselage, parasite drag, and compressibility effects using (9.4), (9.5), and (9.6). Applying this method at the high cruise condition, which corresponds to the most fuel-intensive phase of the mission profile, yields a result of $e = 0.64$. This is lower than the assumed value of $e = 0.7$ taken for the fuel budget generation. This calculation was done at a late stage of the design process so its effect was not considered in the sizing of the aircraft. Referring to the sensitivity analysis concerning the fuel burn shown in Table 7.4, it is evident that the Oswald efficiency factor is the parameter with the least effect of those considered. Reductions in C_{D_0} or an increase in M could offset the effect of losing some efficiency.

The effect of this change is accounted for in the detailed flight profile calculations in Section 13.1 and in the rest of Chapter 13.

$$e_{\text{theo}} = \frac{1}{1 + f(\lambda - \Delta\lambda)A} \quad (9.2)$$

$$e = \frac{k_{e,M}}{Q + P\pi A} \quad (9.3)$$

$$Q = \frac{1}{e_{\text{theo}}(1 - 2\left(\frac{d_F}{b}\right)^2)} \quad (9.4)$$

$$P = 0.38C_{D_0} \quad (9.5) \quad k_{e,M} = -0.001521 \left(\frac{M}{0.3} - 1\right)^{10.82} \quad (9.6)$$

It may be seen that this method only takes into account a limited number of design variables, namely A , λ and M . λ was selected to be 0.45 as suggested by [57] in order to minimize induced drag. The aspect

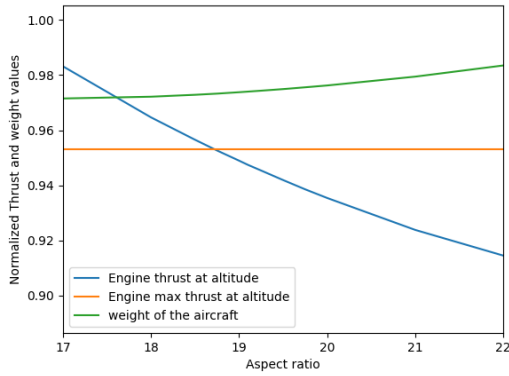


Figure 9.1: Aspect ratio optimization for weight

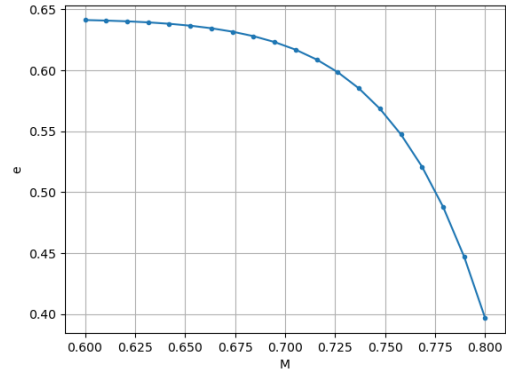


Figure 9.2: Variation of e with M

ratio was selected based on the discussion in Section 9.2. The Oswald efficiency factor is inversely proportional to A , meaning that larger aspect ratios carry an efficiency penalty with them in terms of the lift distribution over the wing. Assuming all variables are independent of each other and keeping the surface area of the wing constant so that $b = \sqrt{SA}$ it was found that $\frac{\partial e}{\partial A}|_{A=19.5} = -0.012$ meaning that increasing the aspect ratio by one lead to a reduction of 0.012 in e . This indicates that at high aspect ratios, the method is insensitive to fluctuations. The dependency of e to M can be seen in Figure 9.2. Evidently, increasing the Mach number leads to a sharp drop in performance. Therefore, a limit was set to $M < 0.7$ for maximum cruise Mach.

Verification & Validation

The method is straightforward so the entire verification was carried out by unit tests with hand calculations. No discrepancies were found within machine precision. Validation is difficult because the regressions used to determine the method are from airliners with significantly lower aspect ratios. In [57], the authors validate their method against an A320, as shown in Figure 9.3. The red and black lines match quite well, suggesting the method is accurate in that domain. It is recommended to use a high-fidelity CFD analysis to validate the result for our aircraft, given its distinct geometry. As a preliminary check data from [80] for a strut-braced wing with an aspect ratio of 19.5 may be seen in Figure 9.4. This polar was obtained using VLM software. By retracing the polar for $M = 0.8$ a value of $e = 0.2$ was found as opposed to the predicted value using Nita’s method: $e = 0.25$. This is a difference of 25%, which is significant. It is therefore likely that at high aspect ratios, the method loses applicability. However, due to a lack of a computationally cheap method for conceptual design, it will remain the chosen approach. A further caveat is that VLM software is not reliable for high Mach numbers, so the polar may be inaccurate.

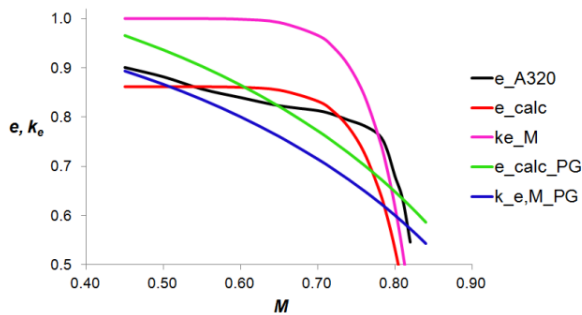


Figure 9.3: Validation of Oswald efficiency factor against A320 data

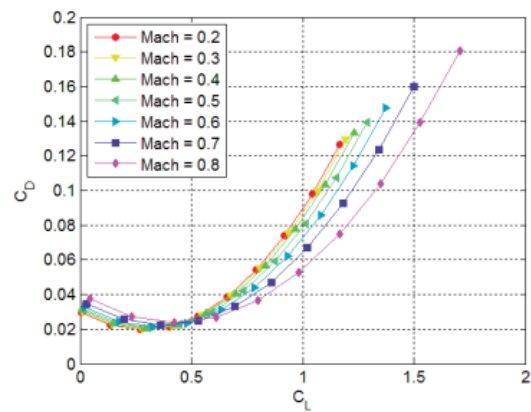


Figure 9.4: Drag polar for NASA strut-braced wing concept

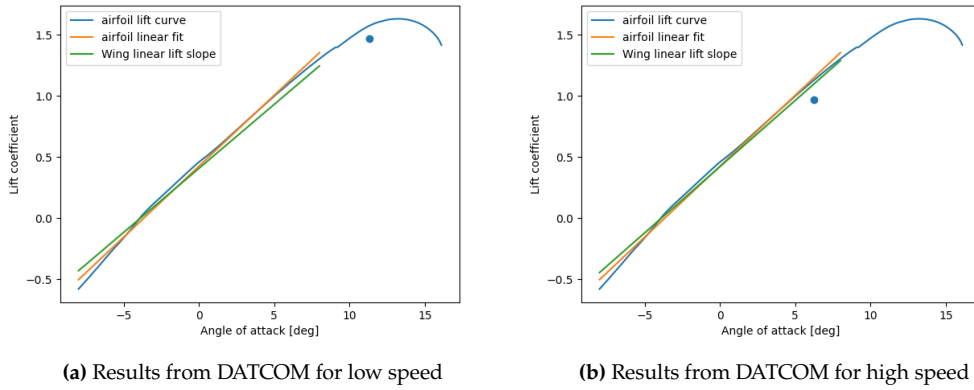


Figure 9.5: DATCOM results

9.3. Wing characterization

9.3.1. DATCOM method

Due to the geometry of the wing, airfoil characteristics do not fully translate to the real case and measures must be taken in order to ensure proper understanding of the aircraft capabilities. In order to convert airfoil characteristics to wing characteristics, a DATCOM [82] method is used. This method yields the lift slope $C_{L\alpha}$, the maximum lift coefficient C_{Lmax} and the stall angle of attack α_{stall} for the wing. This method mainly involves adding correction terms to 2D airfoil calculations with wing planform input.

9.3.2. Vortex Panel method

The aerodynamic characteristics of both 2D and 3D wing of ESRA are also determined by using the Vortex Panel Method with XFLR5 software. The wing planform analysis result is shown in Table 9.3. There are certain limitations of this method as offered in XFLR5. First, the analysis result of lift slope only includes the nonlinear part of close to stall angle of attack for 2D airfoil analysis but not for the 3D wing. Second is its' deficiency in simulating viscous effects. An interactive boundary layer loop couples the change in geometric shape due to boundary layer and flow properties to satisfy both potential and viscous flow models which are not available on the software [22].

For the analysis of control reversal speed which is explained in Chapter 11, the same method in XFLR5 is used. The chordwise position where the aileron begins as sized in Chapter 12 are used as input. The part of the airfoil aft of this position is then deflected by increasing angle of attack which produces a higher lift of the airfoil. Since only a 2D analysis can be done for this setup, this method leads to a $C_{L\delta}$ value that is higher than what the wing can achieve. This is mainly attributed to three reasons, first; the lack of 3D wing effect, second; the fact that ailerons do not run through the entire span of the wing, and lastly due to the flow disturbance caused by the deflection mechanism of the ailerons. Depending on the design of the ailerons, an optimized design may be able to energize airflow over the ailerons and minimize performance loss.

9.3.3. Wing analysis results

Using the inputs given in Table 9.2, the lift slopes described in Table 9.3 and Figure 9.5 are obtained. The DATCOM method was run for both high and low speeds. Two points can be noted, first, the maximum lift coefficient and the stall angle of attack both decrease considerably at higher speeds due to compressibility effects

Parameter	A	Λ	M_s	M_h	$\frac{S_{exp}}{S_{ref}}$	d	b	α_0
Value	19.5	0	0.15	0.65	0.95	1.1	24	-3.9

Table 9.2: Input values for the DATCOM method

Furthermore, it was found that at a design lift coefficient for the wing of $C_{L_{des}} = 0.77$ the design lift coefficient of the airfoil would be $C_{l_{des}} = 0.86$ which corresponds to a drag divergence Mach number of $M_{DD} = 0.73$.

9.4. Wing optimization

Since the aircraft will be cruising at Mach numbers of 0.7 or less, local airflow velocity around the wings is not expected to reach drag divergence Mach number, which is why no wing sweep is introduced as it will decrease lift coefficient. The remaining parameters that can be used as input to optimize wing design are mainly the taper ratio, aspect ratio, and twist distribution of the wings. The optimization results are in Table 9.4, the optimization process was as follows:

A modified version of Prandtl’s lifting line theory takes wing input and computes C_L and C_{D_i} . Using this method, the lift and drag coefficient without any optimization is in the second column of Table 9.4. Upon further derivations, the method can also be used to compute an optimal total twist Ω to minimize induced drag given a certain aspect ratio and linear taper ratio. Keeping the taper ratio and aspect ratio constant, an optimized total twist of 4.451 was obtained, and an induced drag coefficient of 0.0085.

Table 9.4 shows that the single DOF optimization improves and reduces drag by 2.8% by introducing approximately 4.45twist from wing root to wing tip.

	Airfoil (XFLR5)	Wing (DAT-COM, fast)	Wing (DAT-COM, fast)	Wing (XFLR5)
C_{L_α}	0.116	0.105	0.105	0.099
C_{L_0}	0.4597	0.459	0.459	0.361
$C_{L_{max}}$	1.63	1.46	0.96	-
α_s	13.2	11.3	6.54	-
C_{mac}	-0.11	-	-	-0.72

Table 9.3: Wing analysis outputs

-	No twist	optimized twist (°)
Taper ratio	0.45	0.45
Aspect ratio	19.5	19.5
AoA	1.55424	-
C_L	~0.7234248	0.7234248
Ω (°)	0	4.451
C_{D_i}	0.008792	0.0085428

Table 9.4: Wing twist optimization input and results

9.5. Verification and Validation

XFLR5 is a well established and reliable software for preliminary aerodynamic analysis, thus, verification is mainly in ensuring that the input data into the software is correct. Similarly for the DATCOM method which consists of simple algebraic equations, calculations made with DATCOM are verified by comparison with manual computation.

To validate the results generated by XFLR5, analysis of the NACA 64₂215 airfoil has been conducted and its’ windtunnel data has been collected. The simulation input condition is set to that of the experimental condition, which has a Reynolds number of $6 \cdot 10^6$ [37]. A comparison of the values is shown in Table 9.5. Note that data provided in [37] are in the form of diagrams and specific data points have to be estimated and may have a slight numerical inaccuracy. As shown in Table 9.5, airfoil characteristics generated by 3D panel method in XFLR5 has a discrepancy of no more than 7.13% on average excluding C_{L_α} . Lift slope that XFLR5 predicts falls within the limit of 2π according to thin airfoil theory. From the Prandtl-Glauert rule in [6], aerodynamic coefficients are scaled by a factor of $\frac{1}{\sqrt{1-(M_\infty^2)}}$. A larger lift coefficient will result in lift slope that is steeper. It shows from this that the software may not be so accurate especially in the compressible flow regime.

9.6. Recommendations

Currently, the main tool used in aerodynamic analysis is the 3D panel method available on XFLR5, which is has no boundary layer interaction loop built within to accurately simulate viscous effects such as flow transition or unsteady flow behaviour. To progress further with ESRA’s design, simple CFD analysis should be conducted to obtain more detailed design data which can facilitate the

Table 9.5: Comparison of XFLR5 simulation results and windtunnel data of NACA 642215 [37]

	XFLR5	Windtunnel data	%difference
$C_{L\alpha}$	6.1744	9.74	-36.6
$C_{L_{max}}$	1.479	1.55	-4.58
C_{L_0}	0.177	0.18	-1.67
α_0	-1.534°	-1.5°	2.27
C_{d_0}	0.006	0.005	20
C_{m_0}	-0.037	-	-

optimization of ESRA. It was shown that using a modified version of Prandtl's lifting line theory, induced drag coefficient can be optimized by introducing a total twist angle. Using the same theory, further improvements can be achieved by performing a multivariate optimization, however this this would require rigorous computation and appropriate constraints to be applied. For future design and optimization, a trade off will be needed to determine the fidelity of model to be used to take into account possible transonic effects. Other than this, further optimization should also be coupled with other major design groups such as structures and propulsion to prevent adverse effects on other subsystems due to aerodynamics optimizations.

Apart from the wings, the connections between the wings, strut connections and engines will also be a subject of investigation. The aerodynamic forces of the strut may generate a certain amount of lift which is beneficial but may upset stability balance of the aircraft. The drag caused by the interference drag of these components can also affect the overall performance of ESRA. These effect would require models with higher complexity which is out of scope of this report but will be investigated in future design phases.

Airfoil selection was performed in a relatively early stage of ESRA's design phase, at the time, the cruise Mach number was 0.7, which is just high enough to experience possible transonic effects which is why supercritical airfoils were preliminarily chosen for the trade off. Since then, the cruise Mach number as changed to 0.65 which means transonic effects are less likely to occur. Although the selected airfoil is still able to satisfy the performance requirements, it is recommended to expand ESRA's wing airfoil trade off in search for airfoil that better suit ESRA with the lowered cruise Mach number.

In flight the aircraft experiences many different load cases, all of which the aircraft has to withstand for a successful mission. This chapter covers the design of the wing box structure and wing strut. Section 10.1 covers the methodology of the wing box design process. Section 10.2 covers the design parameters and modelling methods of the wing box. Section 10.4 covers the assumptions, methods and tools used to model the wing box. Section 10.5 documents how the normal loads were implemented into the model. Section 10.6 discusses the loading diagrams that were obtained and the coordinate system used for shear, bending and torsion. Section 10.7 covers the methods used to perform failure analysis on the wing box structure, such as stringer buckling. Section 10.8 covers the wing box that was designed using the tool covered in this chapter. Finally, in Section 10.9 the recommendations and future planning considerations for the structures sub-systems are expanded upon.

10.1. Wing box design methodology

The design of a wing box structure contains many different steps that are shown in a flow diagram highlighting the wing box design methodology (Figure 10.1). The design of the wing structure started with the inputs from other sub-systems, such as the wing planform, airfoil and engine placement. From this a wing box design was generated as well as a strut design. The wing box design was fed into a Python script that calculated the cross-sectional properties along the span of the wing box, this also returned the fuel volume storage and wing box empty weight. The aerodynamic loading of the wing in the critical load cases was generated by using simulations in XFLR5,¹ an open source 3D wing modeling software based on Xfoil.² The aerodynamic loading and wing box model were fed into a Python script that calculated the shear, bending moments, and torque along the wing. The implementation of the strut element was done with an iterative method that found the compatibility between the displacement of the wing and strut. With the load calculations performed, a failure analysis was performed again with a Python script. This gave the deflection diagrams and Margin Of Failure (MOF) diagrams, which were used to see if the wing box design was feasible. Figure 10.1 displays the flow diagram of the design methodology described for the wing structure.

10.2. Wing box design parameters

The tool developed to model a wing box required several design parameters as input. This section will discuss these different design parameters and how they were modeled.

10.2.1. Load cases

The main design parameters around which a wing box is generated are the critical load cases. These load cases come from the flight envelope of the aircraft as well as ground operations. From this, limit load factors are obtained which are then multiplied by a factor of 1.5 to obtain the ultimate load factor, against which the wing box structure is designed to not fail structurally.

In accordance with Figure 10.1, the critical load cases should be extracted from the loading diagrams (Figure 10.2 and Figure 10.3) at operational empty weight and maximum take-off weight. The last critical load condition stems from ground operations. According to CS 23.473(a),³ the limit vertical inertial load factor may not be less than what would be obtained when landing. The landing speed is determined to be $1.23V_{stall}$, which resulted in a vertical inertial load factor of 1.3 during landing. This

¹URL <http://www.xflr5.tech/xflr5.htm> [cited 21/6/23]

²URL <https://web.mit.edu/drela/Public/web/xfoil/> [cited 21/6/23]

³URL <https://www.easa.europa.eu/en/document-library/easy-access-rules/easy-access-rules-normal-category-aeropla> 25/6/23]

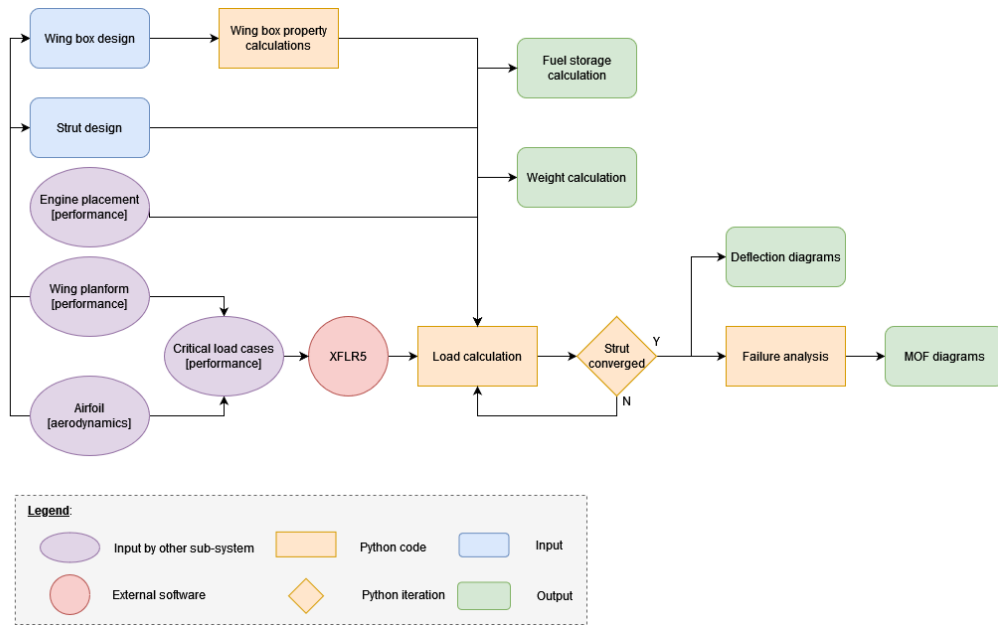


Figure 10.1: Flow diagram for wing structure design

is lower than what is specified in CS 23.437(g)³ and therefore a ground inertial limit load factor of 2 was taken. The most critical loads are then tabulated in Table 10.1.

Table 10.1: Key load cases examined for wingbox failure assessment

Load Case	Speed [m/s]	Weight	N_{max}	N_{ult}	Altitude[m]
1	53.26	OEW	-1.762	-2.643	FL000
2	77	OEW	4.4	6.6	FL000
3	69	MTOW	-1.62	-2.43	FL000
4	99.52	MTOW	4.4	6.6	FL000
5	0	MTOW	-2	-3	FL000

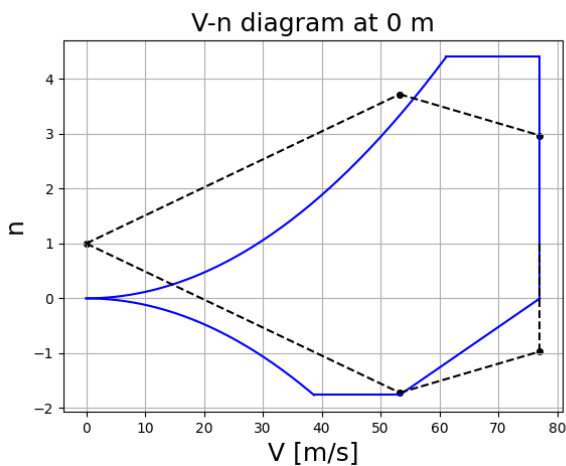


Figure 10.2: Loading diagram at operational empty weight

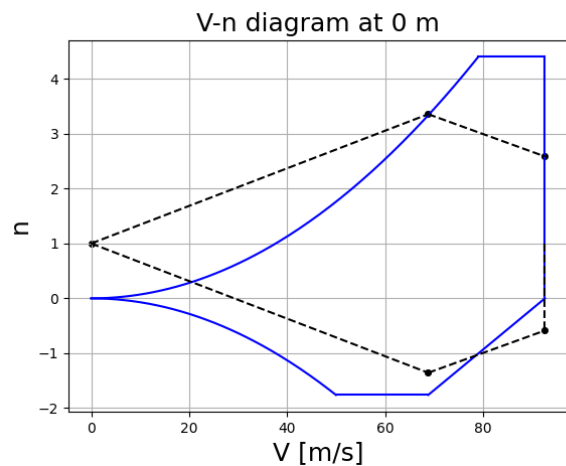


Figure 10.3: Loading diagram at maximum take-off weight

10.2.2. Cross-section Geometry

The cross-section of the wing box was modelled and designed with the following input parameters and assumptions. Firstly, the front and aft spar are located at 20% and 80% of the mean aerodynamic chord and have a defined thickness of 4 and 2 mm respectively. The top and bottom skin of the wing box follow the airfoil curvature and also have a defined thickness of 5 mm. This curved piece of skin

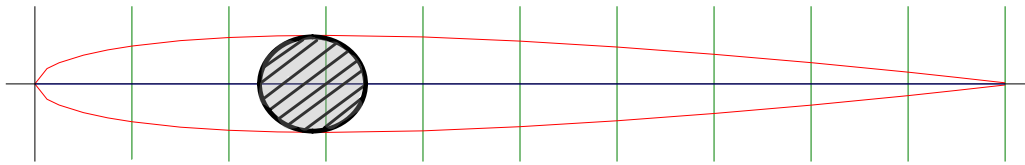


Figure 10.5: Cross-sectional view of the strut with NACA 0010 airfoil

is modelled with a finite amount of straight plates at angles such that they connect and follow the airfoil coordinates. Next, a specified amount of top and bottom stringers are evenly distributed over the top and bottom skin. In the model, the stringers are modelled as point areas with a local moment of inertia. Figure 10.4 shows how the cross section of the wing box was modelled as described.

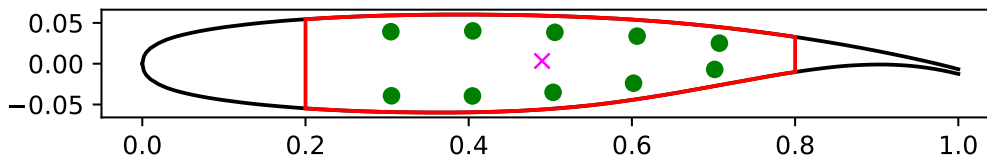


Figure 10.4: Cross section of wing box model. Stringer point areas indicated in green, wing box centroid indicated with a magenta cross, airfoil contour indicated in black and wing box skin indicated in red.

10.2.3. 3D wingbox design

Following from the definition of the cross-sectional geometry, the subdivision of the entire 3-dimensional wingbox should be evaluated. The wingbox can be split up into four general sections, and in each one of these the amount of top and bottom stringers are defined separately. This splitting up is performed so the wingbox design can adapt to the varying internal stresses along the wing.

The tool that was developed to determine the sectional properties of each point along the wingbox can accommodate for the stringers being continuous along the span of the wingbox, assuming that the ribs that are placed perpendicular they will have holes to allow the stringer to pass through them. The continuous stringers will allow for more effective load transfers and distribution of the loads more evenly across the skin.

10.2.4. Strut design

The proper placement of the strut is a crucial aspect of the wingbox design, as it serves as a significant structural element that limits deflections and reduces internal shear and bending stresses at the root of the wing. This, in turn, allows for additional weight reduction in the design.

The telescopic strut is modelled as a circular rod with a certain diameter. This rod is enclosed by a symmetrical airfoil of which the chord length is determined by setting the maximum thickness of the airfoil equal to the rod diameter. At this stage of the design the airfoil is assumed to be the NACA 0010 airfoil. A visual representation of the cross-section of the strut model can be seen in Figure 10.5.

The placement of the strut is defined as follows. The in-board connection point of the strut is attached to the bottom of the engine nacelle, as depicted in Figure 10.6. This was done as passing the strut through, in front or behind the engine was not seen as a viable option, deeming the shown design solution as best suited. The attachment point of the strut at the wing is determined by the outboard location set as a design parameter. These two inputs give as a result the strut angle, as is shown in Figure 10.6.

During the evaluation of the strut, a crucial assumption is made regarding its deflection behavior. It is assumed that the bottom attachment point of the strut will deflect in a similar manner to the engine, while the top attachment point will deflect along with the wing. This assumption considers the interdependence of the strut's behavior with the surrounding components. The resulting internal

tensile and compressive forces generated by this interaction will be fed back into the design tool for further analysis and iteration.

The strut braced wing allows for a bending moment relief in the wing structure. As the strut is a long slender member it's critical load case is buckling. This critical load case significantly increases the weight of the strut. To prevent this it was decided to implement a telescopic strut mechanism, which allows the strut to only carry loads in tension and be an inactive member when negative lift is produced [55]. In order to account for the movement of the strut a sleeve is fitted at the connection point in the engine.

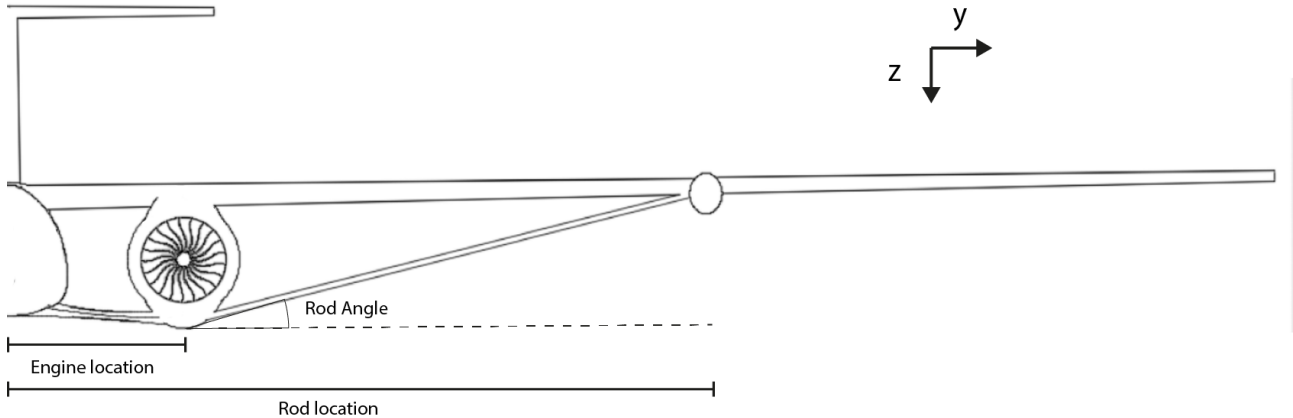


Figure 10.6: Front view of the aircraft showing the strut placement.

10.2.5. Stringer selection

For the stringer selection a multitude of stringers were considered. These and their properties are listed in Table 10.2. From this list of possible stringers the Z stringer shape was chosen. This was chosen because of the ease of manufacturing and inspection of the stringer type while also still performing well in specific moment of inertia ($\frac{I_{xx}}{A}$). In Figure 10.7 a cross section and the definition of the length and thickness of the stringer can be observed.

Table 10.2: Table presenting stringer properties

Stringer Geometries	Stringer properties							
	L	Z	J	C	U	I	POT	HAT
Area	2bt	2bt	$\frac{5bt}{2}$	3bt	3bt	3bt	3bt	3bt
y centroid	$\frac{b}{4}$	$\frac{b}{2}$	$\frac{2b}{5}$	$\frac{b}{2}$	$\frac{b}{3}$	$\frac{b}{2}$	$\frac{b}{2}$	$\frac{b}{2}$
I_{xx}	$\frac{5b^3t}{24}$	$\frac{b^3t}{3}$	$\frac{13b^3t}{30}$	$\frac{7b^3t}{12}$	$\frac{11b^3t}{36}$	$\frac{7b^3t}{12}$	$\frac{5b^3t}{12}$	$\frac{5b^3t}{12}$
$\frac{I_{xx}}{A}$	$\frac{5b^2}{48}$	$\frac{b^2}{6}$	$\frac{13b^2}{60}$	$\frac{7b^2}{24}$	$\frac{11b^2}{72}$	$\frac{7b^2}{24}$	$\frac{5b^2}{24}$	$\frac{5b^2}{24}$

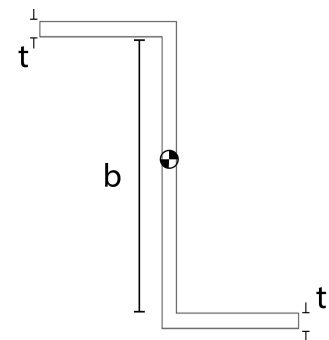


Figure 10.7: Cross-sectional view of the Z-stringer

10.3. Material selection

At this stage of the design, it was known that the critical parts of the aircraft, such as the wing box, were to be produced out of aerospace grade aluminum alloys. This was done for several reasons. Firstly, composite materials typically have an-isotropic materials and therefore their behaviour is harder to model, this in turn increases development costs and time and also operational issues such as being observed on the Boeing 787 program.⁴ Certification of these novel materials in critical structural components such as the wing or strut also are significantly higher compared to more conventional

⁴URL <https://www.technologyreview.com/2008/04/18/34770/boeings-composite-problem/>[cited 21/6/23]

materials such as aerospace grade aluminum [70]. This section will cover a more detailed material selection for the wing structure, strut structure and the fuselage structure.

10.3.1. Material selection

For the structure of the aircraft, several materials have been listed as viable for different part of the aircraft. These are listed in Table 10.3. All of the selected materials are aluminium alloys, only differing in alloy composition and treatment. This choice was made to accommodate a minimal material cost while also keeping the tooling cost down. As an added bonus, certification, inspection and maintenance will be more simple as well. Different alloys will be chosen for different parts of the aircraft as tensile strength and fatigue strength differ between them, and this difference in properties will make them suited for certain applications and less so for other parts of the structure.

Table 10.3: Material types and properties considered for the wing and strut material

Material name	Density [kg/m^3]	Ultimate tensile strength [MPa]	E [GPa]	Fatigue strength [Mpa]	Price [$$/m^3$]
AL6061-T6 ^{5,6}	2700	310	68.9	96.5	71550.34
AL7075-T6 ^{7,8}	2800	572	72	159	92806.94
AL2024-T3 ^{9,10}	2780	483	73.1	138	94925.82
AL7050 ^{11,12}	2700	552	71.7		161950.24

Strut material selection To determine what type of material is best suited for the strut, its function has to be analysed. As the strut uses a telescopic mechanism which allows it to only carry tensional loads, it's main load case will be high axial stress. Therefore the main material property needed for the strut is a high yield strength and E-modulus. The strut compared to other parts such as the wing box has relatively low mass and production complexity, therefore the cost of the material has less of a priority. For this purpose, aluminium 7075-T6 was found to be the best match with these requirements, featuring a high E-modulus and the highest tensile stress of the selected materials.

Wing box material selection In similar fashion as the strut, the loading case of the wing will first be considered to make a well-informed decision about the material to be used. As the wing box has to deal with mainly bending loads, due to the deflection caused by the lift force. As these forces can fluctuate during the flight, and the wingbox is arguably the most important component to ensure structural integrity on, a combination of high tensile strength and high fatigue strength is required. Additionally, the E-modulus should not be too low, as deflection in a wing box negatively affects the performance of the wingbox and the aircraft as a whole. Taking this situation into consideration, the material with the best properties for the job would again be aluminium 7075-T6. The combination of high tensile strength, Young's modulus and fatigue properties make it the preferred choice. On top of that, making use of fewer different materials will make production of different components more straightforward as less different machines and processes are needed. Large quantity discounts could also be better negotiated this way.

Fuselage material selection For the fuselage, the situation is different than for the wingbox and strut. The loads that will be carried by body panels are pressure loads for the pressurized section of the

⁵URL https://www.matweb.com/search/datasheet_print.aspx?matguid=1b8c06d0ca7c456694c7777d9e10be5b [cited 19/6/23]

⁶URL <https://store.buymetal.com/aluminum-plate-6061-t6-t651-0.5.html> [cited 23/6/23]

⁷URL <https://www.matweb.com/search/DataSheet.aspx?MatGUID=4f19a42be94546b686bbf43f79c51b7d> [cited 20/6/23]

⁸URL <https://store.buymetal.com/aluminum-sheet-7075-t6-bare-0.05.html> [cited 23/6/23]

⁹URL <https://www.matweb.com/search/DataSheet.aspx?MatGUID=57483b4d782940faaf12964a1821fb61> [cited 19/6/23]

¹⁰URL <https://store.buymetal.com/aluminum-sheet-2024-t3-0.05.html> [cited 23/6/23]

¹¹URL <https://www.matweb.com/search/datasheet.aspx?matguid=a8298bba8d02486c97c06990a3c215d9> [cited 19/6/23]

¹²URL <https://store.buymetal.com/aluminum-plate-7050-t7451-0.5.html> [cited 23/6/23]

aircraft, and will in general be not as high as for the other parts of the structure. Critical points for the pressurization will be extra reinforced, and in sections with the sharpest radii, in the front and rear of the cockpit, additionally reinforced bulkheads will be installed. This also means that the material that can be used for these sections does not have to be as strong as the wingbox or strut, and fatigue is less of a problem as well. As body panels make up a large portion of the aircraft, attention can be shifted towards weight saving and the minimization of cost. This is why aluminium 6061-T6 will be used for the fuselage. It is significantly cheaper than the other options while also weighing the same or less. As the material is still aluminium, the overall decrease in strength is not extreme, so thinner panels can be used, preferably formed by cheap and efficient processes such as rubber forming, even further reducing the production cost of the aircraft.

10.4. Wing box modelling

For the assessment of the internal stresses of the wingbox and to evaluate its performance, a tool was developed that evaluated the wingbox by subdividing it into finite sections.

10.4.1. Lower wing modelling

The analysis of the wing structure was made with the assumption that the lower wing does not act as a structural member and does not carry any force. In practice, the assumption is incorrect. However, the addition of the lower wing will add stiffness to the total wing structure and therefore it was decided that not including the stiffness of the lower wing would only lead to a more conservative wing box design of the upper wing structure.

10.4.2. Moment of Inertia calculations

Each section has accompanying properties such as a centroid location and a moment of inertia. From Subsection 10.2.2, it was explained how by utilizing a set of data points that represent the airfoil shape, the spacing between stringers was computed based on the desired number of stringers. The centroid of the stringers is then determined by finding the average location in both the x and y directions, considering the the stringers as point areas with a local moment of inertia.

The centroid of each airfoil part is then calculated to assess the contribution of the plate thickness to the overall centroid of the wingbox. As the plate thickness varies between the top and bottom surfaces of the airfoil, the x and y coordinates of the centroid are determined by considering the plate thickness and the midpoint of each line segment connecting consecutive data points.

The moment of inertia is calculated by revisiting the collection of data points representing the airfoil shape, and treating the wing box plates as elements of finite rectangular plates under a certain angle. Together with the added effect of the stringers, this yields the moment of inertia for every cross-sectional area within the segmented wingbox.

Verification section property calculations To verify the calculations made in the tool on every cross-section, hand calculations were performed on a simplified cross-section. This cross-section was a rectangular wing box with top, bottom plates and aft spar having a thickness of 1 mm. With the front spar being 2 mm in thickness. This cross section also included 2 stringers on the top and bottom and it's cross section is shown in Figure 10.8. The results from the tool and hand calculates are summarized in Table 10.5. No significant deviations were found and therefore this code was deemed verified.

Table 10.4: verification table

Property	Hand calculation	Numerical	Difference %
x_{cg}	0.42038	0.42062	0.05 %
y_{cg}	0.0000	0.0000	[-]
I_{xx}	0.0010703	0.0010442	0.024 %
I_{yy}	0.00089982	0.0009117	0.013%
I_{xy}	0.00	1.694e-20	[-]
J	0.001970120	0.0019755	0.27%

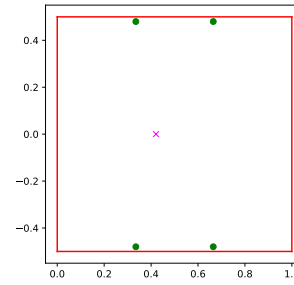


Figure 10.8: Cross section of the rectangular example wing box

10.4.3. Elastic axis determination

Due to the minimal sweep angle of the wing, the elastic axis (EA) of the wing is assumed to coincide with its shear center (SC). The definition of SC is the point where the rate of twist is zero when a shear load is applied [50]. Since the wing box is the main load-bearing structure, the SC of the wing box is calculated which excludes the LE and TE portion of the airfoil. The shear center of the wing box is calculated by first discretizing the wing box and lumping its components into boom areas, as the input file already had the contour of the wing skin plates split into finite small plates this was also used to make a line of small boom areas. At locations where stringers were present the stringers area was added to the boom area, an example of this discretization on the wing box can be seen in Figure 10.9. As a closed section is considered the second step is to split the structure at an arbitrary point along the perimeter. This makes it possible to define a basic shear flow q_b and an unknown closed section shear flow [50]. Here it was assumed that only a vertical shear force V_y acts on the airfoil, resulting in the assumption that the vertical location of the shear center coincides with the vertical location of the cross-sectional centroid. The increment of q_b over a boom area is subsequently calculated using (10.1)[50]. With q_b calculated over the wing box perimeter q_{s0} can be calculated using (10.3). The last step is to use the fact that there should be no rate of twist if a shear force is applied at the SC, which means the sum of moments due to any shear force and internal shear flow of the structure about the SC should be zero. To do this a moment equivalency equation between the moment caused by shear flow and moment caused by shear force of a shear force V_y a distance ξ from a reference point, in this case, the LE of the local cross-sectional airfoil. The moment caused by the shear flow between two boom areas is calculated using the moment (10.2). Where A_{12} is the area enclosed by the two boom areas and the centroid[52]. This is then integrated over the perimeter to get the total moment M_q . The SC is then determined by using (10.4).

$$\Delta q_b = -\frac{V_y I_{yy}}{I_{xx} I_{yy} - I_{xy}^2} [B_r y_r] + \frac{V_y I_{xy}}{I_{xx} I_{yy} - I_{xy}^2} [B_r x_r] \quad (10.1)$$

$$\Delta M_{12} = 2A_{12}q_{12} \quad (10.2)$$

$$q_{s0} = \frac{\oint \frac{q_b}{t} ds}{\oint \frac{1}{t} ds} \quad (10.3)$$

$$V_y \xi = M_q \quad (10.4)$$

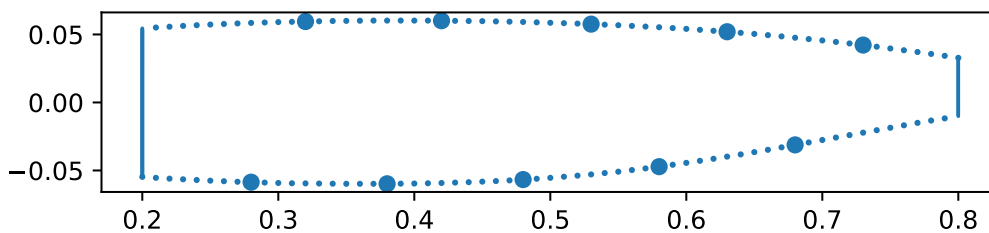


Figure 10.9: boom area model for shear center calculations, blue dots indicating the boom x_r areas and their respective area in size

Verification shear center calculation Two forms of verification on the shear center calculation were performed. The first test example was with a rectangular wing box with an equal thickness of one millimeter, dimensions of one by one meter, and no stringers attached, of which hand calculations showed that the shear center should be at the half chord position. The second example was also a rectangular wing box but with a two-millimeter front spar instead of 1 millimeter. Table 10.5 summarizes the verification of the shear center calculation tool.

example	analytical [m] result	numerical [m] result	difference [%]
equal thickness rectangle	0.5	0.4999999	< 0.1
unequal thickness rectangle	0.349	0.352	<1

Table 10.5: Verification results shear center calculation

10.5. Normal Loading

It is important for the wingbox design to determine the forces that are applied normally to the wing box, as vertical loading is the main focus of the analysis as it is most likely to cause wing deflection. If the wing can handle vertical loading and the associated bending stresses, it can also tolerate horizontal loading to some extent.

10.5.1. Aerodynamic Loading

Initially, it is necessary to find the velocity field of the airflow around the wing and convert it into a pressure distribution. This allows for the calculation of pressure coefficients and the determination of aerodynamic forces. To simplify the analysis, drag and lift forces, along with a pitching moment, are commonly used. The XFLR5 tool, which utilizes the 3D Panel Method, is employed to aid in this process. It requires the wing’s external geometry as input and assumes an inviscid and incompressible airflow with a free stream velocity of 10 m/s. The tool provides results for two angles of attack (0 and 10 degrees), including lift and drag coefficients, pitching moment coefficients, and the spanwise distribution of coefficients.

When using XFLR5, the tool will provide the lift coefficient (C_l), drag coefficient (C_d), and pitching moment coefficient (C_m) for each section of the airfoil. However, these exported results are available only for angles of attack $\alpha = 0^\circ$ and $\alpha = 10^\circ$. To determine the aerodynamic force distribution for other lift coefficients, it is necessary to consider the load cases, which specify the load factor n , weight W , free stream velocity V_∞ , and density ρ (which is dependent on altitude). By taking these factors into account, the desired lift coefficient can be directly derived.

Following this it would be preferred to determine the desired lift distribution over the wing as a function of the span (y) of the aircraft. Which follows from performing a linear interpolation and is presented in (10.5). Here $C_{L_d}(y)$, $C_{L_0}(y)$ and $C_{L_{10}}(y)$ are the spanwise lift distributions for the load case, 10-degree angle of attack and 0-degree angle of attack, respectively. $C_{L_{10}}(y)$ and $C_{L_0}(y)$ are obtained from the XFLR5 data. The corresponding angle of attack can be calculated through $\alpha = \frac{C_{L_d} - C_{L_0}}{C_{L_{10}} - C_{L_0}} \cdot 10^\circ$. Where C_{L_d} is the calculated wing lift coefficient for the specific load case. $C_{L_{10}}$ is the wing lift coefficient at 10 degrees angle of attack and C_{L_0} is the wing lift coefficient at 0 degrees angle of attack.

$$C_{L_d}(y) = C_{L_0}(y) + \frac{C_{L_d} - C_{L_0}}{C_{L_{10}} - C_{L_0}} (C_{L_{10}}(y) - C_{L_0}(y)) \tag{10.5}$$

The distribution of $C_{D_d}(y)$ (drag coefficient) and $C_{M_d}(y)$ (pitching moment coefficient) across the wing can be obtained using a similar procedure. To find the normal component, the lift, drag, and pitching moment distributions can be obtained by multiplying the coefficients by the free stream dynamic pressure Q_∞ and a term that describes the chord ($c(y)$). The normal force distribution can be derived by summing up the vertical components of all aerodynamic forces.

$$L(y) = C_L(y)Q_\infty c(y) \quad (10.6) \quad D(y) = C_D(y)Q_\infty c(y) \quad (10.7) \quad M(y) = C_M(y)Q_\infty c(y)^2 \quad (10.8)$$

10.5.2. Inertial loading

By dividing the wing box into finite sections and analyzing the cross-sectional areas, it becomes possible to determine the wing weight. This can be achieved by selecting specific materials for the skin and stringers and calculating the mass per length or distributed loading. However, it's important to note that wing weight is not the only inertial loading factor. The weight of the fuel also plays a significant role.

To accommodate the required amount of fuel, a conceptual fuel tank design has been incorporated in the wing box model. This fuel tank starts from the root of the wing and stops until the required amount of fuel is filled. This assumes that the entire closed area is occupied by fuel. Similar to the distributed structural weight, the fuel weight is expressed as a mass per unit length. This value can be multiplied by a percentage that represents the remaining fuel in the tanks. This percentage was also made an input of the structural analysis code as some critical load cases included zero fuel situations.

10.5.3. Strut and engine loading

The ESRA aircraft configuration has a significant feature where both the engine and strut are attached to the wing, as depicted in Figure 10.6. This arrangement directly influences the internal loading and deflection of the wing tips. These loads are represented as point loads, causing discontinuities in the shear loading diagram.

When it comes to the strut, the force discontinuity arises due to its linear-elastic behavior. The initial displacement of the wing and the engine determines the overall deflection of the strut, as indicated in Subsection 10.2.4. Consequently, the tension in the strut pulls down the wing, affecting its deflection. This inter-dependency between deflection and strut tension necessitates an iterative process that runs until the modeled deflection of the rod meets the calculated distance between the mounting points of the rod.

10.6. Loading diagrams

Once the wing box geometry has been established, discretized, and analyzed, the next step is to generate the internal loading diagrams. These diagrams serve as the foundation for determining the internal stresses, which will be compared against the critical stress values corresponding to specific failure modes and load cases. The process of determining the internal loading involves integrating the distributed aerodynamic and inertial loading discussed earlier.

10.6.1. Coordinate system

Before delving into any meaningful analysis of internal forces and moments, it is essential to initiate a discussion about the coordinate frame. The signs portrayed in the shear and moment diagrams hold significant sway over the failure modes observed. For example, determining whether bending induces compression or tension in the top and bottom plate plays a crucial role in influencing buckling performance. The coordinate system utilized in this context is outlined in the following Figure 10.10.

10.6.2. Shear and moment loading diagram

The impact of the strut on the internal shear and moment loading diagrams is depicted in the subsequent pair of figures, Figure 10.11 and Figure 10.12). The presence of the strut is evident from the considerable decrease in the root internal shear force and root internal moment. There is a slight discontinuity located just below 8m, which represents the strut exerting a pulling force on the wing box at that specific location. Additionally, a discontinuity can also be observed at a distance of 1.8m due to the engine. This discontinuity is observable in both diagrams, but it becomes more pronounced in the strut diagram due to the reduced shear forces caused by the strut.

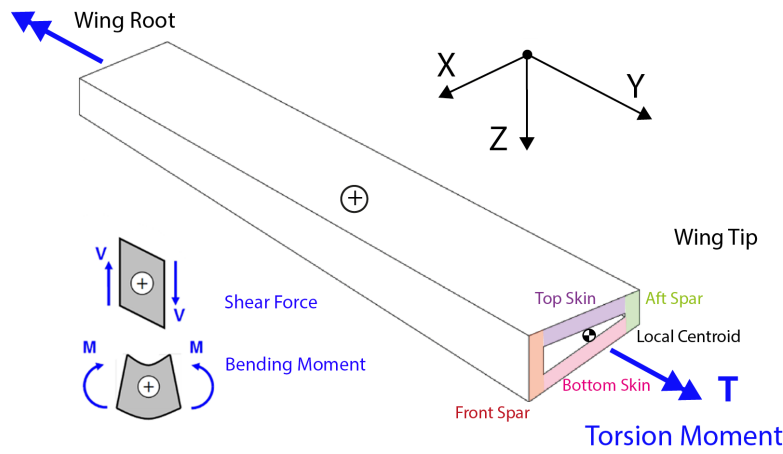


Figure 10.10: Definition of the wing box coordinate system

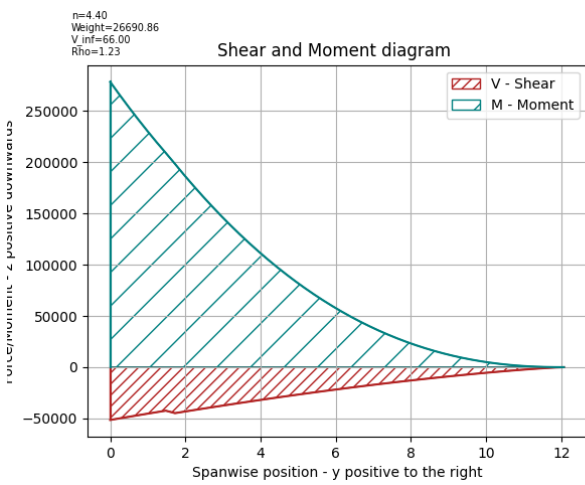


Figure 10.11: Shear and moment diagram without the strut applied

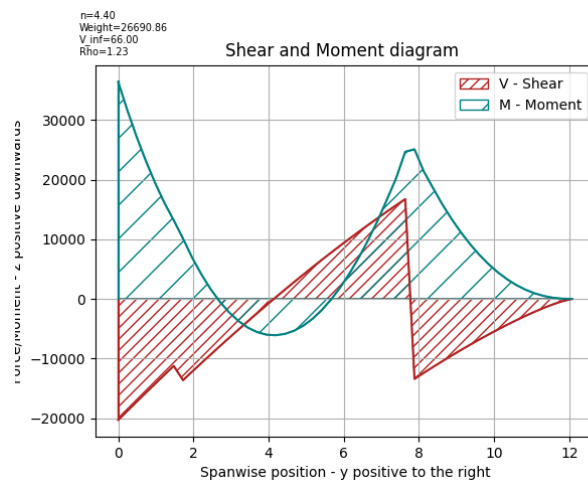


Figure 10.12: Shear and moment diagram with the strut applied

10.6.3. Deflection diagram

Continuing from the shear and moment diagram, by utilizing the information provided in Equation 10.9 and considering the wing box properties at each section, it becomes possible to calculate the deflection in both the strut and strut-less wing boxes. The outcomes for each case are displayed in Figure 10.13 and Figure 10.14. These figures illustrate a significant reduction in deflection for the wing box with the strut, aligning with the decreased internal loads. Notably, the deflection reaches a plateau around the location of the strut and subsequently increases towards the beam, where the wing box resumes its behavior similar to a cantilever beam. Do note that the proper way to interpret the graph in accordance with the sign convention is from right to left.

10.6.4. Torsion and angle of twist diagram

Moving forward, an analysis was conducted on the internal torque and the corresponding angle of twist. It is important to note that in this scenario, the presence of the strut has no additional impact on the diagrams, as the observed discontinuity is solely attributed to the offset between the engine's center of mass and the wingbox's center of mass. To maintain consistency with the chosen sign convention, the graph should once again be read from right to left. It is worth mentioning, as evident from Figure 10.17, that while the engine's contribution to the shear force diagram remains relatively limited, it generates a sharp increase in torque. Therefore the associated angle of twist, given in radians in Figure 10.18, is also fairly limited. The angle of twist of the wing box can then be calculated by calculating $\frac{d\theta}{dy}$ with equation (10.10) [51]. Where A_m is the local enclosed area of the wing box. This local variable is then integrated along the span to get $\theta(y)$.

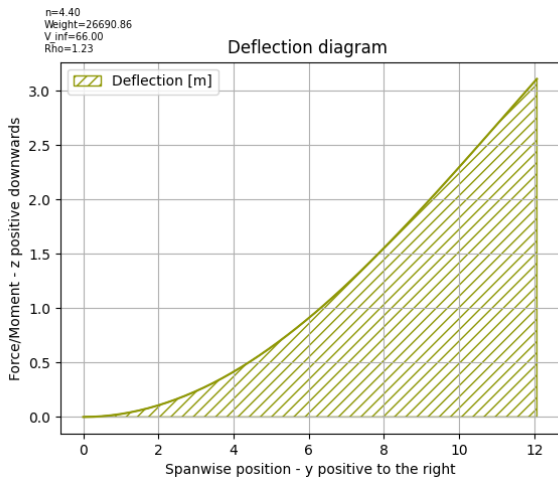


Figure 10.13: Deflection diagram without the strut applied

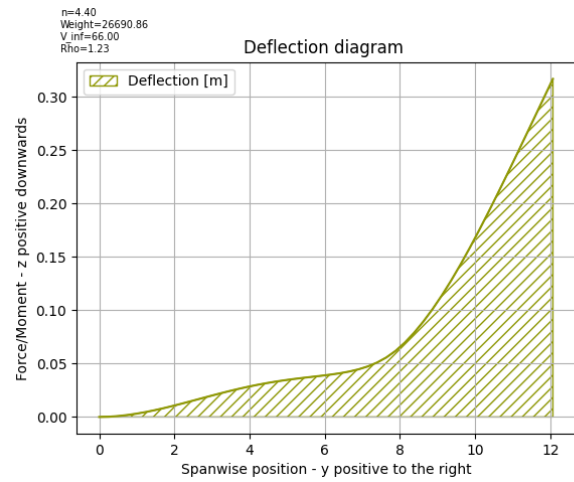


Figure 10.14: Deflection diagram with the strut applied

$$\frac{dv^2}{dz} = \frac{M(z)}{EI_{xx}(z)} \quad (10.9)$$

$$\frac{d\theta}{dy} = \frac{T}{4A_m^2 G} \oint \frac{1}{t} ds \quad (10.10)$$

10.6.5. Verification loading diagrams

For the verification of the loading diagrams a simplified beam model of a rectangular wing box with a constant chord and a length of ten meters. The cross-section taken was the same as the one used for the verification of the section property calculator seen in Figure 10.8. For the deflection calculation, a point force of 1000[N] was applied at the tip. For the torsion verification a point moment of 1000[nm] was applied at the tip. The results are summarized in Table 10.6. Additionally, verification by inspection for the loading diagrams themselves. The expected result was a constant shear force / torsion throughout the wing box. These results are shown in Figure 10.15 and Figure 10.16.

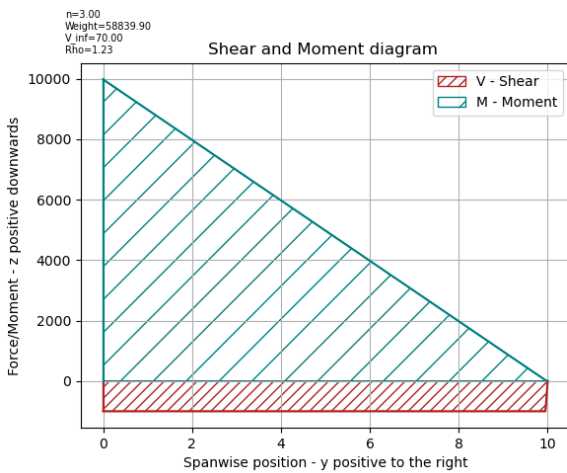


Figure 10.15: Shear and bending moment for verification load case

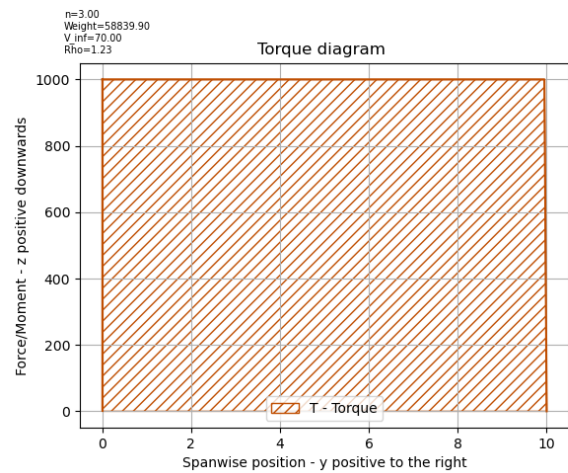


Figure 10.16: Torque for verification load case

[-]	Hand calculation	numerical result	difference
deflection at wing tip	0.0043667 [m]	0.0043010 [m]	1.5 %
angle at wing tip	0.017904 [°]	0.017874 [°]	0.1727%

Table 10.6: Verification loading diagrams with simplified rectangle wing box

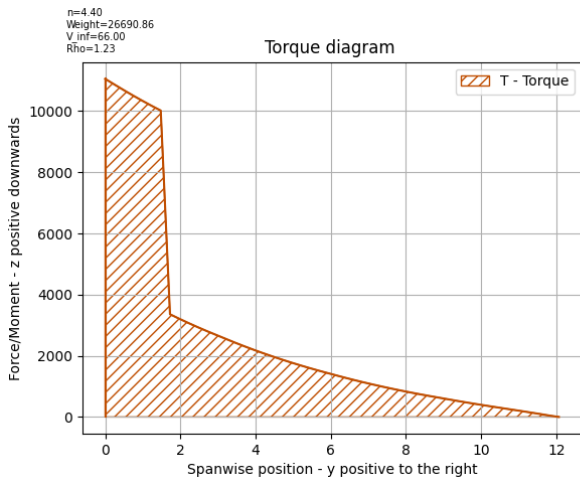


Figure 10.17: Torque diagram with the strut applied

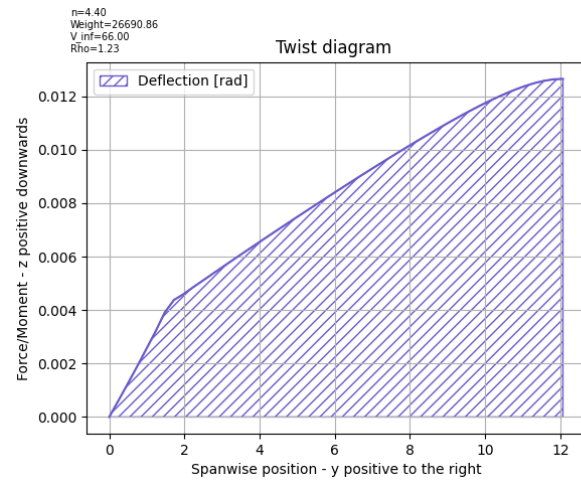


Figure 10.18: Twist diagram with the strut applied

10.7. Failure analysis

Finally in order to determine the validation of a given wing box configuration, a series of possible failure modes should be analyzed. The goal of this exercise is to compare the internal stress with the critical stress and to obtain the margin of safety (*MOF*) given by Equation 10.11, preferably this value is close to 1 but never goes below 1, as going below would imply failure. The internal stresses are determined at the critical loading conditions as specified in Subsection 10.2.1.

10.7.1. Spar buckling

Under shear load, the spar webs are susceptible to buckling. The governing equation is given by:

$$MOF = \frac{\sigma_{internal}}{\sigma_{critical}} \quad (10.11)$$

$$\tau_{crit} = \frac{\pi^2 k_s E}{12(1 - \nu^2) \left(\frac{t}{b}\right)^2} \quad (10.12)$$

Here, t represents the thickness of the spar, b denotes the short side of the plate, and k_s is a coefficient dependent on the plate aspect ratio (a/b). The aspect ratio of the plates is determined by the rib spacing, the placement of the ribs determines the value of a . The selection of the value of k_s was done based on Figure 10.22. It can be seen that the boundary conditions, meaning the way in which the edges of the spar pieces are clamped determine the rest of the wing box structure and determine the value for k_s . To ensure a conservative design approach and prevent premature failure of the wing box, the k_s values for hinged edges will be used. While it is not entirely certain whether clamped or riveted edges should be employed, the decision was made to go with the more critical scenario, which in this case is the hinged edges.

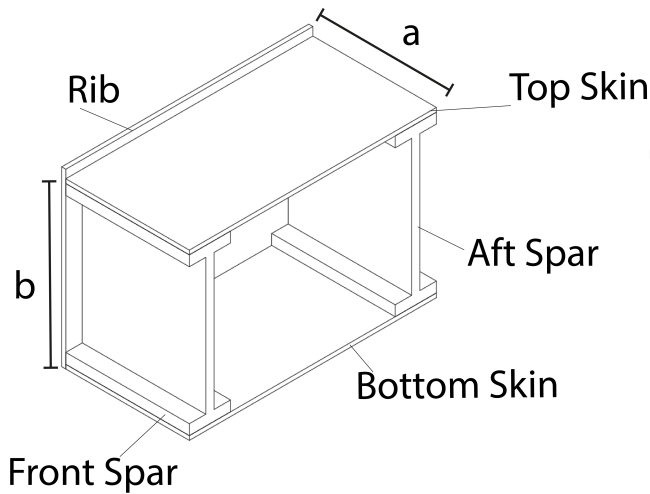


Figure 10.19: The selection of the values a and b for a generalized wing box section

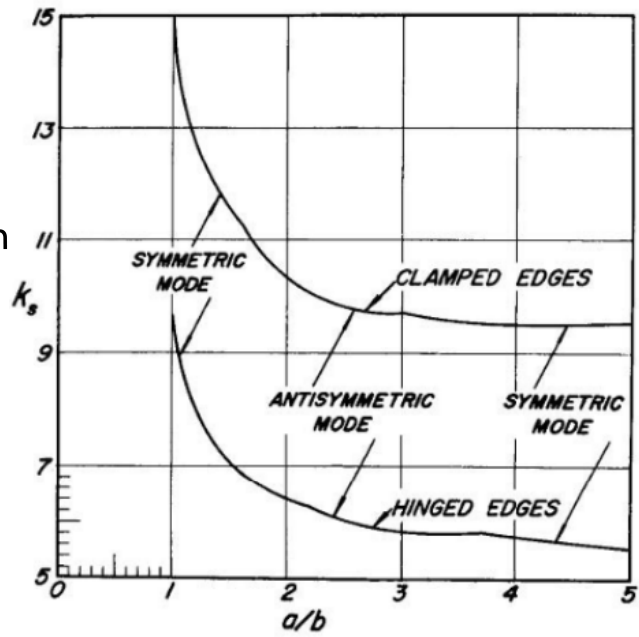


Figure 10.20: k_s values for different a/b ratios[11]

To streamline the analysis process, it is practical to make the assumption that the shear flow induced by the shear force is solely carried by the spar webs. Consequently, a simplification technique can be employed, which involves multiplying the average shear stress over the cross-sectional area of both the front and aft spar by a factor denoted as k_v , as can be seen in Equation 10.13.

$$\tau_{max, shear} = k_v \tau_{ave, shear} \tag{10.13}$$

$$\tau_{ave, shear} = \frac{V}{h_f t_f + h_a t_a} \tag{10.14}$$

Here, $\tau_{max, shear}$ represents the average shear stress in the spar webs due to the shear load, and $\tau_{ave, shear}$ is the average shear stress calculated using Equation 10.14. Where V is the internal shear force at the considered span-wise station of the wing (previously calculated in Figure 10.12), h_f is the height of the front spar, h_a is the height of the aft spar and t_f and t_a are the respective thicknesses of the front and rear spars. The shear stress due to torsion needs to be added to $\tau_{max, shear}$. The shear flow distribution due to torsion can be straightforwardly computed using (10.15)

Where A_i is the enclosed area of the wing box cross-section. Finally, the sum of the maximum shear stress due to the shear force and the shear stress due to torsion can be compared with the critical buckling stress.

10.7.2. Skin buckling

The primary failure mode for the wing skins is skin buckling. The governing formula for skin buckling remains the same as described in Equation 10.16 but with a different constant, k_c , as can be seen in Equation 10.16.

$$q = \frac{T}{2A_i} \tag{10.15}$$

$$\sigma_{cr} = \frac{\pi^2 k_c E}{12(1 - \nu^2)} \left(\frac{t}{b}\right)^2 \tag{10.16}$$

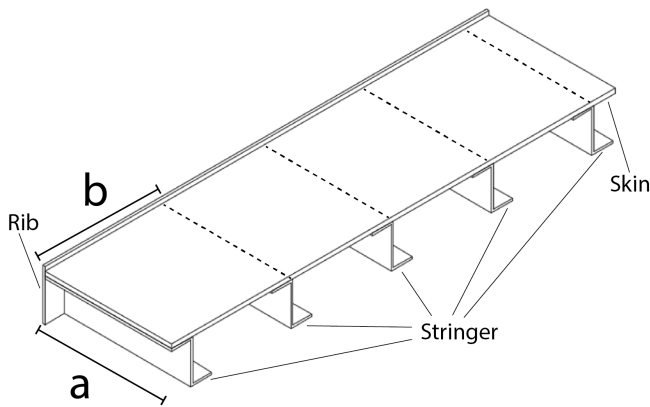


Figure 10.21: The selection of the values a and b for a generalized wing box section

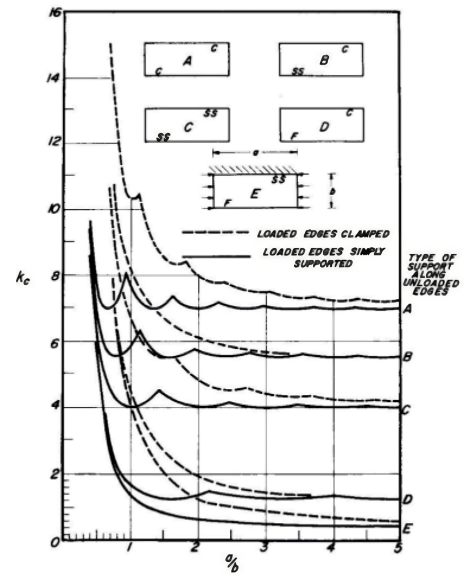


Figure 10.22: k_c values for different a/b ratios[11]

Figure 10.22 illustrates plots displaying various values of k_c for different support configurations. This value is associated with the type of support imposed on the skin and is dependent on the (a/b) factor of the panel under analysis. The value of b represents the distance between the stringers, and the value of a once again represents the length between sections separated by the ribs Figure 10.21.

Given the assumption that the wing skin will be attached to the stringers and ribs using rivets, an appropriate k_c line can be selected based on a rivet connection, as indicated in Figure 10.22. Among the options in Figure 10.22, case C represents the load case for the wing skin panel. In this figure, option C is depicted by a dashed line and a full line. The dashed line corresponds to simply supported edges, while the full line represents clamped edges. However, accurately determining the appropriate choice requires a deeper understanding of how rivets connect structures.

To simplify the analysis, it was assumed that the rivets allow for the skin panel to be simply supported. This assumption implies that the rivets support the skin panel while still permitting rotation of the skin. This choice was made because it will result in a lower k_c value, which, at worst, will underestimate the critical failure stress.

To determine the margin of safety, it is necessary to evaluate the actual internal stress on the skin. This can be achieved by utilizing the flexure formula for bending, as described in Equation 10.17. In this formula, z represents the distance from the centroid, M denotes the internal bending moment at the specific section, and I represents the moment of inertia of the section around the y -axis. By applying this flexure formula, the actual internal stress for the skin can be determined.

10.7.3. Column buckling

The stringers within the wing box can be treated as slender columns. During normal flight, some stringers, particularly those connected to the top plate, experience compressive loads. These stringers are susceptible to a failure mode known as column buckling.

Column buckling is a complex phenomenon compared to other failure modes, such as axial loading. While a detailed mechanical analysis is beyond the scope of this report, it is necessary to understand the physical nature of column buckling to make valid assumptions and select an appropriate calculation method.

However, analyzing the real-case scenario with all load variations and complexities is too challenging. Thus, a simplification is applied to analyze the buckling behavior of stringers analytically. It is assumed that all stringers are perfectly straight columns within the segmented parts of wing box and that the

effects of secondary loads (shear force, bending moment) can be neglected. Resulting in four different critical buckling stresses if the wing box is segmented into four sections, for both top and bottom stringers. Furthermore, even though the axial load is distributed, the stringer is treated as a column loaded with a point force at one end. This simplified case is shown in Figure 10.24.

Under these assumptions, the critical buckling stress can be determined using Euler’s formula for column buckling, Equation 10.18.

$$\sigma = \frac{Mz}{I_{xx}} \quad (10.17) \qquad \sigma_{\text{critical}} = \frac{K\pi^2 EI}{L^2 A} \quad (10.18)$$

Where E represents the elastic modulus, I is the moment of inertia of the stringer’s cross-section, and L is the length of the stringer. In this analysis, the length L is considered as the distance between two ribs, representing the length of a wing box section.

The coefficient K in the formula reflects the end conditions of the stringer, such as whether it is clamped, pinned, or free. The following values of K are assigned based on the end conditions:

- $K = 1$; both ends are pinned
- $K = 4$; both ends are clamped
- $K = 1/4$; if one end is fixed and the other end is free
- $K = 0.7$ or $K = 1/\sqrt{0.7}$; if one end is pinned and the other end is free

Since ribs provide stable fixed support for the stringers, $K = 4$ is chosen to represent clamped ends. To simplify the analysis of wing box buckling, a crucial assumption is made. In general buckling scenarios, if an element within the wing box buckles, it no longer carries any additional load as the overall load is increased. In essence, when an element reaches its critical stress (σ_{critical}), it can be conceptually "removed" from the problem, and the remaining load is redistributed as if the element is not present. This redistribution results in a different centroid, a moment of inertia, and load distribution throughout the structure.

Considering the wing box consists of numerous elements and requires multiple iterations and calculations, it becomes impractical to account for individual element buckling. Therefore, for the sake of simplicity and workload reduction, it is assumed that if any element within the wing box buckles, the entire wing box will buckle as a whole. This assumption allows for more straightforward analysis and avoids the need to iterate through multiple calculations for each individual element’s buckling.

10.7.4. Crack failure

Throughout its operational lifespan, the wing box will experience various loads that gradually induce fatigue and initiate crack formations within the material. Areas with stress concentrations, where there are steep changes in the geometry, are particularly susceptible to crack initiation.

The structural integrity of the wing box, in terms of damage tolerance, depends on its performance when cracks are present. A damage-tolerant structure exhibits the following characteristics [7]:

- It can withstand the limit load even in the presence of a certain-sized crack.
- It can endure a prolonged period without failure in the presence of cracks.
- Cracks within the structure exhibit slow growth.
- It incorporates mechanisms to impede or halt crack growth before they become critical.

The design of the wing box must therefore ensure its ability to withstand anticipated loads, even with existing damage, until the damage is detected through inspections. In other words, the wing box needs to tolerate the presence of cracks within its structure.

Failure due to crack analysis is determined based on the following failure criterion, Equation 10.19. With $K_I(\sigma_{\text{yield}}, a)$ being defined as is shown in Equation 10.20

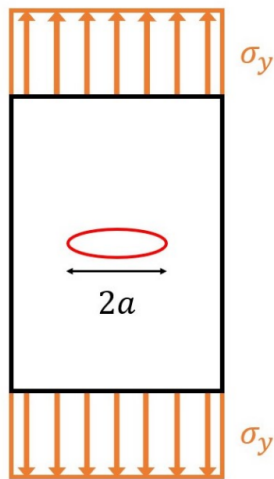


Figure 10.23: Diagram illustrating a cracked plate subjected to tensile loading.

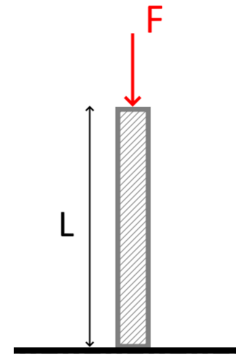


Figure 10.24: Simplified column buckling

$$K_{IC} \leq K_I(\sigma_{yield}, a) \quad (10.19)$$

$$K_I(\sigma_{yield}, a) = \sigma_{yield} \sqrt{\pi a} \quad (10.20)$$

$$\sigma_{fail} = \frac{K_{IC}}{\sqrt{\pi a}} \quad (10.21)$$

In this equation, K_{IC} represents the fracture toughness, a material constant determined through experimental testing, and a is the dimension illustrated in Figure 10.23.

For a given material, the maximum allowable tensile stress can be determined based on the size of the crack. It is assumed that the smallest crack size detectable during visual inspections is 5 mm [A-12]. With the known crack size and material properties, the failure stress can be calculated. By rearranging Equation 10.19 and Equation 10.20, Equation 10.21 was obtained.

10.7.5. Failure analysis of the wing truss

As the wing strut also carries force, a failure analysis also needs to be performed on this member. As the strut uses a telescopic mechanism, only yielding failure of the strut is considered.

10.8. Wing box design

With the wing box generating code developed, and the failure analysis defined and implemented. For the scope of this report, a manual design methodology was used, where the most optimal wing box design was created by giving manual inputs and analyzing the failure modes. This was done as the wing box design tool had many variables, and making an additional tool that could optimize this multi-variable, multi-load case problem was not possible within the time constraint of the project. However, the wing box design presented in this section is a first step towards producing the wing structure for ESRA.

10.8.1. Strut placement

The position of the strut has been proven to influence the aircraft's performance characteristics, such as the drag which is discussed in Subsection 7.2.3, and also the fluttering speed of the aircraft which is discussed in Subsection 11.0.2. With this in mind, design options were generated with different strut placements. From manual generation and selection the outboard strut position of 8[m] was deemed to be the most effective. This was determined by analyzing the shear diagrams and trying to make the maximum absolute bending moment as low as possible. This was done because after an initial structural analysis of the wing box it was found that most often the critical failure mode was stringer buckling or top/bottom skin buckling. Thus a lower maximum bending moment would allow for lower skin thickness and stringer amounts. This resulted in shear diagrams as shown in Figure 10.12.

Here it must also be mentioned that the attachment points of the strut to the wing were assumed to be

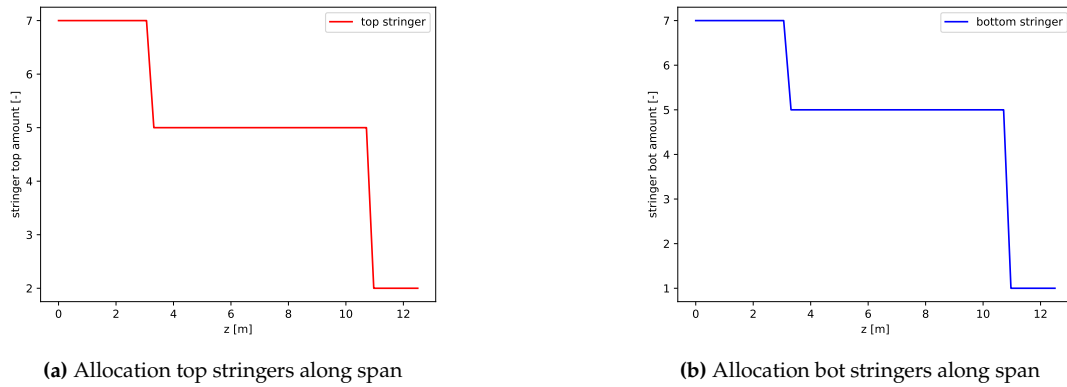


Figure 10.27: Stringer allocation on the wing box design

at the shear center, to introduce no bending moment.

10.8.2. Rib and stringer placement

The ribs placement of the ribs mainly determined the critical buckling stress of the stringers as well as the skin. This resulted in evenly distributed ribs along the span with the rib spacing halving near the root.

Placing the stringers determined the stiffness of the cross-sections, but also the skin buckling as that was determined by the length between stringers. The stringer placement resulted in a near-equal distribution of top and bottom stringers as can be seen in Figure 10.27. This result is different from conventional wing configurations as there often more top stringers are needed to prevent buckling of the top skin and stringers. This showed the effectiveness of the strut in tensional loading.

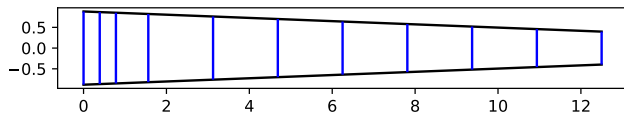


Figure 10.25: Rib placement along the span of final wing box design

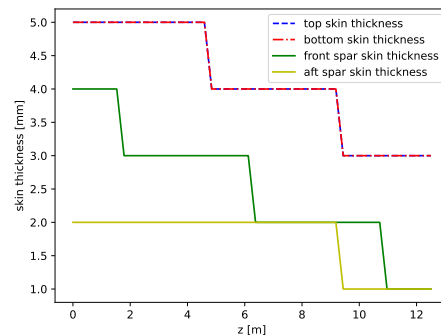


Figure 10.26: Skin thickness along the span of final wing box design

10.8.3. Skin thickness

The wing thickness on the top and bottom influenced the wing stiffness and buckling of the wing skin. Therefore at the root a thickness of both the bottom and top skin of $5[mm]$ was chosen. This thickness reduces over the span until reaching $3[mm]$ as indicated in Figure 10.26. The thickness of the front and aft spar was determined by the spar shear buckling. Due to the torsional loading of the lifting force and engine thrust the front spar needed to be made thicker than the aft spar as can be seen in Figure 10.26.

10.8.4. Wing box characteristics

With the aforementioned design choices, a final wing box design could be generated. Table 10.7 summarizes the characteristics of the wing box. The total calculated structural weight of the wing structure has been determined to be $732[kg]$, this is higher than the mass budget calculated in Subsection 7.2.2 but within the expected range of wing weights. This 12.5% difference was deemed to stem from the manual method of designing the wing box, with no optimization scheme implemented.

Table 10.7: Characteristics of the design wing box

Property	Value
Front spar %	0.2 %
Aft spar %	0.8 %
Wing box length	12.465 [m]
stringer length b	40 [mm]
stringer thickness t	0.003 [mm]
Wing box weight	662 [kg]
Total strut weight	70 [kg]
Total wing weight	732 [kg]

However, the 12.5% difference also gives confirmation that the class II weight estimation and sub-system design were within the same range of weight.

10.8.5. Margin of failure diagrams

The margin of failure plots shows that for the negative loading cases, namely Figure 10.28a and Figure 10.28c, the root of the wing is the most critical place. This falls in line with the usage of the telescopic strut, as the bending moment is then expected to be highest at the root. In the positive load factor cases this does not apply as can be seen in Figure 10.28b and Figure 10.28d, here it can be seen that compressive forces both occur at the top and bottom of the wing box along the span. This could also be seen in the bending moment diagram Figure 10.12. These results from the failure analysis showed that if a non-strutted wing design was chosen, more reinforcement would have been needed for the same assumptions/model. Proving the effectiveness of a structured wing design. The wing structure was also analyzed under critical load case five, as shown in Figure 10.28e. Which also showed that the aircraft could withstand the required ground operational loading cases.

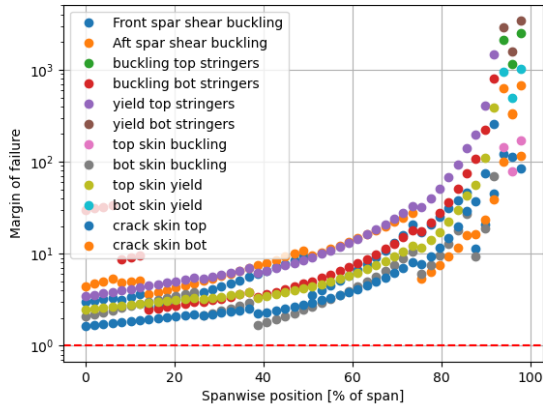
10.9. Recommendations

With the wing box design performed. The design team has several recommendations for future work on the structures sub-system of the ESRA project. Firstly, a viable model of the telescopic strut structure should be designed. To prove that such a mechanism is theoretically useable.

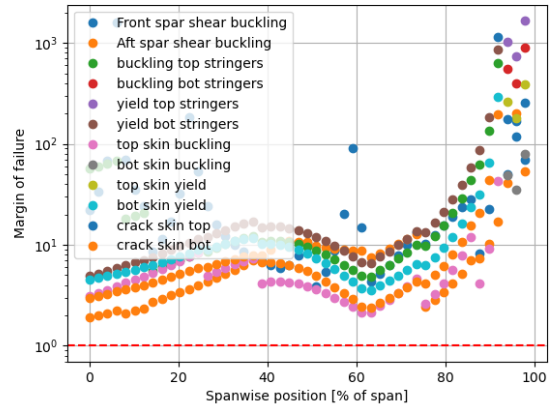
The next recommendation is to model the wing box structure with a higher fidelity model, and further analyze the behavior of the truss structure on the wing. Such analysis should also include the development of an optimization tool to determine the optimal strut placement for the given load cases such as done in [30]. Next to this more fidelity could be added in terms of the internal loading of the wing structure now only the vertical load of the truss was considered. However, compressional loads will also be present which have not been modeled at this point.

Another recommendation is to include structural analysis of the lower wing, the design team expects that this addition will make the wing structure stiffer, which might allow for less total wing structure weight.

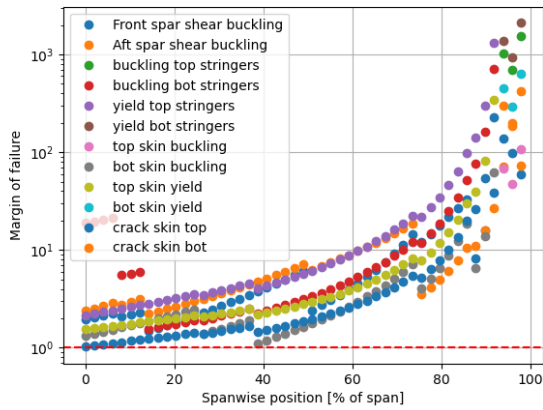
Finally, the use of different materials could be considered in future iterations of design or production. Using aluminum only is beneficial for the overall production cost of the aircraft as fewer machines and processes are needed to produce the aircraft. This is however not ideal from a performance point of view. Making use of titanium alloys in the wing box and composite materials in sections such as the fuselage or tail could easily drive down the weight of the aircraft, while not losing or even gaining overall structural strength. This would however increase the cost of the aircraft and it would require new supply chains and production facilities, which is why this was not considered a viable option for now.



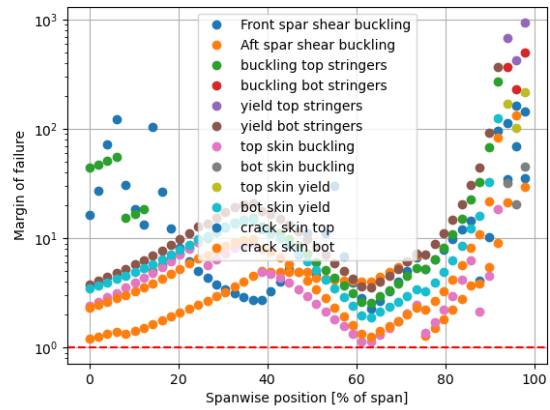
(a) Margin of Failure plot load case 1



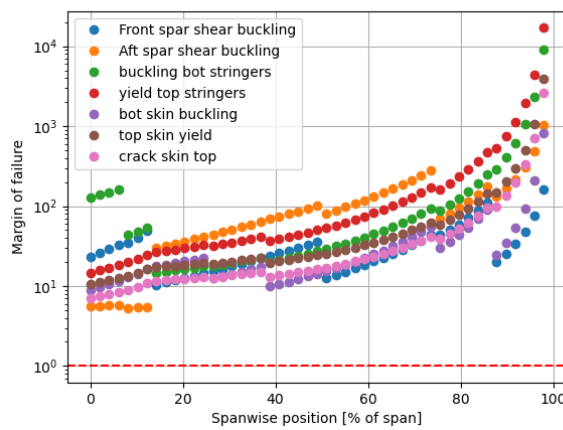
(b) Margin of Failure plot load case 2



(c) Margin of Failure plot load case 3



(d) Margin of Failure plot load case 4



(e) Margin of Failure plot load case 5

Figure 10.28: Margin of failure plots for the wing box

Aeroelasticity

Aeroelasticity involves the interaction of elastic structural deflection and aerodynamic forces, which poses a serious danger should it occur. Certification requires the aircraft to be free of aeroelastic effects at any point in the flight envelope [78]. Aeroelasticity will be analyzed at altitudes of 0km, 11km, and 20.5km. These effects are separated into static and dynamic behavior, with the former further divided into torsional divergence and control reversal.

In the aeroelasticity analysis below, the model shown in Figure 11.3 is used. Cross-sectional properties at a 75% span location between the wing-strut connection and wing tip are used in the calculations. Using the cross-sectional properties at this location produces speed boundaries that are conservative due to the reduced stiffness compared to the cross-section at the wing root. Other than this, the mass balancing effect of different spanwise and chordwise engine locations is also neglected. For chordwise engine position, as long as the CG of the engines is placed in front of the CG of the wing, it will only increase the damping of the system's vibrations. In Figure 11.3, if the lift is assumed to be only a function of the geometric AoA, this results in a steady model where Pine's equation can be applied directly to obtain the flutter speed. Alternatively, the vertical speed can be taken into account which introduces an additional damping term in the system, this is termed the low-frequency model.

Since aeroelasticity describes the interaction of elastic structural behavior and aerodynamic forces, it requires both structural and aerodynamic input. The structural property input is namely the distance between EA and CG expressed in percentage half chord (x_θ), the radius of gyration about EA (r_θ), eccentricity factor (e), bending stiffness (K_h), torsional stiffness (K_θ) and mass per unit span (m). As most of the inputs are calculated about the elastic axis, the majority of work is in the determination of the location of the elastic axis. Calculation of wing section geometrical properties was presented in Subsection 10.4.3 and the values are shown in Table 11.1. Aerodynamic input are determined in Subsection 9.3.3 and are listed in Table 11.1.

Table 11.1: Aeroelastic analysis input

Structural input	x_θ [-]	r_θ [-]	K_h [N/m]	K_θ [Nm/rad]	m [kg]
Value	0.20828	0.35908	40800.3128	160218.1268	10.8387
Aerodynamic input	C_{L_α} [rad^{-1}]	C_{L_δ} [rad^{-1}]	$C_{m_{ac}}$	$C_{m_{ac\delta}}$ [rad^{-1}]	-
Value	0.099	0.0411	-0.175	-0.1211	

11.0.1. Static analysis

At the torsional divergence speed, a wing twist disturbance will diverge into further deflection as the aerodynamic moment becomes too large. Positive aileron deflection increases a wing's effective angle of attack, whilst generating a pitch-down moment that tends to reduce the angle of attack. Control reversal speed is the speed where an aileron deflection has no net effect due to the pitching moment, canceling out the change in the effective angle of attack. These speeds are calculated with the steady model presented in [35]

11.0.2. Dynamic analysis

For preliminary analysis, only two degrees of freedom (DOF), namely vertical translation and rotation, flutter will be considered here. Flutter happens when the direction of the lift force aligns with the vertical movement of the wing section. This results in the wing undergoing uncontrolled oscillations, reaching a point where it continues to oscillate without limits. Mathematically, flutter occurs when the eigenvalue of the system shown in Figure 11.3 has a positive real part and an imaginary part,

indicating a positive growth factor and oscillation frequency. Using the steady model, Pine’s condition shows that flutter speed V_f can be calculated using the structural input in Table 11.1. The flutter speeds calculated are shown in Table 11.2

The flutter speed of the low-frequency model cannot be computed with Pine’s equation due to an additional damping term. The method used here is to solve the system’s characteristic polynomial and plot the imaginary and real parts of the roots against dynamic pressure. The imaginary part of the roots corresponds to the frequency of oscillation, while the real part represents a growth rate. The flutter speed can then be found by identifying the point where the growth rate and frequency are both positive. Frequency and growth rate plots against flight velocity for both the steady and low-frequency model are shown in Figure 11.1 and Figure 11.2. The flutter speed results from the steady model and the low-frequency model are shown in Table 11.2. The last column of Table 11.2 is $1.2V_D$ which is a certification requirement that any aeroelastic behavior shall not exist below that speed[78].

Table 11.2 shows that all speeds at which aeroelastic effect occur are higher than the limit speed $1.2V_D$ specified by regulations. Thus it can be concluded that ESRA should be free from aeroelastic effects.

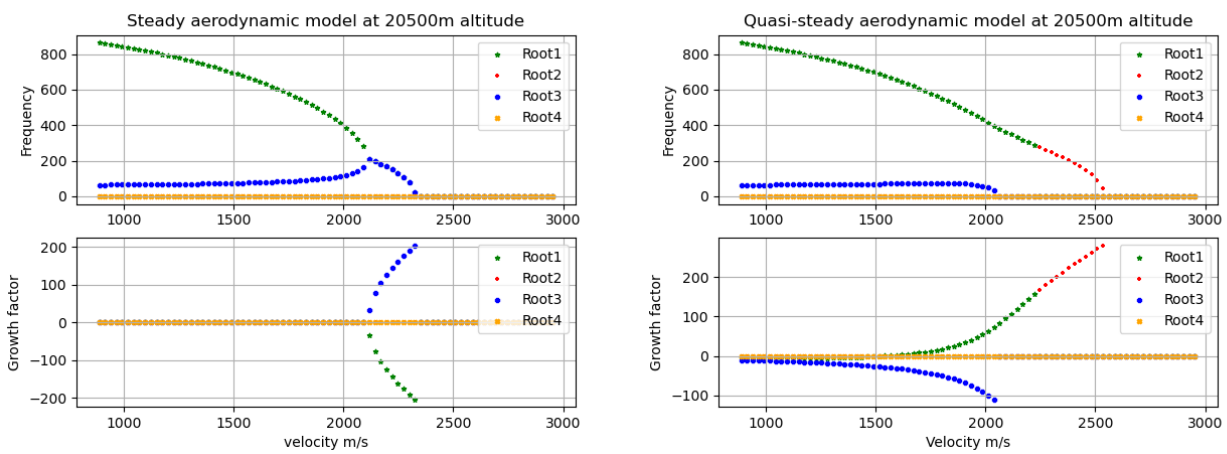


Figure 11.1: Growth rate and frequency plot of steady model at 20.5km altitude **Figure 11.2:** Growth rate and frequency plot of low-frequency model at 20.5km altitude

A few sets of wing box design data with varying strut position were also used to investigate the potential aeroelastic effects of ESRA. Wing bending stiffness increases with strut placement towards the wingtips, all other parameters are constant since the struts are assumed to take only bending loads. The results are shown in Figure 11.4. The increase in flutter speed 1 can be attributed to the increase in bending stiffness with strut position. The exact explanation for the decrease of flutter speed 2 is unexpected and requires further analysis in the future.

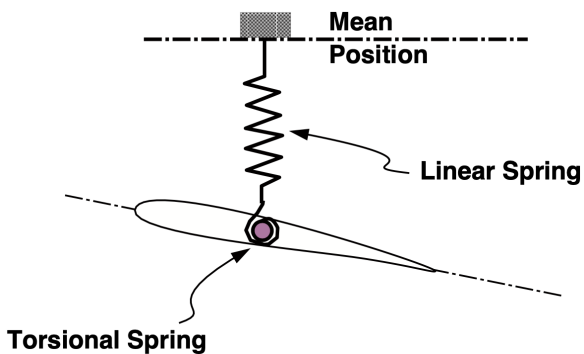


Figure 11.3: Illustration of aeroelasticity model

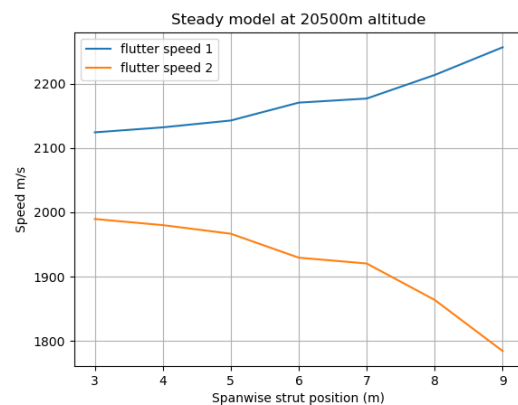


Figure 11.4: Flutter speed with varying spanwise strut position (Steady model)

Table 11.2: Flutter, divergence, reversal and certification limit speeds

Altitude [m]	V_f [m/s]	V_f LF model [m/s]	Divergence speed [m/s]	Control Reversal speed [m/s]	$1.2V_D$ [m/s]
0	542.77	390.54	873.486	1665.2745	90
11000	996.216	718.21	1603.22	3056.49	165.189
20500	2110.09	1519.06	3395.79	6473.97	349.887

11.1. Verification & Validation

The verification of aeroelastic analysis is mostly done by inspection. Since the majority of numerical computation lies in calculating the roots of a fourth order polynomial, this is done with a readily available function on Python which should yield accurate results. A step that was taken to verify the flutter diagrams was to check whether the frequency at zero velocity is equal to the uncoupled bending and torsional frequency. The respective values are shown in Table 11.3, these values have a maximum discrepancy of -22.4%. After several manual calculations, it was concluded that the discrepancy was not due to any numerical error in evaluating the roots of the characteristic polynomial. Upon further inspection, it has been found that the difference in frequencies is likely to be in the fact that the EOMs are derived with small angle approximation. EOM for the sum of forces in the vertical direction and sum of moments in about the elastic axis is shown in Equation 11.1 and Equation 11.2

Table 11.3: Comparison of frequencies

	Analytic	Solving root	%difference
Bending frequency	61.354	55	10.36
Torsional frequency	767.344	939	-22.37

$$\sum F_Z = m\ddot{h} + L\cos(\theta) + K_h h - S_\theta \sin(\ddot{\theta}) \quad \sum M_{EA} = mx_\theta b \cos(\theta) \ddot{h} + I_\theta \ddot{\theta} + K_\theta \theta - L\cos(\theta)^2 ec \quad (11.2)$$

(11.1)

At the time of writing this report, experimental data and simulation results of more complex software are available. However, there are either still certain input values that are missing or incompatible, or the output results are expressed in other units such as wing tip displacement. To be able to make reasonable comparisons for validation, more data have to be collected or a significant amount of current calculation has to be modified to output appropriate values. This will be done in a later stage of design once the required data have been found or the program modified to produce comparable output.

11.2. Recommendations

Regarding aeroelasticity, the main task to implement is to derive EOMs without small angle approximations to confirm that the discrepancy in frequency observed in Table 11.3 is indeed due to small angle approximations. EOMs without small angle approximations were derived and should be implemented into the current program. Furthermore, it is recommended to conduct a more comprehensive analysis with software that takes into account the mass balancing effect of engine position, as well as unsteady aerodynamics. The aeroelastic behavior of the struts should also be considered. On top of this, commercially available software can also output vibration responses based on velocity or AoA perturbation inputs. This can be valuable to simulate the type of perturbations that ESRA might encounter during missions that require flying close to extreme weather features. It has also been observed that a number of aeroelastic analysis software have tip displacement as output. Analyzing aeroelasticity with a wing deflection perspective in future design work may also be able to provide further insight into structural design of ESRA which could improve overall aircraft performance.

Stability and control

12.1. Longitudinal stability and controllability

During a mission, the center of gravity (CG) position of the aircraft changes significantly. The horizontal tail has to ensure stability and control during the entire mission. To size it first the CG range has to be analyzed. This was done by taking into account possible payload loading scenarios, pilot presence and fuel consumption during the flight. The resulting CG range is represented in Figure 12.1.

A number of assumptions were made to generate the loading diagram. The most significant are outlined below. Firstly, it was assumed that the payload is a point mass of 125 kg (including the payload trolley). This assumption was taken as a worst-case scenario where the scientists want to put all their payload in one compartment. Secondly, both the fuel and pilot are also modelled as point masses, with a magnitude of 1544 and 125 kg respectively. It was assumed that the fuel would be stored within the wings. Thirdly, the weight of the landing gear was not considered in the analysis as it will be installed at a later stage. This follows the procedure outlined in [27].

Two separate loading diagrams were generated and super imposed, as shown in Figure 12.1. In one diagram all the payload is in the middle compartment and in the other all the payload is in the front. To ensure safe operation and limit the c.g. range, it is forbidden to put all the payload in the aft compartment. A loading diagram where the payload is evenly distributed across all three compartments was also generated, but this was found to be less constraining than the other two.

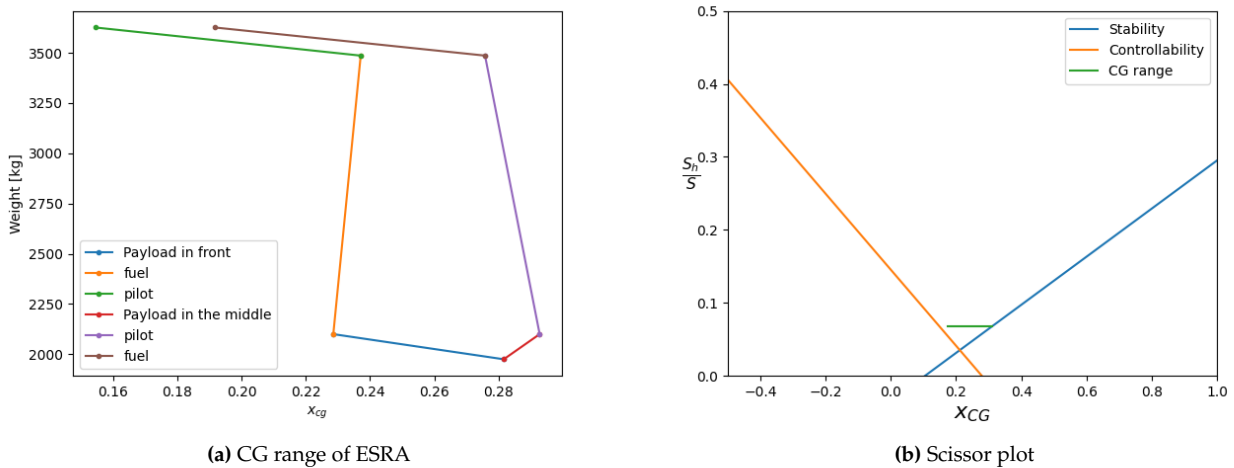


Figure 12.1: CG range of ESRA

The centre of gravity range lies between 0.15 and 0.29 of the MAC. With this in mind, scissor plots can be generated to size the tail. The stability curve of the scissor plot is defined in (12.1)

$$\frac{S_h}{S} = \frac{1}{\frac{C_{L\alpha_h}}{C_{L\alpha_{A-h}}} \left(1 - \frac{d\epsilon}{d\alpha}\right) \frac{l_h}{\bar{c}} \left(\frac{V_h}{V}\right)^2} \bar{x}_{cg} - \frac{\bar{x}_{ac} - 0.05}{\frac{C_{L\alpha_h}}{C_{L\alpha_{A-h}}} \left(1 - \frac{d\epsilon}{d\alpha}\right) \frac{l_h}{\bar{c}} \left(\frac{V_h}{V}\right)^2} \quad (12.1)$$

and depicted on Figure 12.1b as a blue line. Values of S_h/S above the line yield static stability. Torenbeek states that stability should be assessed at high-speed cruise, since the aerodynamic centre shifts forward[82]. The method presented in his book was followed to quantify the effects of the shift in the aerodynamic centre due to the fuselage, and nacelles. Since the horizontal stabilizer is mounted

as a T-tail, the downwash was assumed to be negligible and the ratio of dynamic pressures V_h/V was assumed to be equal to 1. The lift slopes for both the tail and wing were computed using the DATCOM method, which is outlined in Chapter 9. The aircraft is controllable if S_h/S is selected to be above the curve, shown in orange in Figure 12.1b.

The controllability curve is represented by (12.2).

$$\frac{S_h}{S} = \frac{1}{\frac{C_{L_h}}{C_{L_{A-h}}}\left(1 - \frac{d\epsilon}{d\alpha}\right)\frac{l_h}{c}\left(\frac{V_h}{V}\right)^2} \bar{x}_{cg} + \frac{\frac{C_{mac}}{C_{L_{A-h}}} - \bar{x}_{ac}}{\frac{C_{L_h}}{C_{L_{A-h}}}\left(1 - \frac{d\epsilon}{d\alpha}\right)\frac{l_h}{c}\left(\frac{V_h}{V}\right)^2} \quad (12.2)$$

Controllability is most critical at sea level stall, according to Torenbeek [82]. Given the $C_{L_{max}}$ at sea level determined in Chapter 9, the stall speed of the aircraft with no flaps is 40 [m/s] at MTOW. This is lower than the stall speed of the U2 with full flaps (46 [m/s]), so the inclusion of flaps was considered unnecessary.¹ C_{L_h} was determined empirically with $C_{L_h} = -0.35A_h^{1/3}$, to be -0.55 [82]. This is lower than the maximum achievable lift coefficient of the tail with full elevator deflection determined in Section 12.5, thus allowing for extra maneuverability in stall. Torenbeek's methods were used to assess the effect of fuselage and nacelles on C_{mac} , and the aerodynamic center, this time at low speeds.

Knowing the CG range and controllability and stability constraints the tail size can be optimized by varying wing position so that the CG range fits between those constraints at minimum $\frac{S_h}{S}$ ratio. This was done using the method described in [27]. As can be read from the Figure 12.1b the resulting $\frac{S_h}{S} = 0.07$, thus the area of the horizontal stabilizer has to be above $S \cdot 0.07 = 2.6[m]$. With that, the planform design of the horizontal tail was carried out as described in Section 12.3.

12.1.1. Recommendations concerning the strut

For the conceptual design phase, it was assumed that the strut does not contribute to the stability of the aircraft. This is because the lift vector is very close to the center of gravity and, since the airfoil covering the strut is symmetric, the moment it generates is 0. After sizing and placing the strut it was observed that the lift of the strut is acting behind the aft center of gravity. This will make the aircraft more stable but also less controllable. It is recommended to add the strut term to the static stability analysis to quantify the required increase in the tail area-

12.2. Lateral stability

Sizing of the vertical tail was carried out to ensure the tail meets ESRA-STAKE-4-SYS-38, ESRA-STAKE-4-SYS-47 and ESRA-STAKE-4-SYS-21. The methods used were equations 9.59, 9.63 and 9.68 from [82].

The required tail volume was assessed at a stall at sea level, as this was found to be the most critical condition. Torenbeek's methods are rather stiff and only allow the designer a limited number of variables to play with., namely l_{vt} the vertical tail length, $C_{y_{v\alpha}}$ the side force gradient, and the effectiveness of the rudder. For the engine out condition, the lateral position of the engines is also important. Subsection 12.2.1, Section 12.3 and Section 12.5 describe the analysis of the tail length, force slope and rudder effectiveness. Due to time constraints, the sizing procedure consisted of statistical values which were analyzed to ensure they could give adequate performance. Detailed design is recommended. A number of variables are worth considering for the positioning of the engines. For interference drag it is desirable to put the engines outboard, this also helps moment alleviation at the root and helps in dampening aeroelastic response. However, this increases the required tail volume as the yawing moment increases significantly. Furthermore, the joining of the fuselage to the engine, which is the support structure for the strut increases in weight and adds drag. As a compromise, the engine was placed 1.8 meters outboard.

The required tail volume for the three sizing situations is shown in Table 12.1.

¹URL: <https://info.publicintelligence.net/USAF-U2.pdf> accessed on 20/06/2023

Table 12.1: Required tail volume coefficient

	Crosswind	Engine out	Lateral Stability
Tail volume coefficient	0.012	0.013	0.032

It is clear that directional stability is the most driving constraint. The achieved value is 0.06, which is twice what [82] recommends as the minimum. The safety factor was added to improve Dutch Roll damping. The required surface area is 4.4 m^2 .

12.2.1. Wing positioning and fuselage extension

In the longitudinal stability analysis, the wing position was changed to optimize and thus decrease the area of the horizontal tail. This required shifting the wing forward. However, the assessment of lateral stability indicated that a significantly larger arm is required; otherwise, an excessively large vertical tail would be necessary to generate an adequate force. For the initial fuselage length of 9.5m the required vertical tail area would be 5.8m^2 which is 18% of the wing area. Due to the fuselage arrangement, it was impossible to move the wing even further since it would be placed above the cockpit which is not ideal. Therefore the extension of the fuselage was required to extend the arm for the vertical tail.

The extension of the fuselage leads to an increase in structural weight which is undesirable, however, it also decreases the required surface area of both horizontal and vertical tail along with parasite drag decrease. Since the cost of the aircraft is a priority, the optimization for weight is desirable.

Unfortunately, it was impossible to conduct a proper optimization at this stage due to the empennage weight definition. According to the Torenbeek Class II weight estimation method, the weight of the empennage can be either 2-3% of the MTOW or Equation 12.3

$$W_{tail} = k_{wt}(n_{ult}S_{tail})^{0.75} \tag{12.3}$$

Where $k_{wt} = 0.64$ and subscript *tail* stands for both vertical and horizontal. This results in erroneous values of 11 and 24kg for vertical and horizontal tails respectively. This was considered unrealistic and that is why a 3% of the MTOW was utilized to keep a conservative approach. This resulted in 132kg for the entire empennage which seemed more realistic and therefore this value was utilized in further calculations. The problem with such an approach is that the area of the tail is not directly linked with its weight. Therefore it is impossible to establish a relationship between the change of area and weight for the vertical tail and thus not clear how much lighter the tail becomes when elongating the fuselage.

Further analysis should be done later once the structural weight of the tail is known and its relationship with the tail area is established. It should be possible to compare the derivative of the fuselage weight with respect to fuselage length to derivatives of the horizontal and vertical tail areas with respect to their weight. This will allow determination of the optimum fuselage length.

In this design, the extension of 1.5m was required to decrease the surface area of the vertical tail to 4.43m^2 which is 14% of the wing area.

12.3. Tail Planform Sizing

This section presents the determination of the airfoil, sweep angle, aspect ratio and taper ratio for the horizontal and vertical stabilizer.

12.3.1. Vertical Tail

There are a number of requirements that the vertical tail must satisfy. Firstly, it should be able to provide trim with equal efficiency for angles of both negative and positive sideslip. Secondly, it should stall at an angle greater than 20° . This is due to the expected angle of sideslip in transient conditions after a one-engine out event, as suggested by [82]. Thirdly, compressibility effects should be avoided. Fourthly, the horizontal stabilizer should not be blanketed by the wing.

To satisfy the trim and compressibility requirements the symmetric airfoil SC – 0010 was chosen.

This is a supercritical airfoil that should postpone adverse compressibility effects while offering an adequate balance of forces. The aspect ratio, half-chord sweep, and taper ratio were all selected from statistics and are shown in Table 12.2.

An analysis of the 3D performance of the fin was carried out using the DATCOM method, as described in Chapter 9. The objective was to ensure compliance with the stall angle of attack requirement and to quantify the lift slope of the stabilizer. The results are shown in Table 12.2. It was determined that the stall performance of the vertical tail was most constrained at altitude, so the results are shown for $M = 0.67$ at 20.5 km. Evidently, the requirement is met. Furthermore, the minimum height required to ensure the horizontal tail is not blanketed by the wing is 1 m which is well below the span of the tail.²

12.3.2. Horizontal Tail

A similar analysis was conducted for the horizontal tail. The requirements for the tail are that it must not encounter compressibility effects before the wing, and it must stall after the wing. Again, the critical condition is high cruise, as the $C_{L_{max}}$ decreases due to compressibility effects. A sweep of 10° was selected to postpone drag divergence and increase the stall angle of attack. An aspect ratio of 4 was selected from statistics compiled in [66] The lift coefficient of the tail in high altitude loiter is -0.328. This is low enough that drag divergence is unlikely to occur. For reference, the wing is at a C_L of 0.77 and still flies below M_{dd} . SC-0010 was chosen again as the airfoil for the tail to minimize any pitch-up moments which may be caused by an upside down cambered airfoil. The required angle of incidence is discussed in Subsection 12.3.3. Table 12.2 shows the stall angle and 3D lift slope of the stabilizer. The stall angle of attack, coupled with the negative incidence, shows that the tail will not stall before the wing. For the analysis of the 3D wing, consult Chapter 9.

Table 12.2: Empennage Planform Characteristics

	Horizontal tail	Vertical tail
$A[m]$	4	1.2
$\lambda[m]$	0.5	0.5
$\Lambda_{c/2}$	10	40
$b [m]$	3.23	2.3
Lift slope [1/rad]	4.30	2.33
α_{stall}	9.6	23

12.3.3. Incidence angle

The angle of incidence is the angle between the chord of the airfoil and the longitudinal axis of the aircraft. It is needed to decrease the drag of the aircraft during the longest mission stage - cruise flight. It decreases drag since the front-view area of the aircraft does not increase when the aircraft is flying under the cruising angle of attack because only the wing is inclined with respect to the flow. It is also beneficial for the stability of the aircraft since it ensures that the horizontal tail will stall after the main wing.

To calculate the angle of incidence the $C_{L_{des}} = 0.77$ determined in Section 9.4 was used. From $C_L - \alpha$ curve Figure 9.5b of the wing the α corresponding to $C_{L_{des}}$ is 3.5° . Thus $\alpha = 3.5^\circ$ is the incidence angle for the wing.

Now once the wing incidence angle is known the corresponding incidence angle of the horizontal tail has to be determined. It yields from the moment equilibrium equation during the cruise. The horizontal tail has to provide a sufficient C_{L_h} to satisfy the moment equilibrium equation. The angle of attack for the horizontal stabilizer that can provide such C_{L_h} is thus the angle of incidence for the stabilizer.

²This value was computed from equation 6.61 in http://aero.us.es/adesign/Slides/Extra/Stability/Design_Tail/Chapter%206.%20Tail%20Design.pdf

The desired moment equilibrium around the center of gravity leads to the following equation

$$\frac{1}{2}\rho V^2 S C_L (x_{ac} - x_{cg}) + M_{acwing} = \frac{1}{2}\rho V_h^2 S_h C_{L_h} l_h \quad (12.4)$$

The aerodynamic moment of the horizontal tail was omitted due to the fact that for symmetric airfoils for angles of attack close to zero $C_m \approx 0$. Dividing by $\frac{1}{2}\rho V^2 S \bar{c}$ and expressing C_{L_h} leads to the following relationship

$$C_{L_h} = \left(C_L \frac{x_{ac} - x_{cg}}{\bar{c}} + C_{mac} \right) \frac{\bar{c}}{l_h} \left(\frac{V}{V_h} \right)^2 \frac{S}{S_h} \quad (12.5)$$

Due to the T-tail configuration the $\frac{V_h}{V} = 0$. Plugging in all the values results in $C_{L_h} = -0.328$.

Note that during the cruise stage, the centre of gravity does not change significantly since all the fuel is stored in the wing, very close to the CG location. It can also be seen from Figure 12.1.

The symmetric airfoil SC-0010 is used for the horizontal stabilizer, assuming a slope of 2π and knowing that $C_L = 0$ at $\alpha = 0$, the required $\alpha_h = -3^\circ$. This further ensures that the tail will stall after the wing.

12.4. Dynamic stability

This section focuses on the analysis and control of the dynamic modes of the aircraft. [60] specifies levels of flying quality ranked from I to III for different categories of aircraft, also ranked I to III, under different flight conditions, defined as A, B, and C. A flying quality of I is desirable as it indicates adequate handling for the flight phase. ESRA is a category II aircraft operating in category B flight during normal operations and category C for take-off and landing.

This leads to the requirement ESRA-STAKE-4-SYS-46: ESRA shall have flying qualities of Level I as defined in [60] for all phases of flight and for all longitudinal and lateral eigenmotions.

To evaluate the dynamic response of the system the lateral and longitudinal stability and control derivatives were evaluated using methods from [38], [68] and [9] and substituted into the full linearized equations of motion described in [9]. The methods used are semi-empirical in nature and are generally functions of the geometry of the aircraft. Due to the difficulty in estimating a number of lateral motion derivatives, the eigenmotions of the asymmetric case were computed using simplified models described in [FD].

The simplified models used for the dynamic stability analysis made a number of assumptions, detailed below. For the rolling eigenmotion only roll was considered, neglecting yaw and sideslip. This is a rigorous simplification which will be assessed in Subsection 12.4.2. For the dutch roll, the rolling motion was neglected. This means the effect of C_{l_β} on the Dutch Roll will not be quantified. However, as the dutch roll is already stable, and the spiral lies within the limits of acceptability, it is unlikely a modification of the dihedral, taken to be 1° in Section 9.2 is necessary. Concerning the spiral mode, the simplified model neglects linear and angular accelerations.

Section 12.4 shows the results of the dynamic stability analysis. The responses were analysed for several different altitudes, velocities, and weights. It was found that the most critical condition is cruise at $M = 0.65$ at 20.5 km with MTOW minus the fuel burnt in cruise. Although this corresponds to a category B phase of flight, the flying quality is presented for the most demanding category (C) to ensure proper handling at all phases of flight. Note that the difference between category B and C is slight, and for certain motions, such as the Dutch Roll, these categories are grouped together.

Table 12.3: Dynamic Stability Results

Eigenmotion	Eigenvalue	ζ	$\omega_n[rad/s]$	$\tau[s]$	$T_{0.5}[s]$	Flying quality
Short Period	$-0.447 + -2.168i$	0.202	2.214	-	1.550	II
Phugoid	$-0.002 + -0.0689i$	0.0298	0.069	-	337.5	II
Roll	-2.313	-	-	0.432	-	I
Dutch Roll	$-0.0506 + -1.389i$	0.0364	1.391	-	13.7	II
Spiral	0.01593	-	-	-	-43.5	I

The motions that fail to meet the requirement are the short period, phugoid, and dutch roll. The driving handling requirements for these motions are shown in Table 12.4.

To conform to the required characteristics a gain controller will be implemented on the aircraft as a stability augmentation system. The methodology for this is described in the following section.

12.4.1. Gain Control Tuning

To implement the gain controller for the longitudinal motions the linearized equations were first converted to state-space format. The longitudinal equations operate on the state vector $\bar{x} = [u \ \alpha \ \theta \ q]^T$ with the control vector $\bar{u} = [\delta_e]^T$. The output of the system was defined to be the same as the state vector, such that $\bar{x} = \bar{y}$. The controller will adjust the elevator to control the pitch rate q and the pitch angle θ , therefore, the gain matrix is $K = [0 \ 0 \ K_\theta \ K_q]^T$. Figure 12.2 shows a block diagram of the system.

Table 12.4: Handling Requirements for Misbehaved Eigenmotions

Eigenmotion	Driving Requirement
Short Period	$\zeta > 0.35$
Phugoid	$\zeta > 0.04$
Dutch Roll	$\zeta\omega_n > 0.15$

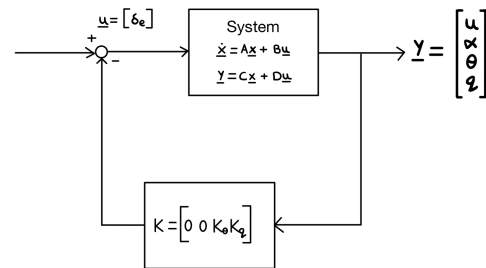


Figure 12.2: Block diagram of the controller system.

Gain tuning was carried out with the root-locus method. The minimum gains to achieve the required damping are $K_\theta = -0.0046$ and $K_q = -0.2$. Section 12.4.1 shows the eigenvalues of the new system.

Table 12.5: Improved Dynamic Stability Results

Eigenmotion	Eigenvalue	ζ	$\omega_n[rad/s]$	$\tau[s]$	$T_{0.5}[s]$	Flying quality
Short Period	$-0.870 \pm 2.135i$	0.37	2.306	-	0.796	I
Phugoid	$-0.003 \pm 0.0663i$	0.0434	0.0664	-	240.64	I

With these control modifications ESRA-STAKE-SYS-46 has been met for the longitudinal motions. To ensure a properly damped Dutch Roll a similarly configured yaw damper will be implemented that operates on the rudder. Due to time constraints, this has not been designed and is left for future teams.

12.4.2. Verification and Validation

Computation of the dynamic stability characteristics requires 17 stability and control derivatives to be implemented. The first level of verification was to unit test each of the functions against a hand calculation, until no discrepancies to 10^{-12} were found. The second layer of verification involved checking the sign of the derivatives against those from a Cessna Citation II, for which data was experimentally available. No discrepancies were found, however, there were a number of parameters

Table 12.6: Explanation of large discrepancies in stability derivatives

Derivative	Citation II value	ESRA value	Remark
C_{Z_u}	-0.37	-1.5	A change in velocity will induce a significantly larger change in the vertical force since ESRA operates at higher lift coefficients than the Citation in cruise.
C_{Z_q}	-5.66	-1.95	This derivative is a function of the tail length l_{ht} normalized by the MAC. This parameter is less for ESRA than for the citation, owing to the rather short fuselage.
$C_{m_{\dot{\alpha}}}$	0.18	0	This derivative is a function of the downwash. Since ESRA has a T-tail aircraft it has no effect.
C_{n_r}	-0.21	-0.034	This parameter is heavily influenced by the parameter l_{vt}/b . Since the vertical tail length is small and the span is large the magnitude of the derivative decreases relative to the Citation.

that had a significantly different magnitude. The nondimensional stability and control derivatives, despite being aircraft specific, should all lie "in the ballpark" of each other. Table 12.6 shows the parameters for which there was a significant discrepancy and a reasoning for this.

The derivatives with the largest discrepancies all have reasonable explanations in terms of the unique geometry of ESRA. Further verification and validation is warranted, however, it is outside the scope of this project. For now, the stability derivatives can be assumed verified to a moderate degree of confidence.

It is strongly recommended to implement the full equations of motion for the lateral eigenmotions. The simplified models can offer accurate results if the geometry of the aircraft is such that the neglected derivatives play little effect, however, this cannot be guaranteed for ESRA.

12.5. Control surfaces

12.5.1. Ailerons

To design ailerons the target roll performance has to be defined. Lower speeds are more critical since they require bigger control surfaces to perform a maneuver, whereas at high speeds even a small deflection of the aileron can cause a significant roll rate. Nevertheless, it would be unwise to design control surfaces for a stall speed because during the turn one of the wing tips will experience a lower velocity than V_{stall} and thus will stall. Therefore it is impossible to perform turning at stall speed and approach speed, V_{appr} , equal to $1.3V_{stall} = 54.6[m/s]$ will be used instead. It is also important to note that the analysis and sizing will be done for the MTOW since it constrains the maximum $\Delta\alpha$ the most. During the approach at sea level, the required $C_L = 0.7464$ while $C_{L_{max}} = 1.2614$, from $C_L - \alpha$ curve of the wing Figure 9.5a, $\Delta\alpha_{max} = 5$. This is the maximum change of the angle of attack that is allowed during the turn maneuver at sea level at MTOW. This constraints the roll rate which can be seen in Equation 12.6

Thus the maximum roll rate should not exceed this value at low speeds.

ESRA is not designed to be the most maneuverable aircraft since there is no need for this. Therefore the most liberal airworthiness requirements were chosen, mainly to perform a bank of 30° within 1.5s. Gladly this requirement can be met with the $P_{max} = 0.38215$.

To begin the design the following geometry has to be assumed Figure 12.3a.

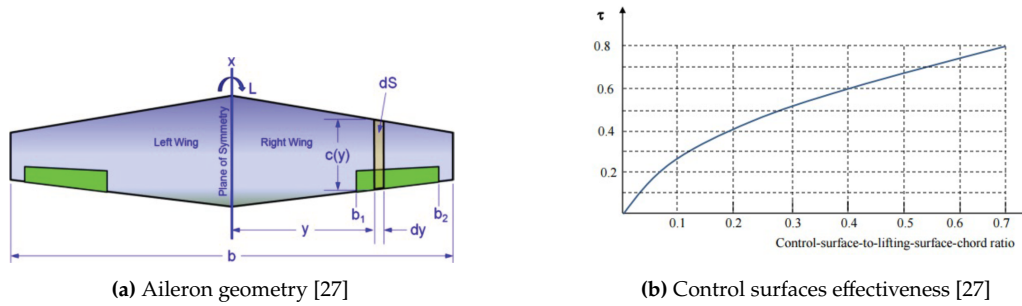


Figure 12.3: Aileron design

Ailerons are the most effective at the tip of the wing, nevertheless, in order to decrease the structural loads a 1[m] gap was left between the tip and b_2 (read from Figure 12.3a, thus $b_2 = \frac{b}{2} - 1$). Next, the aileron chord length had to be chosen. It is directly linked to aileron effectiveness represented by the aileron chord to local wing chord ratio and depicted in Figure 12.3b. The control-surface-to-lifting-surface-chord ratio of 0.2 has been chosen that gives the aileron effectiveness, $\tau = 0.41$.

The roll rate of the aircraft due to aileron deflection can be estimated from the relationship seen in Equation 12.7

$$P_{\max} = \frac{2V_{\text{apr}} \tan \Delta\alpha_{\max}}{b} = 0.38215 \quad (12.6) \qquad P = -\frac{C_{l_{\delta a}}}{C_{l_p}} \Delta\alpha_{\max} \left(\frac{2V_{\text{arr}}}{b} \right) \quad (12.7)$$

where $\Delta\alpha_{\max}$ is the maximum deflection of the ailerons and is assumed to be 25 degrees as the most common value for non-military aircraft.

$$C_{l_p} = -\frac{4(c_{l_\alpha} + c_{d_0})}{Sb^2} \int_0^{\frac{b}{2}} y^2 c(y) dy \quad (12.8) \qquad C_{l_{\delta a}} = \frac{2c_{l_\alpha} \tau}{Sb} \int_{b_1}^{b_2} c(y) y dy \quad (12.9)$$

So far the only unknown variable is b_1 . Several iterations have been performed increasing b_1 and thus the length of the ailerons in order to meet the above-stated requirements. This resulted in the overall length of the aileron being equal to 2.5[m].

Further analysis of the effect of choosing different values for aileron effectiveness and another gap from the wing tip is recommended however does not fall in the scope of the preliminary design.

12.5.2. Elevator

Several rather dense methods for the elevator design were found [72], [32]. These methods were considered to be too involved for the preliminary design so an alternative approach has been implemented. The typical elevator characteristics such as span, $b_e = 0.9b_h$, chord, $c_e = 0.2c_h$ and maximum deflection angle of 25° were obtained from Mohammad H. Sadraey's book [72]. A 3D model of the horizontal tail with elevator deflected to the maximum angle was simulated and analyzed for low Reynolds numbers³ in XFLR 5 software. This resulted in the $C_{L_h} - \alpha$ curve for the horizontal stabilizer with maximum elevator deflection. At the incidence angle determined above, $\alpha = -3^\circ$ and upward deflected elevator the C_{L_h} of -0.94 was obtained and considered to be satisfying. The proper analysis of both take-off and landing will be described in Chapter 13 and prove that this elevator configuration satisfies take-off and landing requirements. Further discussion and optimization are needed, and more cases and manoeuvres have to be considered, however, this falls beyond the preliminary design scope. The highlight of this subsection is that the current horizontal tail and elevator configuration do satisfy primary needs.

³These values correspond to take-off and landing conditions, which were considered the critical scenarios for the elevator deflection.

12.5.3. Rudder

The sizing of the rudder was conducted similarly to the elevator. From statistics [69] the rudder hinge was assumed to be at 80% of the chord and the span was taken to be 90% of the tailplane span. A simulation was run using XFLR5 to determine the increase in side force due to a deflection of 25°, which is a typical maximum rudder deflection [82]. The parameter $\tau_v \delta_r$ was substituted into Torenbeek’s formula and its value was found to be 0.91 (in dimensionless terms) which proved satisfactory for both the engine out and cross-wind conditions, as shown in Section 12.2.

12.6. Gear design and placement

12.6.1. Gear sizing

Gear sizing has been done based on Raymer’s statistical wheels and tire sizing table. Since there was no place available in the fuselage due to payload priority it has been decided that the most effective place for the main landing gear would be in the bottom wing-like structure that is part of the struts, since it would not create new nacelles and thus no extra parasite drag. That’s why the width of the landing gear had to be minimized and authors decided to proceed with two main wheels. Knowing the number of wheels and MTOW the load per wheel can be easily obtained. Analyzing a table with reference aircraft the following dimensions were chosen for nose and main landing gear[63].

Table 12.7: Gear dimensions

	Wheel radius[m]	Tire radius [m]	Tire thickness [m]
Main landing gear	0.254	0.48	0.11
Nose landing gear	0.203	0.406	0.1

12.6.2. Retraction mechanisms

To minimize the parasite drag it is beneficial to hide gears during the flight. The following mechanisms were created to satisfy this need. For the nose landing gear, the four-bar linkage mechanism was utilized whereas the main landing gear simply fold into the bottom wing rotating around pivot points.

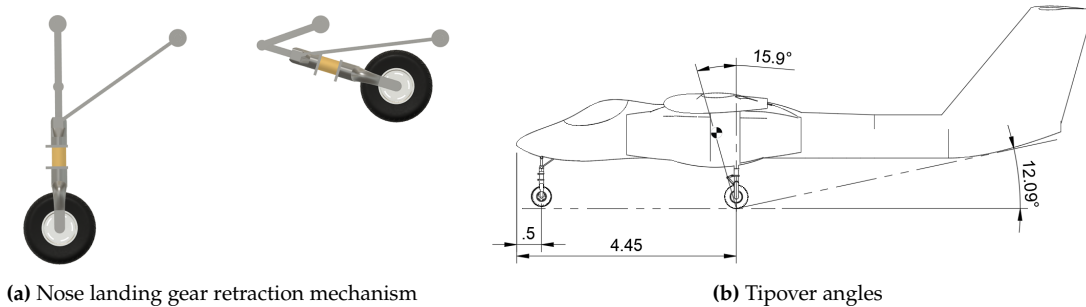
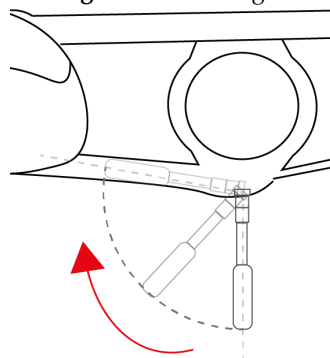


Figure 12.4: Nose gear retraction and tip over angles



(a) Main landing gear retraction mechanism

Figure 12.5: Nose gear retraction and tip over angles

12.6.3. Gear placement

The longitudinal and lateral placement of the gear has to ensure aircraft stability on the ground. During the placement procedure, the following aspects were considered - clearance, longitudinal stability (tip-over), lateral stability (turnover) and steering. The latter is driven by the percentage of the total weight of the aircraft that falls on the nose wheel. It is recommended to keep this percentage within a range from 8 to 15%. The 13% value was used in this design. Due to fuselage geometrical constraints, the nose landing gear was first placed at 0.5 m behind the nose of the fuselage Figure 12.5a. Knowing the location of the center of gravity, previously determined in this chapter, the corresponding placement of the main landing gear has been determined from the simple sum of moment equation. This resulted in the tipback angle of 12.09° which is smaller than the 15.9° requirement shown in Figure 12.5a.

To satisfy the lateral stability requirement the Ψ angle has to be smaller than 55° [82]. This was satisfied by placing gear at 1.65[m] outboard from the symmetry line. This resulted in $\Psi = 48.4^\circ$.

Due to the high-wing configuration and the inboard engine position, the clearance requirements are met.

Performance Analysis

13.1. Detailed Profile Characterization and Optimization

This section presents a detailed quantification of the flight profile and a preliminary optimization procedure. This is required to evaluate the margins to the fuel budget outlined in Section 7.2 with higher fidelity and to assess the effect of decreasing e to 0.64 on the overall performance of the aircraft. This section will first discuss the evaluation of the fuel-intensive phases of flight (outgoing cruise, loiter on station, return cruise, and diversion cruise) and then the evaluation of the climb and descent profiles.

13.1.1. Fuel intensive phases

The assumptions and methodology are outlined as follows. For calculation of the fuel burnt the differential form of the Breguet range and endurance equations were used (13.1) (13.2). A tool was developed to numerically integrate these using the Forward Euler method. A number of assumptions were loosened. Firstly, altitude was not assumed constant. The Breguet range equation describes a cruise climb procedure meaning that as the aircraft burns fuel it gains altitude. Secondly, we assume a constant angle of attack and a constant C_{D_0} . As shown in Subsection 7.2.3 C_{D_0} increases with Mach number and altitude. For computational efficiency, C_{D_0} at an average altitude of 20.5 km was taken, with the value of 0.022. This is conservative for the first cruise phase and unconservative for the second phase, with the net effect that the assumption is valid. Thirdly, c_j was assumed to be a function of altitude and Mach number, using available engine data.

$$dR = \frac{V}{g c_j} \frac{L}{D} \frac{1}{W} dW \quad (13.1)$$

$$dE = \frac{1}{g c_j} \frac{L}{D} \frac{1}{W} dW \quad (13.2)$$

Optimization of the cruise profile for minimum fuel was carried out in the following way. The objective function to be maximized is the specific range: $\frac{V}{g c_j} \frac{L}{D}$. A number of operational constraints were introduced for safety. M was allowed to vary between [0.65, 0.7]. The lower bound was chosen to ensure a low mission time and a margin of 0.02 M to stall at high altitudes. The upper bound was chosen to provide a safe margin to drag divergence, computed to occur at $M = 0.73$ in Chapter 9, and to ensure high Oswald efficiency. The excess power should be greater than 100 N for both cruise phases and greater than 80 N for the loiter phase (a definition of the excess power may be found in Subsection 13.3.1). Furthermore, at each stage of cruise, the aircraft should be able to achieve at least 1 m/s rate of climb to avoid flying too close to the ceiling. After initial analysis it was shown that this is not possible for the loiter phase, so the constraint was relaxed to 0.6 m/s, meaning the aircraft will fly just under its ceiling. Following the analysis of the performance in the loiter phase it was found that the achievable rate of climb increases from 0.67 to 0.93 m/s as fuel is burnt.

The constraints discussed above may be plotted on a contour plot showing the specific range as a function of M and altitude. Such a plot is shown in Figure 13.1 for the weight at the start of the first cruise segment. This contour plot corresponds well with the recommendation in [71] to fly high and fast, as well as the similar conclusion drawn in Subsection 7.2.1. From these contours, a determination of the optimum starting altitude and velocity may be made. In this case, the value is $M = 0.672$, $h = 19600m$. The final value was determined iteratively, by ensuring the constraints are met at every stage of the cruise climb. Because of the increase in the specific fuel consumption with growing altitude, the best optimum starting value changes slightly.

Since the loiter altitude is specified by ESRA-STAKE-1-SYS-1, the optimization consisted in maximizing the rate of climb within the velocity constraints. It may be seen in Figure 13.1 that flying slow is best to

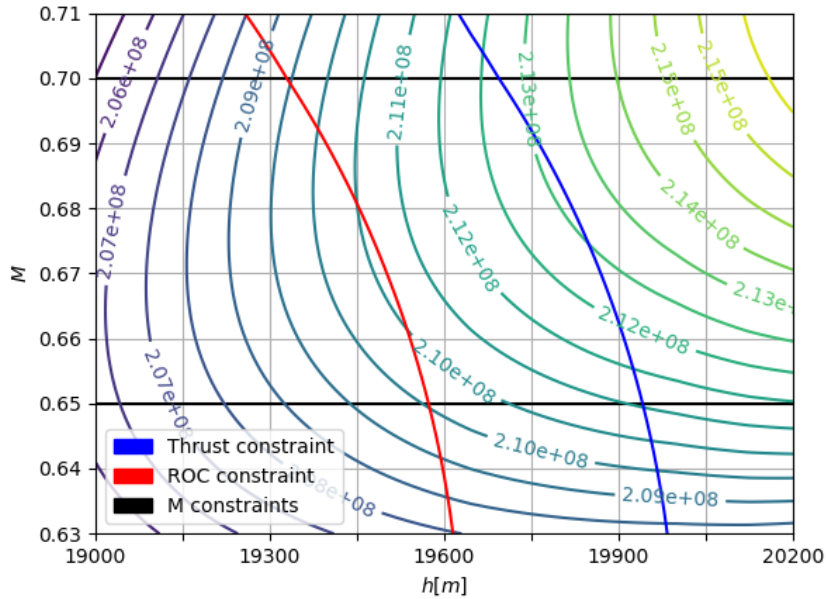


Figure 13.1: Specific range as a function of M and h , with performance constraints at $W = W_{cruise_1}$

maximize the rate of climb for a given altitude. Therefore, the loiter speed was set to $M = 0.65$.

Table 13.1 shows the results of the profile calculations with optimization of the fuel-intensive phases.

13.1.2. Climb and Descent Procedures

In Subsection 7.2.1 no climb or descent procedures were detailed, and the fuel burnt during those stages was calculated with statistics from [62]. This section presents the results of an analysis of these segments.

From the ER-2 experimenter’s handbook, the climb is carried out at constant IAS up to a crossover altitude, where the climb is continued at a constant Mach number. This is the procedure that ESRA will follow. To optimize for fuel consumption, the descent will be carried out using a continuous descent operation (CDO), as explained in [1]. In this procedure, the thrust is idle throughout, excluding the final approach where some thrust may be necessary to hold the required glideslope. This operation is already being implemented in a number of airports, including Schiphol. With a CDO, the fuel burn is close to 0. In order to remain conservative, the statistics were maintained from Raymer in the descent calculations, to allow for some fuel burn.

Using the program referred to in Subsection 13.3.1 it was determined that minimizing fuel burn is best achieved by climbing at a fast CAS with the thrust setting at 100%, as this minimizes the time to climb. The dive speed of the aircraft is 75 m/s EAS so a constraint was set to climb at a maximum of 70 m/s CAS. At the crossover, the altitude climb will be continued at cruise Mach number for ease of operations.

Since descent does not burn any fuel there is more freedom to choose a profile. It was decided on the descent at cruise Mach number followed by descent at constant CAS of 65 m/s to allow for a quick descent with some margin to the dive speed. Near landing, speed brakes will have to be used to achieve the speeds indicated in Section 13.2. Table 13.1 shows a summary of key performance metrics for the climb and descent phases of the profile. Table 13.2 shows a breakdown of the induced drag over the fuel-intensive phases of the mission. Given the improved resolution of the profile calculations, this should be taken as the budget for future design.

The key conclusion is that when taking into account altitude effects and proper evaluation of the fuel burnt in climb, the aircraft is unable to complete ESRA-STAKE-4-SYS-27. The diversion cruise must be

Table 13.1: Detailed profile calculations

Phase	Time spent [hr]	Starting altitude [km]	Ending altitude [km]	Distance covered [km]	M	Fuel Burnt [kg]
Warm up, taxi and take off	0.17 (approximate)	0	0	0	~0.15	75.23
Climb to cruise altitude	0.62	0	19.45	377.05	Detailed in text	213.28
Outgoing cruise	3.66	19.45	20.23	2622.95	0.675	482.06
Loiter on station	1.00	20.50	20.50	0	0.65	118.34
Return cruise	3.79	20.3	21.12	2700.00	0.67	431.85
First descent	0.85	21.12	0	347.64	Detailed in text	31.25 (from statistics)
Climb to 11 km	0.089	0	11.00	26.47	70 m/s CAS	70.28
Diversion cruise	0.24	11.00	11.00	175	0.7	65.1
Second descent	0.33	11.00	0	120.18	65 m/s CAS	29.61 (from statistics)
Landing and shut-down	0.17 (approx.)	0	0	0	0	23.22 (from statistics)
Total	10.89	-	-	6444	-	1540.22

Table 13.2: Induced drag over the fuel intensive phases of flight.

Phase	Induced drag, counts
Outgoing cruise	115
Loiter	137
Return cruise	113
Diversion cruise	3.5

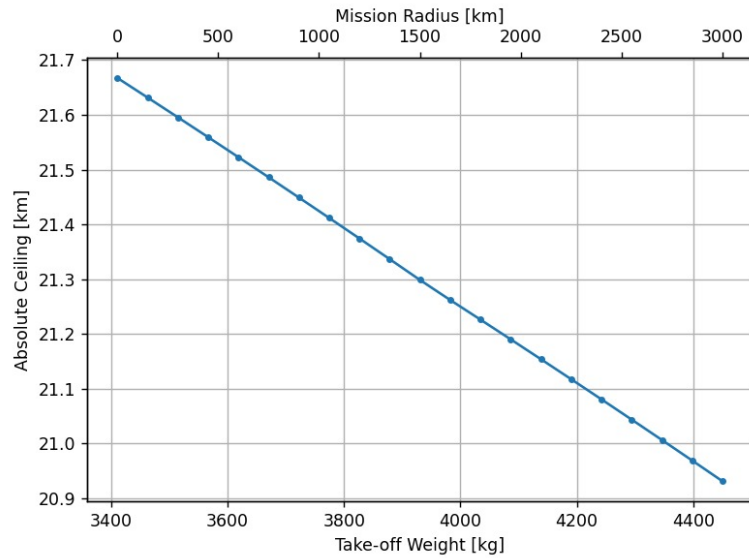


Figure 13.2: Sensitivity of the service ceiling to outgoing range (with take-off weight)

Table 13.3: Verification of the detailed profile calculations

Phase	Mf detailed	Mf simple	Remark
Warm up, taxi and take off	0.983	0.983	Both models used statistics
Climb to cruise altitude	0.951	0.98	
Outgoing cruise	0.884	0.875	
Loiter on station	0.968	0.968	
Return cruise	0.879	0.875	
First descent	0.990	0.990	Both models used statistics
Climb to 11 km	0.977	0.98	
Diversion cruise	0.978	0.951	Diversion cruise reduced from 500 km to 175 km for the full model
Second descent	0.990	0.990	Both models used statistics
Landing and shutdown	0.992	0.992	Both models used statistics
Final fuel fraction	0.35	0.35	

reduced from 500 km to 175 km, although some distance may be made up in climb and descent. The aircraft is also unable to cruise for 6000 km unless the distance covered in climb and descent is taken as part of the cruise. Since this distance is quite significant, the assumption is believed to be valid. To account for this, when operating at the critical mission profile, care should be taken to ensure a suitable alternative airport is within 175 km.

Sensitivity analysis

Figure 13.2 shows the absolute ceiling of the aircraft for a range of altitudes and weights. This graph is an indication of how high the aircraft can go for a given weight and the operational radius of the mission that that weight corresponds to. The ceiling is always evaluated at mid-mission and diversion is always included in the profile. Note that the absolute ceiling is generally around 250 m higher than the service ceiling, so this correction should be accounted for.

Verification and Validation

Verification of the fuel burn tool was carried out by comparing the results of the detailed analysis to those of the simplified model in Subsection 7.2.1. The results are shown in Table 13.3.

It is clear that the tools agree to a substantial amount, indicating that the numerical program is running correctly. The greatest discrepancies lie in the fuel burnt during climb and during diversion. This is

reasonable as the climb is to twice the altitude of a typical airliner and the diversion profile has been significantly altered.

Due to the general agreement of both the simplified and higher-fidelity models validation remains the same as in Section 7.2.

13.2. Take-off and Landing

The objective of the take-off and landing analysis is to ensure compliance of ESRA with ESRA-STAKE-8-SYS-26 and to show that the take-off maneuver can be completed with the selected configuration.

13.2.1. Take-off condition

To take off the aircraft should be able to accelerate, rotate around its main landing gear and generate enough lift force to become airborne. This requires the solution of the dynamic problem depicted on the Figure 13.3.

The start of the rotation is defined as the instant when the nose landing gear has just left the ground and thus normal force \vec{N}_n and friction force \vec{F}_n are equal to zero. Note that drag forces have been omitted for simplicity due to their relatively small magnitude at take-off speeds. Since drag generates a pitch-up moment around the landing gear, this assumption is conservative and valid. The acceleration in the y-direction is considered to be zero since the aircraft is still in the translation stage. Concerning the lift forces, the C_L of the wing is assumed to be 0.77 and $C_{L_H} = -0.95$ for the tail. These correspond to the C_L of the wing at 3° angle of incidence and the C_{L_H} of the tail at -3° angle of incidence with -10 degrees of elevator deflection.

By summing the moments around the main landing gear the required lifting force of the horizontal tail can be determined. The resulting equation is Equation 13.3

$$\sum M_{main} = Ty_{thrust} - Lx_{ac} + Wx_{cg} + L_h l_h = ma_x + \alpha(I_{yy} + md^2) \tag{13.3}$$

where all distances are with respect to the point where the main landing gear is touching the ground. The moment of inertia was obtained from the CAD model, using the mass of the components obtained in Subsection 7.2.2. The above equation can be satisfied by choosing the appropriate take-off speed and thrust settings to ensure rotation.

Raymer suggests that the take-off velocity should be at least $1.1V_{stall}$, thus $46.2[m/s]$ [62]. The maximum take-off speed is limited by the dive speed which is $77.8[m/s]$ to ensure the structural integrity of the plane. The required take-off speed to satisfy (13.3) is $V_{TO} = 59[m/s]$ which is within range, meaning the aircraft can rotate safely during take-off with no tailplane adjustments necessary. The analysis was also run at 50% thrust, to simulate engine failure during the take-off run. This had an insignificant effect on the required tail area as the moment due to the horizontal inertia of the aircraft works to offset the moment due to thrust.

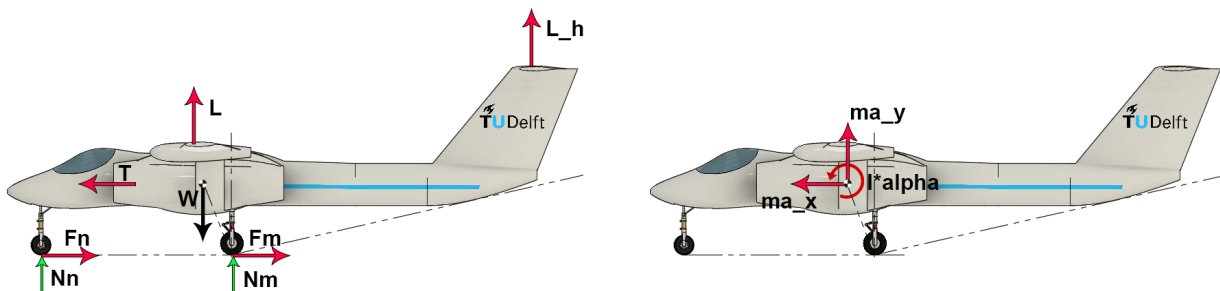


Figure 13.3: Take-off FBD

13.2.2. Take-off and Landing Distance

Once the take-off speed is known, the take-off distance can be calculated. This distance consists of the ground roll, transition to climb, and climb phases. In some cases, the required altitude to clear 50 ft (specified by [62] to be the necessary altitude for obstacle clearance) can be reached in the transition to the climb phase in which case the distance in the climb phase can be omitted. The ground roll distance was obtained from the following relations:

$$S_G = \int_0^{V_{take-off}} \frac{V}{a} dV \quad (13.4) \quad a = \frac{g}{W} [T - D - \mu(W - L)] \quad (13.5)$$

where $\mu = 0.03$ is the friction coefficient for a dry concrete runway[62]. For both the takeoff and landing calculations MTOW was assumed, as a worst-case scenario.

The transition distance, S_T , is obtained from the following equations:

$$S_T = R \sin \gamma_{climb} \quad (13.6) \quad R = \frac{V^2}{g(n-1)} \quad (13.7) \quad S_{appr} = \frac{h_{obs} - h_{flare}}{\tan \gamma_{appr}} \quad (13.8)$$

γ_{climb} was obtained using (13.12) assuming $V = 1.05V_{TO}$. It was calculated as $\arcsin \frac{ROC}{V} = 33$. The altitude reached during the transition stage is $R(1 - \cos \gamma_{climb}) = 34.2[m]$. This is above the required obstacle clearance of 35 ft [62], thus the climb phase analysis can be omitted. The total take-off distance is $S_G + S_T = 411 + 129 = 540[m]$. This conforms to ESRA-STAKE-8-SYS-26.

To study the possibility of take off with one engine out, the analysis was re-run at 50% thrust. In this case, $S_G = 926$ and $\gamma = 13$. $S_T = 58[m]$ but, since the climb angle is lower, the achieved height is less than the required obstacle clearance. It is necessary to compute the climb distance, given by (13.8), with h_{flare} being the height achieved at the end of the transition phase and $\gamma_{appr} = 13$. The result is $S_C = 37[m]$. The total distance is $S_{TO} = 1021[m]$, still below the requirement.

Analysis of the landing distance was also carried out. The landing procedure consists of three phases: approach, flare, and ground roll. The approach begins by clearing an obstacle of 50 feet as specified in [62]. This must be done at a certain glideslope angle, set to 3° for ESRA, as is the case for most transport aircraft. The flare height was assumed to be 20 feet, taken as the average of the typical height of large airliners and small general aviation aircraft. The approach distance may be calculated with (13.8), and the flare distance with (13.6), taking γ_{climb} to be $\gamma_{appr} = 3$. The flare velocity v_f was defined to be $1.23V_{stall}$ and n assumed to be 1.2, as indicated by [62]. Note that $V_{stall} = 40[m/s]$ as specified in Chapter 12.

The ground run follows from (13.4) with the integration limits set from $V_{land} = 1.15V_{stall}$ to 0, the thrust at idle and μ to 0.3, which is a normal value for friction with brakes applied on a concrete runway. The result of the total landing distance is $S_{land} = 1,030m$. Regulations specify that the landing distance be $\frac{10}{6} \cdot S_{land} = 1,717m$, which is well below ESRA-STAKE-8-SYS-26.

13.3. Flight Envelope, Climb and Descent Performance

It is necessary to establish the performance limitations of the aircraft. There are a number of constraints on the operation of ESRA. Aerodynamically, the aircraft is constrained by stall at low speeds and by drag divergence and Mach buffeting at high speeds as discussed in Chapter 9. In terms of power, for a given altitude there is a range of velocities where the power available is in excess of the power required to overcome drag, that is $TV - DV > 0$. The boundaries of this region set the power limitations of the aircraft. Note that at high altitudes the excess power may not be sufficient to fly at stall speeds, in which case the aircraft is power limited at low speed. The point where the achievable rate of climb is 0 is defined as the absolute ceiling. Mathematically, this occurs when the excess power is null and the power required and power available curves are tangent to each other, as shown in (13.9). The service ceiling of the aircraft is the point where the achievable rate of climb at the best climb speed is 0.5. The aircraft should not be expected to fly beyond this boundary. A detailed analysis of the climb performance of ESRA is shown in Subsection 13.3.1.

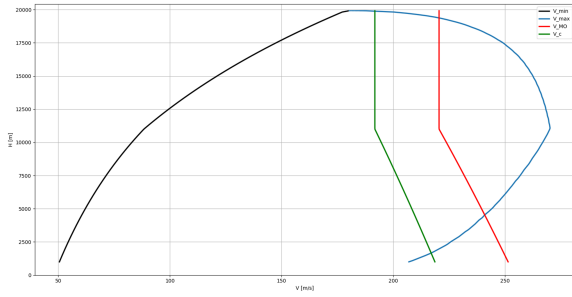


Figure 13.4: Flight envelope at MTOW

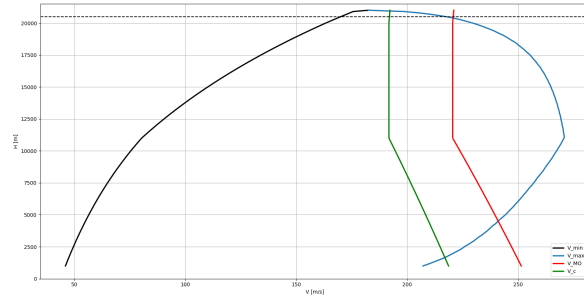


Figure 13.5: Flight envelope halfway through the mission

Flight envelope diagrams were generated showing the combination of altitudes and speeds in which the aircraft can operate. A number of assumptions were made. The most significant are as follows. Firstly, $C_{Lmax} = 0.96$. This is the C_{Lmax} at high altitudes and high M. This assumption is conservative, as compressibility effects reduce the value of this parameter. The effect is that at low altitudes the envelope will be wider. Secondly, thrust is a function of altitude and Mach number. This is a relaxation of an assumption made in [64] as engine data is now available. The effect is that the envelope is of higher fidelity. Thirdly, M_{dd} denotes the aerodynamic buffet boundary. Drag divergence occurs when a strong shockwave separates the flow at a certain point over the airfoil, leading to a sharp increase in drag. The interaction of the shock with the boundary layer may also lead to the periodic motion of Mach buffet [6]. Fourthly, the aircraft is flying at a load factor of one. An increase in the load factor both increases the stall speed and reduces the speed at which Mach buffet occurs [6]. The purpose of the envelope is to showcase the performance of the aircraft flying straight and level on the station, so the assumption is valid. Section 13.4 considers the increase in load factor when analyzing turn performance. Fifthly, C_{D0} and e are constant at all altitudes and Mach numbers. As shown in Subsection 7.2.3 this assumption is conservative for the parasite drag, as C_{d0} decreases with increasing altitude and Mach number. Finally, the thrust setting is 100%. The PW 535A engine is certified to fly at continuous maximum power, so this assumption is valid [83].

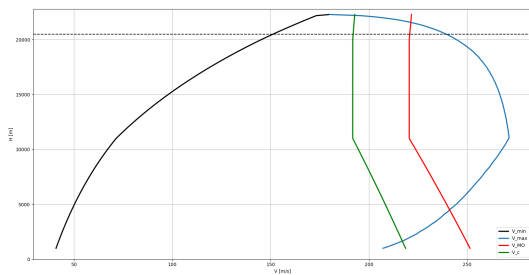


Figure 13.6: Flight envelope at the end of the mission

Figure 13.4, Figure 13.5, Figure 13.6 show the flight envelope at MTOW, halfway through the mission when the aircraft is expected to operate at 20.5 km, and at the end of the mission.

Analysis of these figures leads to the following conclusions. While on station, the aircraft flies 155 m below its service ceiling. As the aircraft stays on station and burns fuel the margin increases. The margins to stall are 21 m/s and 25 m/s to engine flame out. The range of operations is greater to the U-2, which can fly as little as 2.5 m/s above stall [25]. The aircraft is power limited before being aerodynamically limited, as the power boundary is reached before the over speed limit in Figure 13.5. This shows that, while on the station, the aircraft is flying at the edge of the engine performance. This may lead to increased engine maintenance and overhauls. Note in Figure 13.6 that the absolute ceiling increases past 22 km when the aircraft is flying on very low fuel. This is higher than the greatest recorded ceiling of the ER-2 and opens the possibility for research to be carried out at greater altitudes than 20.5 km, provided the aircraft takes off with significantly less fuel. This is illustrated in

$$\left. \begin{aligned} TV - DV &= 0 \\ \left(\frac{\partial T}{\partial V} V + T \right) - \left(\frac{\partial D}{\partial V} V + D \right) &= 0 \end{aligned} \right\} \quad (13.9)$$

Figure 13.2.

13.3.1. Climbing Performance

The climb performance of the aircraft should be assessed at sea level to show compliance with ESRA-STAKE-4-SYS-42 and at different stages of the mission to show compliance with ESRA-STAKE-4-SYS-41. Assuming symmetric flight with small climb angles ($\gamma < 15$) the rate of climb C is given in (13.10) [62]. This is equivalent to (13.11)

$$C = \frac{(T - D)V}{W \left(1 + \frac{V}{g} \frac{dV}{dH}\right)} \quad (13.10) \qquad C = V \sin(\gamma) \quad (13.11)$$

Due to the relatively large thrust-to-weight ratio of our aircraft, it is likely the assumption of small climb angles does not hold at certain conditions such as take-off. However, in later stages, this model is appropriate.

Results for the general climb performance of the aircraft are given in Table 13.4 by assuming a steady rate of climb, such that

$$C = \frac{(T - D)V}{W} \quad (13.12)$$

Table 13.4: Aspects of climb performance.

Parameter \ Weight	MTOW	Start of loiter	End of mission
Max C (sea level) [m/s]	44	-	-
Max C (20.5 km) [m/s]	Not achieved	0.6	2.3
γ (sea level) at TO speed and full thrust [°]	33	-	-
γ at loiter speed (20.5 km) [°]	Not achieved	0.19	0.7
Climb gradient at take off [-]	0.52	-	-

The climb gradient is required by CS-23 to be greater than 0.083 to ensure proper clearance of obstacles around the airport.¹ There are some points worth noting. The small angle approximation is invalid at low altitudes, as the climb angle at sea level is 30°. The climb gradient at sea level is 52%, conforming to regulations.² At the start of the loiter phase a climb rate of only 0.6 m/s can be achieved. This means the engines are already operating close to their limit. Note however, that towards the end of the mission the achievable rate of climb is considerably better, 2.3 m/s. To ensure the longevity of the engine the critical mission profile should be flown sparingly and Figure 13.2 should be taken as a reference of the achievable altitude for a range of mission radii.

Climb and Descent Profile Analysis

As mentioned in Section 13.1 the climb profile for ESRA is ascent at a constant CAS of 70 m/s up to the crossover altitude, where the true airspeed equals the cruise Mach number. The climb is then continued at a constant Mach number. This is similar to most airliners and to aircraft such as the ER-2 and WB-57 [25, 34]. The rate of the climb follows from (13.10). V_{CAS} must be translated to V_{TAS} to compute $\frac{dV}{dH}$ for the first part of the climb. This may be done using the conversion described in [71].

$\frac{dV}{dH}$ was computed numerically throughout the climb profile. A program was written in Python to evaluate the performance in climb, specifically, the time to climb (13.13), the distance in climb (13.14) and the fuel burnt during climb (13.15). For the calculation of the fuel burn a thrust setting of 100% was assumed, as this gave the best fuel performance (see Subsection 13.1.2).

¹URL: <https://www.easa.europa.eu/en/document-library/certification-specifications/cs-23-amendment-6-and-amc-gm-cs-23-issue-4> consulted on 22/05/2023

²URL: <https://www.easa.europa.eu/en/document-library/certification-specifications/cs-23-amendment-6-and-amc-gm-cs-23-issue-4> consulted on 22/05/2023

$$t_{climb} = \int_0^{h_1} \frac{1}{C} dh \quad (13.13)$$

$$s_{climb} = \int_0^{t_1} V \cos \gamma dt \quad (13.14)$$

Table 13.1 shows the results.

The descent profile was determined to be a continuous descent operation (CDO) for maximum fuel efficiency. The equations for climb still apply, with the caveat that $\gamma < 0$. Results for the descent time and distance are also shown in Table 13.1.

13.3.2. Verification and Validation

Verification of the time to climb and ceiling tool was conducted in [64] by thorough unit testing. Validation was also performed by considering a simplified model for thrust lapse (13.16) and using data from the U2 to predict its time to climb. The ceiling calculator was validated against data from the Gulfstream G550. The results of the validation were: the time to climb to 50,000 ft was predicted to be 12.6 min, as opposed to the true value of 12.5 min. The ceiling of the Gulfstream was predicted to be 50,000 ft, against the true value of 51,000 ft.

$$f_{climb} = \int_0^{t_1} T c_j dt \quad (13.15)$$

$$T = T_{TO} \left(\frac{\rho}{\rho_0} \right)^n \quad (13.16)$$

Regression-based sensitivity analyses were performed on both tools, with the results shown in Table 13.5 and Table 13.6 [64].

Table 13.5: Sensitivity of the ceiling calculator, $R^2 = 0.99$ **Table 13.6:** Sensitivity of the time to climb calculator, $R^2 = 0.95$

Parameter	Range	SRC
C_{D_0}	[0.014, 0.02]	-0.424
$T_{TO}[N]$	[112,800, 150,400]	0.435
e	[0.65, 0.85]	0.206
n	[0.75, 1]	-0.718
A	[7, 8.5]	0.142
$W_{TO}[kg]$	[38,420, 45,200]	-0.244
$S[m^2]$	[89.4, 119.2]	-0.003

Parameter	Range	SRC
C_{D_0}	[0.014, 0.02]	0.289
f_{Tto}	[0.75, 1]	-0.663
e	[0.65, 0.85]	-0.048
n	[0.75, 1]	0.658
A	[10, 12]	-0.018
f_W	[0.98, 1]	0.064
$S[m^2]$	[47.4, 64.1]	0.081

It can be seen for both tools that the result is most sensitive to parameters that affect the thrust, namely T_{TO} , f_{Tto} and n . f_{Tto} denotes the throttle setting, with 1 being 100%. Because of this high sensitivity both tools were validated to moderate degrees of confidence, as the simplified thrust model is not necessarily indicative of actual engine performance. The excellent results presented above for the validation were obtained by model matching both tools, varying the sensitive parameters within the ranges shown in Table 13.5 and Table 13.6. Because accurate results were obtained with model matching, the tools were deemed valid and verified in [64].

It is worth noting the sensitivity of both the time to climb and the ceiling to the parasite drag. Although it is not the most significant parameter it has a significant effect. Care should be taken to reduce parasite drag as much as possible to maximize performance at altitude.

13.4. Turning Analysis

Level-turning flight analysis has been done. It resulted in the following results summarized in the Figure 13.7. Results comply with the minimum turn radius requirement ESRA-STAKE-9-SYS-44. The plots in Figure 13.7 demonstrate the turn radius envelope together with the time required to perform a full turn at different cruise velocities. The maximum load factor of 1.12 indicates that the maximum bank angle is 26°.

There was a concern that due to the low range of cruise speeds available at service altitude, the wing tip may stall during the turn. A simple analysis has been performed to verify whether this is a serious

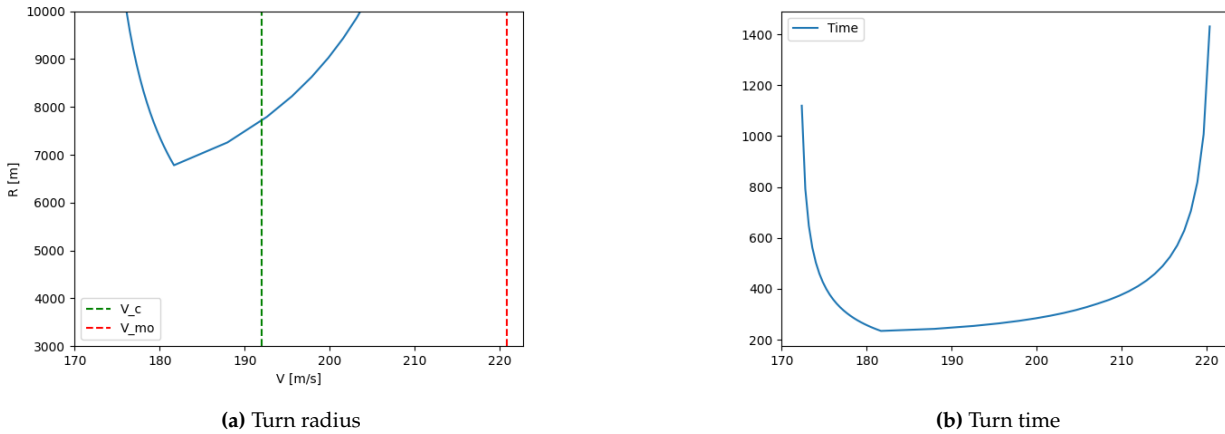


Figure 13.7: Turn performance
Table 13.7: Summary of horizontal turn analysis

	R_{min} [m]	T_{min} [s]	n_{max}
ESRA	6781	181	1.12

threat, it involved the calculation of the speed difference between the root chord and inner wing tip chord during the turn at the maximum bank angle stated above yielding the Equation 13.17.

$$V_{inner} = V_{cg} \left[1 - \frac{b}{2R} \cos \phi \right] \tag{13.17}$$

where V_{inner} is the speed that the inner wing's tip experiences, whereas V_{cg} is the speed at the center of gravity. However, the analysis showed that due to high speeds and a big Radius of around 6.7 km, the difference in speeds is negligible, therefore stall of the wing tip during the turn is unlikely to happen, and could always be avoided by deflecting ailerons to increase a C_L when needed. However, for low speeds, this can become an issue and is addressed in control surfaces sizing Section 12.5.

Internal layout and aircraft systems

Work on different subsystems has been documented in the previous chapters with performance analysis in Chapter 7, propulsion analysis in Chapter 8, operation in Chapter 16 and so on. The aforementioned systems are all required for flight but they cannot operate in a vacuum. This section will deal with the interconnections between different aspects of the aircraft and the layouts and connections between different crucial systems of ESRA. First, the general system communication layout will be presented, this will be followed by a presentation of the aircraft electrical system as it is central to the ESRA system layout. Following this, the fuel distribution system will be presented before attention is given to the hydraulics layout.

14.1. System communication

ESRA is a complex aircraft with many systems interacting internally as well as externally. Figure 14.1 shows a preliminary layout of communication channels between systems as well as some of the components of each system.

The ESRA system is mostly self-contained though it will interact with a ground element composed of Air Traffic Control (ATC) as well as the mission scientists. The airborne element is composed of multiple communicating elements such as the cockpit, the Flight Control System (FCS), the navigation and communication system (NavCom) and so on.

It was decided to use a Fly By Wire (FBW) system in order to reduce pilot workload by the implementation of control augmentation systems. This is achieved by routing all pilot and autopilot inputs through the two redundant flight computers. These computers are furthermore fed telemetry (such as airspeed, altitude, and attitude...) that is gathered via measurement devices. Given all required inputs, the flight computers will give commands to all actuators as well as the propulsion system. It can also be noted that the flight computer data also feeds into the Flight Logging System (FLS) along with the cockpit voice recordings.

The NavCom system includes the equipment required by ESRA for successful navigation (GNSS receiver and weather radar) as well as communication with the system ground element. The communication part of the NavCom system is composed of a VHF radio which connects the pilot to ATC as well as the mission scientists. Furthermore, ESRA is equipped with an ADS-B transponder which enables it to be tracked by ground control. Furthermore, ESRA also offers the option to be equipped with a datalink system in order to enable the mission scientists to collect data in real time and make small changes to the flight plan. However, it has been decided in Chapter 16 that the datalink is not a default part of ESRA and the mission scientists are responsible for its installation and operation.

Furthermore, a life support system was included in order to provide pressurization and heat to the pilot and the payload. Environmental sensors are placed both in the cockpit and in the regulated payload bays that feed data back to the life support system which in turn feeds air and heat where it is needed.

14.2. Electrical subsystem

As mentioned in Section 14.1, ESRA relies heavily on electrical systems such as the FCS and NavCom systems. The Electrical Power System (EPS) must therefore provide sufficient redundancy for the aircraft to land even if all power-supplying systems are lost. The EPS shown in Figure 14.2 can be seen to be built primarily around an Alternating Current (AC) system with two main busses. These buses are centralized power distribution systems that take power in from a generator for example and distribute it across several systems.

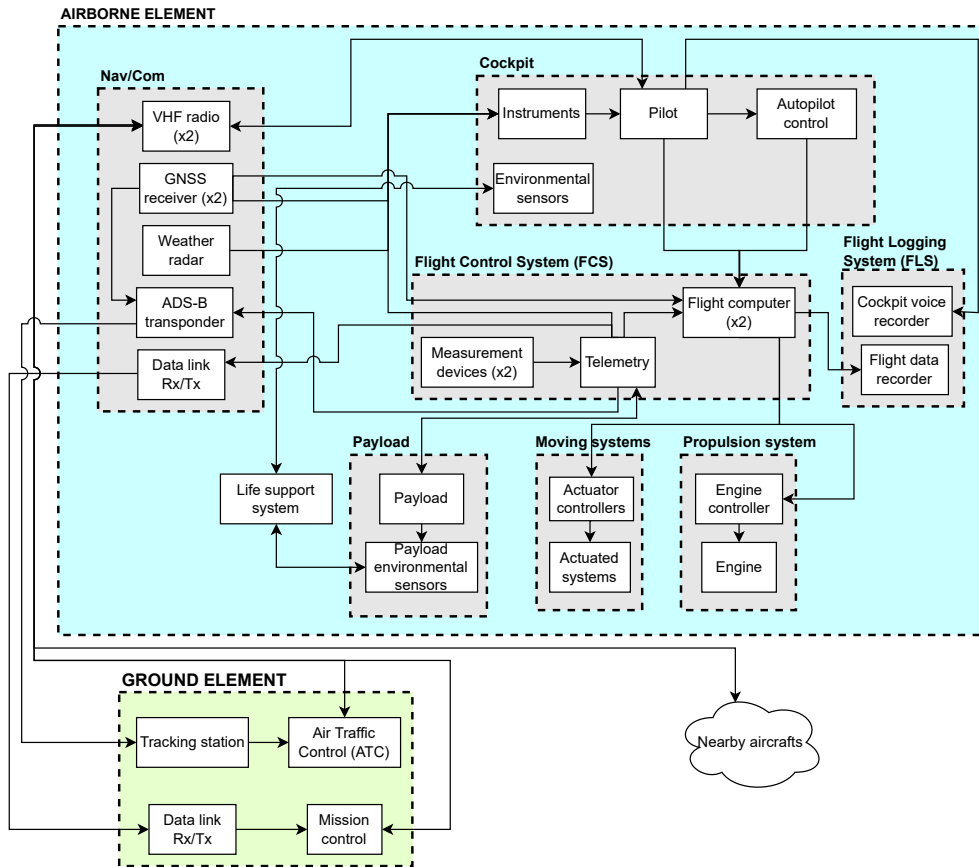


Figure 14.1: System communication diagram

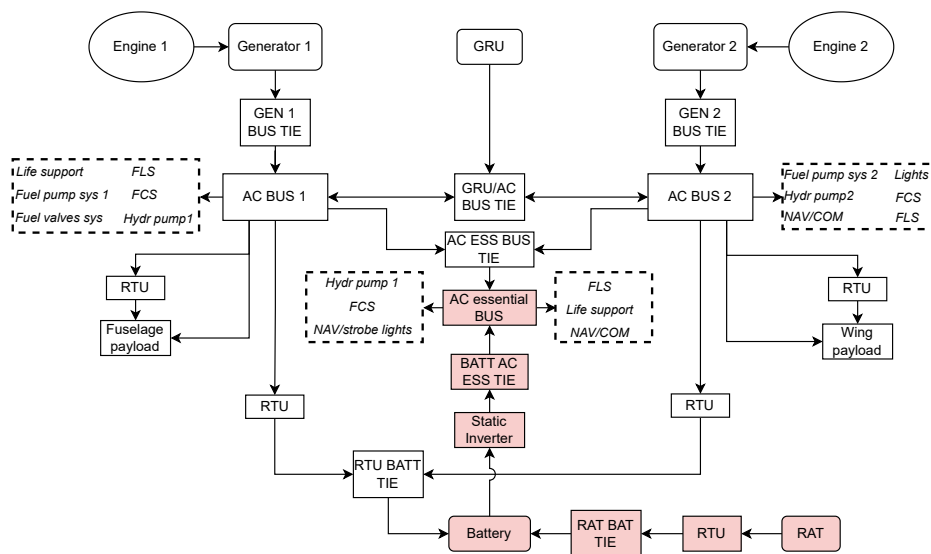


Figure 14.2: Electrical subsystem diagram

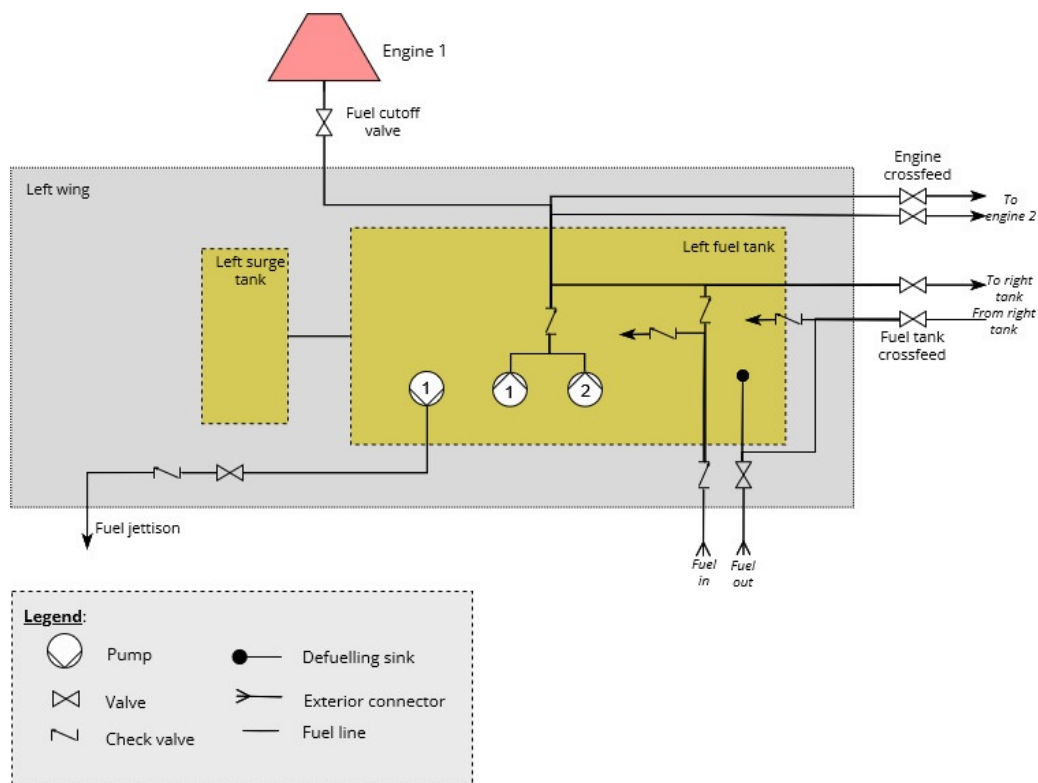


Figure 14.3: Fuel distribution subsystem diagram

Figure 14.2 shows that the electrical system is powered by two generators that are in turn powered by the engines. Multiple "ties" can be noticed throughout the EPS, these ties are components of the EPS that connect different components such as the generators and busses. Furthermore, the GPU/AC BUS TIE has the important role of connecting the two AC buses such that they can share power in the event of a generator or engine failure. This tie also connects the electrical system to a Ground Power Unit (GPU) to provide the aircraft with power when before during start-up. It was decided to use a GPU instead of an onboard Auxiliary Power Unit (APU) to save on weight and simplify the design.

All electrically powered systems are connected to AC BUS one and two and some of them are connected to both in order to provide some redundancy. These more important systems include the FCS and the FLS as these systems cannot be allowed to fail. Redundancy is also added by connecting different fuel and hydraulic pump systems to the different busses such that fuel supply from both tanks is assured even in the event of a main bus failure.

The last layer of redundancy is provided by the battery that is connected to the AC essentials bus. This bus powers the most critical electrical systems of the aircraft that are needed to safely land such as the FCS, hydraulic system one, and the Nav/Com system. The battery itself is constantly powered by the AC busses via Rectifier Transformer Units (RTU) and another tie. In the event of both busses failing, the critical systems will be powered by the battery which in turn can be powered by a Ram Air Turbine (RAT).

14.3. Fuel subsystem

The aircraft needs thrust to fly and in order to produce thrust it needs a reliable fuel supply. A basic diagram for the fuel distribution system is given in Figure 14.3.

Figure 14.3 shows that ESRA is equipped with one main fuel tank in each wing with each of them paired with a surge tank further outboard in the wing. The purpose of the surge tanks is to cope with any change in the volume of the fuel due to a change in temperature for example.

Attention was also given to redundancy within the fuel system with the engine crossfeed lines being doubled to ensure that both engines can be supplied from one side of the aircraft even if one of the

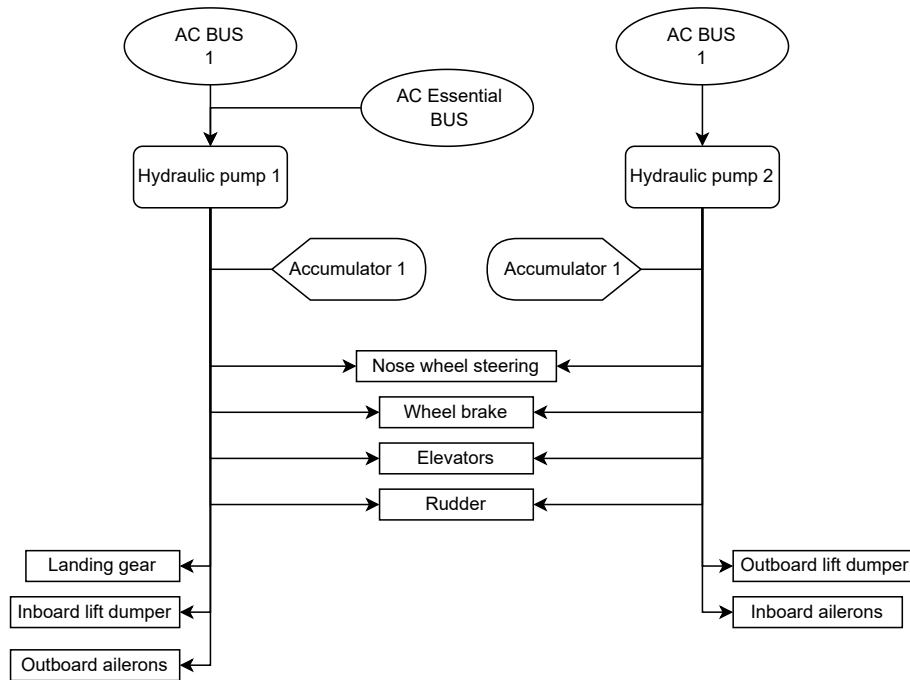


Figure 14.4: Hydraulic subsystem description

crossfeed lines had failed. Furthermore, there are two main fuel pumps that supply the engine as well as the engine and fuel tank cross feeds, which are each powered by a different electrical system in order to provide an additional layer of redundancy. A fuel jettison system is also included in order to enable the aircraft to lighten itself in case an emergency landing is required. Lastly, in case of an engine failure, a fuel cutoff valve is included such that the aircraft is able to starve the powerplant of fuel to rapidly shut it down.

It is furthermore possible to fuel and defuel the entire aircraft from a single location on the aircraft. This is achieved by routing fuel into the tank as well as the tank crossfeed line such that both tanks can be filled simultaneously. A similar approach is used to defuel the aircraft whereby the far tank is defuelled via the crossfeed line and the close one simply via a port in the tank. This method does mean that at least one of the fuel pumps in the far tank has to be active during defuelling thus requiring the aircraft be on ground power during the operation.

14.4. Hydraulic subsystem

The hydraulic subsystem of the aircraft is critical to its safe operation and comfortable use. Indeed many subsystems rely on hydraulic pressure derived from the engines to function and actuate properly. A visual summary of the hydraulic subsystem layout as well as the different subsystems attached to it is given in Figure 14.4.

Figure 14.4 shows that the aircraft is equipped with two independent hydraulic systems with electric pumps respectively driven by the two electrical systems. Furthermore, it can be seen that both hydraulic systems are equipped with an accumulator which is a pressure vessel meant to help the system cope with sudden demands and reduces the power required from the hydraulic pumps.¹ Subsystems attached to each hydraulic system are also shown in Figure 14.4 and two types can be distinguished: systems such as the brakes, elevator actuators, and rudder actuators were judged

¹URL: <https://www.fst.com/sealing/products/accumulators/hydraulic-accumulators/>[cited on 14/06/2023]

important enough that they were connected to both hydraulic systems so that they can still function in case one hydraulic system fails. On the other hand, some systems such as the landing gear, ailerons, and lift dumpers were connected to only one system. This choice was not made because the concerned systems are of lesser importance but because they have a different kind of redundancy. If system one were to fail, for example, the inboard ailerons and outboard lift dumpers would still function and provide the aircraft with control. Furthermore, the landing gear can use gravity and its drag to deploy and lock and if that is still insufficient, a positive load factor maneuver can also be used to help deployment. In the unlikely scenario of a double engine failure, both principal electrical systems would also lose power and thus the hydraulic pumps would not be able to run. In order to prevent a complete loss of control due to a double engine failure, hydraulic system one was also connected to the emergency electrical system that is powered by the battery such that the pilot can bring the aircraft down safely even with such a failure.

14.5. Recommendations

The systems presented in this chapter have only been designed conceptually without any components being sized or characterized beyond their primary role. In future phases of design, it is recommended that investigations take place into the required characteristics of certain subsystems. Furthermore, the EPS shown in Figure 14.2 should be completed with the power requirements of different systems thus enabling the generators, the battery, and the busses to be sized. The same can be said for the fuel distribution system and the hydraulics system where pumps and tanks should be sized and selected. Furthermore, it is recommended that geometrical constraints for the mentioned systems be considered such that large components can be placed.

Finally, it is recommended to perform a RAMS analysis for the systems of ESRA in order to validate the selected layout in terms of how redundancy was implemented for safety. Thus, measures can be added where needed and removed where they are not necessary and it can be ensured that maintenance is easily achievable.

15.1. Aircraft system characteristics

Now that all of the subsystems are designed and the integration of the subsystems is complete, a summary containing all of the technical data can be made.

Table 15.1: Physical measurements of ESRA

Metric	Value	Unit	Description
l	11.03	m	Total length
l_{fus}	10.41	m	Fuselage length
d_{fus}	1.08	m	Fuselage diameter
b	24.98	m	Wingspan
S	32.00	m ²	Wing surface area
$c_{r,w}$	1.77	m	Root chord length main wing
$c_{t,w}$	0.80	m	Tip chord length main wing
c_{MAC}	1.34	m	MAC
z_{MAC}	5.46	m	Spanwise location of the MAC
$c_{r,h}$	1.08	m	Root chord of the horizontal tailplane
$c_{t,h}$	0.54	m	Tip chord of the horizontal tailplane
S_h	2.61	m ²	Surface area of the horizontal tailplane
$c_{r,v}$	2.42	m	Root chord of the vertical tailplane
$c_{t,v}$	1.28	m	Tip chord of the vertical tailplane
S_v	4.43	m ²	Surface area of the vertical tailplane
cg_{fwd}	3.84	m	Most forward location of the CG as measured from the nose
cg_{aft}	4.03	m	Most aft location of the CG as measured from the nose
$x_{lg,fwd}$	0.51	m	Location of the front landing gear as measured from the nose
$x_{lg,aft}$	4.45	m	Location of the aft landing gear as measured from the nose
$d_{eng,cow}$	1.07	m	Engine cowling diameter
$d_{eng,fan}$	0.81	m	Engine fan diameter
$d_{eng,exh}$	0.7	m	Engine exhaust diameter
$z_{lg,aft}$	1.66	m	Main landing gear track width
z_{eng}	1.66	m	Engine lateral position as measured from the fuselage center
$d_{lg,fwd}$	0.406	m	Nose landing gear wheel diameter
$d_{lg,aft}$	0.48	m	Main landing gear wheel diameter
z_{payl}	6.64	m	Lateral position of the wing-mounted payload pods as measured from the fuselage center
$l_{strut,hor}$	1.66	m	Horizontal strut length
$l_{strut,dia}$	5.13	m	Diagonal strut length

Table 15.2: Aerodynamic metrics describing ESRA

Metric	Value	Unit	Description
-	SC(2)-0612	-	Airfoil number of the main wing
-	SC(2)-0010	-	Airfoil number of the vertical stabilizer
-	SC(2)-0010	-	Airfoil number of the horizontal stabilizer
$C_{L_{des}}$	0.77	-	Lift coefficient of the main wing
$C_{l_{des}}$	0.86	-	Lift coefficient of the airfoil
A	19.5	-	Aspect ratio of the main wing
t_{root}	0.21	m	Maximum thickness of the main wing
A_h	4	-	Aspect ratio of the horizontal stabilizer
A_v	1.2	-	Aspect ratio of the vertical stabilizer
e	0.7	-	Oswald efficiency factor of the main wing
C_{D_0}	0.022	-	Zero lift drag coefficient
M_{DD}	0.73	-	Drag divergence mach number

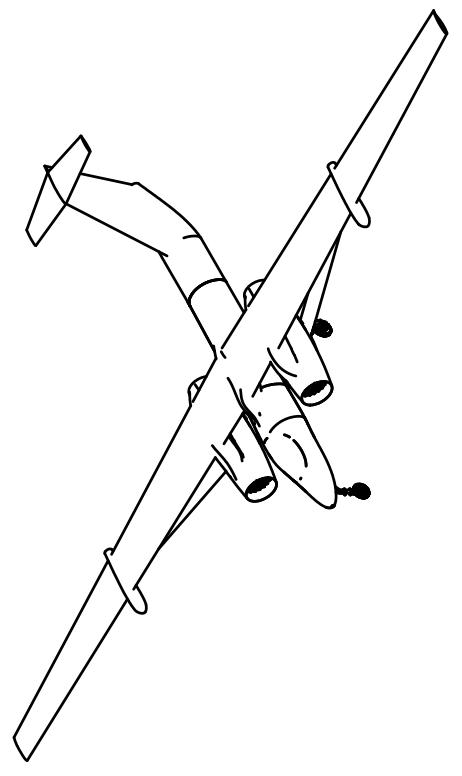
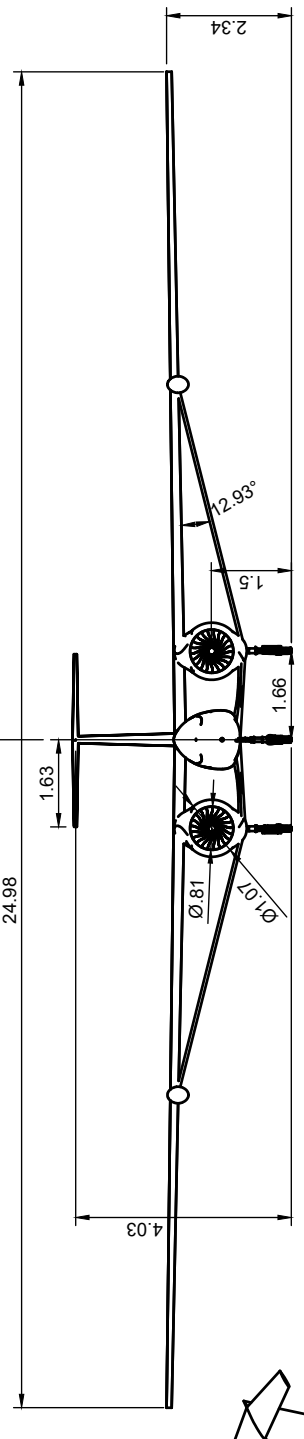
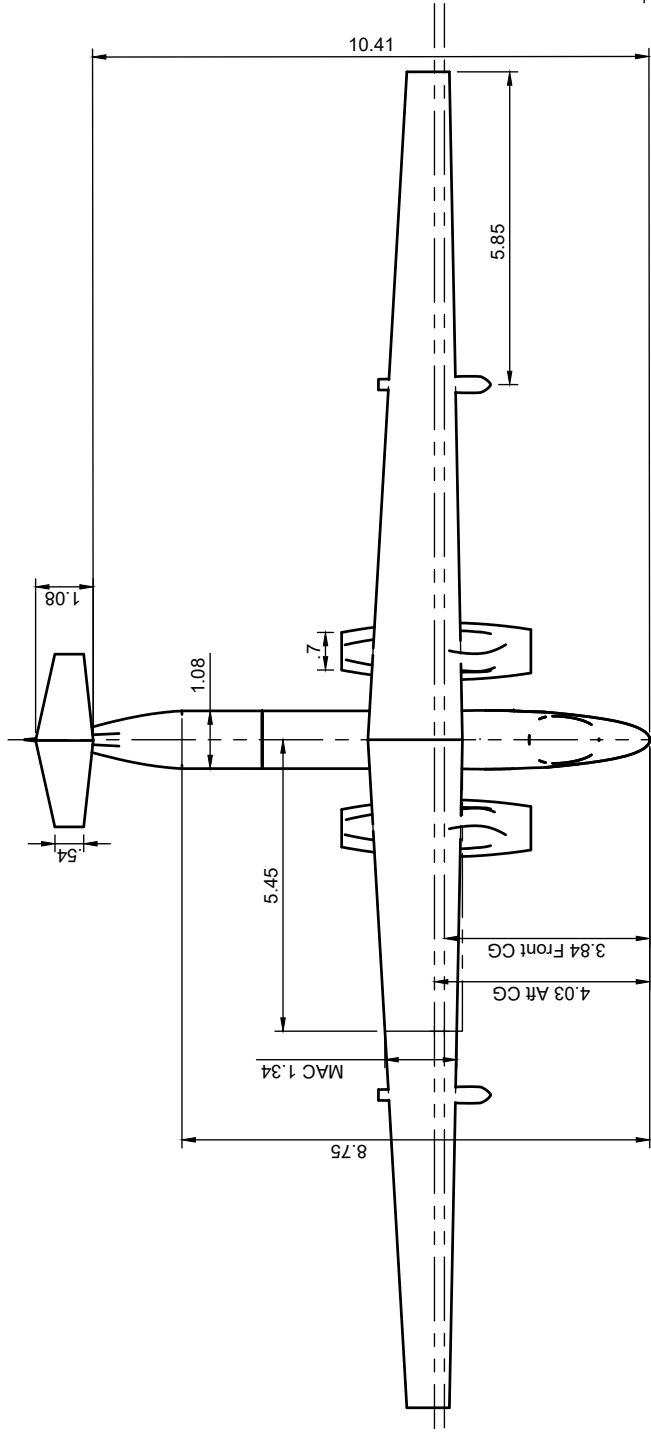
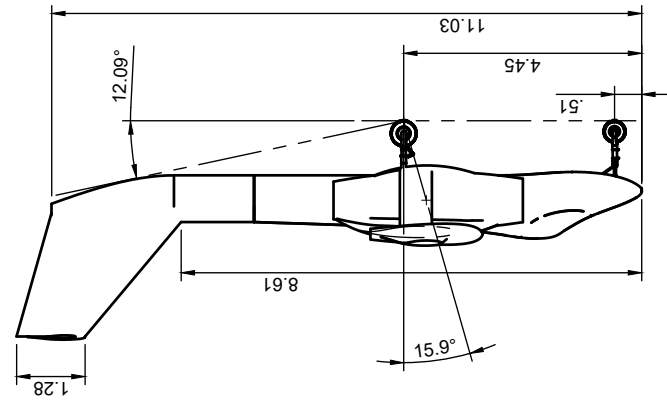
Table 15.3: Performance metrics describing ESRA

Metric	Value	Unit	Description
V_{cruise}	200	m/s	Cruise speed
M_{cruise}	0.65	-	Cruise mach number
$V_{D_{SL}}$	77	m/s	Dive speed at sea level
$V_{stall_{SL}}$	42	m/s	Stall speed at sea level
$V_{stall_{ceiling}}$	185	m/s	Stall speed at ceiling
h_{ceil}	20500	m	Service ceiling
h_{cruise}	19200	m	Cruise altitude
E	1	hr	Endurance on station
R	6000	km	Range
RC	32	m/s	Climb rate at sea level
T_{SL}	15.47	kN	Thrust at sea level conditions
T_{cruise}	1.73	kN	Thrust at cruise conditions
$TSFC_{SL}$	13.3	$\frac{g}{kN*s}$	TSFC at sea level conditions
$TSFC_{cruise}$	19.5	$\frac{g}{kN*s}$	TSFC at loiter conditions
d_{TO}	1000	m	Takeoff distance
d_{ldg}	1030	m	Landing distance
-	26.54M	\$fy2023	ESRA acquisition cost
-	4217	\$fy2023 / hr	User fee
-	304703	\$fy2023	Total cost for standard campaign

Table 15.4: Metrics describing the structure of ESRA

Metric	Value	Unit	Description
$MTOW$	4445.98	kg	Maximum takeoff weight
$MZFW$	2885.29	kg	Maximum zero fuel weight
OEW	2665.29	kg	Operating empty weight
W_F	1560.69	kg	Fuel weight
W_{payl}	100	kg	Payload weight
V_{payl}	2.56	m^3	Maximum payload dimensions
n_{max}	4.4	-	Maximum positive load factor
n_{min}	-1.762	-	Maximum negative load factor
$n_{max,land}$	-2.0	-	Maximum landing load factor

15.2. Technical Drawings



Dept.	Technical reference	Created by Group 14	Approved by
		Document type 6/19/2023	Document status
		Title ESRA	DWG No. 3
		Rev.	Date of issue
			Sheet 1/1

Having a working aircraft is important but ESRA must be operated as well. In order to ensure successful operations, plans are developed in this chapter. First of all, a discussion will be held on possible bases of operation for ESRA. Following this, flight operations will be addressed followed by ground operations and finally by a discussion on the operational limits.

Operations and Logistics

16.1. Home bases for operation

Table 16.1: Airport Information

Location	IATA code	Zone served	Runway length
Cagliari, Italy	CAG	Europe	2804m
Anchorage, USA	ANC	North Pacific	3780m
Manila, Philippines	MNL	South and East Asia	3737m
Johannesburg, South Africa	JNB	Africa	4421m
Ushuaia, Argentina	USH	Antarctica	2804m
Christchurch, New Zealand	CHC	Oceania, South Pacific	3288m
Mexico City, Mexico	MEX	Central and North America	3900m
New Dehli, India	DEL	Asia	4400m
Salvador de Bahia, Brazil	SSA	South America, South Atlantic	3003m
Wake Island, USA	AWK	Central Pacific	3000m

In order to facilitate ESRA's global operations, it is crucial to distribute the fleet of aircraft across various regions worldwide. To achieve this, a total of 10 different airports, listed in Table 16.1, have been selected to serve as the home bases for ESRA operations. The goal is to have an aircraft parked at each of these bases, readily available for operations at all times. By dispersing the aircraft across different locations around the world instead of concentrating them in a single airport, significant time and cost savings are achieved. This eliminates the need to schedule a ferry flight to move the aircraft from the central home airport to the specific airport of operation.

The selection of airports listed in the table complies with the criterion set before ESRA-STAKE-8-SYS-26. This criterion ensures that the aircraft can safely take off and land within a distance of 2500 meters. Furthermore, these airports are strategically situated in politically stable countries across the globe, enabling ESRA to conduct research activities on a global scale. To visualize the operational reach of the aircraft from these bases, circles representing a 3000 km operational radius are displayed around the identified airports, as depicted in Figure 16.1. These circles highlight the main areas of interest for research, such as the Pacific's Ring of Fire, the Indian monsoon region, and areas in proximity to the poles. It is important to note that if operations extend beyond these areas, the aircraft's range limitation of 6000 km prevents it from returning to the home base. In such cases, the aircraft would need to land at a different airport to accommodate the extended range requirements, making operations more inconvenient.

16.2. Flight Operations

16.2.1. Flight Profile

A regular mission profile during a campaign begins with a brief takeoff roll, followed by a steep initial climb. Within 40 to 45 minutes of launch, depending on the aircraft's weight, it will reach the intermediate cruise altitude of 19.6 kilometers. From here, cruise climb is initiated. During this phase, the aircraft flies very close to the critical Mach number. As fuel is consumed, the aircraft's weight decreases, allowing it to ascend to an altitude of 20.5 km. At this point, the aircraft performs station

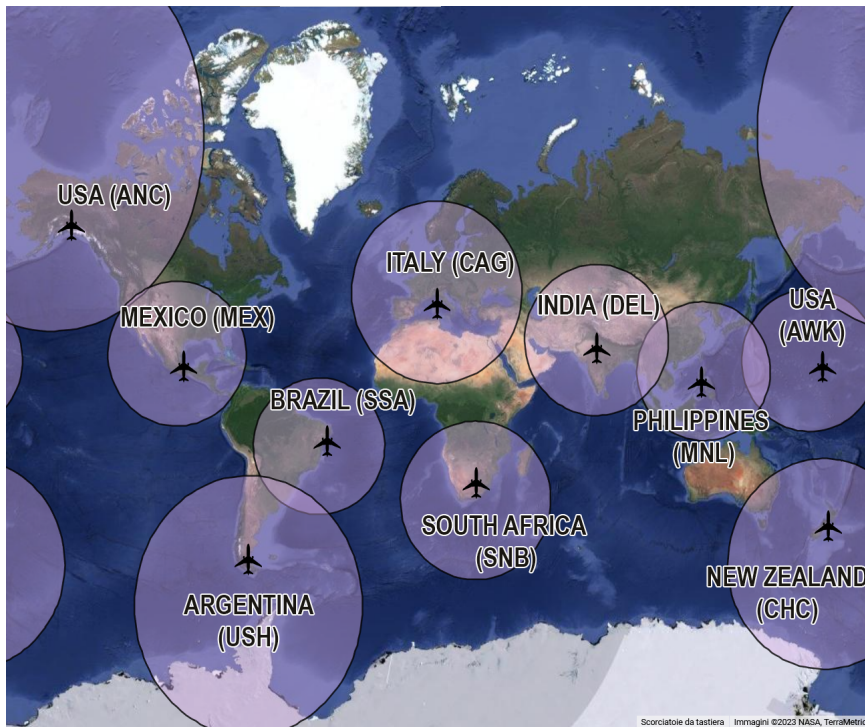


Figure 16.1: Map of the world and the range ESRA aircraft would have when operating from these airports.

keeping for 1 hour at this altitude to take measurements. In the second part of the flight, the aircraft descends quickly to 20 km, where it begins the second cruise climb, in which the altitude is gradually increased until the maximum ceiling, of around 20.8 km, is achieved. The height of the maximum ceiling depends on the weight of the payload on board. Approximately 30 minutes before landing, the descent from a high altitude will be initiated, and the aircraft will then return to the airport. The critical, 11 hours flight profile, described above, is displayed in Figure 16.2.

16.2.2. Frequency and Duration of Flights

The routine flight duration for the ESRA is 6 hours. However, if the mission requires it, the flight can be extended to a maximum of 11 hours, as mentioned in the section above and in Figure 16.2. The duty day for the pilot and the rest of the crew is 12 hours, it begins at pre-mission report time and ends with engine shutdown after the mission. Pilots and maintenance crew must have 12 hours of off-duty time between two flight sessions. Pilots who will fly a mission for more than 8 hours will be given one day after the flight to recover. As described in Chapter 1 a typical 5-weeks campaign includes 8 flying days of 6 flying hours per day.

16.2.3. Pre-flight Operations

Before the start of the flight, the aircraft needs to pass the preflight checks on the instruments that are performed by the maintenance crew, and the pre-flight inspections. These checks need to be completed at least 2hrs prior to the scheduled time for takeoff. After this, the aircraft is fueled and the oxygen tanks are replenished. 1 hr prior to launch, external power is connected to the aircraft. In order to prevent damage to the instruments due to voltage spikes, the instruments will be shut off until the engines have been switched on, and internal power is selected. The engine is started approximately 15 minutes prior to taking off. Due to the restricted mobility of the pressure suit and the possible heat build-up in the suit, the pilot will wear the suit and enter the aircraft only 30 minutes before launch. For the same reason, delays aside, the aircraft is taxied to the runway as soon as possible following engine start-up.

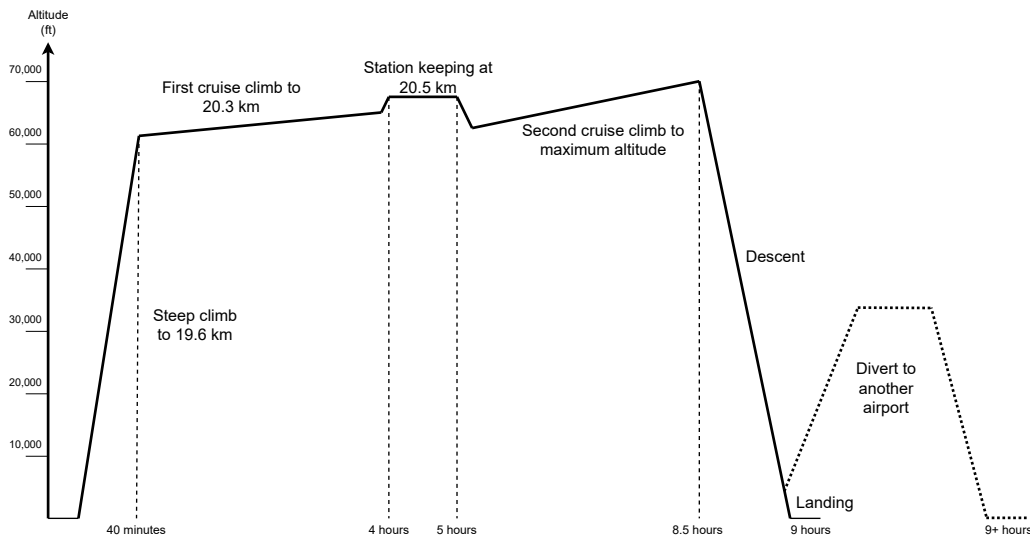


Figure 16.2: Critical flight profile for the ESRA. Altitude and time elapsed are shown as well.

In-flight Operations

During high-altitude operations, it is important to adhere to the performance limitations of the aircraft. The desired altitude and range must fall within these limitations to ensure the safety and efficiency of the mission. Additionally, other factors such as turbulence, altitude winds, temperature, and lack of a visible horizon for attitude reference may impose further restrictions. The pilot holds the authority to assess these conditions and make informed decisions regarding the continuation of the mission.

During operations, the operations crew will maintain radio communications at all times with the pilot. A designated member of the ground crew should remain in contact at all times with scientists from each instrument team, enabling communication in case of instrument-related issues or changes in the expected return time.

Post-flight Operations

Once the mission tasks are completed, the descent from high altitude is initiated. Following landing, the instruments are usually turned off, although they may remain powered for a brief period for sensor calibration. After ESRA has landed, a considerable amount of time is required for towing, inspection and servicing. Scientists should anticipate a waiting period of 30 minutes to 1 hour following engine shutdown before accessing the instruments. Following each flight, a mission debriefing is conducted to gather insights from the pilot, including observations on weather conditions and instrument performance.

16.3. Ground Operations

Payload

The fuselage-mounted payload will be integrated into the aircraft through a hatch in the rear of the fuselage. The payload dollies are slotted onto two rails and secured once they have reached their flight position, this system was inspired by that present on the WB-57, allowing for easy accessibility to the payload [34]. Once the payload has been slotted and pinned into place, it is electrically connected to the airplane's electrical system. The payload under the wing must be hoisted, fixed, and electrically connected. This procedure is taken directly from the mounting of a 3-foot pallet from the WB-57 [15]. The 3-foot pallets are equipped with pre-drilled holes, allowing experiments to be securely bolted onto the payload pallets. In the event that an experiment requires a different hole configuration than what is available, it is possible to drill additional mounting holes. However, it is important to ensure that the added holes do not compromise the strength and integrity of the pallet.

All payloads must conform to the given dimensions of either the dollies or the wing pods. The mass distribution within these payload areas must be approved before each mission by the mission manager and flight engineer independently to ensure that the CG of the airplane does not migrate outside the allowed safety limitations.

Electrical Power

The payload of the aircraft is provided electrical power according to requirements: ESRA-STAKE-7-SYS-29-PW-1 and ESRA-STAKE-1-SYS-1-PW-2. When the aircraft is in flight the power is given by generators powered by the bleeding air of the engine, however, once the aircraft is down on the ground the electrical power is provided by the infrastructure on the ground. The requirements for electrical power have been designed such that the aircraft on the ground is operated by a standard European power grid, therefore when operating in countries whose power grid is different a converter will be necessary.

In order to protect instruments from an electrical surge during aircraft power-up, it is recommended to turn them off when changing the aircraft from ground power to internal power. Similar recommendations are given to analogous research aircraft [25].

Data Handling

There will be no in-flight data transmission possibilities unless specifically organized by the scientists. All data will need to be recorded on a hard drive present in the payload compartment, this hard drive needs to be removed from the aircraft at the end of each flight, and it is the responsibility of the scientists to download and securely store the data.

16.4. Operational Limitations

16.4.1. Limitations due to flight planning

Some limitations of the ESRA's operation are dictated by the amount of time that a pilot can operate the aircraft. This time is referred to as the duty day and is determined by regulations set by EASA [24], as well as requirements established by US authorities for the ER-2 [25] and WB-57 [34] aircraft. In accordance with these regulations and to facilitate pilot transition among the stratospheric aircraft fleet, the ESRA fleet adheres to the same duty day and rest cycle requirements. Currently, the maximum duty day for the ESRA pilot is set at 12 hours, starting from engine startup until engine shutdown. Furthermore, a minimum of 12 hours of off-duty time is mandated between duty days [25, 34]. These two requirements for the pilot are in the form of ESRA-STAKE-4-SYS-48-LS-3 and ESRA-STAKE-4-SYS-48-LS-4.

16.4.2. Wind conditions

Flight operations will cease if wind speed or projected wind speed in any direction reaches or exceeds 30 knots. Additionally, if the wind speed or projected wind speed includes a crosswind component equal to or more than 20 knots, flight operations will be suspended.

16.4.3. Pilot control of instruments

Another limitation concerns the amount of control the pilot has over the instrumentation on board used for experiments. The ESRA is designed as a single-seat platform, which means the pilot has multiple responsibilities other than flying the aircraft. This includes operating communication and navigation systems, and managing various aircraft systems. While some systems may require minimal attention, others demand the pilot's full focus to ensure flight safety. Monitoring these systems is further complicated by the restrictive nature of the pressure suit which, coupled with the compact size of the cockpit, imposes constraints on the pilot's movement and adds complexity to even the simplest of tasks. Consequently, the pilot's available time dedicated to operating the scientist's instruments is limited, and it needs careful coordination to ensure the mission's safety and completion.

Sustainable Development Approach

This chapter covers the sustainable development approach of the ESRA project. In Section 17.1 the climate impact and emissions of ESRA are modelled and presented. Section 17.2 covers impact on social sustainability of the ESRA project. At last, Section 17.3 covers the End of Life strategy.

17.1. Climate impact and emissions

Any quantification of the climate impact of aviation is convoluted as the effects of different emissions don't directly correlate to an overall or immediate impact on the climate. Although precise predictions cannot be made, the effects of CO_2 and NO_x in the atmosphere can be modelled with a certain degree of certainty using a host of climate metrics[47]. These metrics include but are not limited to: GTP (Global Temperature-change Potential), GWP (Global Warming Potential) and ATR (Average Temperature Response). For the analysis of the climate impact of the ESRA design, ATR will be used as a value as it is specifically developed for aircraft and it models sustained emissions more precisely than the other methods [49]. This niche metric also helps correlate direct design choices in aircraft to the overall climate impact of a design. Even though ESRA will only be produced in small batch sizes with low operational hours relative to commercial aircraft, and thus the overall impact of the operation of this aircraft on the climate will be marginal, climate effects should be considered to some extent when making a future-proof design.

17.1.1. Average Temperature Response (ATR)

Before calculating the ATR of the aircraft, the definition of ATR should be considered. The ATR is calculated with the following expression:

$$ATR_H = \frac{1}{H} \cdot \int_0^{\infty} \Delta T_{sust,H}(t) \cdot w(t) dt \quad (17.1)$$

In Equation 17.1, H represents the time horizon over which the climate effects are considered. Here the operational lifetime of the aircraft (30 years) will be used, as in this time span the modeling of the climate effects is still quite precise [19]. The term $\Delta T_{sust,H}(t)$ signifies the time-varying global mean temperature change, caused by operating the aircraft for H years, and depends on the emission rates of the aircraft that is being considered. The final term, $w(t)$, is an additional weighing function that can for example be used to vary the impact in different phases in (or after) the operational time of the aircraft. For the sake of simplicity, no additional weighing will be considered in this report, the emissions will be assumed to conform with the chosen temperature response model.

Using the logic above, the calculation of the ATR is reduced to modeling the emissions of the aircraft. This is done through a Linear temperature response model (LTR), which considers altitude impacts.

$$e_i = EI_i \cdot W_{fuel} \quad (17.2) \quad E_i(t) = e_i \cdot U(t) \quad (17.3)$$

The first step is to quantify the emissions, which is done through Equation 17.2. The values used for EI_i (emissions index) are a function of the composition of the fuel and are assumed constant, so that $U(t) = U$ for all time instances t [19]. This assumption holds for all the emitted gasses, except for the NO_x emissions as they vary too much, especially at high altitude [17]. The values used for this calculation can be found in Table 17.1.

Table 17.1: Emissions Index (EI) of different emitted gasses

Species	Emissions Index (EI) [kg/(kg fuel)]
CO ₂	3.16
H ₂ O	1.26
SO ₄	2.0 · 10 ⁻⁴
Soot	4.0 · 10 ⁻⁵
NO _x	See models below [4]

Table 17.2: Fuel capacity of ESRA and the WB-57

Aircraft	Fuel capacity [kg]
ESRA	1400
WB-57	10115

As the values for both Soot and SO₄ are significantly smaller than the ones for the other emitted gasses, they will be disregarded in this analysis. For the estimation of the Emissions Index of NO_x [17][33], two models have been proposed. The first model was proposed by DLR [17], and uses the atmospheric conditions at the entrance of the combustion chamber of the engine as inputs. The second method is proposed by NASA and is based on empirical methods[33], taking the same inputs but is significantly less complex, and will be used for validation purposes. The Emissions index for NO_x decreases with altitude, as the atmospheric conditions change: the pressure and air density change. When the assumption is made that the temperature in the combustion chamber and the fuel flow are constant, and thus irrespective of altitude, overall emissions at higher altitudes are lower than at lower altitudes. As a result, from an environmental point of view, a higher cruise altitude is advantageous. In reality, however, the thrust-specific fuel consumption will reach a minimum and after that increase again. Depending on the specific engine and conditions, the actual fuel consumption might increase.

$$\Delta T(t) = \int_0^t G_i(t - \tau) \cdot \left[\sum_i RF_i(\tau) \right] d\tau, i = CO_2, NO_x \quad (17.4)$$

$$G_T(t) = S \cdot \left[\frac{\alpha_t}{\tau_{t1}} \cdot \exp\left(\frac{-t}{\tau_{t1}}\right) + \frac{1 - \alpha_t}{\tau_{t2}} \cdot \exp\left(\frac{-1}{\tau_{t2}}\right) \right] \quad (17.5)$$

Now, Equation 17.4 can be used to calculate the temperature change, which corresponds to $\Delta T_{sust,H}$ in Equation 17.1. The overall change in temperature can be seen as the sum of the temperature changes caused by the separate emission gasses. Each contribution is quantified using the so-called radiative forcing (RF), which expresses the energy transfer to the atmosphere, and incorporates long and short-term effects of the gasses considered. This is necessary as NO_x emissions will cause both heating and cooling effects, through short and long-lived ozone. Once the radiative forcings of all of the considered gasses have been calculated using Equation 17.6, the ATR can be calculated. The distinction between the radiative forcings of different gasses is achieved through different forcing factors $s(h)$, if the effect of the expulsion of the gas differs with altitude. The empirical functions $G_i(t)$ also differ as they quantify the absolute impact for each gas. The specific formulae and values used can be found in [19].

$$RF_i(t) = s(h) \cdot \int_0^t G_i(t - \tau) \cdot E_i(\tau) d\tau, i = CO_2, NO_x \quad (17.6)$$

When using the model for ESRA, the following conclusions can be made. First of all, due to the limited production numbers and flight hours, the overall impact on the climate by operating the aircraft is minimal. Considering this minor impact and the urgent nature of climate research, the emissions of the aircraft will most likely be of lesser importance than other considerations like cost or mission suitability. Furthermore, the operational lifetime also greatly influences the ATR value. As such, when considering this as a performance value, considering the temperature change is considered more useful, as the ATR will linearly increase with increasing lifetime. In addition, using ΔT as a metric makes it easier to consider the impact over time.

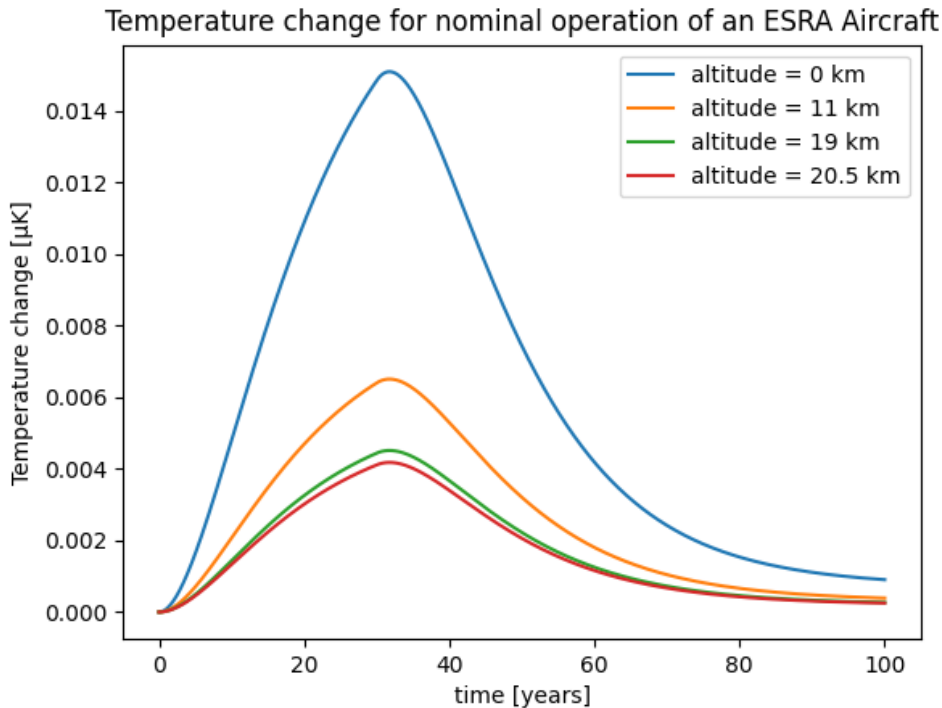


Figure 17.1: ΔT variation in time for operation at different altitudes for the nominal operation of ESRA

In Figure 17.1, the ΔT can be seen over the span of 100 years. From this, one could conclude that the cumulative impact of years of sustained operation can amount to a significant temperature change during operation, especially considering this is just for one aircraft. After some time, the temperature change does settle down as after the retirement of the aircraft, the change in temperature is tempered down and settles in the end. Note that for any of the altitudes, the value the temperature change settles to is not equal to zero. In practice, this means that there is a remaining effect of the emissions on the global climate, however small. Again, for a fleet size of 10 aircraft, the effect on the planet is negligible, but the combination of all aircraft worldwide does have a clear impact on the environment is significantly higher, in the order of 10's of mK.

Furthermore, a difference in temperature response can be seen for different operating altitudes. In general, the higher an aircraft operates, the less temperature change it will cause. This can be explained through fuel usage: at higher altitudes, there is less air resistance, causing less drag. This will allow an aircraft to burn less fuel, and thus emit less.

When comparing the climate impact of the ESRA aircraft to its competition that is currently operational, a clear difference can be spotted in emissions. As a case study, the WB-57 was used as a reference because the NO_x emissions of both engines are comparable, so they can be discarded in the comparison. The qualitative comparison then reduces to the amount of CO_2 produced by both engines, which itself is directly proportionate to the amount of fuel burned. As a result, comparing the fuel usage of both aircraft will result in a representative comparison. ESRA has a fuel capacity of 1400kg while the WB-57 has a fuel capacity of 10115kg as shown in Table 17.2. From the ratio of fuel capacity between the two aircraft and thus the emissions, ESRA's emissions are estimated to be 13.8% of those produced by the WB-57. The large disparity can be attributed to the smaller mass, engines, and payload capacity of ESRA.

Even though the impact of the ESRA fleet on the climate will be incredibly small, effort should still be put in optimizing design and operations in such a way that the effect is minimized. This can be achieved in a few ways. By burning less fuel, less gasses will be emitted and the impact will be reduced. This can be achieved by making the overall design lighter. New, cleaner engines can be developed and used. This will be especially effective if they are optimized to be more efficient at high altitudes.

Another option could be to use a novel, zero emissions type of engine in the more distant future. The operational side of things can also be modified to limit climate impact. In Figure 17.1, one can see that the more time is spent at high altitude, the smaller the change in temperature and thus climate effects. The engines can also be modified to run on sustainable aviation fuel (SAF). As the general aviation industry is moving in that general direction, it is not a stretch to assume that for future operations SAF will be present at more and more airports, making operation on SAF feasible.

17.1.2. Verification and Validation

For the estimation of the ATR, a tool was made. As such, it should be verified and validated to ensure correct and accurate results. A direct comparison of different aircraft simulations is provided in [19]. The values provided there were run and the results were compared to the ones provided. The difference in results was 5% at most, so the tool can be considered correct. This type of verification was combined with a unit test of the different functions constituting the program. An additional check was performed by comparing the data provided for the total ATR of all aircraft in 2005. This check was done by assuming that all aircraft were equal to the current design. This is a grave underestimation, so an additional 50% emissions on average was assumed. The results were in the same order of magnitude then the numbers provided in [19], and differed on average about 5% to a maximum 10%. The ATR model is validated in [19], and uncertainty margins are provided as well.

17.2. Social sustainability

Social sustainability covers the societal impact of the design, production, operation, and end-of-life of ESRA. The consequences range from socio-economic to the general well-being of the population.

Noise: To reduce aircraft noise near residential areas, several measures can be taken. One approach is to avoid using older engines, which tend to generate more noise, as well as straight jet engines or engines with afterburners. Instead, employing newer engines with low bypass ratios can ensure a balance between performance and noise reduction. Additionally, selecting operating bases in relatively remote areas or at busy airports can minimize the number of affected individuals. Remote airports limit the impact on nearby communities, while busy airports are advantageous due to their infrastructure designed to handle heavy aircraft traffic.

Socio-economic impact: The establishment and production of a new aircraft can have positive effects on the local population through job creation, investments in the region, and increased economic activity. This impact extends to areas where research and development, production lines, end-of-life facilities, and operational bases are located. Supporting companies that provide services such as catering, construction, and maintenance of facilities also contribute to additional economic activity. Moreover, both existing and new suppliers of specific aircraft parts benefit from the demand. Additionally, the presence of an aircraft or high-tech company often stimulates innovation and development in the technological sector.[40].

Emissions: Emissions can have a negative impact on the health and overall well-being of the population, especially those living near the bases of operation, where the direct impact will be the most noticeable. Excessive pollution of the local atmosphere can cause or worsen smog in highly populated areas. A direct correlation between air quality and general health has been proven.¹ As a constructor or designer of an aircraft, this should always be taken into account. As fuel consumption is directly related to the emission of harmful gasses, fuel consumption, and emissions should be kept to a minimum low to the ground or in populated areas. Considering the small amount of aircraft being produced, the overall impact on the general health will be minimal.

Scientific progress: As a science aircraft, the main purpose of ESRA is the collection of data that can be used to fasten scientific progress or provide data for hypothesis confirmation. Either way, the general population benefits from progress in the field of atmospheric research, which can help to better understand climate change, one of the most relevant problems today.

Ethical considerations: In order to be truly socially sustainable, ethically mined resources, ethical

production processes, and supply chain transparency should be used. This ensures that the people making any part of the aircraft or anywhere in the supply chain are treated with respect and dignity, as well as being paid a fair wage for their work.

17.3. End of life

As the aviation industry is readily increasing with an estimated 5.1% passenger and 5.6% freight traffic growth increase per year until 2030 [65] the End Of Life (EoL) strategy of aircraft becomes increasingly more important. The landfilling of any aircraft is not a viable option anymore even though no legislations are in place for aircraft recycling [65]. Therefore, the ESRA design philosophy will ensure that EoL strategies are considered.

Unlike the automotive industry, there are no common guidelines on design or EoL strategies for aircraft recycling[44] due to the difficulty stemming from the complexity of different components, the relations between production departments and the lack of regulations regarding EoL. As such, designing for sustainable EoL is not straightforward. Keivanpour et al. and Franz. K have shown that based on aircraft sustainability data, the waste hierarchy, also known as the ladder of Lansink approach, best applies to aircraft EoL strategies [44, 41]. This approach emphasizes designing for waste management and ranks the possible methods to do so. Firstly disassembled parts are re-used where possible. The remainder of the parts are recycled into raw material. If this isn't possible then the part is burned for energy recovery. Finally, if none of these methods are technologically feasible, then landfilling is chosen [43]. This philosophy is followed by Airbus in their *Process for Advanced Management of End-of-Life of Aircraft (PAMELA)* project and it will be used as a guideline for the EoL strategy of ESRA.

After being decommissioned, inspected and cleaned, a decision can be made to on whether to retire ESRA. In case of retirement, a planned systematic and fully catalogued disassembly procedure can be started. Possible reusable components will be the engines, landing gear, avionics, RAT and other small general cabin components such as wiring harnesses etc. [65]. The integration method for the possible reusable parts stated above will be designed for disassembly from the system without damaging said part and easy integration into the new system. Therefore, bolting assembly for metal structural components is to be considered and simple assembly of avionics such as screws to allow for disassembly. These reusable parts called usable serviceable material (USM) will be kept as spares for the ESRA fleet or for any other compatible aircraft. The parts have to be re-certified, inspected and if necessary worked on.² Additionally, any fluid in the aircraft such as lubricant and hydraulic oil can also be re-used. Since the ESRA design is a conventional fixed-wing aircraft, many simpler components are commonly used in other small aircraft and can thus potentially be sold to other aircraft manufacturers.

Then, more dismantling of the rest of the aircraft is done for each sub-system. Starting from the rivet removal of the outer skin to the airframe itself. Depending on the sizes of components, various cutting tools are to be used ranging from plasma torches to angle grinders to abrasive water jet [65]. The disassembled components are then sorted based on material and then recycled with the respective polarization technique of each material. If the part can be effectively separated and is made up of common aerospace alloys, then it can be recycled if the process adheres to environmental and safety regulations. Some thermoplastic composites can be recycled but is a more complex process that increases cost. More complex thermoset composite can be burned for energy recuperation following the ladder of Lansink approach [86]. This is one of the reasons that ESRA is mostly made up of aluminium which can be smelted, re-formed and then cast into metal ingots for re-purposing. The recycled material can then be sold to various manufacturers. It is important to note that the recycling process is substantial and would increase costs, however, the market for recycled material would limit these extra costs.

¹URL: <https://www.who.int/teams/environment-climate-change-and-health/air-quality-and-health/health-impacts> [cited on 21/06/2023]

²URL: <https://aircraft.airbus.com/en/newsroom/news/2022-11-end-of-life-reusing-recycling-rethinking> [cited on 20/06/2023]

Production Plan, Assembly and Integration plan

The production plan documents the intended concept to materialize ESRA from a design into an actual aircraft. It includes stages from manufacturing main components, assembly, and integrating all subsystems required in the aircraft. The focus will be put on ensuring the balance of product quality and cost efficiency, especially due to the small product series expected.

18.1. Manufacturing

Although the production stage happens at a later stage of the project, it is taken into account in the design to ensure its compatibility with manufacturing, assembly, and integration. This is especially relevant due to the required modularity for payload integration and the short turnover time needed to achieve higher flight hours per year. How the aircraft is assembled and integrated is quite relevant to how maintenance is conducted and the time required. Hence, it will require close contact between the design group and potential manufacturing and production parties whether it be external or internal to prevent a possible clash of design production.

Since a small amount of aircraft will be built, the production plan will differ drastically compared to large-scale high-volume production. Mass production requires large investments in tooling and infrastructure to produce a vast quantity of product, which drives the unit cost down. This method also entails issues such as overproduction and storage, which is likely to reflect sharply in ESRA's cost due to the low product series. Additive manufacturing (AM) can be a method that prevents these issues, as well as offering design freedom with complex geometry, which can bring performance increase through weight and shape optimization. AM also allows the opportunity for rapid prototyping, which can be constructed to provide feedback to the design group to make appropriate improvements. However, note that this requires additional engineering work and there are a number of extra considerations that have to be implemented in the design phase in order to exploit the full potential of AM [29]. This has to be carefully balanced due to the 2030 delivery schedule and cost requirement of ESRA.

At this stage of design, the resolution detail of the design does not allow a fixed set of manufacturing methods to be chosen yet. Further analysis focusing on methods that enhance engineering performance increase and their subsequent cost and engineering workload should be conducted.

Another consideration is the manufacturing of spare parts, unlike commercial airliners where an aircraft will still be in production years since the first of its kind entered service. In this case, parts will still be in production which can easily be sourced and replaced. For ESRA, the reliability and predicted number of replacements should be estimated such that spares can be manufactured to avoid excessively long operational downtime, which will contribute to an increase in DOC. Additional payload pallets and wing pods along with their pressurized and depressurized options should also be manufactured since the operational mode of ESRA is to send researchers the parts to allow them enough time to tailor the payload to their particular needs.

18.2. Assembly plan

As mentioned in the previous section, the design of the aircraft has a large influence on how it will be manufactured and assembled, which then has a direct impact on payload accessibility and maintenance time. Payload accessibility and low maintenance time is significant contributors to high scientific research efficiency and lower DOC, which make ESRA competitive against other competitors. Therefore, it should be stressed that assembly considerations will be included in the design phases. Other than this, a concept assembly process has been formulated and presented in Figure 18.1. Note that parts that are purchased externally are indicated in orange. System integration broadly refers

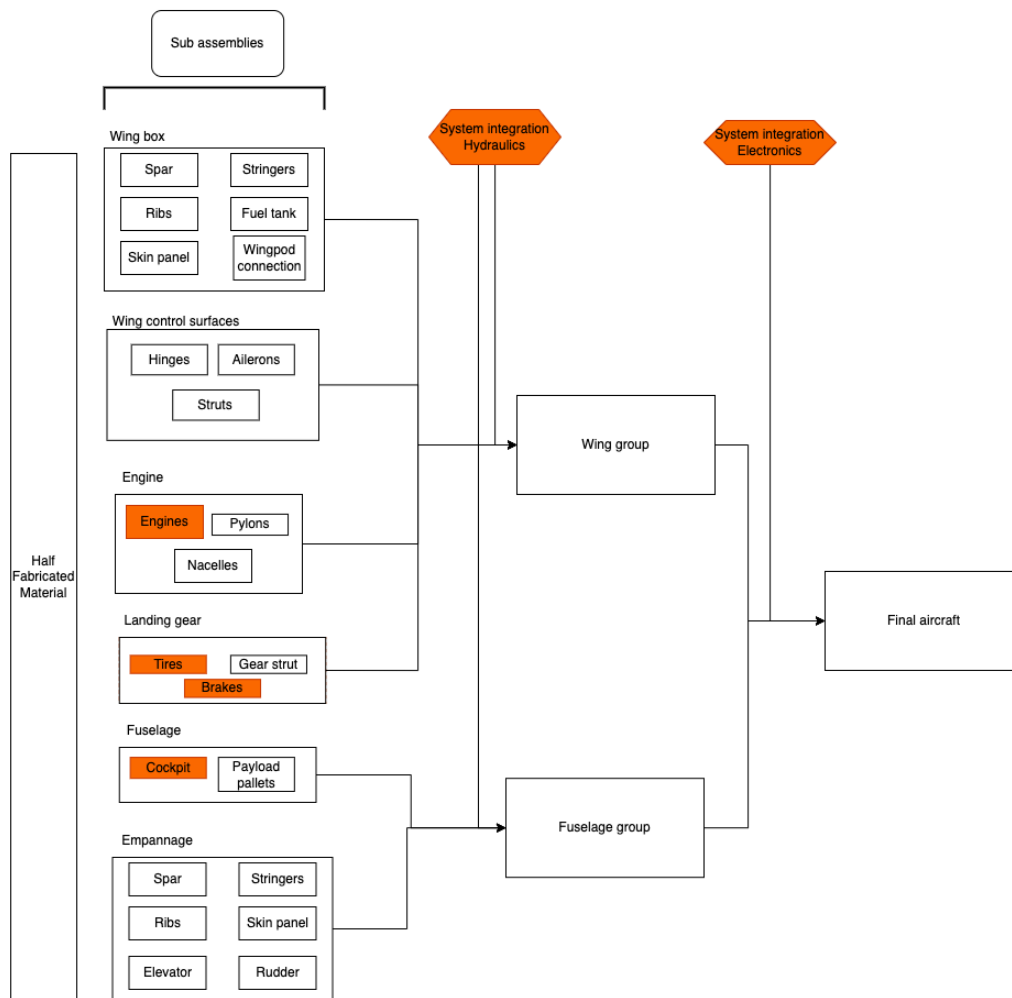


Figure 18.1: ESRA assembly plan

to systems such as hydraulics, electronics, and others which can include pilot life support, cockpit temperature control, etc. They are integrated into separate stages depending on the particular system, for example, hydraulics are integrated before the wing group is fully assembled due to its integral role in the wing group. Other systems such as electronics can be integrated at a later stage.

Technical Risk Assessment

The design of ESRA has been brought to a stage where new risks can be derived, and mitigation strategies can be implemented. Three risk categories are identified for this assessment: Design, Operations, and External Risks. For each risk, a score was given to two criteria: probability of occurrence and consequence. For the probability, each score from 1 to 5 corresponds to a level of probability (very low, low, moderate, high, very high), and for the consequence a score from 1 to 4 to a level of impact on the mission success (negligible, marginal, critical, catastrophic). All risks are described in the section below, and are presented on a risk map in Figure 19.1 to better visualize the most critical ones. The respective mitigation strategies implemented are then described thoroughly, and a new risk map is generated with the mitigated risks, which is shown in Figure 19.2.

Design risks:

R-DES-1 Poor analysis on critical subsystem caused by stretched resources, wrong assumptions, or oversimplification that leads to a belief that a certain analysis isn't required. Due to the tight time constraints and the difficulty of performing certain analyses with currently available tools, this risk was given a **Very High (5)** likelihood and a **Critical (3)** consequence rating

Mitigation of R-DES-1 is achieved by documenting which areas need to be implemented further in the future, to make up for the lack of analysis at the current stage. This reduces the consequence of such a risk to **Marginal (2)**.

R-DES-2 Snowballing weight estimate due to a small change in the design can be severe enough that the aircraft cannot fly. Due to the sensitivity of the design to weight, this risk was given a **Catastrophic (4)** consequence rating. Furthermore, it has been shown through sensitivity analysis that the weight can change easily, thus a probability rating of **High (4)** was awarded

Mitigation of R-DES-2 is difficult to achieve due to the inherent sensitivity of the design. The probability rating can however be reduced to **Moderate (3)** by using safety factors in the design.

R-DES-3 Poor cost estimates are a risk to ESRA as it lies in a category with few competitors. Thus, the models used are tailored to different kinds of aircraft. The impact for this risk is rated as **Critical (3)** and the likelihood is marked as **Very high (5)**

Mitigation of R-DES-3 is achieved by incorporating safety factors as well as by comparing the obtained values with those for current high-altitude aircraft. Thus, the probability rating is reduced to **Moderate (3)**, and the severity is reduced to **Critical (3)**.

Operational risks:

R-OPS-1 Engine Failure is a risk for any powered aircraft. Due to the high altitude of ESRA, the engines will run close to full throttle, thus excessively stressing the engine. It has been shown that ESRA would be able to fly on a single engine if it were to fail during take-off or landing. The main risk related to engine failures lies in the systems that are fed by the engines. Indeed, Section 14.1 shows that the engines power almost all aircraft systems, thus a failure might have a **Catastrophic (4)** impact. Engines are however designed to be reliable, thus the likelihood of failure can be considered **Low (2)**.

Mitigation for R-OPS-1 is achieved first by having two engines. Furthermore, the systems powered by the engines all include multiple levels of redundancy. Thus, the likelihood of a full engine failure is reduced to **Very Low (1)** and the consequence can be reduced to **Critical (3)**

R-OPS-2 EPS failure has the potential to be **Catastrophic (4)** as many systems including the FCS are electrically powered. As with the engines, a full failure of the EPS has a **Low (2)** likelihood due

to the components being designed hastily.

Mitigation for R-OPS-2 was achieved by implementing multiple levels of redundancy in the design. In fact, two generators power the EPS and a RAT is available in case those two fail to power some critical systems. Thus, the likelihood of a full EPS failure can be marked as **Very Low (1)** and the severity as **Critical (3)**.

R-OPS-3 Fuel distribution system failure has the potential to have similar consequences as an engine failure since the engines would shut down. Thus, the same severity rating of **Critical (3)** is given, and a probability rating of **Moderate (3)** is given, as the pumps must operate consistently within a harsh environment and there are many points of failure.

Mitigation for R-OPS-3 was done by including multiple levels of redundancy with two pumps per side to feed the engines as well as multiple cross-feed channels that enable the fuel load to be balanced and one set of pumps to feed the other engine. The causes of a fuel system failure do not change, but the severity of any one failure is reduced to **Marginal (2)** due to the many backups.

R-OPS-4 Avionics or FCS failure is dangerous because of how reliant ESRA is on the computer systems for flight. Indeed, all control inputs are routed through the flight computer, and a loss of this component would render ESRA uncontrollable. A loss of some avionics would not be so critical, as the pilot is able to fly with minimal data available, especially at lower altitudes. For these reasons, the severity of this risk was rated as **Catastrophic (4)** and the likelihood as **Low (2)**.

Mitigation for R-OPS-4 is done by implementing redundancy in the system. It was decided to use two independent flight computers. Furthermore, redundancy is also used for telemetry gathering devices such as Pitot tubes and angle of attack sensors. The likelihood is thus reduced to **Very Low (1)** and the severity to **Critical (3)** due to the extra layer of safety. Furthermore, if there is a failure of one of the flight computers, and it cannot be restarted, the mission should be scrubbed, and the aircraft should land at the closest airfield.

R-OPS-5 Communication system failure is a failure known to happen in civil aviation. In case of such a failure, procedure states that the squawk 7600 shall be entered.¹ This code signals to ATC that an aircraft has lost communication, so they will use visual signals to communicate with the aircraft when in the vicinity of the airfield. For this reason, a severity rating of **Marginal (2)** was given to this risk. Communication is designed for robustness, so a probability rating of **Low (2)** was given.

Mitigation for R-OPS-5 is completed by installing two VHF radios in order to provide a layer of redundancy, thus reducing the likelihood of total failure to **Very Low (1)**.

R-OPS-6 Poor weather conditions may cause excessive loading of the airframe due to heavy gusts and dangerous landings due to unpredictable wind shear or even a crosswind above the aircraft 20 kts limit. the severity of this risk was set to **Marginal (2)** as the pilot can always reject a landing if needed or avoid a region of heavy turbulence as they feel it starts. The likelihood of this risk was set to **High (4)** because the aircraft might operate in proximity to large storm structures.

Mitigation for R-OPS-6 is assured by the integration of a weather radar into the aircraft. This will enable the pilot to have an advanced warning for dangerous weather structures in order to void them, thus reducing the likelihood of this risk to **Low (2)**.

R-OPS-7 Danger to ground personnel due to the aircraft itself (Jet-blast) or due to potentially hazardous substances contained in the payload is considered. Accidents involving the ground crew can be dangerous depending on what system is involved. due to the high potential for injury, this risk was given a severity rating of **Critical (3)**. Considering that ground personnel will have the training, the likelihood of such an event is marked as **Low (2)**.

Mitigation of R-OPS-7 is done by adding a beacon light to ESRA which is active from just

¹URL: [https://wiki.ivao.aero/en/home/flightoperations/Procedures/LMMM/Commfail\[20/06/2023\]](https://wiki.ivao.aero/en/home/flightoperations/Procedures/LMMM/Commfail[20/06/2023])

before the engines are started until after shut down so that personnel is aware of the danger. Furthermore, it was decided to ensure that the ground crew does not come into contact with the payload during operation. This is achieved by having the payload integrated by the mission well before the start of the flight. Thus, the likelihood of the risk is reduced to **Very Low (1)** even though the severity remains the same.

R-OPS-8 Structural failure is considered dangerous as it can be capable of causing a loss of the aircraft, thus it was given a severity rating of **Catastrophic**. Due to the strong loads, the wing was sized for and the unlikelihood of encountering them, this risk was given a probability rating of **Low**.

Mitigation of R-OPS-8 has already been done by including a 50% safety factor. This safety factor also be included in all future structural design work, thus reducing the likelihood and severity of the risk. Both are also to be reduced by regular inspection, as described in Chapter 16. Thus, the severity is reduced to **Critical** and the likelihood of **Very low**.

Market and external risks

R-MA-1 Few qualified pilots may hinder efforts to perform research with ESRA as it is a rare type of aircraft that may require special licensing to fly. Due to the entry in service date seven years from the writing of this document, the severity of this risk was placed at **Marginal (2)** as time remains to devise a training program and find potential pilots. Furthermore, a likelihood level of **Moderate (3)** was assigned to this risk for the same reason.

Mitigation for R-MA-1 can be done by approaching pilots with experiences flying high-altitude aircraft such as the U-2 or WB-57. Furthermore, test pilots would also have sufficient qualifications to fly ESRA with minimal additional training. Approaching and hiring such individuals would reduce the likelihood of this risk to **Low (2)** and the severity to **Negligible (1)**

R-MA-2 Better performing competitor are a risk for any commercialized system. In the case of ESRA, the market is small and with no known competitors in development. Therefore, ESRA will have the benefit of being the first new aircraft on the market and having established itself by the time a new competitor enters the market. Thus, the likelihood of this risk is set to **Low (2)** and the severity to **Marginal (2)**

Mitigation for R-MA-2 would be achieved by minimizing cost while ensuring that ESRA is capable of performing future science missions such as Aerosol injection missions. With these points implemented, the severity of this risk will be reduced to **Negligible (1)** and the probability to **Very Low (1)**

R-MA-3 Too few interested parties would be problematic as the cost of each unit is dependent on the number of units built as shown in Chapter 21. It is possible that some identified parties might not pursue high-altitude research or that they already have a working solution. Therefore, the probability of this risk was set to **Moderate (3)** and the severity was set to **Critical (3)**

Mitigation for R-MA-3 is will be accomplished by approaching potential clients in the future phases of the project so that the severity of the risk can be reduced by more advanced warning. Thus, the severity of the risk was reduced to **Marginal (2)** and the likelihood to **Low (2)**.

R-MA-4 Too few flight hours will have a similar impact as R-MA-3 as the cost will have to be more concentrated and thus the cost per flight hour will increase. The likelihood of this event was set to **Moderate (3)** as it is difficult to predict exact flight hours at this stage of the design and the severity was rated as **Critical (3)**

Mitigation for R-MA-4 is done primarily by including margins in the estimations done and by ensuring the market analysis is updated throughout the future design process. The advance warning provided by the market analysis will reduce the severity of the risk to **Marginal (2)** and the likelihood to **Low (2)**.

		Probability				
		Very Low	Low	Moderate	High	Very High
Consequence		1	2	3	4	5
Catostrophic	4		R-OPS-1 R-OPS-2 R-OPS-4 R-OPS-8		R-DES-2	
Critical	3		R-OPS-7	R-OPS-3 R-MA-3 R-MA-4		R-DES-1 R-DES-3
Marginal	2		R-OPS-5 R-MA-2	R-MA-1	R-OPS-6	
Negligible	1					

Figure 19.1: Risk map of the ESRA program before mitigation

		Probability				
		Very Low	Low	Moderate	High	Very High
Consequence		1	2	3	4	5
Catostrophic	4			R-DES-2		
Critical	3	R-OPS-1 R-OPS-2 R-OPS-4 R-OPS-7 R-OPS-8		R-DES-3		
Marginal	2	R-OPS-5	R-OPS-6 R-MA-1 R-MA-3 R-MA-4	R-OPS-3		R-DES-1
Negligible	1	R-MA-2				

Figure 19.2: Risk map of the ESRA program after risk mitigation has been implemented

Reliability, Availability, Maintainability, and Safety (RAMS) Analysis

Reliability, Accessibility, Maintainability, and Safety Analysis, or RAMS analysis in short is a method to quantify the future availability of the system being designed, making use of four separate factors. Each of these factors could potentially reduce or entirely kill the future availability if not addressed properly. Consequentially, by introducing this type of analysis when designing a product, overall costs are minimized, yielding improved profitability. As the operational cost of the ESRA aircraft is one of the main driving factors for the design, the use of a RAMS analysis is warranted.

20.1. Reliability

The first factor that has to be assessed is reliability. The higher the reliability, the shorter the overall downtime and the lower the maintenance cost. This will lead to both an increase in changeability and a reduction in user fees. Reliability itself is impacted by a few factors, resulting in common pitfalls; Product complexity, TRL of components, Length of the development cycle, Rapid product obsolescence, Customer expectations, and Financial factors.

When considering the reliability of a system, the general failure rate should be taken into account. Generally, the failure rate follows the so-called bathtub rule, where failures are more common in the beginning (burning in period) and in the end (wear out period) of the life cycle. To reduce the number of failures in these periods, some precautions can be taken. As the overall production numbers of the aircraft are not high, and the availability of parts will consequently not be very high, reliability issues in the burning-in period should be kept to an absolute minimum, as resulting downtime would be largely due to the limited availability of spare parts. Though not completely avoidable, the risk of failure can be decreased through inspection, preventive maintenance, and other mitigation measures.

Reliability engineering can be defined as: "Reliability engineering is an engineering discipline for applying scientific know-how to a component, product, plant, or process in order to ensure that it performs its intended function, without failure, for the required time duration in a specified environment." [46]. From this, one can conclude that reliability itself depends on the function of the system, time duration this function has to be performed for and the environment in which it operates. When done correctly, maintenance can be planned in accordance with the estimated rate of failure for each part of the subsystem, thus avoiding failures during flight. For this purpose, the aircraft was subdivided into subsystems and their subsequent parts. For each of these parts, the most common failure modes are listed, together with the estimated impact of stratospheric operation. Using this information, a maintenance and inspection scheme is proposed to avoid failures while still minimizing downtime. According to regulations [3], general inspection happens each 100 flight hours and annually. For some critical components, more frequent inspection and maintenance might be warranted. According to the same regulations, a subsystem breakdown and inspection items is proposed, which is partially adopted here [5].

20.1.1. Fuselage and hull group

The first subsystem that is considered in this breakdown is the Fuselage and hull group. This contains the fuselage structure, skin panels, payload bays and pressurization system for said bays. Due to the pressure differentials during missions requiring the aircraft to go to its service ceiling, some more frequent inspection and maintenance of the payload bays and the pressurization system as well as some skin panels is warranted. The full breakdown can be found in Table 20.1.

Table 20.1: Impact of stratospheric operation on parts of the fuselage and hull group

Part	Signs of failure, detectable by inspection	Additional impact due to operation	Advised maintenance scheme
Fabric and skin	Deterioration, distortion, insecure attachment of fittings	Low - more pressure difference during operation cycle	Post flight visual inspection, Annual non-destructive testing of essential body parts
Systems and components	improper installation, apparent defects, unsatisfactory operation	None	Annual inspection
Envelope, gas bags, ballast tanks	general deterioration	None	Annual inspection
Payload bays and pressurization system	general deterioration, cracks causing air leakage	Medium - High pressure differentials	Inspection every 100 flight hours, Annual non-destructive testing

Table 20.2: Impact of stratospheric operation on lifting surfaces

Part	Signs of failure, detectable by inspection	Additional impact due to stratospheric operation	Advised maintenance scheme
Surface	Poor general condition, skin deterioration, distortion, clear signs of buckling, deterioration of the de-icing system	None	Visual inspection after 100 flight hours
Control surfaces and flaps	Skin deterioration, mechanism failure, defects, improper travel	Low - Mechanisms could freeze due to low temperatures at altitude	Visual inspection after 100 flight hours
General structure	Clear signs of bending or other structural deformations	None	Annual inspection

20.1.2. Lifting surfaces

The lifting surfaces exist out of the main wing, and the vertical and horizontal tail surface. These are invaluable to the operation of the aircraft as they produce the necessary lift and provide control over the behaviour of the aircraft. When either of these functions fail, a catastrophic failure could be the result.

20.1.3. Cabin and Cockpit group

For an aircraft that operates in the stratosphere, the cabin and cockpit group is one of the most affected by the unique operating conditions. For the safety of the operator, additional attention should be paid to the pressurization and life support systems, as well as an ejection system.

20.1.4. Engine and nacelle group

Due to the low pressure and temperatures of the operating altitude in combination with the possible operation in or near extreme weather phenomena, the engine inspection and maintenance should be more frequent and rigorous than advised. The engine that is used, the PW535A should be overhauled every 5000 flight hours and the hot section of the engine should be inspected after 2500 hours of operation as standard. These numbers have been decreased as the aircraft should remain certified for ETOPS (Extended Range Twin Operations approval) plus 180 minutes or more [2], so that the range requirement can be fulfilled. This does imply that the failure rate of the engine can be .01 per 1000 flight hours at most.

20.1.5. Landing gear group

As the landing gear group has a relatively large amount of moving parts and is crucial for successful operation, the overall reliability can be impacted by the landing gear.

Table 20.3: Impact of stratospheric operation on parts of the cabin and cockpit group

Part	Signs of failure, detectable by inspection	Additional impact due to stratospheric operation	Advised maintenance scheme
General state of the cabin	Dirtiness impeding the controls or loose items	None	Visual inspection every 100 flight hours
Seats and safety belts	Poor condition and apparent defects	Low - Special suit might cause damage to seat and belts	Visual inspection every 100 flight hours
Windows, windshields and canopy	Deterioration and breakage	High - High pressure differentials every cycle, high impact to operator	Visual inspection after every flight, non-destructive testing every 100 flight hours, preventive maintenance
Bulkheads	general deterioration, cracks causing air leakage	Medium - High pressure differentials every cycle, high impact to operator	Visual inspection every 100 flight hours, annual non-destructive testing
Instrumentation	Poor condition, mounting, marking, and improper operation	Low - Pressurized suit could impede proper operation	Visual inspection after every flight, calibration every 100 flight hours
Flight and engine controls	Improper installation and improper operation	Medium - Pressurized suit could impede proper operation, high impact on operation	Visual inspection after every flight, calibration every 100 flight hours
Batteries	Improper installation and improper charge	Low - Temperature differences each cycle could deteriorate the state of the batteries	Inspection of battery condition every 100 flight hours, preventive maintenance
Ejection system	Improper installation and apparent defects	Low - Ejection system explosives could deteriorate due to temperature fluctuations	Visual inspection every 100 flight hours, preventive maintenance
Pressurization system	Improper installation and apparent defects, leaks causing pressure loss	Medium - Large pressure differentials have to be achieved and maintained	Pressure test every 100 flight hours, preventive maintenance
Heating system	Improper installation and apparent defects, reduced heating performance	Medium - Large temperature differentials have to be maintained for extended periods of time	Inspection every 100 flight hours, preventive maintenance

Table 20.4: Impact of stratospheric operation on parts of the engine and nacelle group

Part	Signs of failure, detectable by inspection	Additional impact due to stratospheric operation	Advised maintenance scheme
Engine section	Visual evidence of excessive oil, fuel, or hydraulic leaks, and sources of such leaks	Low - Temperature and pressure fluctuations might cause hydraulic and fuel lines to fail faster	Visual inspection every 100 flight hours
Studs and nuts	Improper torquing and obvious defects	Low - Expansion cycles due to temperature differences might cause loosening or fracture	Visual inspection and torque tests every 100 flight hours
Internal engine	Cylinder compression and for metal particles or foreign matter on screens and sump drain plugs. If there is weak cylinder compression, for improper internal condition and improper internal tolerances	High - Extended operation in low pressures, operation in extreme weather	Inspection of the hot section after 1500 flight hours, engine overhaul after 3000 flight hours
Engine mount	Cracks, looseness of mounting, and looseness of engine to mount, for both the upper and lower mounting point	Low - Loosening might happen due to expansion cycles of the material	Visual inspection every 100 flight hours
Engine controls	Defects, improper travel, and improper safetying	None	Visual inspection every 100 flight hours
Lines, hoses, and clamps	Leaks, improper condition and looseness	Low - Lines could rupture due to the high temperature and pressure differences	Visual inspection every 100 flight hours, if accessible without engine demounting, otherwise concurrent with the hot section inspection
Cowling	Cracks and defects	Low - Damage during extreme weather operation	Visual inspection after extreme weather operation or after 100 flight hours

Table 20.5: Impact of stratospheric operation on parts of the landing gear group

Part	Signs of failure, detectable by inspection	Additional impact due to stratospheric operation	Advised maintenance scheme
Shock absorbing devices	Improper oleo fluid level	None	Fluid level inspection once every 100 flight hours
Linkages, trusses, and members	Undue or excessive wear fatigue, and distortion	Low - Linkages might experience large differences in heat during operation, causing loosening	Visual inspection every 100 flight hours
Retracting and locking mechanism	General condition, improper operation	Low - Might experience difficulty locking due to temperature during operation	Visual inspection every 100 flight hours
Hydraulic lines	Leakage	Low - Leaks could occur due to large temperature and pressure differences	Visual inspection every 100 flight hours, preventive maintenance
Electrical system	Chafing and improper operation of switches	Low - Chafing might occur due to fluctuation in resistance, induced by temperature	Resistance and voltage test every 100 flight hours, preventive maintenance
Wheels	Cracks, defects, and condition of bearings	None	Visual inspection every 100 flight hours, annual maintenance or replacement
Tires	Wear and cuts	Low - Rubber can harden when operated in low temperatures, increasing wear	Visual inspection of tread every flight, preventive maintenance
Brakes	Improper adjustment	Low - Reduced braking performance of cold brakes	Inspection every 100 flight hours, preventive maintenance

Table 20.6: Impact of stratospheric operation on other systems and components

Part	Signs of failure, detectable by inspection	Additional impact due to stratospheric operation	Advised maintenance scheme
Radar and communication system	improper installation and insecure mounting, improper routing	Low - Electrical circuits and radar could be impacted by temperature differences	Visual inspection and testing every 100 flight hours
Life support system	Leaks in the oxygen tank, defects in heaters or compression system, defects of pressurized suit or linkage with life support system	Medium - Systems might wear faster or get damaged by extreme weather, large impact for operator	Testing after 100 flight hours
Insulation and shielding	Improper installation, degradation	Low - Temperatures can cause accelerated wear, high impact on operator	Visual inspection after 100 flight hours, preventive maintenance

20.1.6. Other subsystems or components

Subsystems or components that are unique to operation in the stratosphere or not listed yet are considered in Table 20.6. Some of the unique components are the pressurized suit, a complex life support system and radiation and heat insulation.

20.2. Availability

Availability is the amount of time that the aircraft is ready to complete its mission. Operational availability is defined as the percentage of time that the aircraft is available for research purposes it can be calculated using Equation 20.1 [31]. In this equation, MTBM is the average time between both preventative and corrective maintenance actions [31]. The MMT is the average time for preventative and corrective maintenance and MLDT is the logistics time for aircraft maintenance [31].

$$A_o = \frac{MTBM}{MTBM + MMT + MLDT} \quad (20.1)$$

The general method to quantify the availability of the aircraft is shown, however, currently, there isn't sufficient data to complete the availability analysis. The aim would be to maximize the availability of the aircraft to increase the number of hours that it can be rented out for, generating research and revenue for the client.

20.3. Maintainability

The maintenance costs are those that are needed to keep the aircraft flying and conducting research in a safe condition. The maintenance has to be done to the airframe and engines. This maintenance can be divided into four categories: Line/ Ramp maintenance, Base maintenance, and Unscheduled maintenance [42].

Line and ramp maintenance occurs at the airport of operations on the flight line. Typically, it is used to identify arising problems and quickly fix them by replacing parts, it averages 2 man-hours per flight day. This includes thoroughly checking the engines for damage to blades or unusual vibrations.

Base maintenance is usually carried out in a hangar and follows a set schedule. Typically, for commercial operations, there are lettered checks. These are "A", "B" and "C" checks. A-checks typically happen every 80-100 flight hours and maintenance takes 10-20 man hours. B-checks are thorough maintenance for the whole aircraft, they happen every 500-600 flight hours and typically last 100-300 man hours. C-checks happen every couple of years for commercial aircraft and take 10,000-30,000 man-hours.

Typically during C checks the engines are pulled from the aircraft to be disassembled and cleaned [42].

Unscheduled maintenance occurs after some sort of aircraft failure or after some fault is found that grounds the aircraft. Typically this maintenance occurs on the flight line as the aircraft is unable to fly to a maintenance airport.

Maintenance can be measured utilizing the MTBM as shown in Equation 20.2 which comes from [31]. One of its components, the MTBF can be calculated utilizing Equation 20.3 [31], where $R(t)$ is the reliability function and λ is the failure rate of components.

$$MTBM = \frac{1}{\frac{1}{MTBF} + \frac{1}{MTBPM}} \quad (20.2) \quad MTBF = \int_0^{\infty} R(t)dt = \frac{1}{\lambda} \quad (20.3)$$

The ESRA airplane is still in its preliminary stages and therefore a complete analysis of the maintainability cannot be currently completed. The method described in this section will be used once a detailed design and prototype are completed.

20.4. Safety

The primary goal of ESRA is to provide a platform for cutting edge high altitude atmospheric research. In order to deliver such data in sufficient volume, ESRA must be able to operate in a safe and reliable manner. An overview of risks affecting ESRA have been given in Chapter 19. Some of the risks presented, specifically the operational risks, can lead directly to threats to the aircraft operators. These threats and some others are listed in this section along with an explanations of the actions taken during the design phase to mitigate those risks as well as some of the actions that can be taken in case such an incident does happen.

Pressurization failure:

When flying at high altitude, one of the most serious risks for the safety of the operator is a loss of pressure in the cabin. The higher risk relative to lower altitude flight is caused by the larger pressure differential, requiring systems to be more robust. A loss in pressure is detrimental to the health of the operator as at 20.5 kilometers altitude, not enough oxygen is present to remain conscious. Considering the size of the aircraft, depressurization may happen in an explosive manner, possibly incapacitating the operator before there is enough time to react [26]. Considering the altitude, an emergency dive may not be possible either.

This issue can be addressed by pressurizing to a higher altitude, for example 30,000 ft. This will reduce the structural stresses, reducing the risk of explosive depressurization or damage to other systems. Additionally, the bulkheads of the aircraft can be designed to be lighter, reducing the overall weight of the aircraft. The operator does have to wear a pressurized suit at all times, and additional life support systems are necessary to provide oxygen at all times and ensure pressurization of the suit. In this situation, when either the suit or the cabin would (more slowly) lose pressure, there is sufficient time to reach safer altitudes. This design decision does also imply that the cockpit has to be designed in such a way that it can be operated with a pressurized suit. The same goes for an emergency bailout procedure. The aircraft will also have to be serviced at airports where the required pressurized oxygen can be provided.

In the event of a loss of pressure, the life support system shall be reconfigured to prioritize the pressure suit such that the pilot may remain safe. In parallel, the aircraft shall descend at the highest sink rate allowable till ESRA reaches a safe altitude.

Instrumentation or avionics failure:

A failure of the avionics or any instrumentation system could lead to dangerous situations for the operator. When the failure does not actively influence the performance of the aircraft, the risks corresponding to this failure are minimal, as the pilot can still operate the aircraft as normal, only the convenience is impacted. Whenever an aircraft system depends on an input, the situation is more severe. Whenever this happens, multiple scenarios are possible: the system could shut down, reset, use the faulty input as is and cause instability or even make the aircraft uncontrollable. To mitigate

this risk, the operator should be able to manually disable any system and take over control manually. This does not mean that there can be no fail-safes present which try to rectify the error. It is advised to have some redundant sensors for critical systems, especially when the avionics system is fly-by-wire. That way, faulty inputs can be more easily detected and the system or the pilot can intervene before a dangerous situation is created.

Control system failure

It has been discussed in Section 14.1 that ESRA is a fully fly by wire aircraft. Thus a full failure of the flight control system would lead to a loss of control of the aircraft. To mitigate this risk, ESRA has been given two independent flight computers that are each able to individually control the aircraft. Due to the importance of this system, in the event of a computer failure, the aircraft is to land at the nearest possible airport in order to minimize the flight time on a single computer.

Structural failure:

Depending on the location and type, a structural failure can potentially cause catastrophic failure of the entire aircraft. When the failure results in a severe loss of lift or structural integrity, the aircraft might not even be able to keep flying. To minimize the chance of this happening, redundancy can be built in the structure, or safety margins in the design can be increased for critical components of the structure. Preventive maintenance and regular inspections are also key in preventing structural failure.

Communication system failure:

A critical failure in the communication system can cause dangerous situations as contact with air traffic control is also lost. For the operator specifically, this means no information on air traffic in the region, and an inability to request clearance for landing. This in turn may cause collisions or dangerous situations for people in other aircraft. A loss of communication also implies that mission control is unable to communicate dangerous weather phenomena, or precise location data, necessary for the mission to be a success, resulting in a do-over. Communications can also be temporarily disabled due to interference of the atmospheric phenomena being researched. For this loss of communication can and should be planned by mission control. A loss of communication is most commonly mitigated by including a fully redundant communication system in the aircraft.

Engine failure:

When at cruise altitude, the aircraft is not able to generate sufficient to sustain cruise on a single engine. Thus an engine failure would have catastrophic effects of the mission in that the mission would have to be aborted. Due to the effects of thrust lapse, the aircraft will be able to cruise without any issues at lower altitude in order to return to base. Multiple systems are dependent on the engines for power such as the Electrical Power System (EPS). In order to mitigate the risk of an electrical failure due to a single engine failure, the EPS described in Section 14.2 is capable of feeding both electrical busses with a single generator thus ensuring a power supply to the entire aircraft.

In the event of a double engine failure, the aircraft will have to make an emergency landing at the closest airport. If the aircraft is cruising close to its ceiling when the double failure occurs, it will rapidly lose altitude but once the air density increases, ESRA will be able to glide sufficiently well to ensure that it is able to reach an airfield. As both generators are powered by the engines, a double engine failure will cause a complete EPS failure as well. In order to prevent such a failure, critical systems can be powered by a battery which in turn can be powered by a RAM Air Turbine (RAT).

Fuel system failure:

Section 14.3 shows how the fuel system has been designed for redundancy. Indeed, each fuel tank is equipped with two fuel pumps to feed the engines each of which is connected to a different electrical system. This means that in case of a single pump failure, the engine can still be fed by the other pump. In case both pumps on one side of the aircraft were to fail, the aircraft is equipped with two crossfeed channels. The engine crossfeed is able to provide fuel from one side of the aircraft directly to the engine on the other side thus overriding the inoperative pumps. In addition to the engine crossfeed, ESRA is equipped with a fuel tank crossfeed which enables it to balance the fuel load across the two

wing tanks thus mitigating the risk of instability due to the failure of one side of the fuel distribution system.

Dangerous weather:

Harsh weather could create threats for to the aircraft structure and its operations. Encountering strong gusts in flight could excessively stress the structure or even damage it. The aircraft structure has been designed to cope with a load factor for gusts of up to 4.4. Anything beyond this value risks damaging the aircraft. In order to avoid such situations, a weather radar is mounted to the wing in order to give the pilot an advance warning for dangerous weather structures. Another danger posed to ESRA by the weather would be during landing in case of excessive crosswinds and potential wind shear. The aircraft has been sized to cope with up to 20 kts of crosswind. Above this, the aircraft will have to be rerouted to a different airport. The airfield itself is also an important component of the mitigation strategy for weather related risks as they will provide information to the pilot of ESRA thus enabling an informed decision for landing.

Furthermore, ESRA will be used for weather and plume research. This means that ESRA may be required to fly through structures such as volcano plumes. These mission will present similar risks to those already mentioned but will additionally affect the engine as it might ingest soot and ashes. Thus, a detailed engine inspection will be required after such a mission to ensure safe operations in future missions.

Jet blast risk:

Aircraft engines can present many risks to ground crew due to the powerful suction at the front of the engine as well as the high temperature and high speed jet blast aft of the engine. In order to prevent accidents linked to the engines, beacon lights will be used on ESRA that are turned on when the engine start up process begins and are turned off when the engines are shut down. Whenever the beacon light is active, ground crew must stay clear of the aircraft.

Payload risks:

ESRA has been designed to carry a variety of scientific payloads some of which may contain dangerous substances such as aerosols or cryogenics. Contact between the ground crew and the payload should thus be limited and the payload should be designed such that it prevents egress of any substances.

Complete loss of aircraft:

Despite all possible action being taken in order to avoid a loss of the aircraft, the eventuality does have to be considered. In such a scenario, the priority would be to give the pilot an escape route from the aircraft before the aircraft crashes. It was decided to issue a parachute to the pilot and ensure that the canopy could be jettisoned in order to provide an egress route.

20.5. Recommendations

The RAMS analysis was performed at a high level at this stage of design due to the lack of knowledge on specific components. Thus, as the level of detail increases during the design process, attention must be given to update the analysis. For the reliability section, it is recommended to perform a Failure Mode and Effect Analysis (FMEA) in order to identify the overall subsystem and system reliability and find the weak points. The availability and maintainability require subsystem information that can only be obtained with further design, thus it is recommended to refine these analyses such that they can be used to inform the design. Finally, it is recommended that the safety analysis be done at a subsystem level in a more detail than currently presented in Section 20.4.

The utilization of ESRA aircraft is constrained by its costs, as affordability is crucial for scientists to access and utilize the aircraft within their budgetary limits. These costs are governed by the requirement ESRA-STAKE-5-SYS-12. The following chapter provides an analysis of the costs, categorizing it into acquisition costs and direct operating costs. By quantifying and illustrating these expenses, it demonstrates how they will be allocated from the agency to the client, i.e., the scientists. Additionally, recommendations are presented to explore strategies for cost reduction.

21.1. Cost Breakdown Structure

The costs of the ESRA program can be divided into two distinct categories: Acquisition Costs and Direct Operating Costs (DOC). The acquisition costs for the ESRA program include the initial costs incurred in development, production, and infrastructure and are further broken down into Research and Development, Manufacturing, and Certification costs. On the other hand, the DOC encompasses the day-to-day costs associated with aircraft operation, maintenance, and support. These costs can be further divided into Maintenance, Flying, and Logistics costs. In Figure 21.1 the division of the mission costs can be visualized and in the next section, these costs are defined in more detail.

21.1.1. Cost estimation method

There are various cost estimation methods available that can be used to estimate the cost of an aircraft program. The extensive tool developed by Roskam, although dating back to 1989, is still widely used in the aerospace industry given its reliability. The Roskam method was coded in separate files, one for each part of the cost. The costs were then added up to get the cost for each part of the breakdown described in the previous section. To use the Roskam method, general specifications and performance characteristics of the aircraft, such as take-off weight, engine thrust, and cruise airspeed, are inputted into the tool. The tool then calculates the labor hours required for different phases of aircraft development. These labor hours are multiplied by the corresponding hourly rate to determine the cost.

For estimating the Direct Operating Cost (DOC), empirical formulas were used to approximate different cost components, including fuel, operations, and maintenance. These components were combined to derive the total operational cost, measured in dollars per nautical mile. Typically, the Roskam method also incorporates the aircraft's depreciation cost, however, in our case, this cost was excluded due to the assumption made by the commercial model that the client will not resell the aircraft. Instead, the

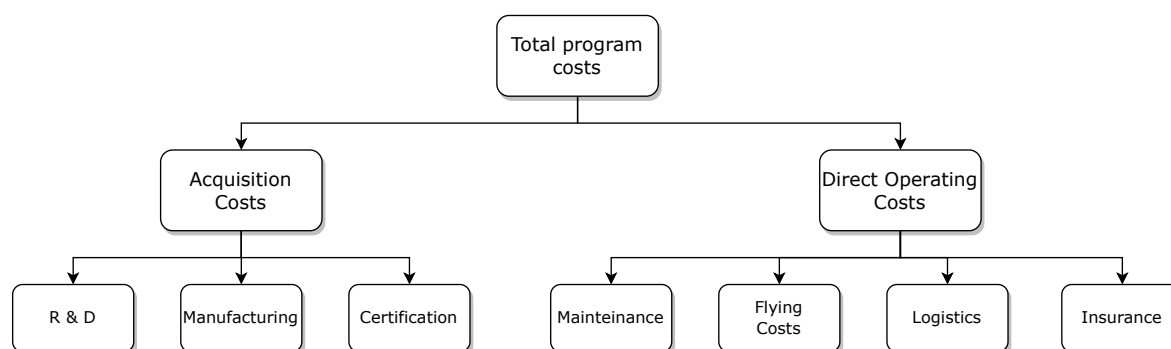


Figure 21.1: Diagram for the cost breakdown ESRA program.

Parameter	Description	Value	Unit
$CPI_{1989-2023}$	Consumer price index from 1989 to 2023	2.51	-
CPI_{fuel}	Consumer price index for fuel from 1989 to 2023	5.8	-
U_{annbl}	Annual flight hours	500	hr
N_{rdte}	Amount of prototype A/C produced in R&D phase	2	-
N_m	Number of aircraft produced	10	#
F_{diff}	Difficulty factor of the airline program	1.8	-
F_{cad}	Difficulty factor of CAD experience of designers	0.8	-
R_e	Hourly rate for an engineer	25	\$1989/hour
R_m	Hourly rate for manufacturing	10	\$1989/hour
R_t	Hourly rate for tooling	Value 11	\$1989/hour
F_{mat}	Correction factor, which depends on the type of materials used in the construction of the airplane,	1	-
N_r	Production rate of aircraft	0.2	AC/month
N_{yr}	Lifetime of the aircraft	30	years
SAL_j	Pilot's yearly salary	69000	\$1989
TEF_j	Travel factor (hotels)	7	\$1989
OD	Oil Density	7.5	lbs/gallon
FD	Fuel Density	7.01	lbs/gallon
R_{lap}	Maintenance labor rate	14.5	\$1989/hour
H_{em}	Hours between overhauls	6000	hr
W_{to}	Aircraft mass at takeoff	10305	lbs
T_{to}	Aircraft thrust at takeoff	6429	lbf
V_{max}	Maximum airspeed	146	knots
N_e	Number of engines	2	#
EP	Engine price	1,500,000	\$2023
W_f	Weight fuel used	3398	lbs
R_{bl}	Range of aircraft + 10% for maneuvering	3239	Nm
$CERT$	Cost of Certification	25,000,000	\$2023

Table 21.1: Parameter Descriptions and Values

aircraft will only be utilized for research purposes throughout its expected lifespan.

It is worth noting that the calculation of DOC and the final user fee relies on the operational hours of the aircraft. These operational hours were determined using a specific tool described in Chapter 1. This tool takes the expected lifetime of the aircraft into account and outputs the yearly operational hours based on the duration of regular scientific campaigns.

During the estimation process, various parameters for the tool needed to be determined, while some are obtained from the configuration described in Chapter 15. A comprehensive list of these parameters, along with their corresponding descriptions, can be found in Table 21.1. The difficulty factor F_{diff} was chosen to be 1.8 because it's a program that involves the use of moderately aggressive advanced technology [69]. The F_{cad} factor was chosen at 0.8 as Computer-Aided Design is a prolific skill in the engineering workplace. Lastly F_{mat} was chosen to be 1 as the airplane is primarily made up of traditional aluminum materials.

21.1.2. Research & Development (RDTE)

The breakdown of the costs for R&D is shown in Table 21.2. The R&D comprises Airframe Engineering and Design Cost and planning for the design, preliminary and detail design, integration, engine tests,

Table 21.2: Different components of R&D cost

Name Component	Symbol	Value	Units
Airframe Engineering and Design Cost	C_aed	6,293,032.87	\$2023
Development Support and Testing Cost	C_dst	2,903,471.23	\$2023
Flight Test Airplanes Cost	C_fta	39,032,946.69	\$2023
Flight Test Operations Cost	C_fto	289,164.32	\$2023
Total R&D costs	RDTE	48,518,613.613	\$2023

Table 21.3: Different components of manufacturing cost

Name Component	Symbol	Value	Units
Airframe Engineering and Design Cost	C_aed	2,441,942.40	\$2023
Airplane Production Cost	C_apc	123,232,952.19	\$2023
Total production cost	AEP	125,674,894	\$2023

wind tunnel models, reliability, and maintainability analysis [69]. The Development Support and Testing Costs are the system, wind tunnel, structural, propulsion, and simulation tests [69]. The Flight Test Airplane's Cost is composed of the engines and avionics, manufacturing labor cost, material cost, tooling cost, and quality control cost [69]. The Flight Test Operations Cost is associated with the salary for certification flight test hours, simulation activities, and innovation in design. The overall formula to describe R&D costs is shown in Equation 21.1

$$RDTE = C_{aed} + C_{dst} + C_{fta} + C_{fto} \quad (21.1)$$

$$AEP = C_{aed} + C_{apc} + C_{fto} \quad (21.2)$$

21.1.3. Manufacturing (AEP)

The manufacturing cost of aircraft is made of the components reported in Table 21.3. The Airframe Engineering and design cost is the cost associated with research done into how the aircraft will be manufactured and the design of the production line. The Airplane production cost is composed of the labor necessary, materials, and space. The flight test operations cost is the test pilot's salary necessary to conduct test flights and the personnel assisting with these flights. The flight tests act as one final quality check, assuring that the aircraft is fit to be delivered to the client. The final manufacturing cost is shown in Equation 21.2.

21.1.4. Certification (CERT)

The certification level for the ESRA aircraft will be type certification. Since 2003, the European Union Aviation Safety Agency (EASA) has been entrusted with the task of certifying aircraft in the EU and certain European non-EU countries. This certification serves as evidence that the particular aircraft type adheres to the safety standards established by the European Union. The type certification is the highest certification standard in EASA, it was chosen as such in accordance with Section 1.1 to be able to market the aircraft to the largest amount of clients.

The certification is hard to estimate, as the existing freely available methods such as DAPCA IV are antiquated and result in certification costs that are too low. Furthermore, the usage of any existing models is dubious as our aircraft is very specialized, with the wingspan of an airliner but the fuselage a fifth of the length, statistical models for the certification might not apply as the ESRA aircraft would be an outlier. The certification must however be estimated, and it is estimated as 25 million US\$. This comes from an estimate in an article relating to certification cost [39] and discussions with Joris Melkert, the senior lecturer at the Flight Performance and Propulsion chair in TU Delft. Joris Melkert has knowledge of the certification, having participated in projects as the certification engineer.

21.1.5. Flying Costs

The flying costs are those necessary to operate the aircraft during a day of flying research, these include fuel, oil, and pilot salary as can be seen in Table 21.4. The method that is used in Roskam is for an airliner and it was thought that this would produce results that were acceptable, since the military

Table 21.4: Breakdown of Flying Costs

Name Component	Symbol	Value	Units
Cost of Crew per nautical mile	C_{crew}	0.83	\$2023/nm
Fuel and oil (pol stands for petroleum oil and lubricants)	C_{pol}	1.50	\$2023/nm
Total Flying costs	DOC_{flt}	2.33	\$2023/nm

Table 21.5: Breakdown of Maintenance Costs

Name Component	Symbol	Value	Units
Labor cost of airframe and systems	$C_{lab_{ap}}$	0.32	\$2023/nm
Labor cost of engines maintenance	$C_{lab_{eng}}$	0.07	\$2023/nm
Cost of maintenance materials for airframe and engine	$C_{mat_{ap}}$	0.34	\$2023/nm
Engine maintenance	$C_{mat_{eng}}$	1.10	\$2023/nm
Applied maintenance burden	C_{amb}	0.71	\$2023/nm
Total Maintenance Cost	DOC_{maint}	2.54	\$2023/nm

single-seater pilot estimations produced much higher costs due to the liabilities of operating in a warzone. Fuel, oil, petroleum, and lubricants are consumables that must be bought each flight and represent a significant portion of the direct operating cost.

Further, flying costs from using the ADBS, satellite GPS telemetry, are incurred each flight, however, these costs are not modeled as the ADBS represents a minuscule part of the initial acquisition costs, satellite telemetry will be considered on a per-mission basis and the cost of this service will be charged directly to the user. Costs that are not incurred each flight but are still associated with flying include the purchase and replacement of brakes, tires, and sealing O rings of the aircraft, these will not be modeled in the cost tool due to their complexity.

$$DOC_{flt} = C_{crew} + C_{pol} \quad (21.3) \quad DOC_{maint} = C_{lab_{ap}} + C_{lab_{eng}} + C_{mat_{ap}} + C_{mat_{eng}} + C_{amb} \quad (21.4)$$

21.1.6. Maintenance Costs

The maintenance costs are those associated with the upkeep of the ESRA aircraft to keep it safely mission ready. The different components of this cost are shown in Table 21.5 and the overall maintenance cost is displayed in Equation 21.4. The labor cost of airframe and systems and the labor cost of engine maintenance are the salaries of the specialists that maintain airframes and engines. The cost of the spares that are required for maintenance is shown as $C_{mat_{ap}}$. Maintenance burden cost is the cost associated with the management, administration, monitoring, planning, and testing of maintenance activities.

21.1.7. Insurance

The ESRA aircraft will be sold to a space agency (for example ESA) that will then lease it out to scientists in order to conduct their research. In order to mitigate the financial risk of an airframe loss following an accident, the aircraft will be insured and a part of this insurance cost will be passed onto the scientists that lease the aircraft for research. The insurance rate is part of the Direct Operating Cost and has been set at 2% of the acquisition costs for an airplane. 2% is the recommended value from [69]. This leads to a cost per nautical mile of 0.91 US 2023 \$. This will insure the owner of the aircraft in case of an accident that results in an airframe write-off.

21.1.8. Logistics costs

The costs associated with logistics are those of transporting or flying the aircraft to the chosen research location and moving the necessary personnel and equipment to keep the aircraft running while not at home base. Furthermore, any specialized perishables will need to be transported along with the aircraft.

The personnel that needs to be transported when the aircraft is deployed on a campaign is composed

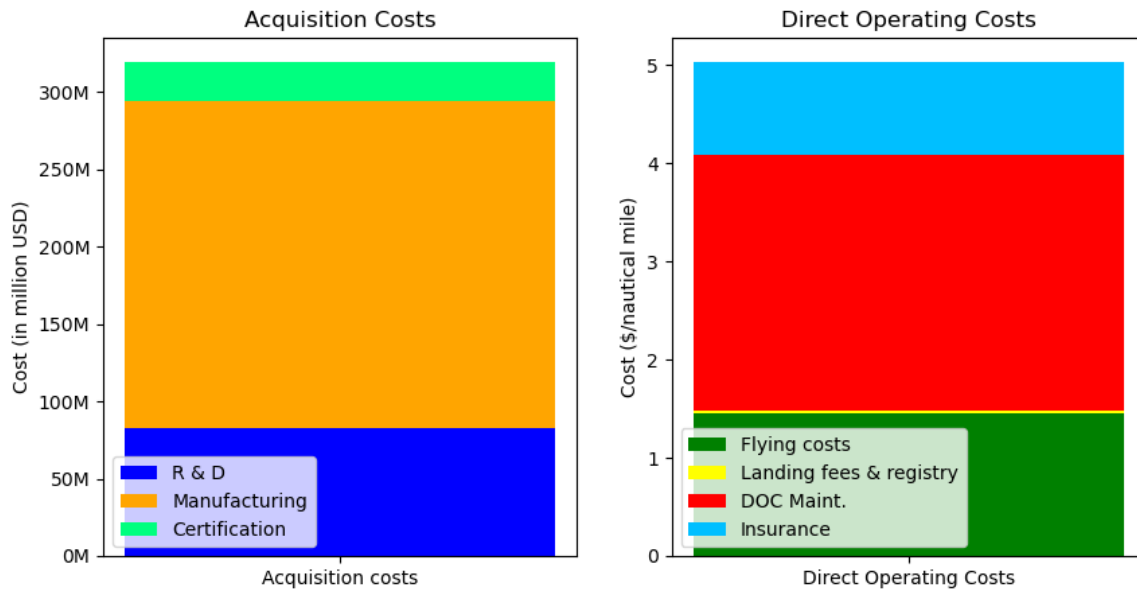


Figure 21.2: Breakdown of the different components of the acquisition costs and DOC.

of 2 pilots and 3 maintainers. Four of these crew members (all except the pilot flying research aircraft) will need to be transported via a flight to the deployed base of operations. Their equipment will need to be transported along with them, for this a standard 20-foot shipping container will be allocated. Additional costs are those of the crew accommodation and the renting of a sufficiently big hangar to store the aircraft while it is on deployment.

These costs are all highly variable, depending principally on the distance between the deployed base and the home base for the transport, and on the local accommodation/ renting rates in the specific country of deployment. For example, shipping container rates vary from 3500-14000 US\$ [16] based on size and distance traveled. It is therefore not possible to produce a general estimate for the logistical costs, as it needs to be calculated on a per-campaign basis. However, all logistics and operations costs from a deployed base will be directly charged to the client.

21.1.9. Breakdown of the cost for ESRA

It is now possible, to sum up all the costs for the two categories: acquisition costs and direct operating costs, these can be visualized in Figure 21.2. The acquisition costs are those shown for the entire fleet of 10 series planes plus 2 prototypes. The total acquisition cost of 319 million USD leads to an acquisition cost per airplane of 26.54 million USD. As can be seen in the left bar chart of Figure 21.2 the manufacturing cost of the aircraft is the main contributor to the initial acquisition costs and is a cost that will vary with an increasing number of aircraft unlike certification and R&D costs. The right-hand side of Figure 21.2 shows the direct operating costs associated with running the aircraft per nautical mile (as defined in the Roskam costing book [69]). The total cost is 5.05 USD per nautical mile flown which is mainly composed of the maintenance burden to be conducted once the flight lands. The second largest contributor to the per nautical mile cost is the fuel, oil, lubricant, and crew costs. The direct operating costs increase linearly with increasing nautical miles flown.

21.2. User Fee and campaign costs

Now that all the costs associated with the program have been calculated, the user fee can be determined. The user fee represents the hourly price that will be charged to the final customer and includes not only the direct operating costs but also all the other expenses related to the development and manufacturing of the fleet. To calculate the user fee, the following steps were followed: Firstly, the total acquisition costs for the fleet (TOT_ACQ) are obtained, as shown in Equation 21.6, by summing up all the fixed

Table 21.6: Costs of ground crew per day of the campaign

Person	Number	Salary	Hours Per day	Cost Per Day US \$
Mechanic	3	30	10	900
Engineer	1	55	10	550
Mission Manager	1	55	10	550

costs for each aircraft. Next, the (DOC) needs to be converted from the value calculated in \$/nautical mile to \$/hour. This conversion is performed in Equation 21.5 by multiplying the DOC by the cruise ground speed, which was assumed to be constant at 191 m/s throughout the entire flight duration. To determine the DOC in \$/hour, it was multiplied by the total hours flown by each aircraft during its lifetime (TOT_HOURS) and the number of aircraft produced (N_m). Finally, the user fee is calculated by combining the total acquisition costs and DOC costs and dividing the result by the number of aircraft and the total hours flown, as demonstrated in Equation 21.7. This gives a user fee of, \$4217/hour, if the scientists are charged this value then the client (space agency) will recuperate the money spent for the acquisition of the aircraft within the 30 years of expected lifespan of the aircraft.

$$TOT_DOC = N_m \cdot TOT_HOURS \cdot 3600 \cdot V_{gs} \cdot 0.00053996 \cdot DOC \quad (21.5)$$

$$TOT_ACQ = RDTE + AEP \cdot N_m + CERT \quad USER_FEE = \frac{(TOT_ACQ + TOT_DOC)}{N_m \cdot TOT_HOURS} \quad (21.6) \quad (21.7)$$

One of the primary objectives of this project is to increase the affordability of stratospheric research, thereby making it more accessible to scientists compared to the existing options. Consequently, it is crucial to assess the position of ESRA in the market, in relation to other aircraft currently operating. To facilitate this comparison, the cost, and payload of each aircraft have been graphically represented in Figure 21.3, alongside ESRA. An immediate observation is that ESRA stands out as the most cost-effective option among the alternatives. It is worth noting, however, that other aircraft exhibit much higher payload capacities. At the same time, it is important to consider that the majority of scientific payloads nowadays have been miniaturized enough and often weigh less than 100 kg. In this context, ESRA emerges as a highly valuable asset in the market, as scientists' main priority is conducting research at the most economical price possible.

The total costs for a campaign are taken by applying the costing model to a standard campaign as shown in Table 1.6. For a standard campaign with 45 science flying hours and 14 testing and integration hours, the total costs would be 248,803 2023 US\$ for a campaign from a home base. The salaries of all those employed during the campaign are shown in Table 21.6. All hourly rates for Mechanics, Flight engineers and Mission managers were taken from the Bureau of labor statistics. Mission managers and flight engineers were assumed to have the same salary in both specialized positions. The total cost for personnel for a 50-day standard campaign as seen in Table 1.6 would be 55900 USD. This would bring the total campaign costs to 304703 US dollars for a 50-day 45 flying science hour campaign.

21.3. V&V of the cost tool

The single calculations from the Roskam [69] book were implemented into the code and they were checked by hand to ensure that their outputs were mathematically correct. The Roskam [69] method for cost estimations was coded in Python and was verified by inputting numbers from a costing exercise present in the Roskam book. The values that resulted from inputting the original values turned out the same as the answers in the book, therefore the tool has been correctly coded as indicated in the book.

⁴URL: <https://www.bls.gov/ooh/installation-maintenance-and-repair/aircraft-and-avionics-equipment-mechanics-and-htm> [cited 20/06/2023]

⁴URL: <https://www.bls.gov/ooh/architecture-and-engineering/aerospace-engineers.htm> [cited 20/06/2023]

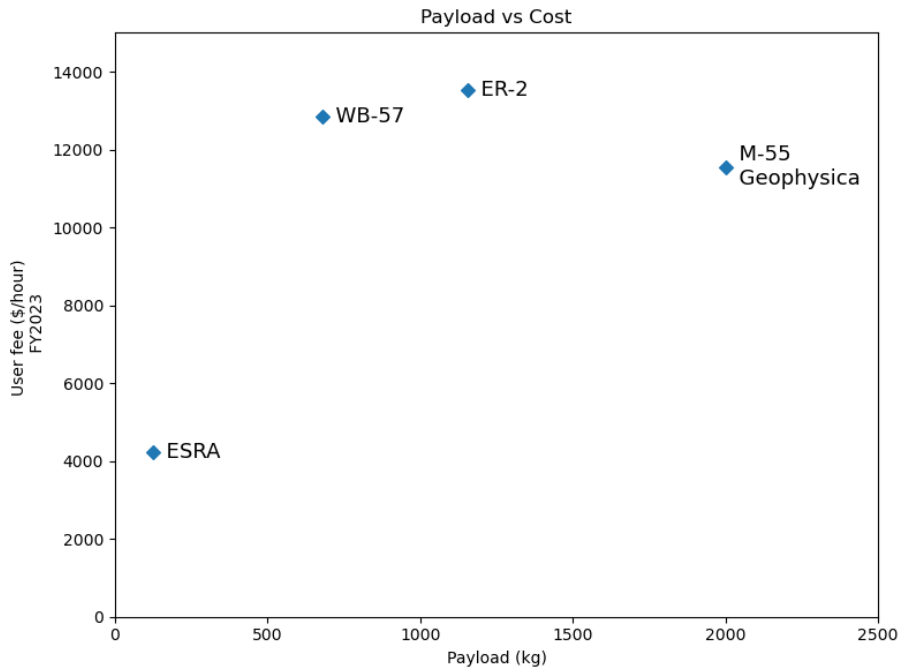


Figure 21.3: Overview of cost and payload capability of all current options on the market.

Table 21.7: Percentage change of the user fee when different inputs are varied by 20%

Component	Final Change User Fee (%)
W_to	10.58
T_to	0.0388
V_max	12.41
V_cr	-15.08
W_a	0.1825
W_f_used	2.578
T_cl	1.019

21.4. Sensitivity Analysis

Given that lowering the costs is one of the main concerns for the ESRA design bureau, it is fundamental to understand what are the parameters that have the biggest impact on the different costs of the ESRA program. Therefore, a sensitivity analysis was conducted on the cost tool to determine what inputs created the largest changes in the outputs. This was done by varying the inputs by 20%, and recording how the changes affected the acquisition, DOC, and user fee. A result of this analysis is presented in Table 21.7 in which it can be seen how each parameter affects the cost for the user fee. Given that the configuration of the aircraft has already been finalized, there is limited flexibility in modifying key aircraft parameters such as takeoff weight, fuel weight, and maximum airspeed as doing this could impact the overall aircraft performance. Nonetheless, it remains crucial to understand which of these parameters has the most substantial influence on the final cost. This understanding will facilitate future optimization efforts aimed at cost reduction.

On the other hand, there are additional parameters utilized in the cost estimation tool that exert a significant influence on the final cost and can be further modified to optimize for cost. These are respectively the number of aircraft, lifetime of an aircraft, and number of operational hours per year.

The relationship between the number of aircraft and the user fee, acquisition costs, and DOC can be observed in the figure below. The number of aircraft produced (N_m) shows an inverse relationship with user fees. It is worth noting that the R&D costs remain constant, as they are fixed regardless of the number of aircraft produced. In other words, one approach to reducing the hourly fee is to increase the production and sale of the aircraft. By doing so, the research and development (R&D) costs can

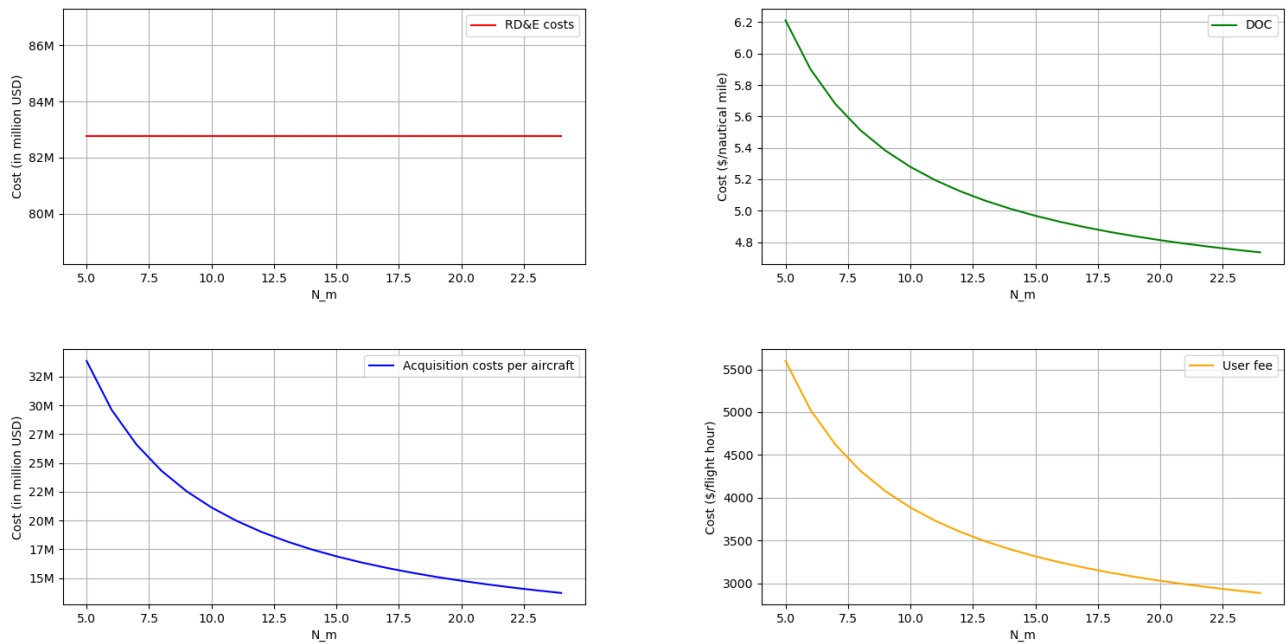


Figure 21.4: Relationship between the number of units built (N_m) and costs.

be distributed across a larger fleet. The specific value for N_m depends on the level of interest from potential buyers of the ESRA. Currently, it was decided that 10 aircraft will be sold based on the market analysis and mission requirements. However, if additional organizations express interest in acquiring the aircraft for research purposes after certification, the number of aircraft produced can be increased, resulting in lower overall hourly fees. This represents a highly practical approach to cost reduction and enhances accessibility to the aircraft for researchers.

Looking at Figure 21.5a and Figure 21.5b, a similar relationship can be observed for the user fee in relation to the number of operational hours per year (Op_hours) and the program’s lifetime in years (N_yrs). As these two parameters increase, the hourly rate decreases. To estimate the operational hours, previous scientific missions and the frequency of campaigns conducted by the existing stratospheric fleet were taken into account. This estimation yielded approximately 500 operational hours per year, which is significantly higher than the current stratospheric aircraft, however, given that the aircraft is new it is expected that it will be highly available. Although it is unlikely for the yearly flying hours to increase further, an increase in research interest regarding atmospheric studies may lead to more missions in the future, ultimately resulting in lower prices for scientists.

The estimated lifetime of the aircraft is around 30 years, which is a realistic value for a newly developed aircraft. Existing stratospheric aircraft have been in operation for over 50 years, and it is possible that the ESRA could remain operational even costs beyond the 30-year timeframe. However, accurately estimating the operational lifespan during the preliminary design phase is challenging.

21.5. Recommendations

The main goal of ESRA from a cost point of view was to produce an aircraft that had a lower acquisition and operating cost than the competitor aircraft. This would open up stratospheric research to a larger community. In this section, recommendations and suggestions to lower the price will be discussed.

To minimize aircraft acquisition costs without the need for significant redesign or major alterations, the most effective approach is to expand the marketing efforts to target additional space agencies globally. As illustrated in Figure 21.4, when more aircraft are ordered, economies of scale come into play. This results in reduced manufacturing costs since materials can be purchased in bulk at a larger discount, and the experience gained from manufacturing processes enables faster aircraft production. Moreover, with a growing number of aircraft purchases, the costs associated with research and development

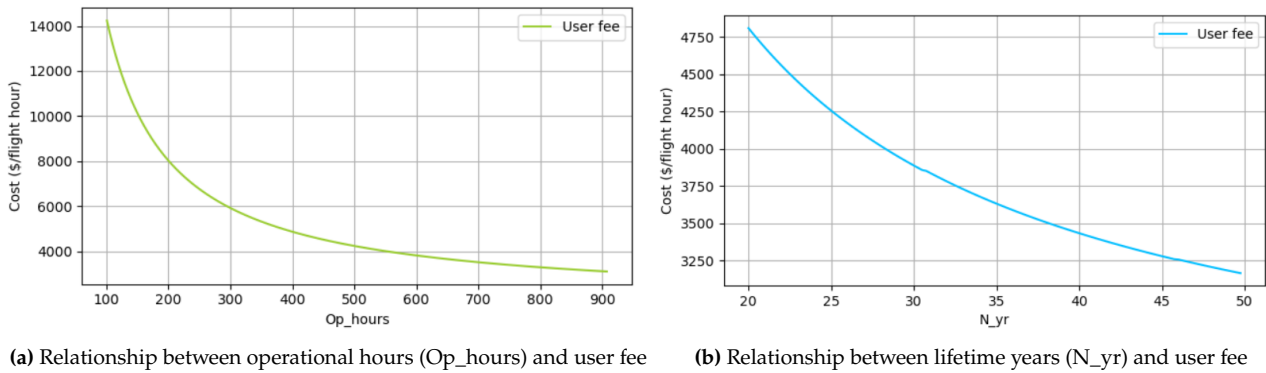


Figure 21.5: Changes to user fee when varying operational hours and lifetime years.

(R&D) and certification are divided among a larger number of aircraft, thereby lowering the individual aircraft price.

To lower the operational expenses of the aircraft, it's crucial to consider the right-hand side of Figure 21.2. The costs associated with flying the aircraft primarily consist of crew and fuel expenses. Unfortunately, these costs are unlikely to decrease in the foreseeable future. To achieve fuel savings, one option is to install new engines or reduce aircraft drag. However, both approaches would necessitate significant redesign efforts and lead to increased research and development (R&D) costs.

On the other hand, maintenance costs can be reduced by implementing a design that allows for easy access to aircraft parts and standardization. This ensures that spare parts can be readily found worldwide. Although these design decisions have already been made, any further cost reductions related to improving the aircraft's maintainability would be minimal.

As the aircraft accumulates more flight time and demonstrates its safety record, insurance costs are expected to decrease gradually. However, in general, reducing the DOC without a major and expensive redesign is challenging to accomplish.

The user fee is inversely related to the aircraft's acquisition and DOC. This relationship is demonstrated in Figure 21.5a and Figure 21.5b. As yearly operational hours and years in service increase, the user fee decreases accordingly. Anticipated improvements in familiarity among maintainers and research crews are expected to result in a slight increase in yearly operational hours once the aircraft is deployed. Moreover, with proper maintenance, the operational lifespan of the aircraft can exceed 30 years. Notably, competitor aircraft such as the WB-57 and ER-2 have successfully remained in service for 40-50 years [25]. Once the aircraft surpasses the 30-year operational milestone, the acquisition cost is recouped, leading to a significant drop in the user fee.

There is potential for further cost reductions in the ESRA project. Thanks to the the current affordability of the aircraft compared to competitors, a larger segment of the scientific community now has the opportunity to engage in high altitude research. However, it is still valuable to consider recommendations for cost reductions.

Requirement compliance

22.1. System Requirements

Req. ID	Requirement	✓	Reference
ESRA-STAKE-1-SYS-1	The aircraft shall be able to fly at an altitude of 20.5 km or higher	✓	Section 13.3
ESRA-STAKE-6-SYS-2	The aircraft shall have 1-hour endurance on station at altitude	✓	Section 13.3
ESRA-STAKE-9-SYS-3	The aircraft shall be able to stay in a radius of 9.26 km (5 nm) from an object of study at altitude	✓	Section 13.4
ESRA-STAKE-9-SYS-4	The aircraft shall be able to determine its location within 200 m precision in the research area	✓	Future Design
ESRA-STAKE-9-SYS-5	The aircraft shall be able to transmit telemetry data to the ground base during scientific experiments	✓	Future Design
ESRA-STAKE-7-SYS-7	The aircraft shall have a modular payload interface relevant to current research operations	✓	Chapter 6
ESRA-STAKE-3-SYS-8	The aircraft shall have a sustainable end-of-life solution	✓	Section 17.3
ESRA-STAKE-3-SYS-9	The aircraft shall cause a temperature change lower than or equal to $0.016 \cdot (10)^{-6}$ [K] considering a time horizon of 100 years	✗	Subsection 17.1.1 ¹
ESRA-STAKE-5-SYS-10	Operation of the aircraft shall have at least 60% research efficiency during a scientific research campaign	✓	Future Project
ESRA-STAKE-5-SYS-12	The direct operating cost of the aircraft shall be no more than \$11557 FY23 USD per hour	✓	Section 21.2
ESRA-STAKE-2-SYS-13	The aircraft shall enter operation by 2030	✓	Chapter 23
ESRA-STAKE-4-SYS-14	The aircraft shall adhere to noise pollution regulations as stated in ICAO annex 16 vol.1	✓	Future Project
ESRA-STAKE-4-SYS-15	The aircraft shall be certified according to EASA and FAA standards	✓	Whole report and Future Project
ESRA-STAKE-4-SYS-16	The aircraft shall be statically stable in all operating conditions	✓	Chapter 12
ESRA-STAKE-4-SYS-17	The aircraft shall be controllable in all operating conditions	✓	Chapter 12
ESRA-STAKE-4-SYS-18	The aircraft shall maintain its structural integrity in all operating conditions	✓	Section 10.8
ESRA-STAKE-4-SYS-19	The aircraft shall have a communication system capable of communicating with air traffic control	✓	Future Project
ESRA-STAKE-4-SYS-20	The aircraft shall be able to land in 20 knots crosswind conditions	✓	Chapter 12
ESRA-STAKE-4-SYS-21	The aircraft shall be able to land in minimum visibility conditions of 366 mm of visual range	✓	Future Project
ESRA-STAKE-8-SYS-24	The aircraft shall be serviceable with existing airport infrastructure	✓	Section 16.1
ESRA-STAKE-5-SYS-25	Routine maintenance of the aircraft shall take less than 2 hours between flights	✓	Section 16.2

ESRA-STAKE-8-SYS-26	The aircraft shall be able to land and take off on runways of 2500 m length	✓	Section 13.2
ESRA-STAKE-4-SYS-27	The aircraft shall have 500 km of airport diversion capability	✓	Chapter 7
ESRA-STAKE-4-SYS-28	The aircraft shall be able to loiter for 45 minutes after an aborted landing	✗	Not complied with due to a decrease in Oswald factor: Chapter 13.
ESRA-STAKE-7-SYS-29	The aircraft shall provide more than 8050 W of power to the payload for payload operation	✓	Chapter 6
ESRA-STAKE-7-SYS-30	The aircraft shall provide flight data to the payload for payload operation	✓	Chapter 6
ESRA-STAKE-9-SYS-32	The aircraft must have the capability to activate or deactivate the payload	✓	Future project
ESRA-STAKE-9-SYS-33	The aircraft shall be able to start and stop the measurements performed by the scientific payload	✓	Chapter 16
ESRA-STAKE-9-SYS-34	The aircraft shall be able to control the pressure and temperature in the environment containing the payload	✓	Subsection 20.1.3
ESRA-STAKE-7-SYS-35	The aircraft shall have a minimum total payload carrying capacity of 100 kg (excluding the pilot)	✓	Chapter 7
ESRA-STAKE-6-SYS-36	The aircraft shall have a minimum operational radius of 3000 km	✓	Chapter 13
ESRA-STAKE-4-SYS-37	The aircraft shall have longitudinal static stability throughout the entire flight envelope	✓	Chapter 12
ESRA-STAKE-4-SYS-38	The aircraft shall have lateral static stability throughout the entire flight envelope	✓	Chapter 12
ESRA-STAKE-4-SYS-39	The aircraft shall have directional static stability throughout the entire flight envelope	✓	Chapter 12
ESRA-STAKE-4-SYS-40	The aircraft shall have stable symmetric and asymmetric eigenmodes. Spiral mode is allowed to be unstable	✓	Chapter 12
ESRA-STAKE-4-SYS-41	The aircraft shall have a climb rate of 0.5 m/s at 20.5 km	✓	Chapter 7
ESRA-STAKE-4-SYS-42	The aircraft shall achieve a climb gradient of 8.3% at take-off	✓	Chapter 13
ESRA-STAKE-9-SYS-44	The aircraft shall have a turning radius of 9260 meters at 20.5 km altitude	✓	Chapter 13
ESRA-STAKE-4-SYS-45	The aircraft power system will comply with certification	✓	Chapter 6
ESRA-STAKE-4-SYS-46	The aircraft shall have flying qualities of level one for all phases of flight and for all longitudinal and lateral eigenmotions	✓	Chapter 12
ESRA-STAKE-4-SYS-47	The aircraft shall possess directional stability in the one-engine-out condition	✓	Section 12.3

22.2. Aerodynamics sub-system

¹This requirement was not proven as not the same metric was calculated.

Req. ID	Requirement	✓	Reference
ESRA-STAKE-1-SYS-1-AERO-1	The aircraft shall possess a load factor that is greater than or equal to 1 at the target altitude of 20.5 km.	✓	Section 13.3
ESRA-STAKE-1-SYS-1-AERO-3	The aircraft shall have 12 m/s speed margin at 20.5 km altitude.	✓	Section 13.3
ESRA-STAKE-4-SYS-15-AERO-4	The aircraft flutter speed shall be higher than $1.2V_d$.	✓	Chapter 11
ESRA-STAKE-4-SYS-15-AERO-5	The aircraft control reversal speed shall be higher than $1.2V_d$.	✓	Chapter 11
ESRA-STAKE-4-SYS-15-AERO-6	The aircraft divergence speed shall be higher than $1.2V_d$.	✓	Chapter 11

22.3. Structure sub-system

Req. ID	Requirement	✓	Reference
ESRA-STAKE-4-SYS-18-STRC-1	The structure must be able to support limit loads without detrimental, permanent deformation. At any load up to limit loads, the deformation may not interfere with safe operation.	✓	Subsection 10.8.5
ESRA-STAKE-4-SYS-18-STRC-1	The structure must be able to support ultimate loads without failure for at least three seconds, except local failures or structural instabilities between limit and ultimate load are acceptable only if the structure can sustain the required ultimate load for at least three seconds.	✓	Subsection 10.8.5
ESRA-STAKE-4-SYS-18-STRC-3	The structure shall be able to withstand oscillatory buffeting load ESRA-STAKE-4-SYS-15-AERO-4 without causing permanent structural deformation.	✓	Subsection 11.0.2
ESRA-STAKE-4-SYS-18-STRC-4	The structure shall be able to withstand vibrational loads according to ESRA-STAKE-4-SYS-15-AERO-5 without causing permanent structural deformation.	✓	Subsection 11.0.2
ESRA-STAKE-4-SYS-18-STRC-5	The structure shall be able to withstand ground load requirements following from taxing and landing scenarios [CS 23.473] ²	✓	Subsection 10.8.5

22.4. Propulsion sub-system

Req. ID	Requirement	✓	Reference
ESRA-STAKE-8-SYS-26-PP-1	The propulsion sub-system shall provide 30 kN take-off thrust at sea level.	✓	Chapter 8.4
ESRA-STAKE-1-SYS-1-PP-3	The propulsion sub-system shall provide 1.7 kN thrust at 20.5 km.	✓	Chapter 8.4
ESRA-STAKE-4-SYS-37-PP-4	The propulsion system shall be integrated in the aircraft in such a way that longitudinal stability is maintained	✓	Chapter 8.2
ESTA-STAKE-4-SYS-17-PP-5	The propulsion sub-system shall become nondispatchable (no flight hours) if the rate at which the engine control system loses thrust control is greater than $1 \cdot 10^{-4}$ failures per hour.	✓	Chapter 20

ESTA-STAKE-4-SYS-17-PP-6	The propulsion sub-system shall become short-time dispatchable (entry-level system = 125 flight hours, mature level system = 250 flight hours) if the rate at which the engine control system loses thrust control is between $7.5 \cdot 10^{-5}$ and $1 \cdot 10^{-4}$ failures per hour.	✓	Chapter 20
ESTA-STAKE-4-SYS-17-PP-7	The propulsion sub-system shall become long-time dispatchable (entry-level system = 250 flight hours, mature level system = 500 flight hours) if the rate at which the engine control system loses thrust control is between $1 \cdot 10^{-5}$ and $7.5 \cdot 10^{-5}$ failures per hour.	✓	Chapter 20
ESTA-STAKE-4-SYS-17-PP-8	The propulsion subsystem shall be capable of operating throughout its operating envelope when subjected to sudden encounters with any 30-second continuous period of hail up to altitudes of 4500 meters.	✓	Chapter 20
ESTA-STAKE-4-SYS-17-PP-9	The propulsion sub-system shall not be exposed to over $0.5[\text{mg}/(\text{hrs} \cdot \text{m}^3)]$ of volcanic ash.	✓	Chapter 20

22.5. Communication sub-system

Req. ID	Requirement	✓	Section 14.1
ESRA-STAKE-4-SYS-19-COM-1	A bandwidth between 108 and 137 MHz will be present throughout the flight for communication.	✓	Section 14.1
ESRA-STAKE-4-SYS-19-COM-2	The communication sub-system shall be able to perform two-way communication.	✓	Section 14.1
ESRA-STAKE-4-SYS-15-COM-3	The communication sub-system shall be equipped with an ADS-B 1090 ES transponder.	✓	Section 14.1

22.6. Power sub-system

Req. ID	Requirement	✓	Section 14.2
ESRA-STAKE-7-SYS-29-PW-1	The power subsystem shall be able to provide 230 V AC at 50 Hz. Three-phase (50 amps max) to the payload, conforming to European standards.	✓	Section 14.2
ESRA-STAKE-1-SYS-1-PW-2	The power subsystem shall be able to provide 28 VDC (400 amps max) to the payload.	✓	Section 14.2

22.7. Payload sub-system

Req. ID	Requirement	✓	Chapter 6
ESRA-STAKE-7-SYS-35-PAY-1	The payload subsystem shall be able to be mounted and removable without making permanent structural changes to the aircraft structure.	✓	Chapter 6
ESRA-STAKE-7-SYS-35-PAY-2	Payload shall be able to be mounted onto the mounting rack without aircraft present.	✓	Chapter 6
ESRA-STAKE-7-SYS-29-PAY-3	The aircraft shall provide a standard power interface for payload integration according to standard US military aircraft connectors.	✓	Chapter 6
ESRA-STAKE-7-SYS-35-PAY-4	Payload bay will be environmentally controlled to a temperature of 16 degrees Celsius.	✓	Chapter 6
ESRA-STAKE-7-SYS-35-PAY-5	Payload bay will be pressurized at an altitude of 9 km when the aircraft is operating at an altitude of 20.5 km.	✓	Chapter 6

22.8. Life Support

Req. ID	Requirement	✓	Reference
ESRA-STAKE-4-SYS-48-LS-1	The cockpit structure must be designed to maintain pressurization at high altitudes, providing a habitable environment for the pilot during stratospheric research missions.	✓	Subsection 20.1.3
ESRA-STAKE-4-SYS-48-LS-3	The cockpit structure must be designed to maintain a temperature of around 16 degrees at high altitudes, providing a habitable environment for the pilot during stratospheric research missions.	✓	Section 16.4
ESRA-STAKE-4-SYS-48-LS-3	The pilot duty hours (pre-flight to engine shutdown) shall be limited to 12 hr.	✓	Section 16.4
ESRA-STAKE-4-SYS-48-LS-4	The entire operational crew shall have a downtime of at least 12 hr between operations.	✓	Section 16.4

22.9. Avionics

Req. ID	Requirement	✓	Future project
ESRA-STAKE-4-SYS-44-AV-1	The off-the-shelf avionics package shall be compliant with aircraft power standards.	✓	Future project
ESRA-STAKE-4-SYS-4-AV-2	The avionics package shall comply with navigational accuracy to within approximately 0.1 nm lateral deviation from the desired course.	✓	Future project
ESRA-STAKE-4-SYS-17-AV-3	The avionics package shall provide an autopilot that will control the aircraft to ± 1 degree in pitch, roll, and yaw.	✓	Future project
ESRA-STAKE-4-SYS-17-AV-4	The avionics package shall be equipped with a supplementary set of analog instruments to complement the digital instruments in case of electrical failure.	✓	Future project
ESRA-STAKE-4-SYS-17-AV-5	The avionics package shall be equipped with a weather radar.	✓	Chapter 6

22.10. Landing Gear

Req. ID	Requirement	✓	Reference
ESRA-STAKE-4-SYS-17-LG-1	The nose landing gear shall have more than 8% MTOW on the ground for steerability.	✓	Chapter 15
ESRA-STAKE-4-SYS-18-LG-2	The nose landing gear shall have less than 15% MTOW on it for its structural integrity.	✓	Chapter 15
ESRA-STAKE-4-SYS-17-LG-3	The aircraft shall have a turnover angle larger than 55 degrees.	✓	Chapter 15
ESRA-STAKE-4-SYS-18-LG-5	The landing gear shall ensure the aircraft has a lateral ground clearance angle larger than 8 degrees.	✓	Chapter 15
ESRA-STAKE-4-SYS-18-LG-6	The landing gear subsystem shall not interfere with other components it is mounted adjacent to.	✓	Chapter 15
ESRA-STAKE-4-SYS-18-LG-6	The aircraft shall have a scrape angle larger than 156 degrees	✓	Chapter 15

Future planning

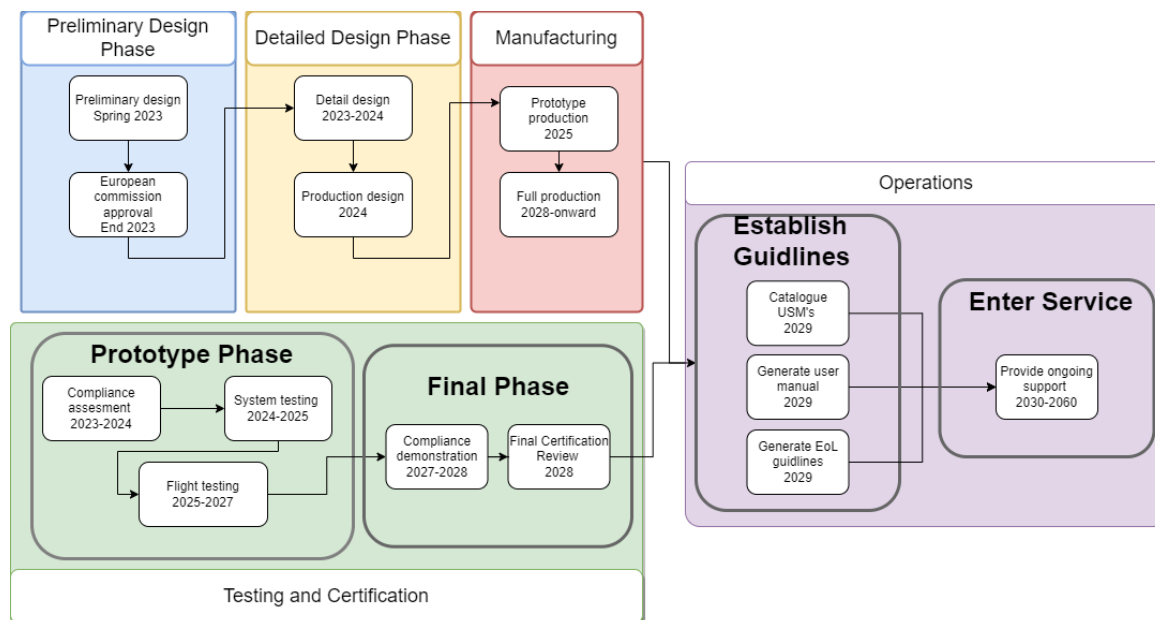


Figure 23.1: Future outlook planning

23.1. Project design and development logic

Preliminary Design Phase

The preliminary design phase, including the original DSE spring further design refinement and acquisition by ESA, was estimated to last 6 months. While awaiting the acquisition by ESA, the detailed design also commences.

Detailed design phase

The detailed design phase focuses on defining the geometry of each component, developing manufacturing processes, and providing a production plan. This phase lasts for approximately 1.5 years.

Manufacturing phase

The manufacturing phase is the time to develop the first set of aircraft after the initial commission, it is estimated to last 3 years.

Certification and Testing Phase

Before entering service, ESRA must undergo rigorous certification and flight tests to ensure compliance with regulations. It was decided that ESRA would be type certified by the European Union Aviation Safety Agency (EASA). Type certification ensures that the aircraft meets the safety standards set by the European Union and is essential for market acceptance and operation within the EU and certain non-EU countries. The certification process will be done concurrently with the design of the aircraft to ensure continuous compliance with the regulatory bodies.

Operations

Once certified, the ESRA aircraft enters the operational phase, delivery to clients, and providing support and maintenance during the operational lifetime estimated at 30 years.

The ESRA design bureau’s role encompasses securing funding, developing the aircraft, expanding its market presence, collaborating with operators, and preparing technical and costing documents for potential buyers. Their effort’s aim to meet the scientific community’s needs for enhanced observational capabilities and facilitate research campaigns conducted by individual scientists.

The day-to-day operations will be conducted by the clients, the ESRA design bureau will supply the clients with comprehensive maintenance plans, including routine inspections, scheduled maintenance, and a reliable supply chain for spare parts. Guidance to skilled technicians with expertise in the new aircraft’s systems will be made available to clients to ensure effective and efficient maintenance.

End-of-Life Phase

At the end of the operational lifetime, an end-of-life procedure is followed, considering ongoing sustainability principles. Once a client decides to discontinue its use of the ESRA aircraft, the ESRA design bureau will similarly discontinue its continued service to the aircraft. The specific disposal of the aircraft, whether it is used for spares or scrapped entirely is up to the discretion of the client but should be in compliance with the EoL guidelines handbook.

The role of the ESRA design bureau is to provide a comprehensive end-of-life plan, similar to the "Process for Advanced Management of End-of-Life of Aircraft" (PAMELA) (see Section 17.3). This plan relates to cataloguing usable serviceable material (USM) and providing guidance to the client of disposable of non-reusable items.

The continued use of parts requiring re-certification and refurbishment will be up to the client.

23.2. Project Gantt chart

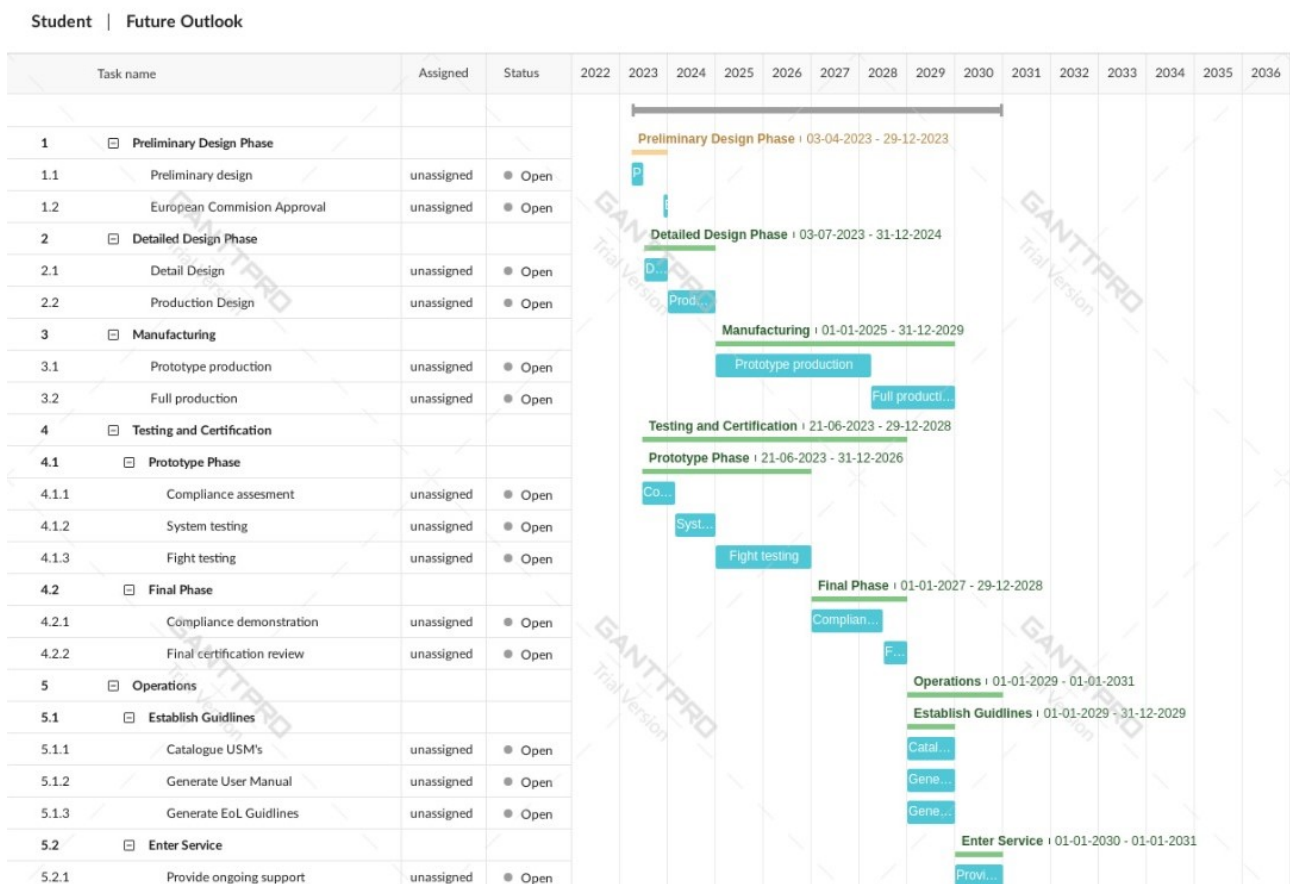


Figure 23.2: Future outlook Gantt chart

Conclusion

The goal of this report was to document the design process of a new European Stratospheric Research Aircraft (ESRA), an aircraft capable of carrying a payload of 100 kg to an altitude of at least 20.5 km and loiter at that altitude for at least one hour. Furthermore, ESRA was required to have an operating range (excluding the one hour loiter time) of 6000 km thus letting it outperform most of the current competition. Previous work was done to select the high level concept for ESRA and perform some initial sizing. Thus was selected the concept of a manned jet propelled aircraft whose design was expanded and built upon in three principal parts in this report.

First of all, the context of the ESRA project was reestablished and completed through an update to the market analysis and revisions of the requirements and subsystem requirements. Important findings of the market analysis were the ESRA roadmap which details how a project such as ESRA could obtain funding from the European Commission and a breakdown of the costs and timelines associated with different stratospheric research missions.

The design of ESRA itself was a complex matter involving many interconnected components that have to combine in the correct way. The first step of design was to select the most appropriate configuration. This resulted in a strutted high wing configuration with podded engines. A big unknown in the configuration was the propulsion layout which was finally set to two wing podded PW535A engines. Thus the tail configuration was set to that of a T-tail. It was decided to size the aircraft fuselage around the idea of payload modularity. Thus, trolleys were designed that contained the payload and could be easily integrated to the fuselage. With those size constraints in place, overall sizing of the aircraft for performance was done. At this stage of the design little optimisation of individual subsystems was done but the overall airframe was sized and characterised such that it could be ensured that ESRA would fulfill the driving requirements. Work was done at a lower level to characterise different subsystems such as the wing structure, aerodynamics and stability and control. Finally, high level designs were made for different systems throughout the aircraft such as the fuel system, the electrical system and the hydraulics system. One of the goals of ESRA was to provide a platform for stratospheric research at a low cost. The first part of that goal was accomplished through the work described above but a detailed cost estimation was required. The design phase concluded with an aircraft capable of fulfilling all driving requirements with a maximum take off weight of 4445 kg, a wingspan of 25 m, a cruise mach number of 0.65 and a unit cost of \$ 26.54M.

Having designed the aircraft, work was focused on the operations of ESRA and the future of the project. First and foremost, an operations and logistics plan was developed where research was done on potential bases that would enable global coverage by ESRA as well as air and ground operations required for ESRA. Furthermore, the sustainability of ESRA was characterised by calculating the Average Temperature Response of the aircraft (ATR) as well as investigating its social sustainability and the end of life plan. A technical risk assessment was performed in order to identify potential threats to the project and identify risk mitigation strategies which have been or will be implemented. It was found that the most pressing threats related to the actual design of ESRA with potential issues with weight or analyses might doom the project. A Reliability, Availability, Maintainability and Safety (RAMS) analysis was performed as a follow up with the safety section taking the risk analysis as an input. It was found that at this stage of the project the RAMS analysis could not be performed to a satisfactory level of detail due to the lack of knowledge on some subsystems. At this point, all activities affecting requirements set up for ESRA had been completed. Thus a compliance matrix was made where it was found that some requirements could not be confirmed yet as the level of detail was too high relative to the work done during this phase of the project. Only one requirement regarding the ATR was failed outright. Due to its relatively low importance, little came from it. Last of all, Plans were made for the future of ESRA including for production and for the overall time line of the project from the writing of this report to 2060 when the predicted service life of ESRA comes to an end.

The goal of this report was to present a design for a Stratospheric Research Aircraft designed for low cost and high performance. The design delivered is however a preliminary design with lots of work remaining to be done. Detailed recommendations for all sections have been given within each chapter but the primary point of improvement lies in further analysis with more capable tools. Indeed, as the first class design, presented in this report, is complete, further work will focus on optimising the aircraft for weight and drag while increasing the design resolution from all sides.

References

- [1] In: *Continuous descent operations (CDO) Manual*. 1st ed. International Civil Aviation Organization, 2010.
- [2] en. URL: <https://www.ecfr.gov/current/title-14/chapter-I/subchapter-C/part-21>.
- [3] Federal Aviation Administration [FAA]. *Aviation Maintenance Technician Handbook– Airframe, Volume 1*. en. FAA, 2018.
- [4] International Civil Aviation Organization [ICAO]. *ICAO Aircraft Engine Emissions Databank*. en. Data set. June 2023. URL: <https://www.easa.europa.eu/en/domains/environment/icao-aircraft-engine-emissions-databank>.
- [5] *14 – Scope and Detail of Items (as Applicable to the Particular Aircraft) To Be Included in Annual and 100-Hour Inspections*. en. URL: <https://www.ecfr.gov/current/title-14/chapter-I/subchapter-C/part-43/appendix-Appendix%5C%20D%5C%20to%5C%20Part%5C%2043>.
- [6] John Anderson. *Fundamentals of Aerodynamics, Sixth Edition*. 6th. McGraw-Hill Education, 2017.
- [7] M.N. van Beijnen. *Damage Tolerance Aspects of a Composite Airplane Fuselage*. Report. July 1993.
- [8] Don C. Bingaman et al. “Stratospheric Aerosol Research Experiments and Aircraft for Solar Geoengineering”. In: *AIAA Scitech 2021 Forum*. DOI: 10.2514/6.2021-1681. eprint: <https://arc.aiaa.org/doi/pdf/10.2514/6.2021-1681>. URL: <https://arc.aiaa.org/doi/abs/10.2514/6.2021-1681>.
- [9] J.H. Blakelock. *Automatic Control of Aircraft and Missiles*. Wiley, 1965. ISBN: 978-0-471-07930-9. URL: <https://books.google.nl/books?id=FXFTAAAMAAJ>.
- [10] Scott A. Braun et al. “NASA’s genesis and rapid intensification processes (GRIP) field experiment”. In: *Bulletin of the American Meteorological Society* 94 (3 Mar. 2013), pp. 345–363. ISSN: 00030007. DOI: 10.1175/BAMS-D-11-00232.1.
- [11] E. Bruhn. *Analysis and Design of Flight Vehicle Structures*. Jacob Publishing inc., 1973.
- [12] D Brunner et al. *The SCOUT-O3 Darwin Aircraft Campaign: rationale and meteorology*. 2009, pp. 93–117. URL: www.atmos-chem-phys.net/9/93/2009/.
- [13] Douglas P. Wells Bryce L. Horvath. “Comparison of Aircraft Conceptual Design Weight Estimation Methods to the Flight Optimization System”. In: (). URL: <https://ntrs.nasa.gov/api/citations/20190000431/downloads/20190000431.pdf>.
- [14] Amir Caspi et al. “A New Facility for Airborne Solar Astronomy: NASA’s WB-57 at the 2017 Total Solar Eclipse”. In: *The Astrophysical Journal* 895 (2 June 2020), p. 131. ISSN: 1538-4357. DOI: 10.3847/1538-4357/ab89a8. URL: <https://iopscience.iop.org/article/10.3847/1538-4357/ab89a8>.
- [15] Lynn Chang. *Payload Mounting Hardware*. Feb. 2021. URL: <https://www.nasa.gov/specials/jsc-aircraft-ops/wb57-design---integration.html>.
- [16] Charlie Clissitt. *International Container Shipping Costs and Rates 2023*. Jan. 2023. URL: <https://www.movehub.com/advice/international-container-shipping-costs/>.
- [17] International Council Of The Aeronautical Sciences. Congress. *Proceedings of the ... Congress of the International Council of the Aeronautical Sciences*. Jan. 1996. URL: https://www.icas.org/ICAS_ARCHIVE/ICAS1996/ICAS-96-4.1.2.pdf.

- [18] RAND Corporation. *Military Jet Engine Acquisition*. en. MR-1596. 2002. URL: https://www.rand.org/content/dam/rand/pubs/monograph_reports/2005/MR1596.pdf.
- [19] Emily Schwartz Dallara, Ilan Kroo, and Ian A. Waitz. "Metric for Comparing Lifetime average Climate Impact of Aircraft". In: *AIAA Journal* 49.8 (Aug. 2011), pp. 1600–1613. DOI: 10.2514/1.j050763. URL: <https://doi.org/10.2514/1.j050763>.
- [20] Edwin F. Danielsen. "Trajectories of the Mount St. Helens eruption plume". In: *Science* 211 (4484 1981), pp. 819–821. ISSN: 00368075. DOI: 10.1126/science.211.4484.819.
- [21] Andrew Dankanich and David Peters. *Turbofan Engine Bypass Ratio as a Function of Thrust and Fuel Turbofan Engine Bypass Ratio as a Function of Thrust and Fuel Flow*. 2017. URL: <https://openscholarship.wustl.edu/mems500https://openscholarship.wustl.edu/mems500/34>.
- [22] André Deperrois. *Theoretical limitations and shortcomings of xflr5*.
- [23] James Drew. "Lockheed disputes U-2 cost comparison: Global Hawk's Cost Per Flight Hour Drops Below \$15K In 2014". In: *Inside the Air Force* 26.9 (2015), pp. 9–9. ISSN: 21648174. URL: <https://www.jstor.org/stable/24804540> (visited on 08/05/2023).
- [24] EASA. *Implementing Rules on Flight and Duty Time Limitations and rest requirements for commercial air transport (CAT) with aeroplanes*. European Aviation Safety Agency. Postfach 10 12 53 D-50452 Cologne, Dec. 2010.
- [25] *ER-2 AIRBORNE LABORATORY EXPERIMENTER HANDBOOK* NASA. National Aeronautics and Space Administration Dryden Flight Research Center, Aug. 2002.
- [26] *Explosive Depressurisation | SKYbrary Aviation Safety*. URL: <https://www.skybrary.aero/articles/explosive-depressurisation>.
- [27] F.Oliviero. *Systems Engineering and Aerospace design*. 2023.
- [28] Saeed Farokhi. *Aircraft Propulsion*. second. John Wiley and Sons Ltd, 2014.
- [29] Andreas Gebhardt, Julia Kessler, and Laura Thurn. *3D Printing*. Ed. by Andreas Gebhardt, Julia Kessler, and Laura Thurn. Second Edition. Hanser, 2019, pp. I–XVI. ISBN: 978-1-56990-702-3. DOI: <https://doi.org/10.3139/9781569907030.fm>. URL: <https://www.sciencedirect.com/science/article/pii/B9781569907023500017>.
- [30] Ohad Gur et al. "Development of a framework for truss-braced wing conceptual MDO". In: *Structural and Multidisciplinary Optimization* 44.2 (Aug. 2011), pp. 277–298. ISSN: 1615-1488. DOI: 10.1007/s00158-010-0612-9. URL: <https://doi.org/10.1007/s00158-010-0612-9>.
- [31] RJ Hamann and MJL van Tooren. *Systems Engineering and Technical Management Techniques - part 2*. Undefined/Unknown. CD-rom, dictaat. LR Ch. System Integration: Aircraft Design, 2004.
- [32] Omran Al-Shamma Rashid Ali Haitham S. Hasan. "AN INSTRUCTIVE ALGORITHM FOR AIRCRAFT ELEVATOR SIZING TO BE USED IN PRELIMINARY AIRCRAFT DESIGN SOFTWARE". In: *Journal of Applied Engineering Science* (2017), pp. 489–494. DOI: 10.5937/jaes15-14829.
- [33] Zhuohui He, Clarence Chang, and Caitlin Follen. *NOx Emissions Performance and Correlation Equations for a Multipoint LDI Injector*. en. NASA/TM—2014-218116. Apr. 2014.
- [34] Raymond G. Heineman. *WB-57 EXPERIMENTERS HANDBOOK*. AOD 33890 Rev C. National Aeronautics Space Administration. Lyndon B. Johnson Space Center Houston, Texas 77058, June 2017.
- [35] Hulshoff and SJ. *Aeroelasticity*. 2011.
- [36] *Janes | L World-leading open source defence intelligence — customer.janes.com*. Jane's Group UK Limited. (Accessed 02-May-2023).
- [37] Renaldo V Jenkins. *SC(2)-07 14 Airfoil Data Corrected for Sidewall Boundary-Layer Effects in the Langley 0.3-Meter Transonic Cryogenic Tunnel*. Langley Research Center Hampton, Virginia, 1989.
- [38] S.R.V. John E. Williams. *THE USAF STABILITY AND CONTROL DIGITAL DATCOM*. 1977. URL: <https://books.google.nl/books?id=FnIVzahqNGUC>.

- [39] DAN JOHNSON. "The cost of certification". In: (Sept. 2012).
- [40] Alenka Pandiloska Jurak. "The importance of high – Tech companies for EU economy – Overview and the EU grand strategies perspective". In: *Research in social change* 12.3 (Sept. 2020), pp. 32–52. DOI: 10.2478/rsc-2020-0013. URL: <https://doi.org/10.2478/rsc-2020-0013>.
- [41] Franz K. et al. *Life cycle engineering in preliminary aircraft design*. Vol. pp. 473–478. Leveraging Technology for a Sustainable World. Springer Berlin Heidelberg, 2012.
- [42] Hans Karlsen. *UK Aerospace Maintenance, Repair, Overhaul & Logistics Industry Analysis*. Tech. rep. Department for Business Innovation and Skills, Feb. 2016.
- [43] Samira Keivanpour and Daoud Ait Kadi. *Modelling end of life phase of the complex products: the case of end of life aircraft*. International Journal of Production Research. Department of Mechanical Engineering, Université Laval, Quebec, Canada, Mar. 2017.
- [44] Samira Keivanpour, Daoud Ait Kadi, and Christian Mascle. *End of life aircrafts recovery and green supply chain (a conceptual framework for addressing opportunities and challenges)*. Tech. rep. Department of Mechanical Engineering, Université Laval, Quebec, Canada, and Department of Mechanical Engineering, École Polytechnique de Montréal, Montreal, Canada, July 2015.
- [45] Philip Matthew Kenul et al. *Sensing Hazards with Operational Unmanned Technology : cost study of Global Hawk unmanned aircraft system operations for high impact weather observations, final report*. Technical Memorandum. 2018. URL: <https://repository.library.noaa.gov/view/noaa/17824>.
- [46] Kiran. "Reliability Engineering". In: *Elsevier eBooks*. Jan. 2017, pp. 391–404. DOI: 10.1016/b978-0-12-811035-5.00027-1. URL: <https://doi.org/10.1016/b978-0-12-811035-5.00027-1>.
- [47] David J. Lee et al. "Aviation and global climate change in the 21st century". In: *Atmospheric Environment* 43.22-23 (July 2009), pp. 3520–3537. DOI: 10.1016/j.atmosenv.2009.04.024. URL: <https://doi.org/10.1016/j.atmosenv.2009.04.024>.
- [48] D.Scholz M.Nita. "Estimating the Oswald factor from basic geometrical parameters". In: (2012).
- [49] Liam Megill. "Analysis of Climate Metrics for Aviation". en. MA thesis. Delft University of Technology, 2022.
- [50] T.H.G. Megson. "Chapter 17 - Shear of beams". In: *Aircraft Structures for Engineering Students (Sixth Edition)*. Ed. by T.H.G. Megson. Sixth Edition. Butterworth-Heinemann, 2017, pp. 537–568. ISBN: 978-0-08-100914-7. DOI: <https://doi.org/10.1016/B978-0-08-100914-7.00017-7>. URL: <https://www.sciencedirect.com/science/article/pii/B9780081009147000177>.
- [51] T.H.G. Megson. "Chapter 18 - Torsion of beams". In: *Aircraft Structures for Engineering Students (Sixth Edition)*. Ed. by T.H.G. Megson. Sixth Edition. Butterworth-Heinemann, 2017, pp. 569–592. ISBN: 978-0-08-100914-7. DOI: <https://doi.org/10.1016/B978-0-08-100914-7.00018-9>. URL: <https://www.sciencedirect.com/science/article/pii/B9780081009147000189>.
- [52] T.H.G. Megson. "Chapter 20 - Structural idealization". In: *Aircraft Structures for Engineering Students (Sixth Edition)*. Ed. by T.H.G. Megson. Sixth Edition. Butterworth-Heinemann, 2017, pp. 605–627. ISBN: 978-0-08-100914-7. DOI: <https://doi.org/10.1016/B978-0-08-100914-7.00020-7>. URL: <https://www.sciencedirect.com/science/article/pii/B9780081009147000207>.
- [53] Ir. J.A. (Joris) Melkert. *Propulsion and Power*. Lecture. Feb. 2022.
- [54] Omar Memon. "How CFM LEAP Engines Enhance The Performance Of The Boeing 737 MAX". en. In: *Simple Flying* (Jan. 2023). URL: https://simpleflying.com/cfm-leap-engines-enhance-performace-boeing-737-max/?newsletter_popup=1.
- [55] Amir H Naghshineh-Pour. "Structural optimization and design of a strut-braced wing aircraft". PhD thesis. Virginia Tech, 1998.
- [56] NASA. *WB57 Experimenter's handbook: Aircraft Operations Division*. July 2017.

- [57] M. Niță and D. Scholz. *Estimating the Oswald Factor from Basic Aircraft Geometrical Parameters*. Deutsche Gesellschaft für Luft- und Raumfahrt - Lilienthal-Oberth e.V., 2012. URL: <https://books.google.nl/books?id=229fuwEACAAJ>.
- [58] Congressional Budget Office. *Usage Patterns and Costs of Unmanned Aerial Systems*. Tech. rep. 57090-UAS. June 2021. URL: <https://www.cbo.gov/system/files/2021-06/57090-UAS.pdf>.
- [59] PWC PW500. en. Aug. 2020. URL: https://customer.janes.com/display/JAE_0487-JAE_.
- [60] B.N. Pamadi. *Performance, Stability, Dynamics, and Control of Airplanes*. AIAA Education Series. American Institute of Aeronautics & Astronautics, 2004. ISBN: 978-1-60086-099-7. URL: <https://books.google.nl/books?id=vR0cxJj4igQC>.
- [61] J.A. Melkert R. Vos. *Aerospace Design and Systems Engineering Elements I*. 2020.
- [62] Daniel P. Raymer. *Aircraft Design: A Conceptual Approach*. Airplane Design. American Institute of Aeronautics and Astronautics, 1989.
- [63] Daniel P. Raymer. *Aircraft Design: A Conceptual Approach*. Airplane Design. American Institute of Aeronautics and Astronautics, 1989.
- [64] M. Reinhard et al. *A New European Stratospheric Research Aircraft*. 2023.
- [65] Júnior Sousa Ribeiro and Jefferson de Oliveira Gomes. “Proposed framework for End-Of-Life aircraft recycling”. In: *12th Global Conference on Sustainable Manufacturing*. Ed. by Praça Marechal Eduardo Gomes Instituto Tecnológico de Aeronautica. Elsevier, 2015.
- [66] J. Roskam. *Airplane Design*. Airplane Design pt. 3. DARcorporation, 1985. ISBN: 978-1-884885-56-3. URL: https://books.google.nl/books?id=%5C_FBLtC3qpr4C.
- [67] J. Roskam. *Airplane Design*. Airplane Design pt. 5. DARcorporation, 1986. ISBN: 978-1-884885-56-3. URL: https://books.google.nl/books?id=%5C_FBLtC3qpr4C.
- [68] J. Roskam. *Airplane Design VI: Preliminary Calculation of Aerodynamic, Thrust and Power Characteristics*. v. 1. DARcorporation, 1987. ISBN: 978-1-884885-52-5. URL: <https://books.google.nl/books?id=0udGAQAIAAJ>.
- [69] Jan Roskam. *Airplane Design: Airplane cost estimation: design, development, manufacturing and operating*. Vol. 8. Airplane Design. Roskam Aviation and Engineering Corporation, 19909.
- [70] Jean Rouchon. “Certification of large airplane composite structures”. In: *ICAS Congress Proceedings*. Vol. 2. 1990, pp. 1439–1447.
- [71] GJJ Ruijgrok. *Elements of airplane performance*. English. 2e editie onderwijsboek met ‘minor adjustments’. VSSD, 2009. ISBN: 978-90-6562-203-7.
- [72] Mohammad Sadraey. *Aircraft Design: a system engineering approach*. John Wiley and Sons, 2013.
- [73] Andrea Saltelli and Paola Annoni. “How to avoid a perfunctory sensitivity analysis”. In: *Environmental Modelling Software* 25.12 (2010), pp. 1508–1517. ISSN: 1364-8152. DOI: <https://doi.org/10.1016/j.envsoft.2010.04.012>. URL: <https://www.sciencedirect.com/science/article/pii/S1364815210001180>.
- [74] William Saric and Helen Reed. “Stability, Transition, and Control of Three-Dimensional Boundary Layers on Swept Wings”. en. In: *IUTAM Symposium on One Hundred Years of Boundary Layer Research*. Ed. by G. E. A. Meier, K. R. Sreenivasan, and H.-J. Heinemann. Solid mechanics and its applications. Dordrecht: Springer Netherlands, 2006, pp. 177–188. ISBN: 978-1-4020-4150-1. DOI: 10.1007/978-1-4020-4150-1_17.
- [75] William S. Saric, Helen L. Reed, and Edward B. White. “Stability and Transition of Three-Dimensional Boundary Layers”. In: *Annual Review of Fluid Mechanics* 35.1 (2003). eprint: <https://doi.org/10.1146/annurev.fluid.35.101101.161045>, pp. 413–440. DOI: 10.1146/annurev.fluid.35.101101.161045. URL: <https://doi.org/10.1146/annurev.fluid.35.101101.161045> (visited on 06/21/2023).
- [76] Cornelius Schiller. *Whitebook ‘Stratospheric Aircraft in Europe’*. European Commission. Aug. 2011.

- [77] Clare E. Singer et al. "Intercomparison of upper tropospheric and lower stratospheric water vapor measurements over the Asian Summer Monsoon during the StratoClim campaign". In: *Atmospheric Measurement Techniques* 15 (16 Aug. 2022), pp. 4767–4783. DOI: 10.5194/amt-15-4767-2022.
- [78] *Standard Specification for Aeroelasticity Requirements*. ASTM International, May 2021. DOI: 10.1520/F3093_F3093M-21. URL: www.astm.org/.
- [79] Phillip L. Swagel. *Usage Patterns and Costs of Unmanned Aerial Systems*. June 2021. URL: <https://www.cbo.gov/publication/57260>.
- [80] Eric Ting et al. "Aerodynamic Analysis of the Truss-Braced Wing Aircraft Using Vortex-Lattice Superposition Approach". en. In: *32nd AIAA Applied Aerodynamics Conference*. Atlanta, GA: American Institute of Aeronautics and Astronautics, June 2014. ISBN: 978-1-62410-288-2. DOI: 10.2514/6.2014-2597. URL: <https://arc.aiaa.org/doi/10.2514/6.2014-2597> (visited on 06/21/2023).
- [81] Owen B. Toon et al. "Planning, implementation, and first results of the Tropical Composition, Cloud and Climate Coupling Experiment (TC4)". In: *Journal of Geophysical Research Atmospheres* 115 (13 2010). ISSN: 01480227. DOI: 10.1029/2009JD013073.
- [82] Egbert Torenbeek. *Synthesis of subsonic Airplane Design*. Delft University Press, 1982.
- [83] *TYPE-CERTIFICATE DATA SHEET EASA.IM.E.048 for PW530 Series Engines*. EASA, 2020.
- [84] Roelof Vos and Saeed Farokhi. *Introduction to Transonic Aerodynamics*. Springer Netherlands, 2015. ISBN: 978-94-017-9746-7. DOI: 10.1007/978-94-017-9747-4.
- [85] Gary A. Wick et al. "The NCAR-NOAA Global Hawk dropsonde system". In: *Journal of Atmospheric and Oceanic Technology* 35 (8 Aug. 2018), pp. 1585–1604. ISSN: 15200426. DOI: 10.1175/JTECH-D-17-0225.1.
- [86] Robert A. Witik et al. *Carbon fibre reinforced composite waste: An environmental assessment of recycling, energy recovery and landfilling*. Tech. rep. Elsevier: Laboratoire de Technologie des Composites et Polymères, 2013.

A

Appendix A

<table border="0" style="width: 100%; border-collapse: collapse;"> <thead> <tr> <th style="text-align: left;">Station</th> <th style="text-align: right;">W</th> <th style="text-align: right;">T</th> <th style="text-align: right;">P</th> <th style="text-align: right;">WRstd</th> </tr> <tr> <th style="text-align: left;">amb</th> <th style="text-align: right;">kg/s</th> <th style="text-align: right;">K</th> <th style="text-align: right;">kPa</th> <th style="text-align: right;">kg/s</th> </tr> </thead> <tbody> <tr><td>1</td><td style="text-align: right;">55.122</td><td style="text-align: right;">288.15</td><td style="text-align: right;">101.325</td><td></td></tr> <tr><td>2</td><td style="text-align: right;">55.122</td><td style="text-align: right;">288.15</td><td style="text-align: right;">101.325</td><td></td></tr> <tr><td>13</td><td style="text-align: right;">39.811</td><td style="text-align: right;">360.83</td><td style="text-align: right;">206.541</td><td style="text-align: right;">55.436</td></tr> <tr><td>21</td><td style="text-align: right;">15.312</td><td style="text-align: right;">364.38</td><td style="text-align: right;">211.579</td><td style="text-align: right;">21.855</td></tr> <tr><td>25</td><td style="text-align: right;">15.312</td><td style="text-align: right;">364.38</td><td style="text-align: right;">209.463</td><td style="text-align: right;">8.246</td></tr> <tr><td>3</td><td style="text-align: right;">14.852</td><td style="text-align: right;">737.47</td><td style="text-align: right;">2094.630</td><td style="text-align: right;">8.329</td></tr> <tr><td>31</td><td style="text-align: right;">13.015</td><td style="text-align: right;">737.47</td><td style="text-align: right;">2094.630</td><td style="text-align: right;">1.149</td></tr> <tr><td>4</td><td style="text-align: right;">13.216</td><td style="text-align: right;">1325.00</td><td style="text-align: right;">2052.738</td><td></td></tr> <tr><td>405</td><td style="text-align: right;">13.829</td><td style="text-align: right;">1300.73</td><td style="text-align: right;">2052.738</td><td style="text-align: right;">1.399</td></tr> <tr><td>41</td><td style="text-align: right;">14.135</td><td style="text-align: right;">1289.24</td><td style="text-align: right;">2052.738</td><td></td></tr> <tr><td>43</td><td style="text-align: right;">14.135</td><td style="text-align: right;">931.77</td><td style="text-align: right;">430.420</td><td style="text-align: right;">1.476</td></tr> <tr><td>44</td><td style="text-align: right;">14.901</td><td style="text-align: right;">922.22</td><td style="text-align: right;">430.420</td><td></td></tr> <tr><td>45</td><td style="text-align: right;">14.901</td><td style="text-align: right;">922.22</td><td style="text-align: right;">421.812</td><td style="text-align: right;">6.403</td></tr> <tr><td>49</td><td style="text-align: right;">14.901</td><td style="text-align: right;">676.98</td><td style="text-align: right;">104.023</td><td></td></tr> <tr><td>5</td><td style="text-align: right;">15.360</td><td style="text-align: right;">674.48</td><td style="text-align: right;">104.023</td><td style="text-align: right;">22.890</td></tr> <tr><td>8</td><td style="text-align: right;">15.360</td><td style="text-align: right;">674.48</td><td style="text-align: right;">101.942</td><td style="text-align: right;">23.358</td></tr> <tr><td>18</td><td style="text-align: right;">39.811</td><td style="text-align: right;">360.83</td><td style="text-align: right;">202.410</td><td style="text-align: right;">22.301</td></tr> <tr><td>Bleed</td><td style="text-align: right;">0.153</td><td style="text-align: right;">737.47</td><td style="text-align: right;">2094.621</td><td></td></tr> </tbody> </table>	Station	W	T	P	WRstd	amb	kg/s	K	kPa	kg/s	1	55.122	288.15	101.325		2	55.122	288.15	101.325		13	39.811	360.83	206.541	55.436	21	15.312	364.38	211.579	21.855	25	15.312	364.38	209.463	8.246	3	14.852	737.47	2094.630	8.329	31	13.015	737.47	2094.630	1.149	4	13.216	1325.00	2052.738		405	13.829	1300.73	2052.738	1.399	41	14.135	1289.24	2052.738		43	14.135	931.77	430.420	1.476	44	14.901	922.22	430.420		45	14.901	922.22	421.812	6.403	49	14.901	676.98	104.023		5	15.360	674.48	104.023	22.890	8	15.360	674.48	101.942	23.358	18	39.811	360.83	202.410	22.301	Bleed	0.153	737.47	2094.621		<table border="0" style="width: 100%; border-collapse: collapse;"> <tbody> <tr><td>FN</td><td>=</td><td>15.12 kN</td></tr> <tr><td>TSFC</td><td>=</td><td>13.3184 g/(kN*s)</td></tr> <tr><td>WF</td><td>=</td><td>0.20137 kg/s</td></tr> <tr><td>BPR</td><td>=</td><td>2.6000</td></tr> <tr><td>s NOx</td><td>=</td><td>0.6204</td></tr> <tr><td>Core Eff</td><td>=</td><td>0.3676</td></tr> <tr><td>Prop Eff</td><td>=</td><td>0.0000</td></tr> <tr><td>P3/P2</td><td>=</td><td>20.79</td></tr> <tr><td>P2/P1</td><td>=</td><td>0.9943</td></tr> <tr><td>NGV Out. 2 Stage HPT</td><td>=</td><td>0.9800</td></tr> <tr><td>P16/P13</td><td>=</td><td>0.9800</td></tr> <tr><td>P25/P21</td><td>=</td><td>0.9900</td></tr> <tr><td>P45/P44</td><td>=</td><td>0.9800</td></tr> <tr><td>P6/P5</td><td>=</td><td>0.9800</td></tr> <tr><td>A8</td><td>=</td><td>0.64931 m²</td></tr> <tr><td>A18</td><td>=</td><td>0.09474 m²</td></tr> <tr><td>P8/Pamb</td><td>=</td><td>1.00609</td></tr> <tr><td>P18/Pamb</td><td>=</td><td>1.99764</td></tr> <tr><td>WBld/W25</td><td>=</td><td>0.01000</td></tr> <tr><td>CD8</td><td>=</td><td>0.93061</td></tr> <tr><td>CD18</td><td>=</td><td>0.97600</td></tr> <tr><td>XM8</td><td>=</td><td>0.09461</td></tr> <tr><td>XM18</td><td>=</td><td>1.00000</td></tr> <tr><td>V18/v8_id</td><td>=</td><td>7.43962</td></tr> <tr><td>Loading</td><td>=</td><td>100.00 %</td></tr> <tr><td>e444 th</td><td>=</td><td>0.85484</td></tr> <tr><td>Pwx</td><td>=</td><td>50.00 kw</td></tr> <tr><td>WCHN/W25</td><td>=</td><td>0.06000</td></tr> <tr><td>WCHR/W25</td><td>=</td><td>0.05000</td></tr> <tr><td>WLC1/W25</td><td>=</td><td>0.03000</td></tr> </tbody> </table>	FN	=	15.12 kN	TSFC	=	13.3184 g/(kN*s)	WF	=	0.20137 kg/s	BPR	=	2.6000	s NOx	=	0.6204	Core Eff	=	0.3676	Prop Eff	=	0.0000	P3/P2	=	20.79	P2/P1	=	0.9943	NGV Out. 2 Stage HPT	=	0.9800	P16/P13	=	0.9800	P25/P21	=	0.9900	P45/P44	=	0.9800	P6/P5	=	0.9800	A8	=	0.64931 m ²	A18	=	0.09474 m ²	P8/Pamb	=	1.00609	P18/Pamb	=	1.99764	WBld/W25	=	0.01000	CD8	=	0.93061	CD18	=	0.97600	XM8	=	0.09461	XM18	=	1.00000	V18/v8_id	=	7.43962	Loading	=	100.00 %	e444 th	=	0.85484	Pwx	=	50.00 kw	WCHN/W25	=	0.06000	WCHR/W25	=	0.05000	WLC1/W25	=	0.03000	<table border="0" style="width: 100%; border-collapse: collapse;"> <thead> <tr> <th style="text-align: left;">Station</th> <th style="text-align: right;">W</th> <th style="text-align: right;">T</th> <th style="text-align: right;">P</th> <th style="text-align: right;">WRstd</th> </tr> <tr> <th style="text-align: left;">amb</th> <th style="text-align: right;">kg/s</th> <th style="text-align: right;">K</th> <th style="text-align: right;">kPa</th> <th style="text-align: right;">kg/s</th> </tr> </thead> <tbody> <tr><td>1</td><td style="text-align: right;">4.203</td><td style="text-align: right;">216.65</td><td style="text-align: right;">5.060</td><td></td></tr> <tr><td>2</td><td style="text-align: right;">4.203</td><td style="text-align: right;">237.93</td><td style="text-align: right;">7.020</td><td></td></tr> <tr><td>13</td><td style="text-align: right;">3.035</td><td style="text-align: right;">298.20</td><td style="text-align: right;">14.310</td><td style="text-align: right;">55.436</td></tr> <tr><td>21</td><td style="text-align: right;">1.167</td><td style="text-align: right;">301.14</td><td style="text-align: right;">14.659</td><td style="text-align: right;">21.865</td></tr> <tr><td>25</td><td style="text-align: right;">1.167</td><td style="text-align: right;">301.14</td><td style="text-align: right;">14.512</td><td style="text-align: right;">8.250</td></tr> <tr><td>3</td><td style="text-align: right;">1.132</td><td style="text-align: right;">615.95</td><td style="text-align: right;">145.122</td><td style="text-align: right;">8.333</td></tr> <tr><td>31</td><td style="text-align: right;">0.992</td><td style="text-align: right;">615.95</td><td style="text-align: right;">145.122</td><td style="text-align: right;">1.156</td></tr> <tr><td>4</td><td style="text-align: right;">1.011</td><td style="text-align: right;">1325.00</td><td style="text-align: right;">142.220</td><td></td></tr> <tr><td>405</td><td style="text-align: right;">1.057</td><td style="text-align: right;">1296.21</td><td style="text-align: right;">142.220</td><td style="text-align: right;">1.544</td></tr> <tr><td>41</td><td style="text-align: right;">1.081</td><td style="text-align: right;">1282.59</td><td style="text-align: right;">142.220</td><td></td></tr> <tr><td>43</td><td style="text-align: right;">1.081</td><td style="text-align: right;">951.78</td><td style="text-align: right;">33.700</td><td style="text-align: right;">1.624</td></tr> <tr><td>44</td><td style="text-align: right;">1.139</td><td style="text-align: right;">935.55</td><td style="text-align: right;">33.700</td><td></td></tr> <tr><td>45</td><td style="text-align: right;">1.139</td><td style="text-align: right;">935.55</td><td style="text-align: right;">33.026</td><td style="text-align: right;">6.297</td></tr> <tr><td>49</td><td style="text-align: right;">1.139</td><td style="text-align: right;">735.91</td><td style="text-align: right;">11.064</td><td></td></tr> <tr><td>5</td><td style="text-align: right;">1.174</td><td style="text-align: right;">729.01</td><td style="text-align: right;">11.064</td><td style="text-align: right;">17.102</td></tr> <tr><td>8</td><td style="text-align: right;">1.174</td><td style="text-align: right;">729.01</td><td style="text-align: right;">10.843</td><td style="text-align: right;">17.451</td></tr> <tr><td>18</td><td style="text-align: right;">3.035</td><td style="text-align: right;">298.20</td><td style="text-align: right;">14.024</td><td style="text-align: right;">22.311</td></tr> <tr><td>Bleed</td><td style="text-align: right;">0.012</td><td style="text-align: right;">615.95</td><td style="text-align: right;">145.122</td><td></td></tr> </tbody> </table>	Station	W	T	P	WRstd	amb	kg/s	K	kPa	kg/s	1	4.203	216.65	5.060		2	4.203	237.93	7.020		13	3.035	298.20	14.310	55.436	21	1.167	301.14	14.659	21.865	25	1.167	301.14	14.512	8.250	3	1.132	615.95	145.122	8.333	31	0.992	615.95	145.122	1.156	4	1.011	1325.00	142.220		405	1.057	1296.21	142.220	1.544	41	1.081	1282.59	142.220		43	1.081	951.78	33.700	1.624	44	1.139	935.55	33.700		45	1.139	935.55	33.026	6.297	49	1.139	735.91	11.064		5	1.174	729.01	11.064	17.102	8	1.174	729.01	10.843	17.451	18	3.035	298.20	14.024	22.311	Bleed	0.012	615.95	145.122		<table border="0" style="width: 100%; border-collapse: collapse;"> <tbody> <tr><td>FN</td><td>=</td><td>0.95 kN</td></tr> <tr><td>TSFC</td><td>=</td><td>19.3539 g/(kN*s)</td></tr> <tr><td>WF</td><td>=</td><td>0.01830 kg/s</td></tr> <tr><td>BPR</td><td>=</td><td>2.6000</td></tr> <tr><td>s NOx</td><td>=</td><td>0.1141</td></tr> <tr><td>Core Eff</td><td>=</td><td>0.4154</td></tr> <tr><td>Prop Eff</td><td>=</td><td>0.6482</td></tr> <tr><td>P3/P2</td><td>=</td><td>20.79</td></tr> <tr><td>P2/P1</td><td>=</td><td>0.9943</td></tr> <tr><td>NGV Out. 2 Stage HPT</td><td>=</td><td>0.9800</td></tr> <tr><td>P16/P13</td><td>=</td><td>0.9800</td></tr> <tr><td>P25/P21</td><td>=</td><td>0.9900</td></tr> <tr><td>P45/P44</td><td>=</td><td>0.9800</td></tr> <tr><td>P6/P5</td><td>=</td><td>0.9800</td></tr> <tr><td>A8</td><td>=</td><td>0.07460 m²</td></tr> <tr><td>A18</td><td>=</td><td>0.09474 m²</td></tr> <tr><td>P8/Pamb</td><td>=</td><td>2.14292</td></tr> <tr><td>P18/Pamb</td><td>=</td><td>2.77158</td></tr> <tr><td>WBld/W25</td><td>=</td><td>0.01000</td></tr> <tr><td>CD8</td><td>=</td><td>0.98000</td></tr> <tr><td>CD18</td><td>=</td><td>0.97600</td></tr> <tr><td>XM8</td><td>=</td><td>1.00000</td></tr> <tr><td>XM18</td><td>=</td><td>1.00000</td></tr> <tr><td>V18/v8_id</td><td>=</td><td>0.72343</td></tr> <tr><td>Loading</td><td>=</td><td>100.00 %</td></tr> <tr><td>e444 th</td><td>=</td><td>0.85975</td></tr> <tr><td>Pwx</td><td>=</td><td>50.00 kw</td></tr> <tr><td>WCHN/W25</td><td>=</td><td>0.06000</td></tr> <tr><td>WCHR/W25</td><td>=</td><td>0.05000</td></tr> <tr><td>WLC1/W25</td><td>=</td><td>0.03000</td></tr> </tbody> </table>	FN	=	0.95 kN	TSFC	=	19.3539 g/(kN*s)	WF	=	0.01830 kg/s	BPR	=	2.6000	s NOx	=	0.1141	Core Eff	=	0.4154	Prop Eff	=	0.6482	P3/P2	=	20.79	P2/P1	=	0.9943	NGV Out. 2 Stage HPT	=	0.9800	P16/P13	=	0.9800	P25/P21	=	0.9900	P45/P44	=	0.9800	P6/P5	=	0.9800	A8	=	0.07460 m ²	A18	=	0.09474 m ²	P8/Pamb	=	2.14292	P18/Pamb	=	2.77158	WBld/W25	=	0.01000	CD8	=	0.98000	CD18	=	0.97600	XM8	=	1.00000	XM18	=	1.00000	V18/v8_id	=	0.72343	Loading	=	100.00 %	e444 th	=	0.85975	Pwx	=	50.00 kw	WCHN/W25	=	0.06000	WCHR/W25	=	0.05000	WLC1/W25	=	0.03000
Station	W	T	P	WRstd																																																																																																																																																																																																																																																																																																																																																																																											
amb	kg/s	K	kPa	kg/s																																																																																																																																																																																																																																																																																																																																																																																											
1	55.122	288.15	101.325																																																																																																																																																																																																																																																																																																																																																																																												
2	55.122	288.15	101.325																																																																																																																																																																																																																																																																																																																																																																																												
13	39.811	360.83	206.541	55.436																																																																																																																																																																																																																																																																																																																																																																																											
21	15.312	364.38	211.579	21.855																																																																																																																																																																																																																																																																																																																																																																																											
25	15.312	364.38	209.463	8.246																																																																																																																																																																																																																																																																																																																																																																																											
3	14.852	737.47	2094.630	8.329																																																																																																																																																																																																																																																																																																																																																																																											
31	13.015	737.47	2094.630	1.149																																																																																																																																																																																																																																																																																																																																																																																											
4	13.216	1325.00	2052.738																																																																																																																																																																																																																																																																																																																																																																																												
405	13.829	1300.73	2052.738	1.399																																																																																																																																																																																																																																																																																																																																																																																											
41	14.135	1289.24	2052.738																																																																																																																																																																																																																																																																																																																																																																																												
43	14.135	931.77	430.420	1.476																																																																																																																																																																																																																																																																																																																																																																																											
44	14.901	922.22	430.420																																																																																																																																																																																																																																																																																																																																																																																												
45	14.901	922.22	421.812	6.403																																																																																																																																																																																																																																																																																																																																																																																											
49	14.901	676.98	104.023																																																																																																																																																																																																																																																																																																																																																																																												
5	15.360	674.48	104.023	22.890																																																																																																																																																																																																																																																																																																																																																																																											
8	15.360	674.48	101.942	23.358																																																																																																																																																																																																																																																																																																																																																																																											
18	39.811	360.83	202.410	22.301																																																																																																																																																																																																																																																																																																																																																																																											
Bleed	0.153	737.47	2094.621																																																																																																																																																																																																																																																																																																																																																																																												
FN	=	15.12 kN																																																																																																																																																																																																																																																																																																																																																																																													
TSFC	=	13.3184 g/(kN*s)																																																																																																																																																																																																																																																																																																																																																																																													
WF	=	0.20137 kg/s																																																																																																																																																																																																																																																																																																																																																																																													
BPR	=	2.6000																																																																																																																																																																																																																																																																																																																																																																																													
s NOx	=	0.6204																																																																																																																																																																																																																																																																																																																																																																																													
Core Eff	=	0.3676																																																																																																																																																																																																																																																																																																																																																																																													
Prop Eff	=	0.0000																																																																																																																																																																																																																																																																																																																																																																																													
P3/P2	=	20.79																																																																																																																																																																																																																																																																																																																																																																																													
P2/P1	=	0.9943																																																																																																																																																																																																																																																																																																																																																																																													
NGV Out. 2 Stage HPT	=	0.9800																																																																																																																																																																																																																																																																																																																																																																																													
P16/P13	=	0.9800																																																																																																																																																																																																																																																																																																																																																																																													
P25/P21	=	0.9900																																																																																																																																																																																																																																																																																																																																																																																													
P45/P44	=	0.9800																																																																																																																																																																																																																																																																																																																																																																																													
P6/P5	=	0.9800																																																																																																																																																																																																																																																																																																																																																																																													
A8	=	0.64931 m ²																																																																																																																																																																																																																																																																																																																																																																																													
A18	=	0.09474 m ²																																																																																																																																																																																																																																																																																																																																																																																													
P8/Pamb	=	1.00609																																																																																																																																																																																																																																																																																																																																																																																													
P18/Pamb	=	1.99764																																																																																																																																																																																																																																																																																																																																																																																													
WBld/W25	=	0.01000																																																																																																																																																																																																																																																																																																																																																																																													
CD8	=	0.93061																																																																																																																																																																																																																																																																																																																																																																																													
CD18	=	0.97600																																																																																																																																																																																																																																																																																																																																																																																													
XM8	=	0.09461																																																																																																																																																																																																																																																																																																																																																																																													
XM18	=	1.00000																																																																																																																																																																																																																																																																																																																																																																																													
V18/v8_id	=	7.43962																																																																																																																																																																																																																																																																																																																																																																																													
Loading	=	100.00 %																																																																																																																																																																																																																																																																																																																																																																																													
e444 th	=	0.85484																																																																																																																																																																																																																																																																																																																																																																																													
Pwx	=	50.00 kw																																																																																																																																																																																																																																																																																																																																																																																													
WCHN/W25	=	0.06000																																																																																																																																																																																																																																																																																																																																																																																													
WCHR/W25	=	0.05000																																																																																																																																																																																																																																																																																																																																																																																													
WLC1/W25	=	0.03000																																																																																																																																																																																																																																																																																																																																																																																													
Station	W	T	P	WRstd																																																																																																																																																																																																																																																																																																																																																																																											
amb	kg/s	K	kPa	kg/s																																																																																																																																																																																																																																																																																																																																																																																											
1	4.203	216.65	5.060																																																																																																																																																																																																																																																																																																																																																																																												
2	4.203	237.93	7.020																																																																																																																																																																																																																																																																																																																																																																																												
13	3.035	298.20	14.310	55.436																																																																																																																																																																																																																																																																																																																																																																																											
21	1.167	301.14	14.659	21.865																																																																																																																																																																																																																																																																																																																																																																																											
25	1.167	301.14	14.512	8.250																																																																																																																																																																																																																																																																																																																																																																																											
3	1.132	615.95	145.122	8.333																																																																																																																																																																																																																																																																																																																																																																																											
31	0.992	615.95	145.122	1.156																																																																																																																																																																																																																																																																																																																																																																																											
4	1.011	1325.00	142.220																																																																																																																																																																																																																																																																																																																																																																																												
405	1.057	1296.21	142.220	1.544																																																																																																																																																																																																																																																																																																																																																																																											
41	1.081	1282.59	142.220																																																																																																																																																																																																																																																																																																																																																																																												
43	1.081	951.78	33.700	1.624																																																																																																																																																																																																																																																																																																																																																																																											
44	1.139	935.55	33.700																																																																																																																																																																																																																																																																																																																																																																																												
45	1.139	935.55	33.026	6.297																																																																																																																																																																																																																																																																																																																																																																																											
49	1.139	735.91	11.064																																																																																																																																																																																																																																																																																																																																																																																												
5	1.174	729.01	11.064	17.102																																																																																																																																																																																																																																																																																																																																																																																											
8	1.174	729.01	10.843	17.451																																																																																																																																																																																																																																																																																																																																																																																											
18	3.035	298.20	14.024	22.311																																																																																																																																																																																																																																																																																																																																																																																											
Bleed	0.012	615.95	145.122																																																																																																																																																																																																																																																																																																																																																																																												
FN	=	0.95 kN																																																																																																																																																																																																																																																																																																																																																																																													
TSFC	=	19.3539 g/(kN*s)																																																																																																																																																																																																																																																																																																																																																																																													
WF	=	0.01830 kg/s																																																																																																																																																																																																																																																																																																																																																																																													
BPR	=	2.6000																																																																																																																																																																																																																																																																																																																																																																																													
s NOx	=	0.1141																																																																																																																																																																																																																																																																																																																																																																																													
Core Eff	=	0.4154																																																																																																																																																																																																																																																																																																																																																																																													
Prop Eff	=	0.6482																																																																																																																																																																																																																																																																																																																																																																																													
P3/P2	=	20.79																																																																																																																																																																																																																																																																																																																																																																																													
P2/P1	=	0.9943																																																																																																																																																																																																																																																																																																																																																																																													
NGV Out. 2 Stage HPT	=	0.9800																																																																																																																																																																																																																																																																																																																																																																																													
P16/P13	=	0.9800																																																																																																																																																																																																																																																																																																																																																																																													
P25/P21	=	0.9900																																																																																																																																																																																																																																																																																																																																																																																													
P45/P44	=	0.9800																																																																																																																																																																																																																																																																																																																																																																																													
P6/P5	=	0.9800																																																																																																																																																																																																																																																																																																																																																																																													
A8	=	0.07460 m ²																																																																																																																																																																																																																																																																																																																																																																																													
A18	=	0.09474 m ²																																																																																																																																																																																																																																																																																																																																																																																													
P8/Pamb	=	2.14292																																																																																																																																																																																																																																																																																																																																																																																													
P18/Pamb	=	2.77158																																																																																																																																																																																																																																																																																																																																																																																													
WBld/W25	=	0.01000																																																																																																																																																																																																																																																																																																																																																																																													
CD8	=	0.98000																																																																																																																																																																																																																																																																																																																																																																																													
CD18	=	0.97600																																																																																																																																																																																																																																																																																																																																																																																													
XM8	=	1.00000																																																																																																																																																																																																																																																																																																																																																																																													
XM18	=	1.00000																																																																																																																																																																																																																																																																																																																																																																																													
V18/v8_id	=	0.72343																																																																																																																																																																																																																																																																																																																																																																																													
Loading	=	100.00 %																																																																																																																																																																																																																																																																																																																																																																																													
e444 th	=	0.85975																																																																																																																																																																																																																																																																																																																																																																																													
Pwx	=	50.00 kw																																																																																																																																																																																																																																																																																																																																																																																													
WCHN/W25	=	0.06000																																																																																																																																																																																																																																																																																																																																																																																													
WCHR/W25	=	0.05000																																																																																																																																																																																																																																																																																																																																																																																													
WLC1/W25	=	0.03000																																																																																																																																																																																																																																																																																																																																																																																													
<table border="0" style="width: 100%; border-collapse: collapse;"> <tbody> <tr><td>Efficiencies:</td><td>isent</td><td>polytr</td><td>RNI</td><td>P/P</td></tr> <tr><td>Outer LPC</td><td>0.9000</td><td>0.9095</td><td>0.994</td><td>2.050</td></tr> <tr><td>Inner LPC</td><td>0.8900</td><td>0.9008</td><td>0.994</td><td>2.100</td></tr> <tr><td>HP Compressor</td><td>0.8700</td><td>0.9032</td><td>1.563</td><td>10.000</td></tr> <tr><td>Burner</td><td>0.9995</td><td></td><td></td><td>0.980</td></tr> <tr><td>HP Turbine</td><td>0.8800</td><td>0.8577</td><td>3.508</td><td>4.769</td></tr> <tr><td>LP Turbine</td><td>0.8810</td><td>0.8601</td><td>1.058</td><td>4.055</td></tr> <tr><td>HP Spool mech Eff</td><td>0.9900</td><td>Nom Spd</td><td>25726 rpm</td><td></td></tr> <tr><td>LP Spool mech Eff</td><td>1.0000</td><td>Nom Spd</td><td>15172 rpm</td><td></td></tr> <tr><td>hum [%]</td><td>war0</td><td>FHW</td><td>Fuel</td><td></td></tr> <tr><td>0.0</td><td>0.00000</td><td>46.200</td><td>Generic</td><td></td></tr> </tbody> </table>	Efficiencies:	isent	polytr	RNI	P/P	Outer LPC	0.9000	0.9095	0.994	2.050	Inner LPC	0.8900	0.9008	0.994	2.100	HP Compressor	0.8700	0.9032	1.563	10.000	Burner	0.9995			0.980	HP Turbine	0.8800	0.8577	3.508	4.769	LP Turbine	0.8810	0.8601	1.058	4.055	HP Spool mech Eff	0.9900	Nom Spd	25726 rpm		LP Spool mech Eff	1.0000	Nom Spd	15172 rpm		hum [%]	war0	FHW	Fuel		0.0	0.00000	46.200	Generic		<table border="0" style="width: 100%; border-collapse: collapse;"> <tbody> <tr><td>Efficiencies:</td><td>isent</td><td>polytr</td><td>RNI</td><td>P/P</td></tr> <tr><td>Outer LPC</td><td>0.9000</td><td>0.9096</td><td>0.086</td><td>2.050</td></tr> <tr><td>Inner LPC</td><td>0.8900</td><td>0.9009</td><td>0.086</td><td>2.100</td></tr> <tr><td>HP Compressor</td><td>0.8700</td><td>0.9038</td><td>0.136</td><td>10.000</td></tr> <tr><td>Burner</td><td>0.9995</td><td></td><td></td><td>0.980</td></tr> <tr><td>HP Turbine</td><td>0.8800</td><td>0.8598</td><td>0.244</td><td>4.220</td></tr> <tr><td>LP Turbine</td><td>0.8810</td><td>0.8653</td><td>0.082</td><td>2.985</td></tr> <tr><td>HP Spool mech Eff</td><td>0.9900</td><td>Nom Spd</td><td>25729 rpm</td><td></td></tr> <tr><td>LP Spool mech Eff</td><td>1.0000</td><td>Nom Spd</td><td>15173 rpm</td><td></td></tr> <tr><td>hum [%]</td><td>war0</td><td>FHW</td><td>Fuel</td><td></td></tr> <tr><td>0.0</td><td>0.00000</td><td>46.200</td><td>Generic</td><td></td></tr> </tbody> </table>	Efficiencies:	isent	polytr	RNI	P/P	Outer LPC	0.9000	0.9096	0.086	2.050	Inner LPC	0.8900	0.9009	0.086	2.100	HP Compressor	0.8700	0.9038	0.136	10.000	Burner	0.9995			0.980	HP Turbine	0.8800	0.8598	0.244	4.220	LP Turbine	0.8810	0.8653	0.082	2.985	HP Spool mech Eff	0.9900	Nom Spd	25729 rpm		LP Spool mech Eff	1.0000	Nom Spd	15173 rpm		hum [%]	war0	FHW	Fuel		0.0	0.00000	46.200	Generic																																																																																																																																																																																																																																																																																	
Efficiencies:	isent	polytr	RNI	P/P																																																																																																																																																																																																																																																																																																																																																																																											
Outer LPC	0.9000	0.9095	0.994	2.050																																																																																																																																																																																																																																																																																																																																																																																											
Inner LPC	0.8900	0.9008	0.994	2.100																																																																																																																																																																																																																																																																																																																																																																																											
HP Compressor	0.8700	0.9032	1.563	10.000																																																																																																																																																																																																																																																																																																																																																																																											
Burner	0.9995			0.980																																																																																																																																																																																																																																																																																																																																																																																											
HP Turbine	0.8800	0.8577	3.508	4.769																																																																																																																																																																																																																																																																																																																																																																																											
LP Turbine	0.8810	0.8601	1.058	4.055																																																																																																																																																																																																																																																																																																																																																																																											
HP Spool mech Eff	0.9900	Nom Spd	25726 rpm																																																																																																																																																																																																																																																																																																																																																																																												
LP Spool mech Eff	1.0000	Nom Spd	15172 rpm																																																																																																																																																																																																																																																																																																																																																																																												
hum [%]	war0	FHW	Fuel																																																																																																																																																																																																																																																																																																																																																																																												
0.0	0.00000	46.200	Generic																																																																																																																																																																																																																																																																																																																																																																																												
Efficiencies:	isent	polytr	RNI	P/P																																																																																																																																																																																																																																																																																																																																																																																											
Outer LPC	0.9000	0.9096	0.086	2.050																																																																																																																																																																																																																																																																																																																																																																																											
Inner LPC	0.8900	0.9009	0.086	2.100																																																																																																																																																																																																																																																																																																																																																																																											
HP Compressor	0.8700	0.9038	0.136	10.000																																																																																																																																																																																																																																																																																																																																																																																											
Burner	0.9995			0.980																																																																																																																																																																																																																																																																																																																																																																																											
HP Turbine	0.8800	0.8598	0.244	4.220																																																																																																																																																																																																																																																																																																																																																																																											
LP Turbine	0.8810	0.8653	0.082	2.985																																																																																																																																																																																																																																																																																																																																																																																											
HP Spool mech Eff	0.9900	Nom Spd	25729 rpm																																																																																																																																																																																																																																																																																																																																																																																												
LP Spool mech Eff	1.0000	Nom Spd	15173 rpm																																																																																																																																																																																																																																																																																																																																																																																												
hum [%]	war0	FHW	Fuel																																																																																																																																																																																																																																																																																																																																																																																												
0.0	0.00000	46.200	Generic																																																																																																																																																																																																																																																																																																																																																																																												

(a) GasTurb performance metrics for the PW535A model, at sea level (b) GasTurb performance metrics for the PW535A model, at 20500m

Figure A.1: GasTurb performance metrics